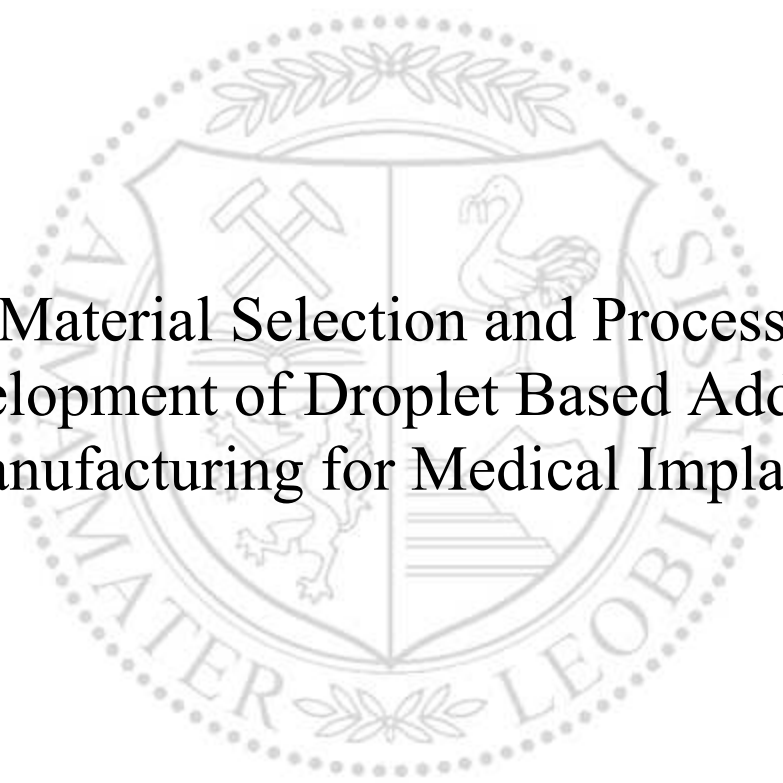Chair of Polymer Processing

Doctoral Thesis

Material Selection and Process Development of Droplet Based Additive Manufacturing for Medical Implants

Dipl.-Ing. Lukas Hentschel, BSc

March 2024

AFFIDAVIT

I declare on oath that I wrote this thesis independently, did not use any sources and aids other than those specified, have fully and truthfully reported the use of generative methods and models of artificial intelligence, and did not otherwise use any other unauthorized aids.

I declare that I have read, understood and complied with the "Good Scientific Practice" of the Montanuniversität Leoben.

Furthermore, I declare that the electronic and printed versions of the submitted thesis are identical in form and content.

Date 13.03.2024

Signature Author
Lukas Hentschel

Acknowledgment

I want to express my thanks to Joamin Gonzalez-Gutierrez for his support in the first years and his guidance in the scientific community. Without him, my first publication would not been published, which may have affected the following papers as well. Even though he left the institute in the middle of my thesis, he still supported me by answering my questions quickly and easily. Also, I want to thank Stephan Schuschnigg and Santiago Cano Cano for the lovely and supportive working group. The discussions we had in the office, lab, or at the bar were astonishing. I learned a lot in rheology, additive manufacturing, and polymer processing in the period of being part of the Institute. In addition, I want to thank my supervisor, the head of the department Clemens Holzer for the opportunity of conducting this thesis at the Institute of Polymer Processing. I am grateful for the last four years working with you and for the support, supervision, and in particular for the examination of my publications.

A special thanks to my continuous co-author Sandra Petersmann. Thanks for all the discussion, ideas, and mechanical testing you did for this thesis. Further, you had the most work in proofreading my written works, which by far is not easy. Without your support, I doubt that this work was even possible. Furthermore, I want to thank Florian Arbeiter for his input and ideas as well.

I want to thank all my colleagues from the institute Anja Wallner, Gernot Weiß, David Zidar, Julia Gössmann, Philipp Beier, Ivan Raguz, Markus Schwaiger, Jutta Geier, Christian Moser, Maria Gfrerrer, Alex Hellmayer, and Martin Hubmann for their support. They always had an open ear for any challenge either workload or emotional and donated their precious time and energy to help me. I am grateful for such a supportive community.

I want to thank all my friends who accompanied me during the journey and held my hand during these challenging times. Special thanks to Patrick, Oliver, Kurt, Michael, Julian, Thomas, Jürgen, Nikolaus, Paul, Eric, Micha, Gregor, Michael, Robin, Maximilian, and Sascha, to name a few of the important ones.

I am grateful to have found the most precious person, in the darkest times of my Ph.D journey. She guided me to find myself and became my better half. Without her, I would not stand there where I am yet. Thus, I thank you for taking this hard trial with me. I love you, Vicky!

Finally, a big thank you to my parents Judith and Karl, and my sister Lisa-Maria who supported and believed in me throughout the whole time. Even though some hard times have come and gone; I am grateful for having my back all the time.

To close it up I want to thank myself! For doing all the work, preserving the pressure, and closing out the work in the end. There was not only one time we wanted to give up, but still finished this journey.

Thank all of you!

Lukas Hentschel

Kurzfassung

Die additive Fertigung (AF), oder auch 3D-Druck, hat sich in den letzten Jahrzehnten von einem Forschungsthema zu einer neuen Fertigungstechnologie entwickelt. Es wurden viele verschiedene Technologien und Anwendungen gefunden, die von Designprototypen bis hin zu hochkomplexen Bauteilen reichen. Vor allem Polymere spielen bei AF im Allgemeinen eine wichtige Rolle. In den letzten Jahren hat der 3D-Druck aufgrund seiner einzigartigen Anwendungsmöglichkeiten ein erhebliches Marktwachstum erfahren. Im Zuge dessen wurde 2006 das ARBURG Kunststoff-Freiformen (AKF) von der ARBURG GmbH Co & KG (Loßburg, Deutschland) entwickelt. Da es sich um neue Technologie handelt, wurde bisher nur wenig Forschung betrieben.

Die AKF-Technologie hat das Potenzial jedes in Granulatform verfügbare Polymermaterial zu verarbeiten, so dass die Herstellung eines Filaments nicht notwendig ist. Bei dieser Technologie werden eine Spritzgusseinheit und eine piezoelektronische Nadelverschlussdüse für das Ablegen von geschmolzenen Polymertröpfchen angewendet. Da diese Technologie einzigartig ist muss der Zusammenhang zwischen Bauteilfestigkeit und Prozessparametern erforscht und ein Verfahren entwickelt werden, um eine gewisse Festigkeit des Teils zu gewährleisten zu können Im Rahmen dieser Dissertation wurden diese beiden Fragestelllungen durch die Erarbeitung eines möglichen Verfahrens zur Parameterqualifizierung und die Demonstration der Parameteroptimierung mittels eines faktoriellen Versuchsplans beantwortet.

Es wurde der Formfaktor (Drop Aspect Ratio, *DAR*) als einer der kritischste Vearbeitungsparameter für die geometrischen und mechanischen Eigenschaften identifiziert. Der DAR wird durch das Verhältnis der Tropfenbreite (*W*) zur Tropfenhöhe (*H*) definiert und dient zur Festlegung der Maschinenbahnen während des Druckens. Im Allgemeinen führt ein niedriger DAR zu einer hohen Teilefüllung und -dichte. Es stellte sich heraus, dass die Teiledichte direkt mit der Zugfestigkeit der gedruckten Teile in Verbindung steht. Außerdem wurde festgestellt, dass die Morphologie teilkristalliner Polymere durch die Bauraumtemperatur während des Druckprozesses beeinflusst wird und so Eigenschaften optimiert werden können. Bei erhöhter Bauraumtemperatur verschwanden die Bindenähte und es konnte eine homogenere Morphologie im Querschnitt der gedruckten Teile erreicht werden.

Die AF findet in der Medizin und im Gesundheitswesen immer mehr Anwendung. Hier werden Modelle, Werkzeuge, Prothesen und sogar Implantate mit dieser Technologie

hergestellt. Bauteile für solche Anwendungen müssen viele Anforderungen wie beispielsweise mechanische Integrität, Funktionalität und Reprodizierbarkeit erfüllen. In dieser Arbeit wurden verschiedene Polymere für die Anwendung als Schädelimplantate untersucht. Dazu wurde eine Standardprothese definiert, in verschiedenen Ausrichtungen und Materialien gedruckt und auf Schlagfestigkeit geprüft. Die Ergebnisse wurden mit jenen einer Knochenzementprobe verglichen. Dabei konnte die Knochenzementprobe eine höhere Schlagfestigkeit erreichen, jedoch erfüllten auch die gedruckten Proben die Anforderungen und können nach weiterer Parameter- und Designoptimierung verwendet werden. Die Ergebnisse zeigten somit, dass Polycarbonat, Polycarbonat-Urethan oder Polymethylmethacrylat für die Herstellung solcher Schädelimplantaten verwendet werden können.

Weiters wurde ein neuartiges Konzept für ein Multimaterial-Rippenersatzimplantat vorgestellt, welches sowohl weiches und hartes Gewebe in einem einzigen Teil imitiert. Insbesondere die Anbindung zwischen zwei Polymeren, mit unterschiedlicher Steifigkeit und Härte, spielte dafür eine bedeutende Rolle und wurde durch Zugversuche analysiert. Es wurden verschiedene geometrische Kontaktflächen entworfen, um die beste Kraftübertragung zwischen den Materialien zu gewährleisten. Einfache glatte Kontaktflächen führten dabei zu den besten Ergebnissen. Basierend auf der Grundlage dieser Erkenntnisse wurde ein Modell eines Rippenimplantats entworfen, erfolgreich gedruckt und in einen menschlichen Körperspender implantiert. Dabei wurde ein Reanimationsversuch durchgeführt, um die Bewegungen des Implantats beobachten zu können, wobei es während des Versuchs zu keinem Versagen des Implantats.

Zusammenfassend lässt sich sagen, dass diese Doktorarbeit das Potenzial des AKF-Verfahrens für medizinische Anwendungen aus technischer Sicht aufzeigt. Es wurde eine geeignete Parameterqualifizierung für alle verwendeten Polymere vorgezeigt und die wichtigsten Einflussfaktoren des Prozesses auf die resultierenden mechanischen Eigenschaften ermittelt. Eine Parameteroptimierung wurde für amorphe und teilkristalline Polymere durchgeführt und kann als Leitfaden für weiterführende Parameteroptimierungen mit der APF-Technologie dienen. Darüber hinaus wurden Implantate hergestellt und auf Schlagfestigkeit getestet, was die Machbarkeit solcher Anwendungen belegt.

Abstract

Additive manufacturing (AM) or 3D-printing has developed from a research topic to an emerging manufacturing technology in the last decades. Many different technologies and applications have been found, ranging from design prototypes, and small batch products to highly complex lightweight aircraft parts. Especially polymers play an important role in AM in general. In recent years, 3D-printing has undergone a significant market growth due to unique applications. The novel AM technology, ARBURG Plastic Freeforming (APF), was developed by ARBURG GmbH Co & KG (Lossburg, Germany) in 2006. Due to its relatively young age, only a small amount of research has been performed.

The APF technology has the potential to process any thermoplastic polymer material available in granulate shape, hence no development of a filament must be done. This technology uses an injection molding unit and a piezo-electronic shut-off nozzle for the deposition of molten polymer droplets. To guarantee a proper part performance, proper processing parameters must be specified. In this context, a procedure must be researched for this technology that allows a suitable set of parameters to be determined. Therefore, high-influencing parameters must be detected as well as a proper qualification procedure. Within the scope of this Ph.D. thesis, these two questions have been answered by describing a possible parameter qualification procedure and the demonstration of parameter optimization.

Therefore, the Drop Aspect Ratio (DAR) was identified as the most critical processing parameter for geometrical and mechanical properties. The DAR is defined by the ratio of the drop width (W) to the drop height (H) and is used for the definition of the machine path. In general, a low DAR led to high part filling and part density. It was found that the part density can be directly related to the tensile properties of the printed part. Furthermore, it has been demonstrated that the morphology of semi-crystalline polymers can be influenced by the print envelope temperature and part properties can thus be optimized. At evaluated print envelope temperature, weld lines disappeared and a homogeneous morphology in the cross-section of printed parts could be achieved. A real isotropic material behavior was not accomplished, but an improvement was also achieved here.

AM also finds increasing numbers of applications in the medical and healthcare sectors. Medical applications like models, tools, prostheses, and even implants can be printed. These devices must fulfill many requirements like mechanical integrity, functionality, and repeatability. In this work, different polymers have been studied for cranial implants. Therefore, one standard prothesis was printed in different orientations and materials and

tested on impact strength. The results were compared with those of a bone cement sample. Although the bone cement sample achieved a higher impact strength, the printed samples also met the requirements and can be used after further parameter and design optimization. The results thus showed that polycarbonate, polycarbonate urethane or polymethyl methacrylate can be established for the manufacture of cranial implants.

A novel concept of a multi-material rib replacement implant was presented, to imitate soft and hard tissue within a single part. This further enhances the possibility of AM for medical devices. Therefore, the bonding between two similar polymers with different stiff- and hardnesses was studied by tensile testing. Distinctive geometrical contact areas were designed to ensure the best load transfer between the materials. Simple plain contact areas led to the best results. Based on these findings a model of the rib implant was designed. The implant was successfully printed and implanted in a human body donor. A reanimation trial was performed, and the movements of the implant were observed. The implant could withstand the upcoming forces and prove its integrity. In conclusion, it was possible to fabricate a multi-material rib replacement implant.

To summarize, this Ph.D. thesis highlights the potential of the APF process for medical applications from a technical point of view. Proper parameter qualification for any given polymer was proposed and the most critical factors influencing the process on the resulting mechanical properties were determined. Parameter optimization was performed on amorphous and semi-crystalline polymers and can serve as a guideline for other parameter optimization using the APF technology. Further, implants were produced and tested mechanically for their impact strength, showing the feasibility of such applications.

Content

1 Motivation and Goal

1.1. Motivation

Additive Manufacturing (AM) has become a well-established manufacturing technology, complementing other traditional manufacturing technologies. This technology experienced rapid development in methods, materials, and applications in recent decades. More complex structures, personalized items, and rapid prototyping are the driving forces of these developments [46, 78, 278] . AM origins back in the 1980s, when first trials showed the potential of generative manufacturing [78]. Today, AM extends the existing manufacturing techniques and is revolutionizing several industries. Different methods for AM have been developed over the last decades, which can be divided into three groups, extrusion-based, vat-based, and powder-based technologies. All of them are based on the same principle of generatively building a part layer-by-layer [75, 78]. Metals, ceramics, and polymers can be used in different AM technologies. However, polymers are the most used feedstock materials for AM due to their good properties, availability and processability. In particular, extrusion-based technologies like fused deposition modeling (FDM®) or fused filament fabrication (FFF) are the most famous and affordable methods, widely used for prototyping, customized production, or low-quantity production. Any thermoplastic polymer available in filament shape can be processed applying extrusion-based technologies, therefore it shows a great potential for industrial applications. Vat- or powder-bed-based systems are limited to photoreactive or special polymer powders, respectively [75, 78, 114, 278].

Material jetting is an AM classification, which per definition builds a part by the deposition of droplets. The Arburg plastic freeforming (APF) belongs to that class of technologies, which was invented by the company ARBURG GmbH + Co KG (Lossburg, Germany) back in 2006. In a nutshell, this technology uses a small injection unit to melt polymer granules and to push the polymer melt towards a discharge unit. At the discharge unit a piezo-electrical shut-off valve is utilized, that opens and closes at frequencies up to 250 Hz. Hence, droplets are formed at the nozzle [73, 97, 276]. These droplets are then deposited onto a moving part carrier and therefore, a polymeric part is fabricated layer-by-layer by deposition of these droplets. Due to the comparable young innovation, not many academic works are available using the APF technology. Further, the impacts of the individual processes or material parameters are not yet well known. Especially, the shape of the drop and the building parameter of the drop aspect

ratio (DAR), which is the ratio of the drop width to drop height, are one of the most important parameters [34, 94, 99, 106, 206]. In contrast to filament-based extrusion methods, the polymer is processed from granules. However, for each polymer, a parameter qualification must be performed to find suitable processing parameters. These procedures are time-consuming and not standardized [97]. The importance of this qualification is of particular interest and must be investigated. Further, parameter optimizations can be performed to enhance the part performance for each application. For such optimizations, it is crucial to understand the influence of different processing parameters, and part orientations on the mechanical properties of either amorphous or semi-crystalline polymers. APF shows a high potential for industrial, high-performance, and medical applications among others [223, 276].

Medical applications are of supreme interest to AM. Here, personalized models, guides, tools, and even implants at very low quantities are required and can complement human healthcare tremendously. In the last few years, several investigations concerning the use of AM in the medical field have been published [110, 149]. Most of them deal with non-invasive parts and only a few tackles implantable devices or even long-term implants. AM can help to improve accessibility for personalized implants by reducing costs and manufacturing time [126]. Nowadays, mostly polyetheretherketone (PEEK) or titanium is used for cranial implants; these materials are expensive and hard to process. Alternative materials like polymethylmethacrylate (PMMA), polycarbonate (PC), or polycarbonate-urethane (PCU) present some advantages in terms of biocompatibility, accessibility, and processability [125, 169, 203]. Currently, cranial implants are mostly manufactured by subtractive manufacturing at an external provider. Hence, delivery time can last up to two weeks. AM, in particular thermoplastic based AM systems, can help by bringing the production of medical devices close to even within the hospital [124]. AM shows a major potential for localized fabrication of medical devices like implants but still must face some challenges like reproducibility, repeatability, reliability, mechanical integrity, or establishment in the medical sector. Furthermore, regulations following the medical device directive and different standards must be considered and reworked to fit these new developments [8, 124, 224, 226].

Due to the generative fabrication of parts, multi-material designs are now possible. Thus, the unique properties of different materials can be combined within a single part [98, 185]. For example, to have rigid construction parts with soft covers or soft hinges with hard mounting parts. One big challenge for such applications is the inter-material adhesion, to transfer the applied loads and to guarantee the function of the part. Not all materials nor all polymers are compatible and hence must be combined with other geometrical techniques [56, 103]. Nonetheless, these approaches are possible with AM technologies. Implants can benefit from multi-material parts, especially in areas where soft and hard tissues are present [98].

The main purpose of this Ph.D. thesis was to study the APF and define parameters and material qualification procedures. Furthermore, parameter optimization for the APF process was performed to show the potential and to point out the different impacts of parameters on the mechanical performance and geometrical accuracy. In addition, the medical implants application with different thermoplastic polymers using APF was studied. Therefore, the presented work shall point out the benefits of AM for medical applications and be used as a guideline for the material qualification and optimization for the studied material jetting AM technology.

1.2. Hypotheses

The following hypotheses were defined prior to the experimental work, based on the current state of the art. In addition to the hypotheses, the used systematic approach is given in a short form and will be further discussed in the individual upcoming sections. Based on the results the statements are then either accepted or rejected.

1. *"A proper qualifications procedure can be used to define suitable processing parameters for the APF technology."*
   A standard operating procedure was developed to identify proper processing parameters based on some material parameters and measuring of the formed droplet. Influences of different processing parameters were investigated and verified by measuring the density, surface appearance, and mechanical properties. Hence recommendations are given for a material qualification.

2. *"A Design of Experiments approach on processing parameters of the APF can be used to improve the mechanical performance of 3D-printed parts."*
   A Design of Experiments was set up and performed on different processing parameters for the fabrication of mechanical specimens. Tensile, bending, and impact parameters were analyzed to indicate the most critical parameters and optimization is performed based on these findings.

3. *"Process parameters optimization can reduce anisotropic properties in APF-manufactured parts made from semicrystalline polymers."*
   A study was performed on printing tensile parts with different infill orientations and different process parameters, to examine the influence on orientation.

4. *Technical or commodity polymers are feasible materials for medical invasive parts, produced by APF.*
   Selected case studies were performed to prove the feasibility to apply polymers with processing conditions below 300 °C as possible implants. Parts were produced and either tested mechanically or used in human body donors.

5. *A hard-soft material combination, manufactured by the APF, can improve the performance of medical implants.*

   This hypothesis was tested by the fabrication of multi-material specimens with different connection designs and the evaluation of the bonding strength. More complex parts were also improved by designing connection areas based on the previously achieved results.

1.3. Outline of the Thesis

This Ph.D. thesis is divided into five parts starting with section 1, motivating this research by providing an introduction, an overview of the hypotheses and the outline of the performed work. Section 2 covers the fundamentals of the topics to further understand the output of the investigations. Section 3 and section 4 form the main part of the thesis and deal with APF and the medical application of 3D-printed parts using that specific technology. Section 3 addresses the problem of parameter qualification of the process and the optimization using APF. These topics are presented in three peer-reviewed journal publications (i.e., publications A, B, and C). Section 4 shows feasibility studies for invasive medical applications in the craniomaxillofacial area, made from different polymers and the concept of a multi-material implant for the rib cage. This was demonstrated in one peer-reviewed journal publication (D) and a peer-reviewed conference publication (E). Section 3 and 4 are built up providing a short state-of-the-art subsection, an introduction to the publications, a slightly adapted version of the publications, and closing remarks summarizing the output. Section 5 ends the thesis with a conclusion and future research outlook. The publications presented in this Ph.D. thesis are summarized in Table 1. The format of the publications was altered slightly from the original form to fit the format of the thesis. The publications are available in open-source journals except for publications D and E. Publication D was submitted but not yet accepted and publication E was accepted but not yet published at the time of finishing this academic work.

Table 1   Overview of all publications abbreviated from A to E. The publications are split into two main topics and are given by their original reference, if available.

3. Parameter Qualification and Optimization for Arburg Plastic Freefroming

A	Hentschel, L.; Kynast, F.; Petersmann, S.; et al.: Processing Conditions of a Medical Grade Poly(Methyl Methacrylate) with the Arburg Plastic Freeforming Additive Manufacturing Process. Polymers 2020, doi:10.3390/polym12112677.
B	Hentschel, L.; Petersmann, S.; Gonzalez-Gutierrez, J.; et al.: Parameter Optimization of the ARBURG Plastic Freeforming Process by Means of a Design of Experiments Approach. Adv. Eng. Mater. 2022, doi:10.1002/adem.202200279.
C	Hentschel, L.; Petersmann, S.; Kynast, et al.: Influence of the Print Envelope Temperature on the Morphology and Tensile Properties of Thermoplastic Polyolefins Fabricated by Material Extrusion and Material Jetting Additive Manufacturing. Polymers 2023, doi:10.3390/polym15183785.

4. Medical Applications of Arburg Plastic Freefroming

D	Hentschel, L.; Petersmann, S.; Gardischar, A.; et al.: Mulit-Material Implant Structures with Medical-Grade Polyurethane via Additive Manufacturing, AIP Conference Proceeding. PPS-38[a]
E	Hentschel, L.; Petersmann, S.;Waly, C.; et al.: Impact properties of Cranial Implants Fabricated by ARBURG plastic freeforming, Journal of Applied Polymer Science[b], submitted 28.12.2023

[a] accepted but not yet published, [b]under review

2.1. Additive Manufacturing

2.1.1 Introduction to Additive Manufacturing

Additive Manufacturing (AM) according to the ISO ASTM52900:2018 [4] is defined as the successive addition of material in layers to form a physical object. In contrast to the traditional manufacturing methods where the amount of material is either constant (formative) or subtracted (subtractive) to put it into shape. AM is also known as 3D-printing, rapid prototyping, or rapid manufacturing among other, less popular synonyms. Especially today, 3D printing has become popular and can be found in design facilities, high-tech manufacturers, and hobby workshops all over the world [75, 78, 121, 189].

AM origins back in the 1980s when the pioneers C. Hull, C. Deckard, and S. Crump reported their first attempts. All of them followed different approaches by photopolymerization or material extrusion (MEX). Stratasys© patented their MEX technology known as Fused Deposition Modeling (FDM®) and released their first machine in 1992. Due to the patent, further development on that technology was hindered until 2006 when it expired, and a revolution started [16, 78]. Since then, many different methods, machines, and new business sectors have formed. 3D printing, especially material extrusion-based methods become community-based open-source projects, which last until today [16, 113, 114]. Some examples are the RepRap Project [215], Voron Design [269], and Klipper3D [133], among others.

Today, AM applications can be found in nearly any industrial branch. From topology-optimized parts in motorsports and aerospace, via personalized medical models, instruments, or implants until design or functional prototypes in any design and development center. Applications with this kind of approach are numerous but it will and cannot replace traditional manufacturing for all applications [16, 78].

2.1.2 General

As aforementioned, AM is defined as creating a physical object by the continuous addition of material. This happens mostly in the form of layer stacking; hence a two-dimensional layer is generated on top of the previously created layer. To achieve this, a computer-aided design (CAD) model must be generated to define the geometry. This model is

then transformed into a standard triangle language (STL) file only giving the information of the surface area of this model. This is digitally sliced into individual layers with a given layer thickness and transformed into a machine code (G-Code), that a standard 3D printer can understand. For the last procedure, open-source software, like PrusaSlicer, or commercial ones like simplyfy3D© can be used for almost any filament-based or photopolymerization machine. High-tech or industrial machines often use corresponding and limited software, due to special features and more reliable usage. However, the G-Codes contain all necessary information from machine parameters and most importantly the geometry which is translated into motor movements for X-, Y- and Z-coordinates, as well as the extrusion motor. Regardless the material, the 3D structure is formed by fusing layer on layer until the solid geometry is formed [16, 78]. In some cases, the parts need post-processing until the final mechanically stable part is reached with the required surface finished and dimensional tolerances. Figure 1 shows an overview of the different steps, from creating the CAD file, preparing the G-Code in an additional software, and finishing the part in the fabrication device.
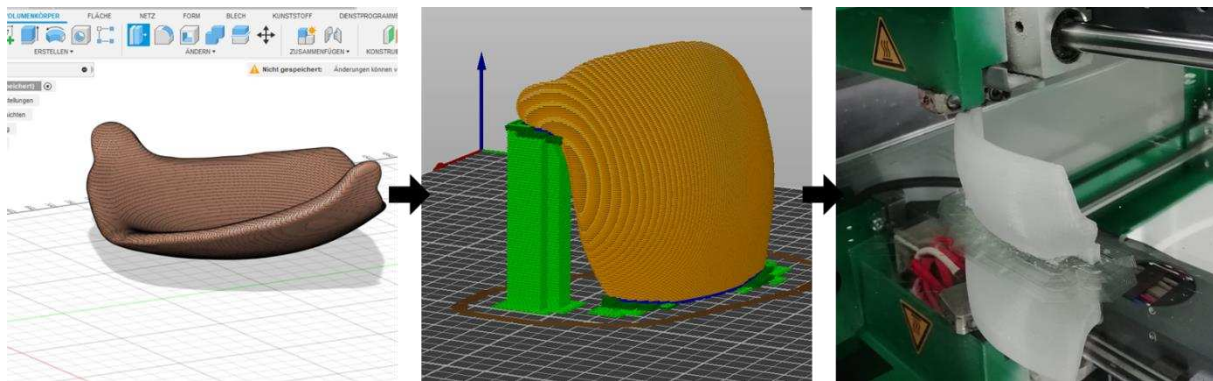
Figure 1   Screenshots from a CAD software (a), slicing software (b) and a picture taken during production (c) of an example cranial implant.

In comparison to AM, in computer numerical control (CNC) machining, unnecessary material is removed from a solid material block to achieve a given geometry, ending up in tons of residual waste depending on the geometry. Formative manufacturing, like extrusion, including injection molding, thermoforming, or forging deforms a feedstock material under constant mass to reach the desired shape. However, a special tool giving the negative form of the shape is needed, which must be formed prior. Such tools are not necessary for AM technologies [78, 121, 189].

In general, AM technologies can be separated into powder bed, vat, or extrusion systems with a few exceptions. Despite the different methods, the basic manufacturing steps of the machines are similar [78, 114]. The first step after uploading the G-code the preparation of the machine which is leveling and pre heating of the building plate for vat and extrusion system machines, since the distance between the toolhead and build bed is crucial for part performance [273]. The offset can also be measured at several points, to compensate for

uneven building plates. For powder-based technologies preparation of the machine include preheating and spreading the first layer of powder in the build chamber. Next the first layer is built onto the building plate, which can be made from metal, glass or polymer and depend on the material and method used. Material is extruded, cured, or melted until the first layer is finished and partly solidified. After finishing the first layer, the next layer is built on top of it and a physical object is created layer after layer. For powder bed and vat systems, a layer of fresh powder or resin must be applied prior. Using the extrusion technologies, material cannot be extruded into the air without support, therefore overhanging edges must be supported by an additional structure, which is also true for vat-based systems. However, for powder-based methods, the not solidified powder can act like a support itself. Such support geometries are created by the software and must be removed in an additional step. For powder-bed and vat-based systems postprocessing like cleaning and post-curing are necessary [16, 75, 78, 114]. Design guides are already available for the different methods of AM [114]. Figure 2 shows schematics of AM machines working with material extrusion (a), vat resin curing (b), and powder bed (c).
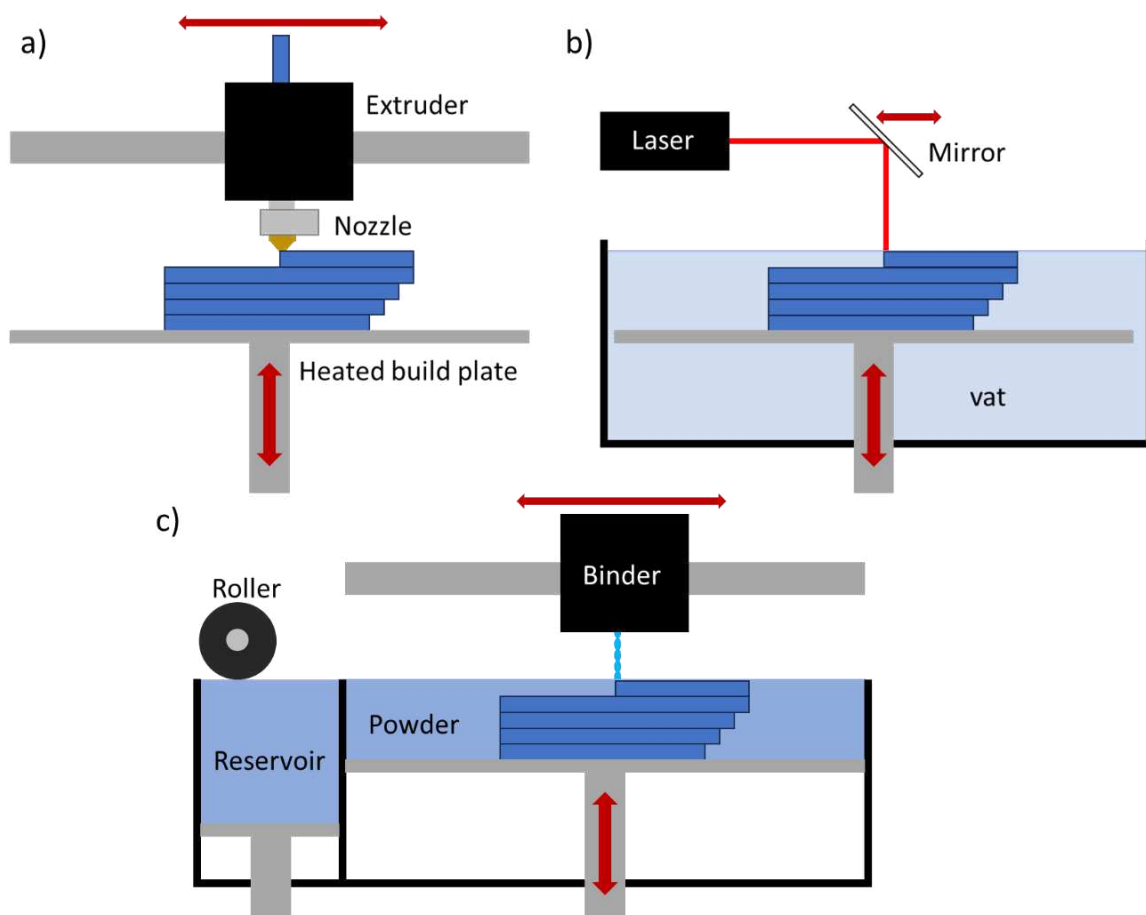

Figure 2   Schematic of a material extrusion-based (a), vat-based (b), and powder bed-based (c) Additive Manufacturing methods.

2.1.3 Methods of Additive Manufacturing

Besides the general classification into extrusion, powder-bed, and vat-based systems, different methods of AM have been developed and are split by the ISO ASTM 59000:2018 [5] into seven categories.

> - Binder Jetting (BJT)
> - Directed Energy Deposition (DED)
> - Material Extrusion (MEX)
> - Material Jetting (MJT)
> - Powder Bed Fusion (PBF)
> - Sheet Lamination (SHL)
> - Vat Photopolymerization (VPP)

The numerous different methods and technologies developed over the last decades may not all be allocated to only one of these categories, nor are some concepts or newer developments even able to fit in these sections. As an example, the Arburg Plastic Freeforming (APF) discussed more in detail in the next section, can be categorized under MEX since the material is extruded through a nozzle but also under MJT due to the formation of droplets throughout the processing [97, 276]. Furthermore, novel AM processes in the biological sector may not fit into either of these categories since bacteria or other microorganisms are used to fabricate 3D structures. However, these techniques gain attention due to the possibility of growing cells by means of AM in order to repair or even replace human tissues [85, 131, 152, 255, 268]. Also, the fabrication of other materials like glass [137], concrete [23], or cellulose [228] may find manifold applications in the future.

BJT is defined as the deposition of a binder onto a powder bed to form a solid layer. Hence, this technology does need a powder bed as well as an added second material that binds the powder particles. However, the powder material can be any material like metal, ceramic polymer, or even sand [238, 285]. As an example, metal casting companies use this technology to form tools made of sand for subsequent metal casting [238]. In this case, this method can also be defined as rapid tooling since the AM is used to form a tool for manufacturing [16, 78].

DED is defined by the application of a directed thermal energy source used to join deposited material by melting. Laser engineering net shaping, direct metal depositing, and direct light fabrication are a few examples of DED. However, the printing process is rather complex and is mainly used for repairing or adding material to existing components [78]. DED tool heads consist of a nozzle providing the feedstock (e.g. metal wire or powder) and an energy source (e.g., electron beam or laser). The material is then molten and deposited on the build plate or

the previously laid layer, like material extrusion, however, the tool head must move with at least four axes. This process can work with polymers and ceramics but is mostly used for metals [78]. The most astonishing application of DED is the production of parts for a rocket engine by NASA [253].

MEX is defined as the deposition of material through a nozzle or an opening. The most common MEX technologies are filament-based technologies named FDM®, fused filament fabrication (FFF), or fused layer manufacturing among other synonyms. Hence, any polymer available in the form of a filament can be processed by this technology. Some limitations due to shrinkage, crystallization, and other morphological properties are present for some materials like polypropylene, polyoxymethylene, and high-temperature polymers like polyetheretherketone [114, 205, 245]. Beside filament-based technologies some machines using a small conventional extruder (i.e., screw-based) are on the market, enabling the processing directly from the granulate usually designed for a higher throughput (e.g., big area additive manufacturing) [236, 264]. Further extrusion can also be performed by a plug-based system, in this case extrusion must not be continuous like for filament or extruder-based systems since cartridges of material are used [264]. MEX technologies are rather rough AM methods with layer height from 0.1 mm for filament-based to a few centimeters when large extruders are used, resulting in a lower resolution at least in Z-orientation [78].

MJT is roughly defined as the deposition of droplets of building material. In contrast to the binder jetting, it is a single material system where no additional binder is needed. Two examples of this category are the Arburg plastic freeforming (APF) and the PolyJet® technology, which could not be more different. The APF used a small injection molding unit in combination with a piezo-electronic shut-off nozzle to form thermoplastic polymer droplets. These are deposited on the build plate or previously formed layer. PolyJet® uses a modified inkjet tool head to deposit photocurable resin on a building plate [193]. After each layer, a light source is applied to cure the resin. It must be noted that this technology is capable of full-color printing like inkjet printing on paper. Nevertheless, the main material is limited to photocurable resin. In contrast, APF can process a great variety of thermoplastics from polypropylene to polyetheretherketone in granulate form, despite some physical or chemical limitations [73, 97, 211, 276]. Further information is given in section 2.1.4.

PBF describes technologies using a heat source to melt controlled areas on a powder bed in order to fuse these powder particles. This technology can be applied to polymers, metals, and ceramics, only by altering the energy input [16, 78]. For polymers, mainly high crystalline polymers like polypropylene or polyamides are processed by such a method but are limited to amorphous or elastomer materials [114, 282]. Selective laser sintering (SLS), selective laser melting (SLM), and electron beam melting (EBM) are a few examples of this technology

[16, 78]. Another limitation of the used materials it the availability in powder shape, with a narrow size distribution, including the peak particle size at around 20 to 45 µm to provide an acceptable resolution. Furthermore, it must be taken care when working with powder, and special safety equipment is needed due to its explosive nature. For all methods, post-processing including removing additional powder and sometimes tempering is necessary [78, 114].

SHL is defined as the formation of a physical object by fusing individual foils. This includes methods like laminate object manufacturing or ultrasonic additive manufacturing. Here sheets of materials are bonded together by adhesives or by ultrasonic fusing technology and subsequently cut after each layer application. This can either be performed by precise laser cutting or CNC milling, depending on the material used. Materials can range from sheets of aluminum, copper, stainless steel, titanium, and different polymers or composites, but mostly paper is used. One main application of this technology is prototyping due to low costs, low energy consumption, and easy handling [16, 75, 78].

VPP, one of the first invented technologies defined as an AM technology, where liquid resin is locally photopolymerized in a vat. Stereolithography (SLA) or digital light processing (DLP) are examples of the VPP [16, 75, 78]. Both methods use a vat filled with a photoactive polymer and a movable building plate, which can be either top-down or bottom-up. Both arrangements have advantages and disadvantages. The top-down variant is easier to build but the material is exposed to oxygen during polymerization, which can lead to interference [151]. Bottom-up is currently more common due to the absence of oxygen but also needs a transparent vat bottom, where resin may adhere to and lead to a process failure [114]. The main difference between SLA and DLP is the light source which is a CO_2 laser or an LCD-display, respectively. Hence, SLA offers a true replication of the outline for every feature greater than the laser spot (~200 µm) but is limited in printing speed due to the reaction kinetics and that the full layer has to be traced by this laser beam [192]. DLP-type technologies can cure the whole layer at once but are limited in resolution by the LCD itself [16, 75, 78, 114]. However, with improving display technologies, the resolution did improve over time and can now go down to an XY resolution of 28.5 µm. Further, layer heights between 0.01 mm to 0.05 mm can be realized making this technology ideal for small functional parts like lab-on-a-chip, personalized brackets, personalized hearing aids, jewelry, or accurate performance part applications among others. However, this technology is limited to photocurable resin materials [114, 192].

2.1.4 Arburg Plastic Freeforming

The APF technology is a rather new technology developed by Arburg GmbH & Co KG (Lossburg, Germany) back in 2006. As aforementioned, it is characterized as MJT but also as

MEX technology since the material is extruded in the form of droplets in theory. The corresponding machine is called freeformer and is available in different variations with 2 or 3 material units or high-temperature applications. Nonetheless, the basic principle remains the same [60, 73, 97].

The technology is based on a small injection molding unit with a barrel diameter of 15 mm with three heating zones including the nozzle zone. A polymer granulate is stored in the hopper, which can be equipped with an on-top circulating dry-air drier. Further, the feedstock is molten by the applied heat and dissipation energy, through shear stress induced by the rotation of the screw. The molten polymer is then pushed to the nozzle by the horizontal movement of the screw. There a piezo-electronic shut-off nozzle is located, which can operate at a frequency of up to 250 Hz, leading to the formation of droplets. A scheme of the machine is shown and explained in Figure 3.
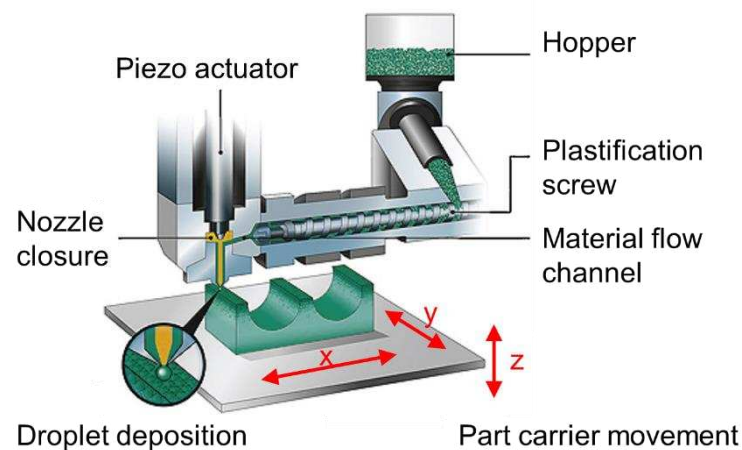
Figure 3   Scheme of the Arburg Plastic Freeforming adapted from [73].

The droplets can reach a height from 0.1 to 0.4 mm depending on the so-called discharge value and a diameter of around 0.2 mm based on the nozzle diameter [34]. The discharge value is a parameter for the screw stroke during nozzle opening and is given in percentage. This value is usually adjusted to form a droplet of 100 % to 125 % of the desired layer height and is rather important for the processing [97]. Further, the needed processing pressure is supplied by the screw as well and should be constant over time, for suitable processing conditions. Decrease or increase in processing pressure over time, or during one dosing cycle may be an indication of degradation due to the high residual time of up to 20 minutes [99]. These values are influenced by the processing temperatures as well as other dosing parameters and must be adjusted for each condition. The parameter settings, consisting of the temperatures, dosing parameters, and discharge values are machine parameters and usually are adjusted directly at the machine [99].

Based on a stable process, the geometrical parameters can be determined. The most important parameter is the drop aspect ratio (*DAR*), which is defined as the ratio of the drop width to the drop height [34, 99, 106, 206]. This value is set in the slicing software for preparation of the machine code, hence this value must be measured and set correctly, otherwise, the final part may be under or overfilled. This value can be measured using a microscope but may be adjusted empirically until a dense part is formed [94, 97]. Measuring the density can be used for the evaluation of the printed parts [99]. Other geometrical parameters are the number of contour lines, the overlap with the contour lines, the infill percentage, and the orientation of the infill among others [34, 53, 92, 99]. A full geometrical parameter set can be saved as ".bbprof" file for the software and a material profile file in addition on the freeformer, which are synchronized by a digital unique identification number (UID). Only the discharge value is not saved and can e.g., be saved in the file name.

Due to the rather young release date of the APF, not many papers have been published before this dissertation. Hence, there was a huge potential for optimization, understanding of different parameters, and qualification procedures, to define suitable processing parameters with low effort. Also, possible applications of this technique must be found based on the properties, despite some applications in the medical sector can already be found in the literature [73, 169, 185, 223, 276].

2.1.5 Challenges

It was expected that 3D printing would one day replace all other traditional manufacturing technologies. In fact, it has become a strong complement to them. Furthermore, design rules must be rethought to either consider the bigger design freedom or to also take the specific needs of the different AM technologies into account [114]. Even with the development of AM technologies, many challenges must be faced or at least considered when working with them. This shall point out topics for further development and improvements to push these technologies even further, rather than point out their weaknesses.

A major drawback of AM methods is the time for manufacturing a single part, which is not competitive to other technologies. AM technologies are not in use for mass production but rather used in low quantity production due to the long processing times [7, 80, 111, 129, 235]. In comparison to injection molding (IM), where numerous parts can be produced in short time, AM may not outrun this technology when it comes to quantity. However, if only a small number of parts is needed, AM may be the cheaper and faster option, taking into account the manufacturing costs and time needed for producing and testing the mold. Figure 5 shows an approximation of the manufacturing costs over quantities for AM and conventional manufacturing like IM [67, 78, 278].
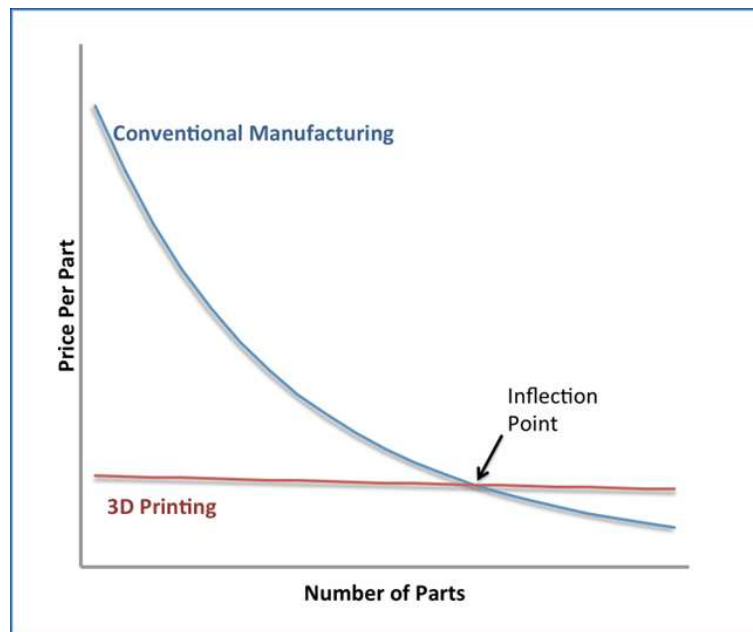
Figure 4   Price evaluation of 3D printed parts and conventional manufacturing (IM) as a function of the number of parts [86].

One possibility to face this challenge is to enhance the printing speed of the machines. However, this is limited to the laws of physics to ensure proper mechanical performance of the solid part [80]. Further, the process speed can be improved in terms of finding a suitable layer height, which is the main influence parameter for the manufacturing time. As an example, a 1 x 1 x 1 m³ prototype must not be manufactured with a layer height of 0.2 mm, otherwise a production time ofa few days could be expected. In contrast, the layer height cannot be too big in order not to lose the resolution of the part [21, 67, 79, 149].

The resolution may be a further challenge, which can again be addressed by the selection of suitable technologies and processing conditions. However, post-processing may also improve the resolution and accuracy of printed parts. The main feature of AM parts is the staircase-like appearance of the outer surface. In rare cases, these layers can only be seen under the microscope, if a layer height of under 0.05 mm is achieved. In contrast, this will again extend the printing time. Hence, a compromise between resolution and printing time must always be found [7, 16, 67, 78, 79, 111, 149, 278].

Further consideration must be taken for the mechanical performance of 3D printed parts. Only speaking about polymers, AM parts mostly show a weaker performance than injection molded, extruded or subtractive manufactured parts, which can also be caused by underfilling the geometry for material or weight reduction. Nevertheless, for performance parts, which have to transfer or withstand loads, the weaker performance must be considered [97, 206]. Furthermore, the parts manufactured by AM show anisotropic properties, which can be correlated with the manufacturing orientation. The performance in the XY plane is significantly

higher than in Z-Orientation, due to the inter- versus intralayer adhesion [100, 242, 247]. However, one possible application for AM is to fabricate topology-optimized geometries, which cannot be done by other technologies. Topology optimization 3D printed structural parts can show a better strength to weight ratio than conventionally manufactured parts. Hence, AM is not meant to replace any traditional manufacturing, but rather enhance the overall manufacturing capability. Anisotropic and the processed induce mechanical properties must be considered to ensure the proper performance of the printed part. This kind of anisotropy is characteristic of 3D printing and is challenged in nearly all AM methods and can also be used on purpose. Anisotropy is highly related to the technology used, the printed geometry as well as processing parameters and materials [16, 78, 114].

Even though AM is primarily used for single-part or small-batch-size production, reproducibility and repeatability are huge concerns [278]. This is important for quality control, predictable part performance, and even environmentally friendly production. By now, variations in the process are present, leading to different results for each print. Reasons can be fluctuations in the powder size, filament diameter, environmental temperatures, molecular mass distribution of the material, and slipping of the extruder drive wheels among others [40, 87, 107, 159, 260]. Few of such errors are controllable, some are monitorable, and some are uncontrollable random errors. The challenge here is to reduce the uncontrollable, random noise to ensure a good repeatability of results [40, 87]. High industrial machines are already capable of reducing variability due to the use of "closed" systems, restricting access to the hardware and software to the user, and in some cases even materials. Stratasys® and Markforged® are some examples of these closed systems, leading to remarkable results but are limited to their portfolio and are more expensive than other open systems. Nevertheless, the user must not be as extensively trained for closed systems as for open systems, which can also be considered as an advantage [16, 78].

In summary, figuring out the highest impact factors to enhance mechanical performance, reduce anisotropy, increase reproducibility and repeatability, and decline the manufacturing time are the most important challenges to face for each individual AM technology and their respective applications [99, 145, 159, 205].

2.1.6 Advantages

In general, most AM technologies are relatively inexpensive, especially for the hobby sector, desktop printers are already accessible for less than 300 €. These are either filament-based MEX or VPP machines designed for home applications. Such printers are provided by numerous suppliers. Further, many different materials with different properties in the shape of filaments are assessable, also resins with different properties are available. However, since

such printers are designed for private use, no quality control tools, expensive features, or compatible software among others are at hand. Industrial printers are more expensive due to such expensive features, higher manufacturing quality, and warranty. Further, such machine purchases are also in combination with company service to ensure printing quality [78]. However, considering the costs of additional tooling, which is needed for IM or CNC machines, AM machines are a low-cost investment [46, 258, 275].

The possibility of complexity is considered as the main advantage of AM, and it is the only technology to produce closed hollow parts in one step. This is especially true for extrusion-based technologies, for powder bed-based or VPP a small opening must be present to get rid of the residual powder or resin [16, 67, 114]. However, internal structures or closed structures are easier to manufacture by AM, such as microfluid channels [88], or other enclosed structures [67]. In that aspect, design freedom for AM parts are higher than for conventional manufactured parts and this fits the market needs of increasing complexity [46]. Especially, in terms of personalization, individualization, and customization of different products, AM seems the way to go [46, 78, 114]. Despite mass production, AM can be used to improve the performance of e.g., in-ear shells, and dental crows, or can be used for jewelry, architecture, and many more [46, 114]. Topology-optimized structures are also a huge advantage of AM since such structures are not economically feasible with traditional manufacturing. This can enhance mechanical performance, reduce weight, and sometimes improve the appearance of a product [16, 46, 75, 78, 114].

Despite the slow production speed, time from scratch to the finished part is short. Hence, improving the design process by the detection of design errors early in the process does save time and money, due to rapid prototyping [41, 78]. This is also interesting for development, fabrication of personalized items, spare parts, or toys in a short amount of time [78, 199, 278]. One must only create a CAD-model of the desired part, convert this into the G-Code and transfer this file to the printer [78]. The printing process itself is fully automatic and can manufacture complex parts in a single step. Post-processing might include the removal of additional support structures.

Some studies have shown that AM technologies are low in energy and material consumption compared to traditional manufacturing [67, 278]. Hence AM can be considered environmentally friendly. Further, such aspects as the reduction of design errors in an early development phase, and the reduction of residual material also can be considered environmentally friendly. The low energy consumption and self-sufficient working principle for most AM machines make them ideal for applications in undeveloped countries. To provide on-demand products in many areas [16, 75, 78, 114, 278].

In a nutshell, AM can be used to enhance existing processes and complement traditional manufacturing. In addition, complex parts like internal structures are now feasible at lower costs, and in economically and environmentally friendly ways [67, 278]. However, AM is not the answer to every challenge given in the present nor the future. It cannot outplay existing manufacturing processes, but rather support them or be an additional worth process. Still a lot of improvements can be made for AM and the corresponding technologies, in terms of their applications.

2.1.7 Applications

Numerous applications for 3D printing can be found today in industries from medical, automotive, aerospace, electronics, and academic institutes among others. As mentioned, starting in private usage, to small series production, but also for high-tech applications like aerospace, and motorsports [16, 75, 78, 114, 149, 278]. The pie chart in Figure 5 gives an overview of the applications of AM.
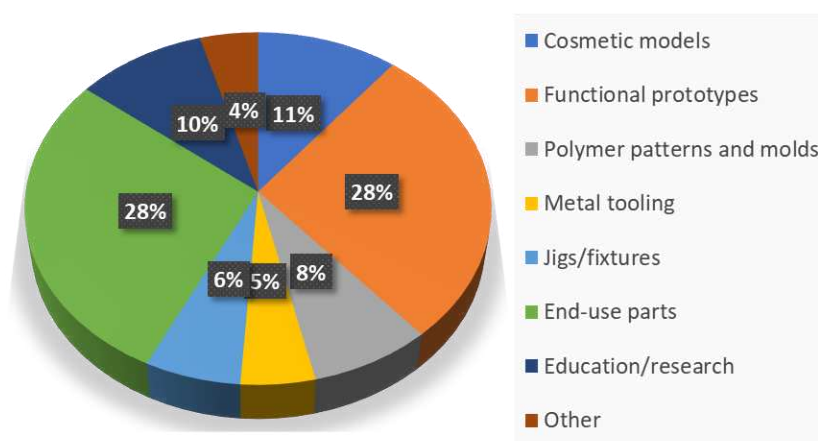
Figure 5   Pie chart of the applications of Additive Manufacturing in the industry based on [278]

This application distribution might change for each sector, but it should give a good overview. Nowadays, AM is already established in applications like shoes, sunglasses, arts, fashion, architecture features, rapid tooling and rapid prototyping, and musical instruments [16, 46, 67, 75, 78, 278]. Another important sector to point out is the medical care sector since AM does help enhance human health. Dental brackets, surgical models, individual prosthetics, and personal implants are just a few examples to name [110]. Personalized implants are still under investigation and are only used in limited cases [10, 62, 125]. However, this might change in the future since AM can enhance implant performance, reduce costs, and increase the aesthetics [126].

2.2. Polymers for Medical Applications

2.2.1 Introduction

Medical applications are always handled as a high-value technology and thus materials are handled the same. The development of medical, surgical, or healthcare instruments dates back to Hippocrates (460-377 B.C.) [28]. He was considered the founder of classical surgery and tools have been developed consistently since then until today. However, the development of such instruments experienced significant growth in the last century. Although first polymers have been synthesized in the early 1900s, the first healthcare applications were only found in 1937 [28]. William Feinbloom developed eye lenses made from polymethylmethacrylate (PMMA) which are nowadays made from silicone elastomers [225, 277]. The positive characteristics of PMMA found other applications in another form as bone cement (e.g., Palacos®). The requirement for materials used for human healthcare such as being sterile, inert, and reliable rose over the years [44, 225, 277].

The variety of synthetic polymers also increased over time and come to the fore of research. In the beginning, polymers in the medical sector were used for packaging, disposable products, and tubing among others [225, 277]. However, most of the applications are not invasive or only for a short period. For invasive applications like long-time implants, mostly inorganic materials have been used. In the last decades, bone cement and poly-etheretherketone (PEEK) have been used more frequently for bone replacement in trauma surgery. They offer some big advantages in post-surgical treatments like X-ray translucency, better acceptance rate, and are cheaper compared to titanium [225, 256]. Prostheses, as an example, also evolved from wood structures to designs made from composite materials due to their high mechanical loading. Implants also experience such a change from metal replacements to polymer parts [210]. In the last decades, the development of polymers for medical applications has increased because of the possibilities biodegradable polymers offer, which are resorbable by the human body [225, 256, 277]. This kind of polymer is especially interesting for tissue engineering since the resorbable polymer gets replaced by biological tissue over time.

2.2.2 Biomechanical Requirements

Synthetic materials, used to either replace living tissue or work together in contact are named biomaterials and can be classified as bioinert, biotolerant, or bioactive. Therefore, such materials must be tested following the classification. The testing of biomechanical properties is regulated according to ISO 10993-1 [22] and includes testing for allergic reactions, irritations, implantation toxicity, cytotoxicity, carcinogenicity, and hemocompatibility. Biomaterials are

currently made of either metal, ceramic, polymer, composite, or natural materials. However, they have to fulfill the same requirements. This includes biocompatibility, functionality, stability, and sterilizability [45, 59, 168, 225, 277].

Biocompatibility is the most important biomechanical property to ensure the integrity of the human body system as best as possible. Materials that do not interact or not significantly are considered bioinert. Such materials are, for example, gold, titanium, stainless steel, zirconia, PEEK, or, although seen as controversial, PMMA. These materials do not induce chemical reactions, inflammation, or any other interaction with the human tissue and hence keep this stability for a lifetime [44, 144, 202, 210, 225, 261]. Due to that, such materials are ideal for long-term applications. Biotolerant materials do interfere with the human body without causing significant harm. However, tissue will be damaged, and hence such biomaterials are only applicable for short-term use. Mostly synthetic polymers are classified as biotolerant and are only used for short-term use applications due to lower costs in comparison to bioinert materials. Bioactive materials are interfering in a significant amount, which are toxic or beneficial for the human body. Mostly such bioactive materials are used as coating for bioinert implants to either enhance their performance or decrease the risk of inflammation, which cannot be neglected [44, 68, 225, 257, 277]. Further, a trend towards drug-loaded implants can be seen to improve the healing process of the patient [157, 276]. Other bioactive materials are bioresorbable, biodegradable or are removed by any microorganismal mechanism and may not cause any changes in the human body environment.

All medical devices must be sterile to be used in the human body environment. That means any organic species, like bacteria, which may cause infections or inflammations, have to be eliminated. Many microorganisms are used to harsh environmental conditions and therefore, the sterilization process must be aggressive to stop cell regeneration or kill those organisms to prevent any interference for the later application [225, 277]. Prior to the sterilization process, a washing step to reduce the contamination of the device to a minimum and ensure a proper sterilization process is performed. The cleaning and disinfection are performed with the help of detergents and biocides [200]. The main sterilization process is realized either by saturated steam, radiation, plasma, or by chemical agents. Saturated air sterilization is performed with an autoclave providing a saturated air environment of 121 °C and 2 bar, or 134 °C and 2 bar. These conditions are applied on the medical devices for 20 min or 5 min, respectively [84, 225, 277]. This technique is most common in hospitals but is not suitable for most polymers since they cannot withstand these extreme conditions. Radiation is most used for disposable products after production. Therefore, either UV, X-ray, or gamma radiation can be applied. High-energy radiation is applied on the surface to disable any biological mechanism. Plasma sterilization is functioning due to the release of UV radiation and free radicals which interfere with organisms and lead to the decomposition of such species. If thermolabile

materials, like polymers which are not resistant to temperatures higher than 120 °C, are used, chemical sterilization is the most applied method. Aggressive chemical agents like formaldehyde, ethylene oxide, or peracetic acid are applied on the pre-washed surface [84, 225, 277]. Again, radical chemical reactions lead to the inactivation of microorganisms. However, for porous or rough surfaces, this may lead to residual chemical agents on the medical device and later interfere with the human body, which makes an additional washing step necessary [277].

Similar to any other technical application, biomaterials have to fulfill the functional requirements as well as to resist the mechanical loads. The biomaterial must be formable, so the needed shape can be provided. Further, the solid parts must withstand the applied forces acting on them. As an example, cranial implants are shaped in accordance with the curvature and sized of the bone to be replaced [225]. This can either be an exact replicate, manufactured from PEEK by means of CNC, or a hand-formed bone cement sample. Both are shapeable with different methods, but the bone cement type may not be as accurate as the CNC replicate. Furthermore, both are able to carry the daily mechanical loads acting on them [10, 256, 261].

In the next subsections, an overview of some important, polymers used for medical applications is given. They offer huge potential to enhance human healthcare due to their processability, biomechanical properties, physical properties, and availability.

2.2.3 Polymethylmethacrylate

Polymethylmethacrylate (PMMA) is a transparent, amorphous thermoplastic polymer, with high mechanical properties, brittle fracture mechanics, and outstanding optical properties. The chemical structure of PMMA consists of a carbon-hydrogen backbone, with an acrylic ester side chain in the repeating segment as shown in Figure 6 [48, 225].

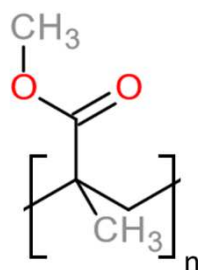Figure 6   Chemical structure of PMMA showing the repeating segment with n units [225].

Since PMMA is an amorphous polymer, the material softens with rising temperatures until a flowable state is reached, further increasing the temperature would lead to chemical decomposition. Hence, these types of polymers do not have a defined melting point, but a recommended processing temperature range can be defined. Amorphous polymers react in

the form of a glass transition, which is defined as the transformation of a glass-like state to a liquid state. For PMMA this state shows around 105 °C, hence it also shows a comparable high-temperature resistance. Further, PMMA shows a high scratch resistance, translucency, and chemical resistance to esters, ketones, and chlorinated and aromatic carbohydrates [9, 48, 188, 225]. Table 2 gives an overview of the physical properties of PMMA.

Table 2   Typical material properties of PMMA polymer materials based on the literature [9, 48, 225, 272].

Material property	Typical value
Density in g cm^{-3}	1.19
Glass transition temperature in °C	105
Heat deflection temperature in °C	90 - 100
Melting temperature in °C	/
Young´s modulus in GPa	2 - 3
Tensile strength in MPa	50 - 75
Elongation at break in %	2 - 5

PMMA is better known by one of its tradename Plexiglas® [48] as a thermoplastic polymer and as bone cement (e.g., Palacos® [101]) for medical use. Bone cement is supplied as oligomer powder and monomeric liquid which is mixed and polymerized just minutes before application. In some cases, in-vitro polymerization is performed but care must be taken since the reaction temperatures can reach up to 70 °C [24]. The heat can lead to harming the surrounding tissue, further residual monomer concentration can lead to inflammation. Bone cement is used in cranioplasty and for fixation of implants for joint replacements (e.g., hip joint). The latter leads to an improved force transmission due to the increased interface surface. Further, bone cement can be drug-loaded to enhance the healing and further prevent inflammation, although PMMA shows a generally low risk of inflammation. Thermoplastic PMMA is used in application as long-period contact lenses due to their optical properties and as bone substitution in non-critical areas [44, 225, 277].

PMMA is also a promising polymer to be used in MEX and MJT AM technologies. In combination with the acceptable biomechanical and mechanical properties, it is seen as an ideal candidate to be used for additively manufactured medical devices [97].

2.2.4 Polyolefins

Polyolefins, like polypropylene (PP) or polyethylene (PE) are usually semi-crystalline thermoplastic polymers. In contrast to amorphous, semi-crystalline polymers have a defined melting range, where the crystalline structure is destroyed, and it converts into a liquid state. These kinds of polymers show melting temperatures ranges from 130 °C to 170°C depending on the side chains, tacticity, molecular weight, and molecular weight distribution. Polyolefins are per definition saturated carbohydrate structures without any other element in the basic chemical structure. The simplest one is PE, followed by PP but can also reach more complex structures depending on the side chains. The chemical structure of PE and PP are shown in Figure 7. Furthermore, copolymers of different monomers are common for polyolefins to improve a certain physical property. Tacticity also influences the crystallinity of polyolefins. As an example, isotactic PP, meaning all side chains are on the same side, and syndiotactic (altering side chains) are semi-crystalline. Atactic (random side chains) PP show a low crystallinity rate or are even amorphous since the formation of crystals is sterically hindered [48, 225].
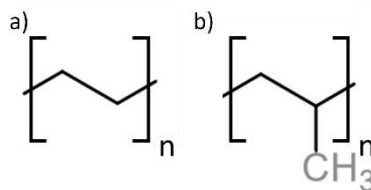
Figure 7   Chemical polymer structure of PE (a) and PP (b) with n repetitions depending on the molecular mass [48, 225].

Polyolefins are ductile, lightweight, and soft polymers with a high chemical resistance to almost any chemical agent. Hence, they are also bioinert and do not interact with any biological species. However, they usually show low mechanical performance, no scratch resistance, and poor UV- and heat resistance. To slightly improve some properties, additives are added to ensure proper material performance [48, 225]. Table 3 gives an overview of some physical properties of PE, PP, and ultra-high molecular weight PE (UHMWPE).

Table 3   Overview of material properties PE, UHMWPE and PP based on the literature [48, 76, 225].

Material property	Typical values		
	PE	UHMWPE	PP
Density in g cm^{-3}	0.91-0.97	0.94	0.86-0.9
Glass transition temperature in °C	-110	-160	-20

Heat deflection temperature in °C	40-90	65-75	50-100
Melting temperature in °C	120-135	130-140	160
Young´s modulus in GPa	0.2-1.4	0.8	1.6
Tensile strength in MPa	11-30	20-25	32
Elongation at break in %	<800	<500	<300

PP is mostly used for packaging, food trays, and disposable containers among many others one-way applications, due to the low price, steam sterilization resistance, and good recyclability. Furthermore, PP is used as suture material, due to its high fatigue strength if stretched properly. UHMWPE is used in joint replacements as an anchor, besides UHMPE, no polyolefin finds application in any invasive application. Further, this polymer cannot be extruded, or injection molded because of the high molecular weight and corresponding high viscosity so it is usually machined to fit the applications [48, 125, 225].

PP did also find its way into 3D printing, although the semi-crystalline structure and considerable high shrinkage potential [245], makes it challenging to process. By now, special types of PP have been found, and an enhanced process development led to better processability of this material. Due to the bioinert characteristics of PP and adjustable properties, it has become an interesting alternative for soft tissue replacements and personalized cranial implants [114, 125, 243, 245].

2.2.5 Polycarbonate

Similar to PMMA, polycarbonate (PC) is a transparent, amorphous thermoplastic polymer. It is known for its solid toughness, impact strength, stiffness, and hardness among others. Further, it shows good optical properties with less transparency but a better refractive index of 1.59, compared to PMMA. Hence, PC is commonly used for glasses or other optics. PC is synthesized from the controversial discussed, cancerogenic monomer Bisphenol A and is classified as polyester, due to the carbon acid ester in the backbone [48, 225]. The chemical structure is given in Figure 8.
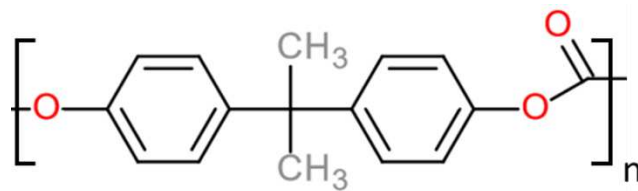
Figure 8   Chemical structure of PC with n repetitions depending on the molecular weight [48, 225].

PC became famous for its usage in CDs which vanished in the last decade and new applications were found in glass substitutes in aerospace, hard cases, transparent housing for cameras, and many more technical applications. PC shows outstanding mechanical performance and has a glass transition temperature of around 150 °C making it nearly a high-performance polymer. Table 4 gives an overview of some physical properties of PC [48, 225].

Table 4   Material properties of Polycarbonate based on the literature [48, 225].

Material property	Typical value
Density in g cm^{-3}	1.2
Glass transition temperature in °C	148-150
Heat deflection temperature in °C	130-138
Melting temperature in °C	/
Young´s modulus in GPa	2.3
Tensile strength in MPa	65-70
Elongation at break in %	<120

PC is used for glasses, contact lenses, and other optics due to the high transmission coefficient and breaking index. Furthermore, e.g. airplane windows are made from PC due to the comparable high-temperature resistance and mechanical performance. If used in applications that are in contact with the human body environment it is seen controversial due to the possible Bisphenol A contaminations [66, 263]. However, PC is used in blood dialysis as filter cartilages, in cardiac surgery as blood reservoirs, filters, and oxygenators, as well as for surgical instruments. Hence, the polymer is already established for invasive short-term medical applications. Those applications benefit from transparency and temperature resistance [48, 225, 277]. Furthermore, almost all known sterilization methods are applicable for PC, in contrast to PMMA or polyolefins [200, 209, 225, 277].

PC also is used in the AM for technical parts. The material is excellently processable by means of MEX-AM and the resulting parts show outstanding mechanical properties. PC is often blended with ABS to improve the impact strength, which also shows positive effects on the processability. Due to the favorable properties and processability in AM, this polymer shows a high potential for personalized medical instruments, devices, and implants, even though long-term applications are not yet established [15, 82, 214].

2.2.6 PC-U

Polycarbonate-urethane (PC-U) is a unique thermoplastic elastomer (TPE) with favorable biomechanical properties. Despite the other polymers, TPEs are famous for their soft behavior and high elongations like classic elastomers. These polymers also develop a network but are only bonded covalently and can be broken up by heat. Hence, this material can be processed like thermoplastic polymers. PC-U is a block copolymer consisting of a linear polycarbonate soft segment and an aromatic urethane hard segment with different ratios available [55, 74, 225]. The chemical structure is given in Figure 9.
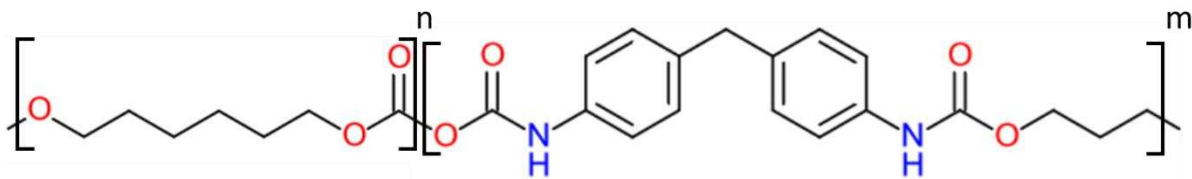

Figure 9   Chemical structure of a typical PC-U as a block copolymer with n repetitions of a linear polycarbonate and m repeating polyurethane segments [27, 74].

The ratios do define the resulting properties and material behavior and are classified by the measured Shore hardness. Higher amounts of urethane segments will lead to more network connection what increases the hardness of the resulting polymer. This can range from around 80A to 75D from soft to hard. Due to the outstanding biocompatibility, mechanical integrity, along with good biostability, this material is used for in-vivo orthopedics [74, 174]. Furthermore, medical applications in pacemakers, catheters, artificial heart valves, and vascular grafts can be found [74, 225].

PC-U is a thermoplastic elastomer and because of that shows low mechanical strength in comparison to other polymers, but high flexibility, elongation and a hyperelastic material behavior. Some material properties are given in Table 5 by the examples of a soft (80A) and hard (75D) grade of Bionate®, supplied by DSM Biomedical (Gelee, Netherlands).

Table 5   Material properties of PC-U of two commercial grades, Bionate® 80A and 75D supplied by DSM Bionmedical [49].

Material property	Typical value	
Shore hardness	*84A*	*73D*
Density in g cm^{-3}	1.19	1.22
Glass transition temperature in ℃	-8	/
Vicat softening temperature in ℃	82.5	56
Melting temperature in ℃	162	/
Flexural modulus in GPa	0.029	1.792
Tensile strength in MPa	54.9	63.2
Elongation at break in %	501	241

PC-U has been shown to be processable in the APF process. Due to the long medical history of these materials, the establishment of 3D-printed implants was already possible. However, this technology is still in its infancy, but a few use cases can already be found in the industry [55, 169, 201, 225].

2.2.7 Other Polymers

Many other polymers are used for medical applications due to their unique properties. Some examples will be given in a short overview in this section.

First, the most famous polyetheretherketone (PEEK) is mainly used for orthopedics in the craniomaxillofacial area. The polymer has outstanding mechanical properties and bioinert nature but is hard to process and extremely expensive. Implants are mostly manufactured by subtractive manufacturing. Thermal resistance up to 200 °C makes them ideal for steam sterilization [202, 225, 277].

Another unique type of polymers are bioresorbable materials. Polylactide-acid (PLA), polycaprolactone (PCL), polyvinyl alcohol (PVA), and polyethylene-glycol (PEG) are the most famous representatives of this kind of material. These polymers can be resorbed by the human body without or only with little interaction to the immune system. PLA and PCL are degraded by human cells at different rates and hence have different durability from a few days to some years [112, 136, 183, 225, 233, 277]. PVA and PEG are soluble in water and hence will just remain for a few days in the human body. Chirurgical sutures are made from either PLA or

PCL due to their relatively high strength and resorbable nature. Therefore, removal of the suture is not necessary, which is interesting if applied to inner tissues. Other applications are resorbable implant fixations or screws which do not need to be removed at an additional surgery. Scaffolds for tissue engineering are also made of PVA or PEG among others, to promote cell growth in orthopedics [159, 225, 277].

For more information on these polymers or other materials used for medical applications refer to the literature [220, 225, 277].

2.3. Manufacturing of Medical Implants

The manufacturing of products for medical usage have to fulfill more and stricter regulations and standards compared to other industrial sectors [225, 277]. In general, medical devices are classified due to their risk of harming the human body's environment. According to the medical device directive (MDD) the following classes are defined [59]:

Table 6   Classification of medical devices according to the medical device directive [59].

Category of Class	Risk Assessment
Class I	Low-risk (corrective glasses, toothbrush)
Class IM	Low-risk measuring device (stethoscopes, blood pressure monitor)
Class IS	Low-risk sterile device (first aid kits, sterile urine bags)
Class IIa	Medium-risk (surgical gloves, short-time implants)
Class IIb	Medium to high-risk (long-term implants, intra-ocular lens)
Class III	High-risk (pacemakers, vaccines)

The classification of medical devices follows different rules, listed in the MDD 93/42/EEC, and considers invasive and non-invasive use, time span, and intervention of the biomechanical system (drug-loading). The MDD is applicable in the EU area, other agencies are responsible for other local regions [225, 277]. Due to the classification, different prerequisites on the material are valid in terms of biocompatibility. These include cytotoxicity, allergic testing, cancerogenic testing, cell growth testing, and many more. Biocompatibility testing is regulated by the ISO 10993 [22] standard as already mentioned in section 2.2.2**Fehler! Verweisquelle konnte nicht gefunden werden.**. However, the device itself also must be validated on quality,

stability, and functionality to ensure no failure at a high probability [225]. This includes a risk analysis in accordance with ISO 14971 [167] and clinical studies in different versions over a relatively long period [59, 225]. Overall, the complete validation process consumes a lot of resources. In addition, the whole production steps must follow quality management regulations according to ISO 13485 [168] to ensure a stable and safe product performance. In summary, medical devices and medical-approved materials follow high standards to ensure human well-being as best as possible. Due to those high standards, materials, devices, software, and services are expensive and need a long time until they are established [225, 277].

Implants are designed on purpose and are custom-made for each specific use case. These person-specific implants (PSI) are mostly manufactured by CNC milling from a solid PEEK block [10, 116, 125, 194, 202, 231, 237]. This procedure is performed at an external manufacturing place and delivered to the operation theater [116, 231]. The total process starts with the imaging of the defect using different digital imaging systems like computer tomography (CT) or magnet resonance tomography (MRT). Based on the digital copy, a PSI is designed virtually and in addition manufactured substantively [125, 126]. Due to the huge variety of geometries, injection molding is not an option for sustainable manufacturing, but AM is already in use for manufacturing PSIs. Here, powder-based AM or MEX-AM technologies with PEEK are used to produce the parts [54, 109, 153, 231, 232]. In terms of medical regulations, a duplicate is always fabricated to replace the first one after failure and is stored in the hospital [124]. In this term, reproducibility of parts manufactured by means of AM is crucial. Furthermore, a classification based on the size, complexity and area may be useful for cranial implants [208]. The complete process from digital imaging, via production request to the final part and surgery, can take up to two weeks [116, 231]. In the worst case the patient must stay under observation during the production time and after surgery, what results in a high consumption of hospital resources. Studies also have shown a positive outcome in terms of geometrical fitting, performance, and rejection rate of professionally manufactured implants compared to hand made bone cement implants [58, 70, 72, 120, 164, 277]. A warranty is given by the manufacturer for the functionality, stability, and biocompatibility of the product [134, 225, 277].

Another established option is the application of hand-formed bone cement implants in the craniomaxillofacial area. Here, the implant is formed either by hand in the operation theater or directly on the patient [24, 44, 123, 130, 180, 225, 277]. As mentioned in the section 2.2.3, bone cement is a reactive polyacrylic system, that is polymerized in the operation theater during the surgery. The reaction only lasts for around 20 min until the final strength of the materials is archived [44, 156]. However, care must be taken on the reaction heat, which can rise to 70 °C and thus harm the surrounding tissue and residual monomer concentration which may cause inflammation. The main advantage of this procedure is the accessibility since the

material is usually in storage, the fast procedure, low material costs, and shorter patient observation times. Nevertheless, implant fitting is comparable low and can lead to dissatisfaction of the patient due to aesthetic reasons, especially in the craniomaxillofacial area [156, 161, 225, 271, 277]. Some pilot studies used rapid tooling in combination with bone cement to enhance the geometrical fitting [123, 130, 180]. There a negative mold is designed for the desired implant geometry and manufactured through AM. Filament-based MEX methods show good results for this usage. The mold is then sterilized and prepared for the surgery. The bone cement is mixed and applied on one mold half in the right amount and the mold is closed for several minutes until the reaction is finished and the solid implant is fabricated. To ensure a good separation of the part from the mold, surgical gloves or similar foils can be used. Studies show great results in terms of fitting, processability, and accessibility [123, 130, 180, 239, 240, 250].

Summarizing, AM is a promising method for the manufacturing of PSI, with less residual materials and fast accessibility. AM can also bring manufacturing into the hospital, shorten supply chains, and reduce costs to produce medical devices, models, and implants among others [124]. Because of to the long time until new technologies are established in the medical sectors, AM usage is still in its infancy but will increase with time.

2.4. Design of Experiments

Experiments are based on the analysis of the variation of results achieved through altering boundary conditions, with defined input parameters. In polymer processing, particularly in AM, a huge number of parameters can be altered to generate the desired results [145, 158]. The so-called design of experiments (DoE) approach is a procedure for setting up experimental parameter studies with the least amount of effort. In the simplest version, a set of parameters (factors) is chosen with an upper and lower value (level), and combinations of these two states are then usually randomized over a series of experiments and analyzed based on the measured results (response) [12, 132, 197]. This design is abbreviated as 2^k DoE, where the number (2) defines the number of different levels for the factors (k). For example, tensile bars are printed by means of MEX-AM at different nozzle temperatures (A) and printing speeds (B), each t a lower and higher level. In total 4 different combinations of parameters are used to fabricate the specimens. These are then tested, and the results are analyzed. Table 7 shows the resulting manufacturing order, after randomizing the combinations with the coded (-upper level- +1, -lower level- -1) and uncoded values for A and B as well as the fictive results of that experiment [12].

Table 7   Example of 2^2 DoE table showing the run order, standard order, factors in coded and value form and fictive results.

Run	Standard Order	A		B		Result in MPa
		A_i	Value in °C	B_i	Value in mm s⁻¹	y_i
1	4	-1	200	-1	10	18
2	1	1	220	1	30	24
3	2	-1	200	1	30	9
4	3	1	220	-1	10	30

Table 7 show the example of a 2^2 DoE, with two factors (2) at two levels (^{2}). The number of different runs equals the mathematical expression of the DoE label (2^2 = 4) and describes the maximum number of different factor combinations and have to be randomized. The factors are labeled with capital letters starting with the nozzle temperature (A) and printing speed (B) leading to a certain tensile strength (y) as the response [12, 132, 197]. For further explanations, the combinations of A and B are sorted and then randomized to avoid any interference of uncontrollable conditions, like changes in humidity or room temperatures as well as fluctuations in the feedstock. However, parameters can be prioritized so that they are not changed too often, as setting the parameter takes too much time. For example, setting the build plate temperature can take up to 30 min depending on the area of the build plate. To further enhance the meaningfulness of the experiment, more measurement points are needed. Thus, the number of samples can be increased by fabrication of replicates or repetitions. Replicates are made at constant processing conditions and repetitions are made later in the experiments after altering the conditions [12, 132, 197].

For analyzing the experiment, a linear regression is performed, assuming the influence of a global constant (0), the individual factors (A, B), and an interaction (AB). The main effects are the effect of the variation of a single factor and interactions are the effect of the variation of both factors on the response. The constant coefficient (α_0) is evaluated as the sum of the response, divided by the number of runs (1). The main effects are the effects of each factor on the response and are calculated by the column sum of the product from the factor times the response, divided by the number of runs. For each factor a coefficient (α_A) is evaluated (2) and per definition the doubled value of the main effect. Such a coefficient (α_{AB}) can also be

calculated for the interaction (AB) which is caused by the altering of both factors. These coefficients are then used to build the linear regression equation (4), for further interpolation of the response variable [12, 132, 197].

$$\alpha_0 = \frac{1}{n}\sum_{i=1}^{n} y_i \tag{1}$$

$$\alpha_A = \frac{1}{n}\sum_{i=1}^{n} A_i\, y_i \tag{2}$$

$$\alpha_{AB} = \frac{1}{n}\sum_{i=1}^{n} A_i B_i\, y_i \tag{3}$$

$$\check{y} = \alpha_0 + \alpha_A A + \alpha_B B + \alpha_{AB} AB \tag{4}$$

Such empirical linear regression equations (4) can only be used for the respective experiment and within its boundaries. Based on this regression main effect plots can be created to point out the correlation of the factors and their interactions. The resulting plots of the example experiment can be seen in Figure 10.
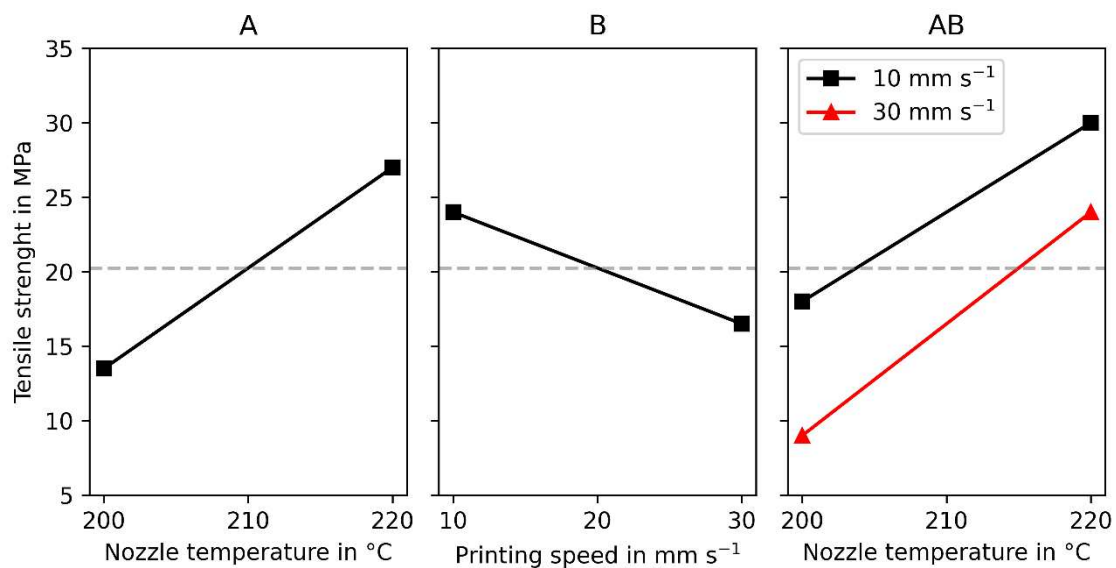

Figure 10   Main effect plot based on the example DoE from Table 7.

The main effects A and B can be correlated with the slope of the curve, in the related plots. The effect of the interactions (AB), in contrast, are present if the two curves shown are not parallel, hence they rise with the angle between the curves. For this example, only a small interaction AB can be observed.

As the evaluation is based on a linear regression model, a linear correlation of the effects is assumed. In nature, however, dependencies are often non-linear. To test the linearity, a

center point can be added to the experiment, by setting each factor to the value in between the initial values and noted as 0. The response of this value must be on the linear regression curve of each main effect plot, otherwise the linear functions are not valid for interpolation. However, based on the resolution of the experiment every relation can be approximated by a linear function [12, 132, 197].

DoEs approaches are designed for the analysis of a series of factors on one or multiple responses. However, the number of runs rises exponentially with the number of factors (2k) and leads to excessively costly and time-consuming experiments. Here a fractional factorial design (2^{k-g}) can be applied to reduce the number of runs. Therefore, a full factorial DoE is set up using k-g factors first, where the remaining factors are generated from the interactions of higher degree. Thus, they are named generators (g). This results in a reduction of runs by the factor 2^{-g} in a total number of experimental runs of 2^{k-g} [12, 132, 197]. Table 8 exemplarily shows a 2^{4-1} DoE which was reduced from 16 (2^4) to 8 (2^3) runs.

Table 8   Standard order of a 2^{4-1} DoE showing the different factor combinations used.

Standard order	A	B	C	D (=A B C)
1	1	1	1	1
2	-1	1	1	-1
3	1	-1	1	-1
4	-1	-1	1	1
5	1	1	-1	-1
6	-1	1	-1	1
7	1	-1	-1	1
8	-1	-1	-1	-1

Using such fractional DoE allows the use of a huge number of factors in a single experiment, however, interactions of higher degrees are usually neglectable in engineering and practice. This approach is useful for screening of different factors when the effects are unknown and then rerunning the experiment with only those factors that show a significant effect. Fractional factorial design can be classified by their resolution. As an examples in resolution III, main effects are not substituted with each other but with 2-factor interactions. In resolution IV, main effects are substituted with 3-factor interactions or higher. Resolutions of higher degree, mean

the substitution of main effects are done by higher degree interactions, that are neglectable. As a rule of thumb, resolution III is not advisable, resolution IV is applicable for screening and resolution V+ can be used without any hesitation [12, 132, 172, 173, 197].

3 Parameter Qualification and Optimization for Arburg Plastic Freeforming

3.1. State of the Art

3.1.1 Parameter Qualification for Additive Manufacturing

Similar to any other polymer processing method, suitable parameters are crucial to provide good part properties of additively manufactured parts. Since injection molding and extrusion are already established processing techniques, processing guides are available for most polymer grades. These guides include processing temperature ranges, throughput, tool temperatures, rheological properties, and shrinkage potential among others. These properties can give the user information on how to process the material and how to setup the process in accordance, although small adjustments may be needed [90, 118, 189]. For many AM methods it is unclear which material properties must be considered for proper processing and individual processing parameters. Filament producers nowadays provide a range for nozzle temperature, build plate temperature, and printing speed for their filaments. However, these are rather broad and affected by the machine used. Further, approximations like a processing temperature around 10 K above the extrusion temperature or build plate temperatures around the glass transition and melting temperature can be made. However, these suggestions are not applicable for all polymers or AM methods [75, 78, 114]. Therefore, there is a need to qualify the process and the process parameters, especially for industrial application.

The DIN SPEC 17071:2019 [2] defines the requirements for manufacturers and manufacturing centers that use any AM technology according to ISO/ASTM 529000:2018-06. The document includes criteria for AM processes and quality factors of the complete production chain. Therefore, internal operations and procedures are defined by the document. In contrast to a standard like ISO 9001, the DIN SPEC 17071 is not mandatory, but manufacturers can benefit from this qualification, particularly if medical devices are manufactured [224]. The complete process chain is defined and separated into individual sequences including data management, material management, machine preparation, process management, machine post-processing, and part post-processing. These sections are critical for quality management and are built up in several steps, defined in the mentioned document. The process qualification is defined by the determination of reproducible and relevant part properties. Therefore, a

significant number of specimens are produced and tested during the qualification process to build a foundation of reproducible parameters. The qualification is valid for the complete process chain with the used material, machine, and parameters set. For any changes in the process chain, it must be re-qualified. Further, the document defines quality management including staff, documentation, tracking, and infrastructure requirements [2].

Even though the qualification is valid for a single parameter set, it is important to mention that parameters can be divided into machine and build parameters. Machine parameters are set on the machine and include processing temperatures and processing speeds among others. Build parameters are set in the slicing program and affect the part resolution, infill percentage, contour lines, and many more geometrical features and appearance properties. Many machine parameters are included in the G-code, at least for desktop MEX printers, hence it is difficult to separate the parameter sets. Other technologies, like the APF machine and building parameters can be saved separately. However, both parameters can affect the mechanical properties and the appearance.

3.1.2 Parameter Impacts for Arburg Plastic Freeforming

As mentioned before, not much research work has been performed using the APF technology. However, Charlon et al. [34] covered the impact of different process parameters on tensile properties, density, and part mass of ABS samples. Machine parameters like the discharge, nozzle temperature, chamber temperature, processing speed, and building parameters like filling density, number of contours, layer height, and processing angles were analyzed intensively. Except for the processing speed and the chamber temperature, all the studied factors show significant impacts on mechanical properties. Young's modulus and tensile strength of the printed samples showed a strong correlation with their density. However, the elongation at break did not show the same correlation.

Hirsch et al. [106] also studied ABS samples, using a design of experiments (DoE) approach. He selected the nozzle temperature, chamber temperature, overlap, layer thickness, and drop aspect ratio (DAR) as factors for the 2^{5-1} DoE. The results of the main effects showed a significant influence of the DAR on the tensile strength and a reciprocal effect on the surface roughness. Hence, a compromise between surface roughness and tensile properties must be taken. Further, the layer thickness showed similar effects on the surface roughness and tensile properties. Eisele et al. [53] showed the same results on printed ABS cubes, concluding that parameters can be found to set either a maximum in mechanical or appearance properties.

Pinter et al. [206] used ABS feedstock to fabricate flexural testing specimens. These samples were tested and compared to filament-based MEX and injection-molded samples, for three-point bending and Charpy impact properties. The tests showed that samples prepared

by injection molding exhibited the highest properties, followed by APF samples. The flexural results showed a linear correlation with the part densities, independent of the manufacturing method. However, impact properties were not affected by the density for the AM technologies but showed a significant increase with increasing density for injection molded samples. Considering the cross-section of the samples, 3D-printed parts showed a significant porosity, which resulted in a significant effect on the impact properties of the material.

Further, the orientation did impact the mechanical properties of additive manufactured parts, which must be considered in the designing and the orientation during the printing process. Two studies showed the impact of orientation on ABS-printed samples [93, 211]. Geometrical properties, economic efficiency, and functionality are further properties to study for AM printed parts and some studies are already available in the literature [73, 94, 223, 226, 227, 276]

3.2. Process Parameter Qualification for Arburg Plastic Freeforming

3.2.1 Introduction to Publication A

Publication A deals with the qualification of a medical grade PMMA. The focus was on defining a proper parameter set for further individual optimization. Processing temperatures of the polymer melt preparation had been defined based on the material data sheet. Building parameters like the DAR and the discharge had been studied empirically, visually, and by measurements of the top surface. Further, the effect of the chamber temperature on the form stability was evaluated. Tensile bars have also been prepared in single and multi-specimen batches in different orientations. The publication can be used as a standard operation procedure for material qualifications of other polymers. It includes a proper approach to define a first parameter set for any polymer. In addition, a specific set of specimens for proper reference values, including mechanical properties were provided and the difference of single and multi-part additive manufacturing was pointed out.

The presented publication is slightly different from the original, to fit the style and language of this work. The original was published as: *Hentschel, L., Kynast, F., Petersmann, S., Holzer, C., & Gonzalez-Gutierrez, J. (2020). Processing Conditions of a Medical Grade Poly(Methyl Methacrylate) with the Arburg Plastic Freeforming Additive Manufacturing Process. Polymers, 12(11), 1-15.*

Beside the publication other related work was published in relation to this topic but is not included into the thesis and listed below:

- Conference contribution: Holzer, C., Hentschel, L., Kynast, F., Schuschnigg, S., & Gonzalez-Gutierrez, J. (2020). *Qualifizierung von Materialien für*

medizinische Anwendungen mittels des Arburg Freeformers. Abstract from Werkstoffe und Additive Fertigung, Potsdam, Germany.

- Magazin contribution: <u>Hentschel, L.</u>, Gonzalez-Gutierrez, J., & Holzer, C. (2020). Eingliederung von Additiven Fertigungstechnologien in einen klinischen Prozess zur Herstellung von medizinischen Implantaten. *Jahresmagazin Kunststofftechnik Ingenieurwissenschaften*, *2020*, 56-61.

3.2.2 Publication A

Processing Conditions of a Medical Grade Poly(Methyl Methacrylate) with the Arburg Plastic Freeforming Additive Manufacturing Process

L. Hentschel, F. Kynast, S. Petersmann, C. Holzer and J. Gonzalez-Gutierrez

Abstract

The Arburg Plastic Freeforming process (APF) is a unique additive manufacturing material jetting method. In APF, a thermoplastic material is supplied as pellets, melted and selectively deposited as droplets, enabling the use of commercial materials in their original shape instead of filaments. The medical industry could significantly benefit from the use of additive manufacturing for the onsite fabrication of customized medical aids and therapeutic devices in a fast and economical way. In the medical field, the utilized materials need to be certified for such applications and cannot be altered in any way to make them printable, because modifications annul the certification. Therefore, it is necessary to modify the processing conditions rather than the materials for successful printing. In this research, a medical-grade poly(methyl methacrylate) was analyzed. The deposition parameters were kept constant, while the drop aspect ratio, discharge rate, melt temperatures, and build chamber temperature were varied to obtain specimens with different geometrical accuracy. Once satisfactory geometrical accuracy was obtained, tensile properties of specimens printed individually or in batches of five were tested in two different orientations. It was found that parts printed individually with an XY orientation showed the highest tensile properties; however, there is still room for improvement by optimizing the processing conditions to maximize the mechanical strength of printed specimens.

Introduction

Additive manufacturing (AM), colloquially known as 3D printing, has started to be a useful tool for the production of medical devices. AM can allow patient-specific medicine and the manufacturing of medical devices with intricate design, which by other methods would be too costly to manufacture. Furthermore, AM technology can be used to shape 3D objects and, using unique materials, reversible-stimuli-responsive functionality can be achieved (i.e., 4D printing) [286] .However, there are still technical limitations of AM that need to be overcome to ensure a safe application in the medical field, such as the identification of materials that can be safely used in long term applications. Further essential aspects, such as identifying cleaning and sterilization methods that can be used with the different materials, have to be defined [42]. Another limitation is that materials need to be certified to produce parts for medical applications. This certification process is time-consuming and expensive. Therefore, material producers go through this certification process for very few materials, particularly for materials for which the certification costs can be recovered in a reasonable amount of time. Altering the material in any way and even altering the processing conditions can render the certification invalid. Thus, it would be reasonable to use materials that have already been certified for medical applications in general. That means that the additive manufacturing equipment should be an open platform, where any material can be used. One example of an open system AM process is the Arburg Plastic Freeforming (APF) process developed by Arburg GmbH +Co KG (Lossburg, Germany).

The APF is a novel material jetting additive manufacturing technology that enables the production of complex thermoplastic components using standard material pellets [106]. In terms of medical application, the processing of granules offers a considerable advantage since no further filament-making is necessary. Thus, no further manufacturing step has to be certified for medical purposes. A plastification unit similar to that of an injection molding machine provides the molten material and the pressure for the deposition process. After plastification, the polymeric material enters the discharge unit, consisting of a nozzle and a piezo-electrical value, which opens the nozzle up to 250 Hz [73, 185]. Since the nozzle opens and closes at such high frequencies, the extruded melt forms droplets instead of a continuous string as is the case of other melt deposition technologies such as material extrusion additive manufacturing (MEX) with filaments (also known as fused filament fabrication (FFF)). Hence, the APF process is sometimes referred to as droplet deposition modeling [276]. The produced droplets are positioned on a Cartesian moveable building platform to form a three-dimensional structure layer-by-layer. A schematic representation of the process is shown in Figure 11. One significant advantage of the APF systems compared to FFF is the higher density that can be achieved in the fabricated specimens. This higher density can lead to better mechanical performance [106, 128].
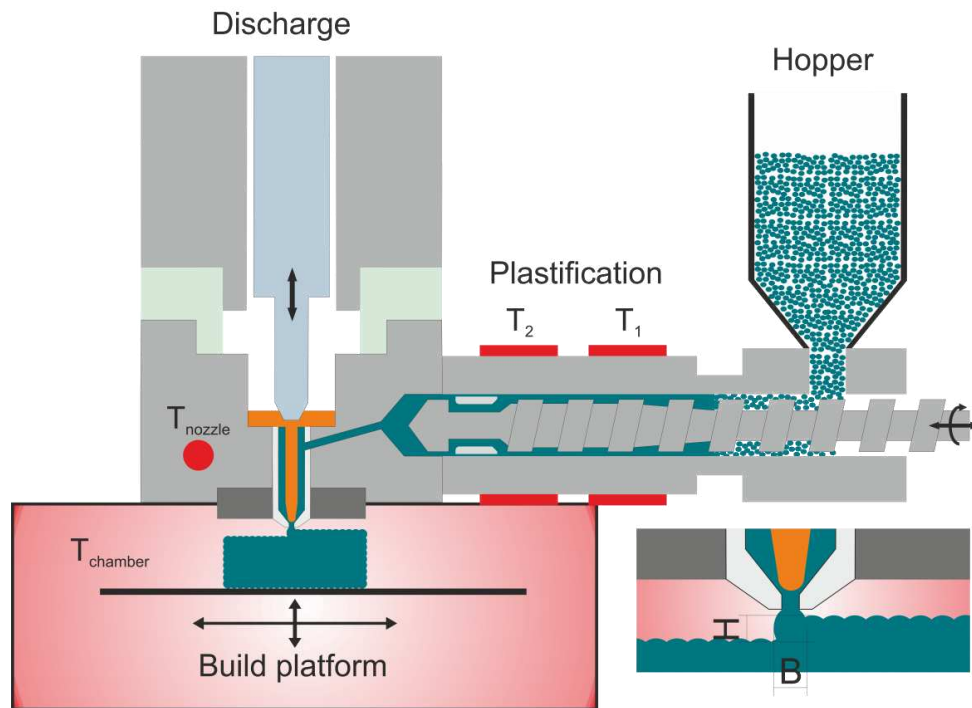
Figure 11   Working principle of Arburg Plastic Freeforming process where T_1 is the temperature in cylinder zone 1, T_2 is the temperature in cylinder zone 2, T_{nozzle} is the nozzle temperature, and $T_{chamber}$ is the chamber temperature. B and H are the width and height of the produced droplets, respectively.

The APF technology is an open system meaning that variations of almost all process parameters are allowed by the manufacturer. This flexibility results in a great variety of processable materials, but it also means that the processing parameters have to be identified by the user. However, some support in finding the right parameters is given directly from ARBURG. The influences and interactions between processing parameters and component quality must be analyzed to optimize the processing parameters and be able to process new materials successfully. Process parameter optimization is a complex task since these interactions are not yet well understood. Thus, the material qualification or optimization of the mechanical properties of new materials has to be done systematically, varying one parameter at a time [106]. Therefore, this investigation aims to give an example of the qualification process to obtain specimens with good dimensional accuracy made of a medical-grade thermoplastic, commonly used for injection molding and extrusion of medical diagnostic devices. Examples of the applications of the selected polymer include diagnostic test packs, microfluidics, and crystallography trays [218]. The processing parameters obtained after this investigation provide a starting point to produce specimens with a good appearance, which do not necessarily have the best mechanical performance achievable by the APF process.

The selected material was a medical grade poly(methyl methacrylate) (PMMA) because PMMA is an inert, biocompatible, transparent and robust thermoplastic [204]. Due to these properties, PMMA has been used in the medical field as intraocular and hard contact lenses,

as bone cement for orthopedic and cranial implants, as an anchor in hip prostheses, in dental applications, or for vertebroplasties and kyphoplasties [184, 213]. PMMA is one of the most widely used polymeric materials for the reconstruction of cranial defects, and its use in cranioplasty dates back to the 1940s [216]. The intraoperative fabrication of PMMA implants by hand is the most common method of manufacturing [62, 138, 161]. However, fabrication by hand is being replaced by the production of molds for casting PMMA implants via thermoforming [180], milling [104], wax elimination [37], and additive manufacturing methods [43, 63, 130, 178, 219, 254, 267]. Currently, the direct printing of implants is being investigated [203], and this investigation represents a preliminary study to find suitable grades of PMMA for implant applications.

Materials and Methods

Pellets of an amorphous thermoplastic compound based on PMMA used in the medical diagnostic industry (CYROLITE® MD H12, Roehm GmbH, Darmstadt, Germany) were selected for this investigation. It has to be noted that this grade of PMMA has not yet been approved for permanent (i.e., more than 30 days inside the body) implants, but rather for other medical devices. All CYROLITE® materials have been approved for food contact, and they are USP Class VI and ISO 10993-1 certified [218]. Nevertheless, the use of this grade as a permanent implant has not been discarded. That is why this investigation and many others are being performed as part of the CAMed (Clinical additive manufacturing for medical applications) project [166] to analyze its suitability as an implant material. Some of the relevant physical properties as supplied by the manufacturer are shown in Table 9.

Table 9   Tensile properties as supplied by the producer.

Parameter	Testing Method	Typical Value
Tensile Strength	ASTM D 638	65.5 MPa
Tensile Modulus	ASTM D 638	3.2 GPa
Tensile Elongation at Break	ASTM D 638	4–6%
Vicat Softening Point 1.8 MPa	ASTM D1525	105 °C
Melt Flow Rate 230 °C & 3.8 kg	ASTM D1238	7.0 g/10 min
Specific Gravity	ASTM D 792	1.19

An Arburg freeformer 200-3X (ARBURG GmbH + Co KG, Lossburg, Germany) additive manufacturing machine was used to fabricate specimens. The print job was prepared in the Arburg freeformer software v2.30 (ARBURG GmbH + Co KG, Lossburg, Germany). The diameter of the nozzle used was 0.2 mm.

The APF process has many process parameters that need to be adjusted for a successful fabrication process. These processing parameters are specific for a given polymer type and even for a given grade of material since they depend on the surface tension, viscosity, melt strength, and thermal properties of each material. For this investigation, the initial printing conditions for another non-medical type of PMMA previously tested by ARBURG were used. These processing conditions are shown in the second column of Table 10.

Table 10   Printing conditions for PMMA and the support material

Parameter	PMMA Initial Values	PMMA Final Values	Support Material Values
Temperature zone 1 (T_1) in °C	195	200	140
Temperature zone 2 (T_2) in °C	225	230	180
Nozzle temperature (T_{nozzle}) in °C	240	245	200
Chamber temperature ($T_{chamber}$) in °C	100	100	100
Dosing stroke in mm	8	8	6
Backpressure in bar	30	40	50
Screw speed in m/s	4	4	8
Discharge rate in %	70	67	100
Droplet overlap in %	50	25	40
Drop aspect ratio (DAR) in -	1.26	1.29	1.65
Layer height in mm	0.2	0.2	0.2
Scale factor X-direction in -	1.000	1.015	1.000
Scale factor Y-direction in -	1.000	1.015	1.000
Scale factor Z-direction in -	1.000	1.000	1.000

A brief description of the APF processing parameters is given here. The position of the different heated zones (T_1, T_2, T_{nozzle} and $T_{chamber}$) is shown schematically in Figure 11. Dosing stroke, similar to injection molding, is the distance that the screw travels backward and controls the volume of the shot. The back pressure is the applied pressure to keep the screw secure during the deposition process. The screw speed defines the turning speed of the screw and is equal to the speed occurring on the bottom of the flow channel. The discharge rate is the volume of material being deposited. The drop overlap is how much the drops overlap each other during deposition. The drop aspect ratio (DAR) is the ratio between the width (B) and the height (H) of the droplet being extruded from the nozzle of the APF (insert in Figure 11 and Figure 12). The DAR is influenced by its material properties and the processing conditions.

The layer height is the distance the build platform moves down during the deposition to determine the layer thickness.
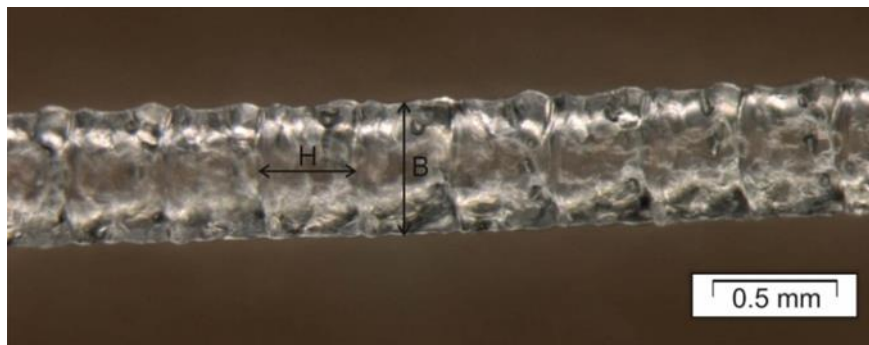

Figure 12   Micrograph of a string of droplets obtained using the initial printing conditions in Table 2. H values are from 0.22 to 0.25 mm and B values from 0.28 to 0.32 mm, giving a drop aspect ratio (DAR = B/H) of approximately 1.26.

Using the initial processing values shown in Table 10 and with the help of an optical microscope (Figure 12), the initial drop aspect ratio (*DAR*) was estimated to be 1.26.

Since it was observed that the initial values shown in Table 10 did not yield accurate specimens for the medical grade PMMA, the *DAR*, the discharge rate, melting temperature, build chamber temperature, and droplet overlap were adjusted systematically. After each adjustment was made, the height along the x- and y-direction of each printed specimen was measured at 25 spots using an analog dial gauge with a measuring range between 0.01 and 10 mm (No. 2048-10, Mitutoyo Corporation, Kanagawa, Japan).

Cube specimens with dimensions 20 mm × 20 mm × 20 mm were printed with conditions between the initial and final values in Table 10 to check the geometrical accuracy. Additionally, dog bone specimens, according to ISO 527-2 1A, were printed with the "PMMA final values" in Table 10 to characterize the tensile properties of the specimens with excellent dimensional accuracy. All specimens were built up with a single contour line and a 100 % and ±45° rectilinear infill strategy. Two building orientations were investigated and labeled according to the plane of the silhouette, thus, XY was used for the laying samples and XZ for the standing samples on the long edge (Figure 13a). Furthermore, single and multiple parts were fabricated at the same time to study the influence of the batch size. In total, 60 dog bone specimens were printed and distributed in different batches, as shown in Table 11. The water-soluble support material ARMAT11 (ARBURG GmbH + Co KG, Lossburg, Germany) was used beneath the parallel zone of the tensile specimen and on the grip zone to prevent tilting and platform detachment of the specimens during printing (yellowish material in Figure 13b) to print specimens in the XZ orientation successfully. The values of the processing parameters for the support material are shown in Table 10.
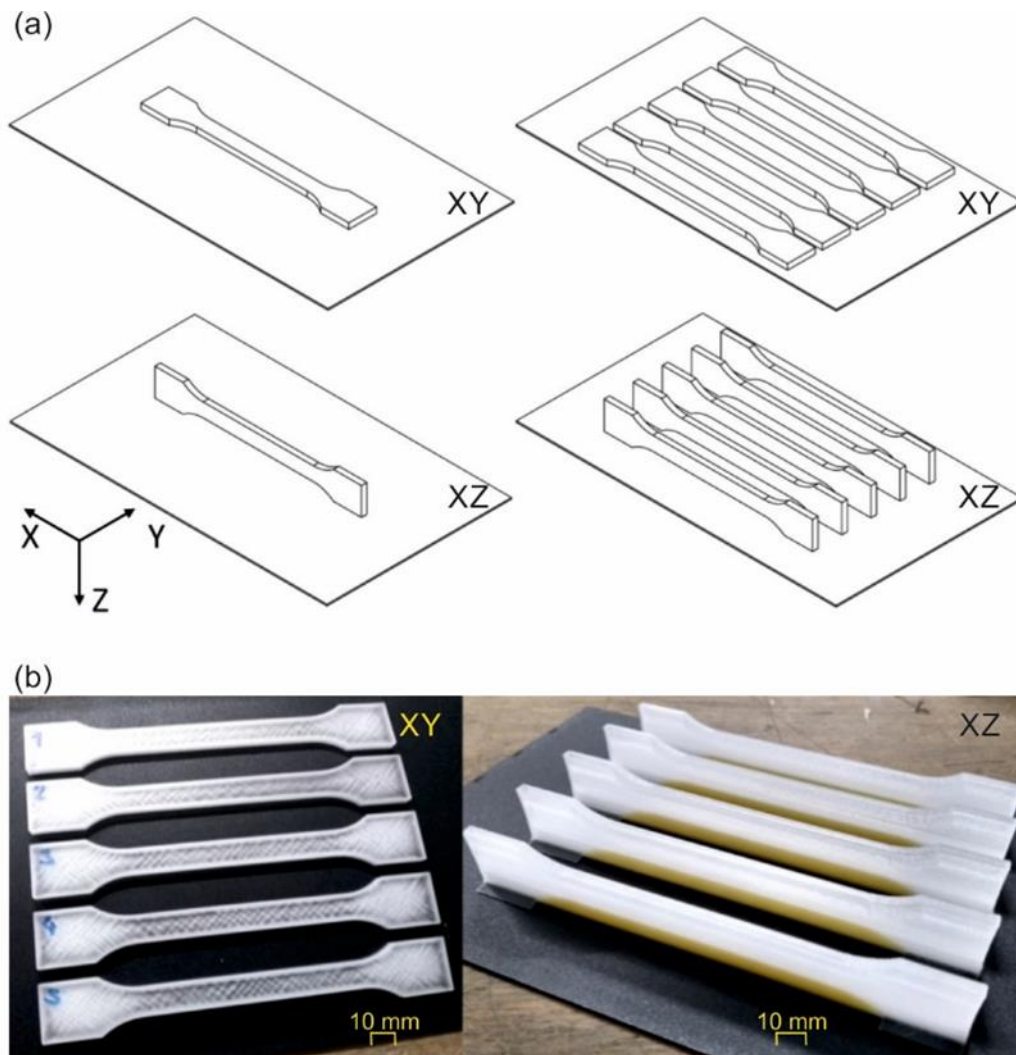
Figure 13   (a) Schematic representation of different orientations (XY or XZ) and arrangements (single or multiple) of tensile bars during printing, and (b) examples of printed parts without support material and with support material (yellowish material).

Table 11   The number of batches and specimens prepared in different orientations.

Build Orientation	*Processing Conditions	Total Single Batches	Total Single Specimens	Total Multiple Batches	Total Multiple Specimens
XY	PMMA final	15	15	3	15
XZ	PMMA final	15	15	3	15

*Processing conditions as defined in Table 10

Tensile testing was performed on the universal testing machine Zwick Z250 (ZwickRoell GmbH + Co KG, Ulm, Germany) at a testing speed of 1 mm min^{-1} until an elongation of 0.25% was reached for measuring of the tensile modulus and 50 mm min^{-1} afterwards until rupture occurred. The use of two testing speeds is in accordance with ISO 527-1, and it is used to speed up the testing procedure. The maximum loading with this machine is limited to 10 kN. Mechanical grips were used for clamping, and the deformations were evaluated by digital image correlation using a Mercury RT System (Sobriety s.r.o., Kuřim, Czech Republic).

Results

Optimized Processing Parameters

The printing results using the "PMMA initial values" according to Table 10 that had a discharge rate of 70 %, yielded a cube that seems to be overfilled and shows warped corners (upper row in Figure 14). Besides, the print job stopped with warning errors such as "discharge value out of range" or "axis reading errors". Since this was unacceptable, the discharge rate was reduced from 70 to 65 %. This discharge reduction led to a more stable process with no errors or warped corners (lower row in Figure 14).
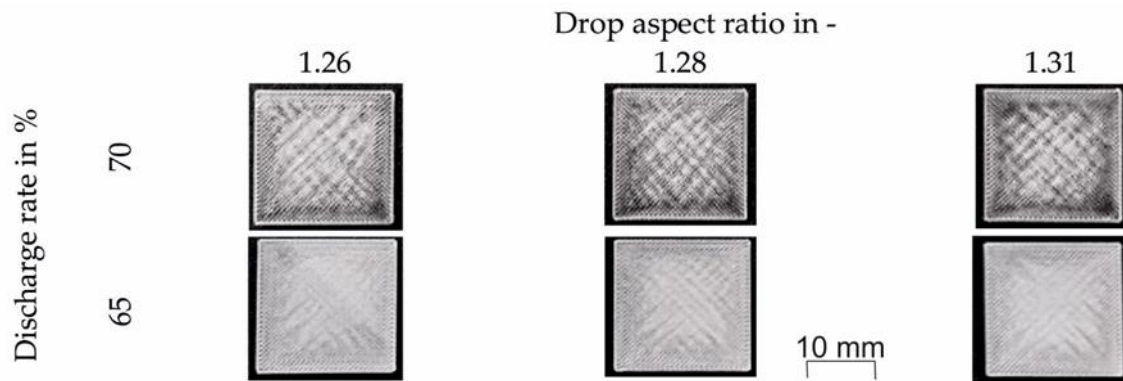

Figure 14   Cubic specimens printed at a chamber temperature of 100 °C with three different drop aspect ratios (1.26, 1.28, and 1.31) and discharge rates of 70 and 65 %. Other processing temperatures were T_1 = 195 °C, T_2 = 225 °C, and T_{nozzle} = 240 °C.

After further inspection of the cubes, it was observed that the drops did not weld together sufficiently. This insufficient welding had to be improved by increasing the energy input. Thus, the temperature of the building chamber was increased to 120 °C. Increasing the build chamber temperature led to a better appearance, but the welding was still not good enough. Therefore, the temperature of zone 1 was increased from 195 to 200 °C and the temperature of zone 2 from 225 to 230 °C. Also, the nozzle temperature was increased from 240 to 245 °C to decrease the process pressure. The cubes produced with the increased temperatures still showed warping and tapered edges regardless of the *DAR* used. Thus, the new strategy was to decrease the building chamber temperature from 120 to 100 °C, and the drop overlap from 50 to 25 %. The resulting print jobs for all chamber temperatures and *DAR*s are given in Figure 15.
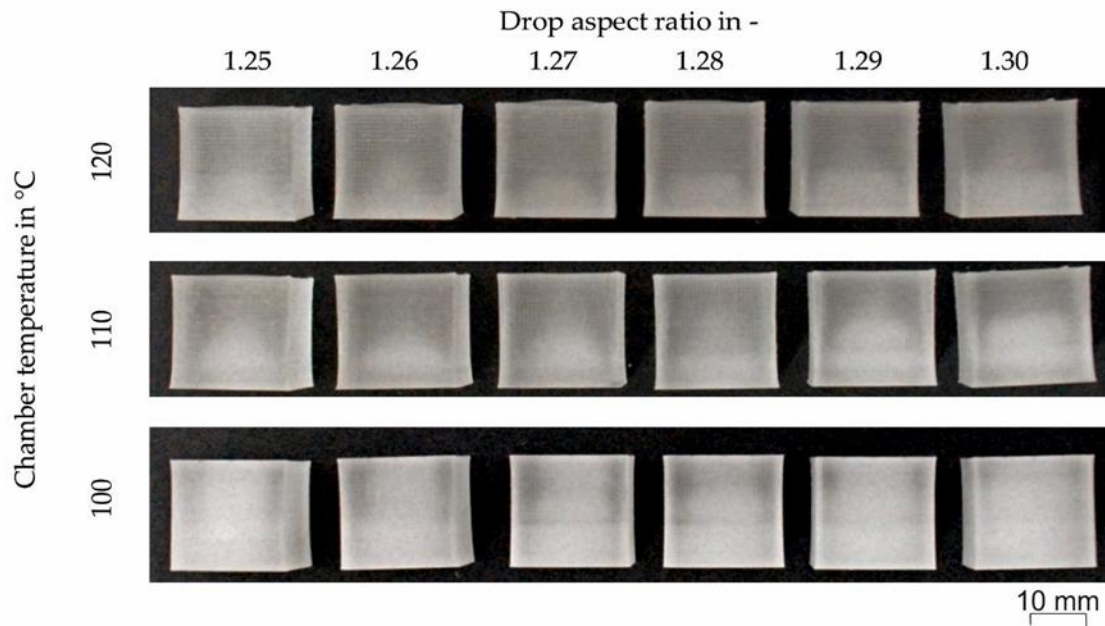
Figure 15 . Printed cubes with six different values for the drop aspect ratio between 1.25 and 1.30, and three different chamber temperatures ($T_{chamber}$) and decreased drop overlap of 25 %. Other processing temperatures were T_1 = 200 °C, T_2 = 230 °C, and T_{nozzle} = 245 °C.

The height at 25 locations along the top surface was measured to get a more accurate picture of the geometrical accuracy of the printed cubes. Figure 16 shows the cubes printed with different *DAR* (1.25 to 1.30) and $T_{chamber}$ of 120, 110 and 100 °C. Please note that the surface roughness on the specimens was not considered in the height measurements since the roughness is smaller than the resolution of the measuring device used. As can be seen in Figure 16, reducing the chamber temperature led to a more uniform height. Variations in the *DAR* were also necessary to improve the flatness of the top surface. However, the *DAR* that improves the flatness was also dependent on the chamber temperature. For example, the most uneven surface for cubes printed at a chamber temperature of 120 °C was reached with a *DAR* of 1.27. On the other hand, at a chamber temperature of 110 °C, the most uneven surface was measured when the *DAR* was 1.25. Finally, when the chamber temperature was 100 °C, the most uneven surface was obtained with a *DAR* of 1.26. Therefore, there is no clear trend regarding *DAR* and surface evenness. Nonetheless, it was observed that a cooler chamber resulted in improved evenness and thus geometrical accuracy. However, care should be taken not to go too low as there could be low adhesion between the droplets and layers.
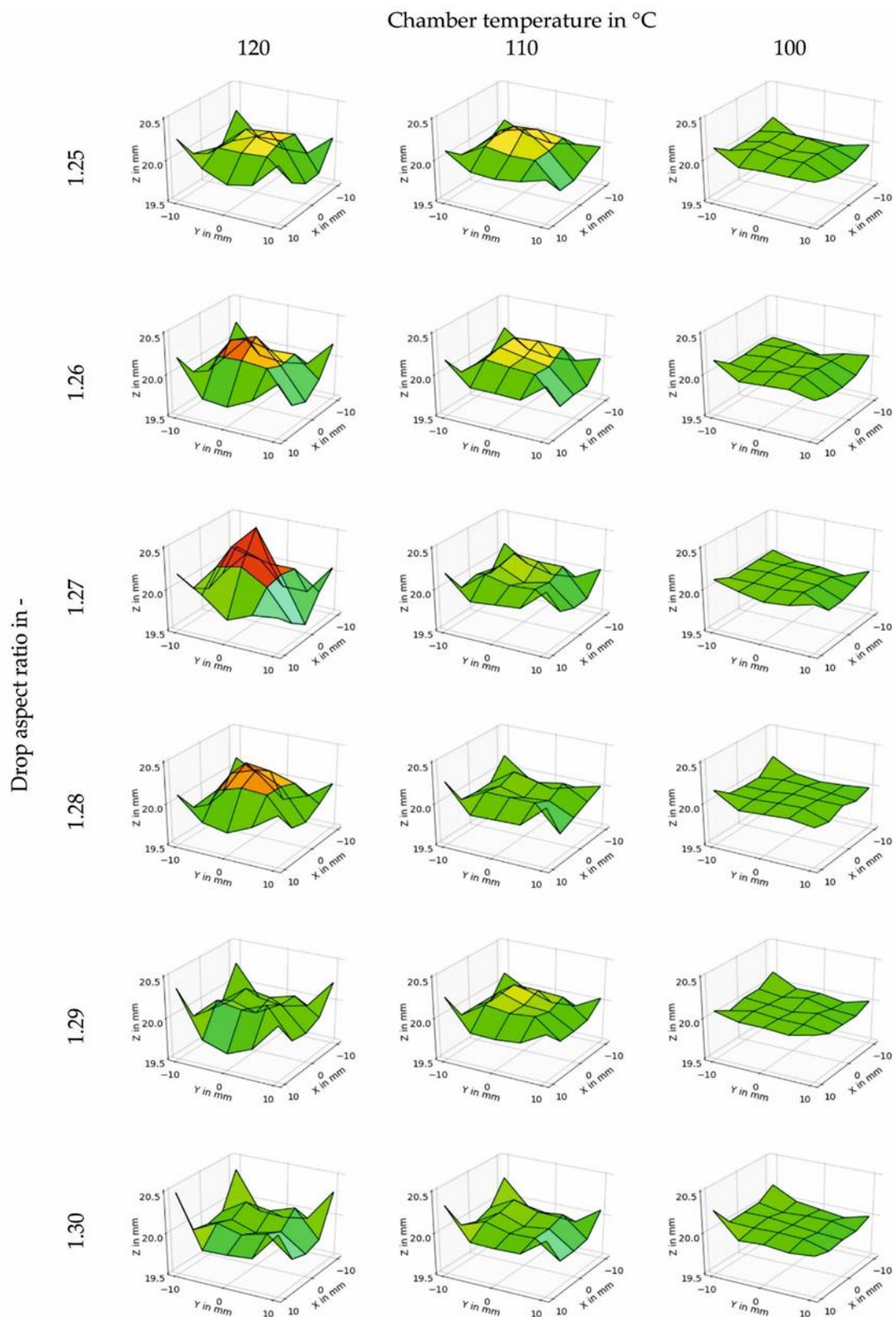
Figure 16 Surface plots of the height measured for cubic specimens printed at different chamber temperatures between 120 and 100 °C and different drop aspect ratios between 1.25 and 1.30. Other processing temperatures were T_1 = 200 °C, T_2 = 230 °C, and T_{nozzle} = 245 °C.

As a final step, the discharge rate was varied from 65 to 68% in increments of 1% to obtain better adhesion between droplets and layers. Figure 17 shows the resulting cubes at three different discharge values (65, 66 and 67 %). It has to be mentioned that a discharge value of 68% was not possible due to an axis error during the build job. Thus, 67 % was set as the discharge value. The specimen processed with DAR = 1.29 had the best appearance with an even color and the best evenness.
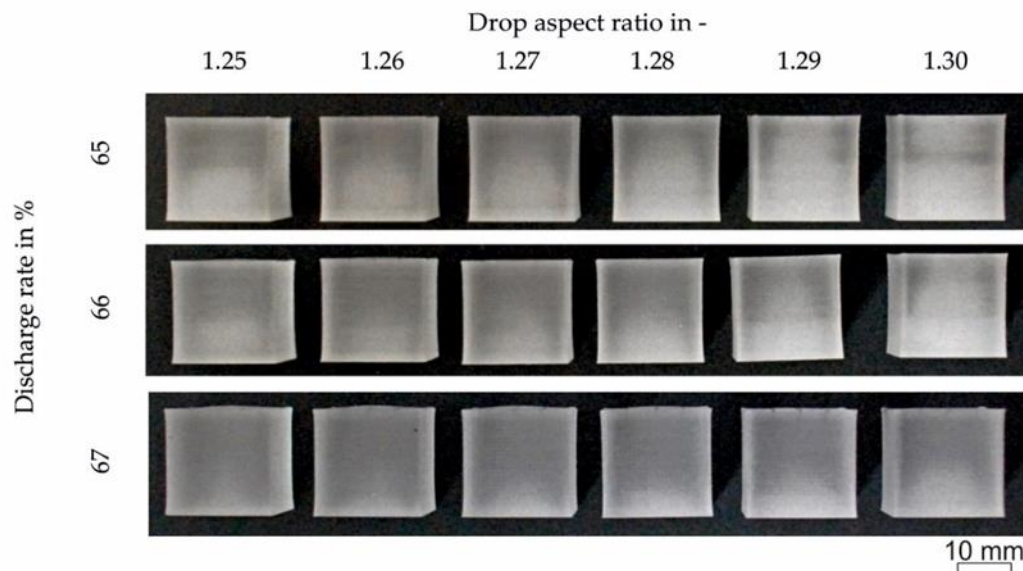

Figure 17   Cubic specimens printed at different discharge rates (65, 66 and 67 %) and drop aspect ratios between 1.25 and 1.30. Other processing temperatures were T_1 = 200 °C, T_2 = 230 °C, T_{nozzle} = 245 °C, and $T_{chamber}$ = 100 °C.

Since thermoplastics shrink after fabrication, this shrinkage has to be compensated by using a scaling factor in the slicing software. For this purpose, five cubes 30 mm × 30 mm × 30 mm were printed individually using the final values shown in Table 10. The dimensions of the specimens were measured in the three axes (Figure 18). It was found that there was anisotropic shrinkage with the cube shrinking more in X- and Y-direction. Therefore, scale factors for each of the directions were calculated: X-direction = 1.015, Y-direction = 1.015, and Z-direction = 1.00 to improve the geometrical accuracy of the printed specimens.
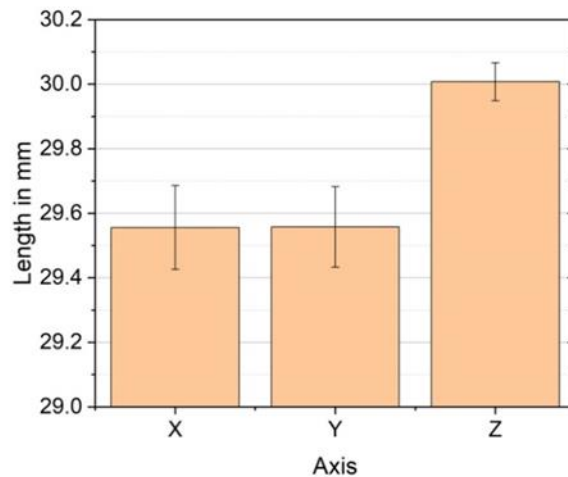
Figure 18　Shrinkage in each printing direction for cubic specimens 30 mm × 30 mm × 30 mm.

Tensile specimens and other geometries such as possible cranial or dental implants were printed using the optimized values of the processing parameters (i.e., "PMMA final values" in Table 10). Examples of such printed specimens are shown in Figure 19. The quality of the printed geometries was considered acceptable based on their appearance, but further characterization on the parts to determine their mechanical performance, internal microstructure, biocompatibility, and long-term stability is ongoing and will be reported in future publications.

Figure 19　Benchmark "implants" printed with the optimized printing parameters ("PMMA final values" in Table 10).

Tensile Properties

All tensile specimens were printed with the final processing values in Table 10, which were determined to obtain good geometrical accuracy. Printed dog bone specimens with different building orientations (XY or XZ) and produced in batches of one (Single) or five (Multi) specimens were tested. Examples of the stress-strain curves and the calculated tensile modulus, tensile strength, and tensile elongation at break for specimens printed with different parameters are shown in Figure 20. Please note that the exact conditions (e.g., strain rate) at which the producer tested their specimens are not known, and since the tensile properties of PMMA are rate dependent, this might have an effect on the actual values of the specification.

Therefore, the values provided are illustrative only to indicate that there is room for improvement that can be archived by modifying the printing parameters.
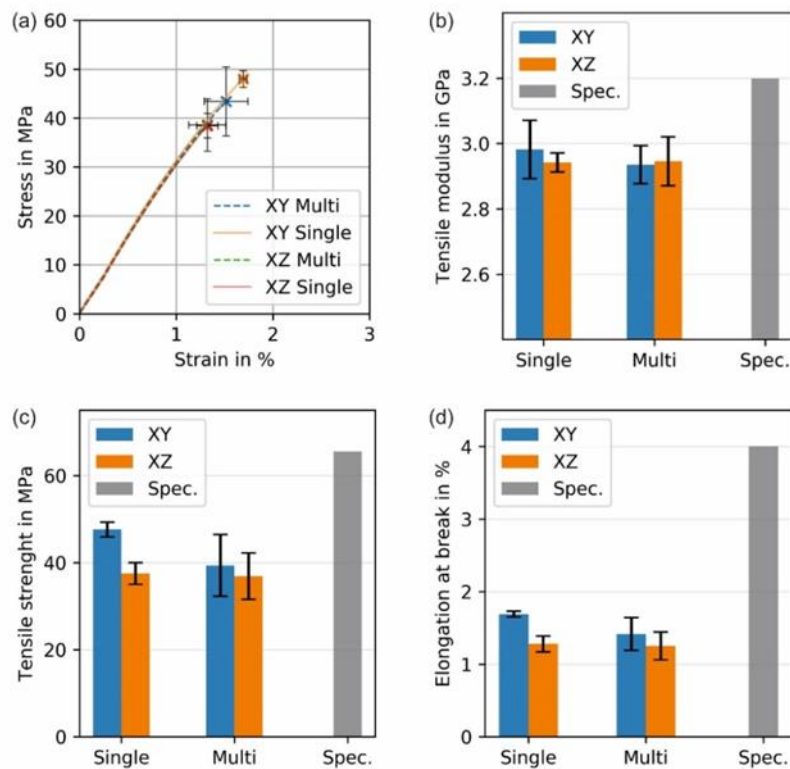

Figure 20   Tensile mechanical properties of printed specimens in two orientations (XY and XZ) and the batch of one specimen (Single) or five specimens (Multi):. (a) stress-strain curves, (b) tensile modulus, (c) tensile strength, and (d) elongation at break. Specifications (Spec.) for the neat (most likely injection molded PMMA) given by the producer are given for comparison. Individual stress-strain curves can be seen in the supplementary information (Figure S1).

In Figure 20, it can be seen that the orientation of the parts affects the measured tensile properties. For example, the tensile values for the specimens printed in the XY-plane appear to be slightly higher than those printed in the XZ-plane. However, the only significantly different values are the tensile strength (Figure 20c) and the tensile elongation at break (Figure 20d) for the specimens printed individually. These results suggest that the specimens printed in the XY-orientation are exposed to a more intense localized heating that promotes a better droplet welding, which leads to higher strength and strain at break. A denser structure can be observed mainly in the surface of the parallel zone of the tensile specimens, where the specimens have sections with higher transparency when printed in the XY-orientation due to better welding (Figure 21a,b), and more opaque sections when printed in the XZ-orientation, since the individual layers are visible and diffract the light (Figure 21c,d). Specimens printed in the XZ-orientation have a larger surface area to volume ratio exposed to the surrounding air in the build chamber, resembling the fins of a convection heat exchanger. Therefore, even though

the path within one layer is smaller, the welding to the next layer is weaker since the temperature of the previous layer might be colder, which leads to weaker tensile properties.
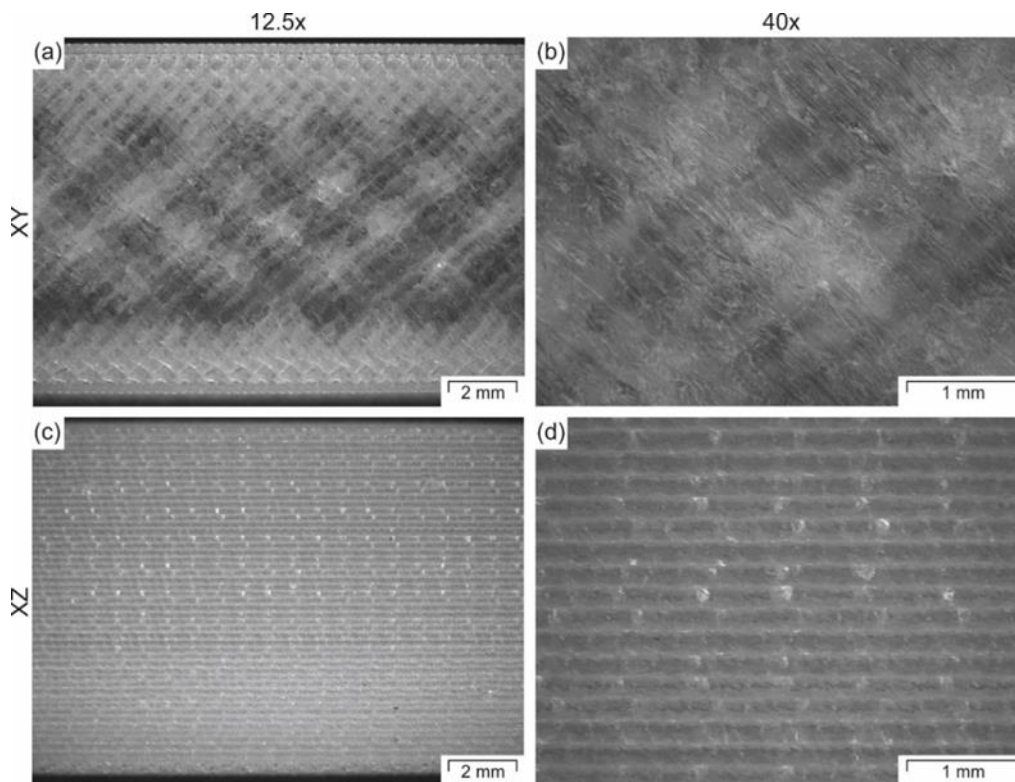

Figure 21   Microscopy images of tensile specimens printed in (a,b) XY-orientation or (c,d) XZ-orientation recorded at two different magnifications (12.5 and 40). All images were taken from the top view and laying the specimens in the XY-plane.

The effect of the build orientation has already been investigated for ABS in the APF process [106]. It was observed that samples printed in the XY-orientation showed considerably higher values for the tensile strength, elongation at break, and the tensile modulus compared to parts built in the YZ-orientation (i.e. upright orientation). Similar results were observed in studies dealing with FFF of polylactide (PLA) [32] and amorphous polyetherimide (PEI) [283]. For this reason, the YZ-orientation was not considered in this study. Additionally, the FFF studies [32, 283] compared the mechanical properties of printed parts in the XY-plane and the XZ-plane, and it was observed that the XZ-orientation showed the highest mechanical properties. It is essential to mention that for PLA specimens, the strands were deposited in the loading direction (at 0°), while for PEI specimens, the strands were deposited at 0° or ±45°. Regardless of the deposition angle, the specimens printed in the XZ-plane were stronger than the specimens printed in the XY-plane [283]. However, based on the work done using ABS in the APF [106], it appears that the angle of deposition that yields the highest tensile properties is 90°, which is the complete opposite to the one that yields the maximum tensile properties in FFF (i.e. 0°). Therefore, it can be expected that the results obtained with parts produced by APF do not necessarily follow the same trends as the parts made by FFF since the deposited

shapes are not the same (i.e. strings of droplets for the APF and cylindrical rods for FFF) and the infill orientations are not equal. Another difference between the FFF printers used in the two studies and the APF is that the build chambers are of different dimensions and for the printers used to produce PLA specimens, the temperature was not actively controlled. These discrepancies make a direct comparison between the different studies difficult.

In general, the "Single" printed parts show slightly higher properties compared to the parts produced in "Multi"-part batches (Figure 20). However, the results are not significantly different. The only statistically different results are the tensile strength and elongation at break between the single printed specimens in the XY-plane and XZ plane (Figure 20c,d). The different thermal history can explain the variability in results. During single part print jobs, the thermal history for each specimen is more similar to each other. Therefore, each specimen produced in separate batches is more similar to each other, and thus the standard deviation for the tensile properties is smaller. In contrast, the thermal history of each specimen within a multi-part batch is slightly different at each position on the build platform. These different thermal histories lead to higher variability in mechanical data. Furthermore, the individually printed parts have better welding between the different layers since it takes less time to build a new layer on top of the previous one. That way, the previous layer is colder, and the contact temperature is lower [150] when printing multiple parts batches than when printing one specimen at a time. This difference in welding can be observed in the specimens shown in Figure 22. The specimens printed individually are more transparent (Figure 22a,b) than the ones printed in batches of five specimens (Figure 22c,d). This difference in transparency suggests better welding between droplets and layers for single printed specimens.
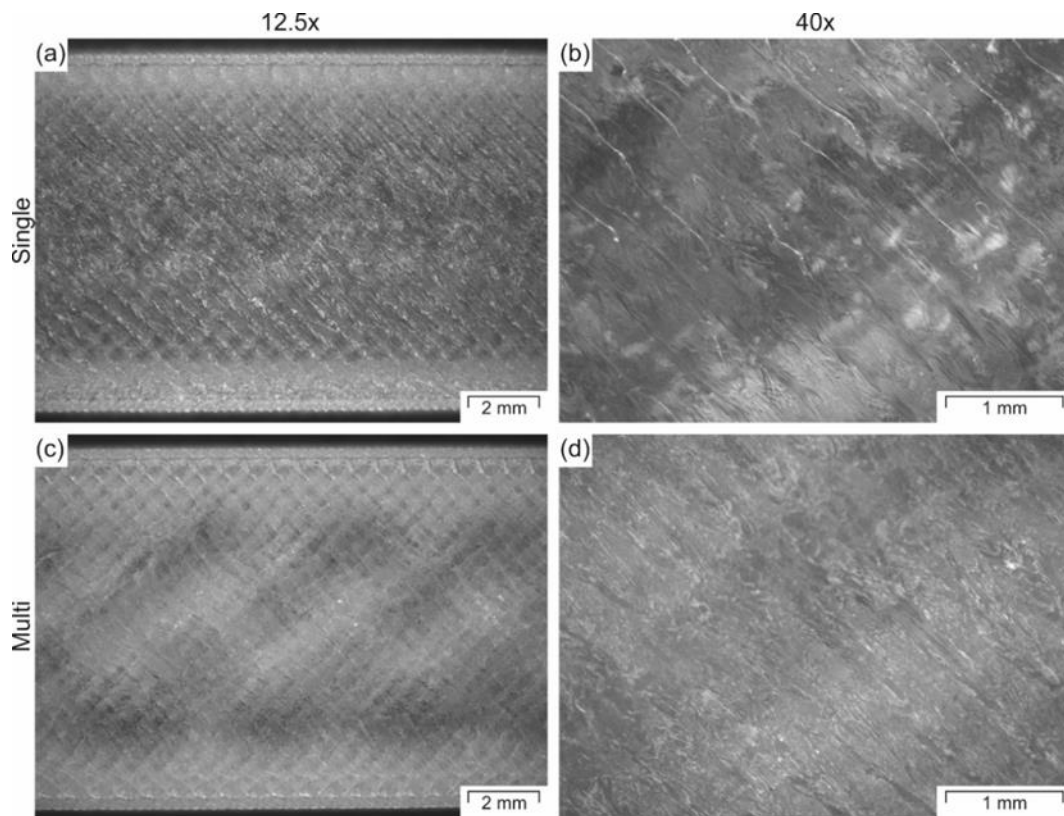
Figure 22 Microscopy images of tensile specimens printed in (a,b) batch of one specimen (Single) or (c,d) five specimens (Multi) recorded at two different magnifications (12.5 and 40). All images were taken from the top view and laying the specimens in the XY-plane.

When comparing the measured tensile properties to the specifications supplied with the raw material, it was found that parts printed individually with an XY-orientation showed the highest tensile properties with a tensile modulus of 93 % and tensile strength of 72 % in comparison to the supplier's specifications (Table 9). As with many other additively manufactured specimens, the elongation at break is low for the APF specimens, having a strain at break of only 42 % of that given in the specification for the raw PMMA material. Thus, it is clear that similar to FFF [146], the processing conditions that lead to the best appearance do not necessarily lead to the optimal tensile properties. There is always a trade-off between geometrical accuracy and mechanical properties in AM technologies since the shape cannot be constrained as it happens inside a molding tool. Therefore, further research is needed to optimize the tensile performance of medical-grade PMMA in APF.

Conclusions

This investigation illustrates a possible way to qualify medical grade materials for the Arburg Plastic Freeforming (APF) process and obtain geometrically accurate specimens. The research also shows the versatility of the APF process to use thermoplastic materials that have not been specifically tailored for an additive manufacturing process in their standard granular form. The material selected to illustrate the qualification process was a medical-grade

poly(methyl methacrylate) (PMMA) material used in the injection molding or extrusion of medical diagnostic devices. The qualification processes started by estimating an initial drop aspect ratio (*DAR*) by extruding a string of droplets at processing conditions for another non-medical grade PMMA. Printing with the initial conditions led to overfilled specimens with warped corners, thus the discharge rate was decreased, the processing temperatures were increased, and the *DAR* was varied at different temperatures. The chamber temperature was varied, and the *DAR* was readjusted until the printed specimens had a smooth surface. Finally, the anisotropic shrinkage was compensated in each printing axis to improve the geometrical accuracy. Once the processing conditions were defined, exemplary geometries for orthopedic implants and tensile specimens were printed in different orientations and batches with a different number of specimens. The highest tensile properties were obtained for parts printed in batches consisting of one specimen in the XY-printing orientation (i.e., laying on the platform). Since the processing conditions were selected to give specimens with good geometrical accuracy, the tensile properties were not maximized. Therefore, a future investigation of the processing parameters is planned to maximize the tensile properties.

Acknowledgments

3.2.3 Closing Remarks on Publication A

Publication A showed a procedure for a proper material qualification for a medical grade PMMA. Optical properties studied visually, and mechanical properties were used to validate the processing parameters. However, an additional work published in a biannual magazine was performed and showed a significant correlation between part density and tensile properties [96]. The correlation was replicated in the upcoming section and also found in the literature [34, 99, 206]. Hence, the part density can, similar to the tensile properties, be used as reference value. However, the density is easier measurable than tensile properties. In conclusion, the first hypothesis "*A proper qualifications procedure can be used, to define suitable processing parameters for the Arburg plastic freeforming technology*" can be accepted.

3.3. Parameter optimization of ARBURG plastic freeforming for mechanical properties

3.3.1 Introduction to Publications B and C

Publication B extends the findings from Publication A and deals with a systematic design of experiments of experiments (DoE) to optimize tensile properties. The first 2^{5-1} DoE was set up to find the parameters of the highest effect and further extended by a full 2^3 DoE for detailed investigation. Therefore, the same material as in Publication A was used. In contrast, Publication C, deals with a semi-crystalline polypropylene and the effect of the chamber temperature on the morphology. Furthermore, the correlation between the build orientation and the build envelope temperature was discussed. The term "build envelope temperatures" was used to describe the chamber temperature and the build plate temperature for the APF and MEX technology used, respectively. Thus, Publication B can be used as a reference for parameters optimization for amorphous polymers and Publication C as a reference for semi-crystalline polymers. Even though Publication C compares APF and filament-based MEX technologies, APF is be highlighted in context of this thesis.

Publication B was original published as: _Hentschel, L.; Petersmann, S.; Gonzalez-Gutierrez, J.; Kynast, F.; Schäfer, U.; Arbeiter, F.; Holzer, C. (2022) Parameter Optimization of the ARBURG Plastic Freeforming Process by Means of a Design of Experiments Approach, Advanced Engineering Materials, 2200279_
and Publication C as: _Hentschel, L.; Petersmann, S.; Kynast, F.; Schäfer, U.; Holzer, C.; Gonzalez-Gutierrez, J. (2023) Influence of the Print Envelope Temperature on the Morphology and Tensile Properties of Thermoplastic Polyolefins Fabricated by Material Extrusion and Material Jetting Additive Manufacturing. Polymers 15 (18), 3785_

In addition to these publications, further contributions of the authors were made in order to support the work. These are not included into the thesis but are listed for further information:

- Conference contribution: _Hentschel, L.; Petersmann, S.; Steinert, T.; Gonzalez-Gutierrez, J.; Kynast, F.; Holzer, C. Impact factors on mechanical properties of poly(methyl methacrylate) manufactured by ARBURG plastic freeforming and filament-based material extrusion additive manufacturing. Presentation at EUROMAT 2021, Graz (online), Austria, September 16, 2021_
- Conference contribution: _Hentschel, L.; Maurer, C.; Gonzalez-Gutierrez, J.; Kynast, F.; Schäfer, U.; Holzer, C. The effect of coalescence and diffusion on the part generation in the ARBURG plastic freeforming. Poster presentation at 31. Leobner Kunststoffkolloquium, Leoben, 2023_

3.3.2 Publication B

Parameter Optimization of the ARBURG plastic freeforming process by means of a Design of Experiments Approach

L. Hentschel, S. Petersmann, J. Gonzalez-Gutierrez, F. Kynast, U. Schäfer, F. Arbeiter, C. Holzer

Abstract

Additive manufacturing finds more applications every day, especially in medical devices, ranging from models, tools, protheses to implants. The fabricated parts have to withstand the mechanical loading applied during their lifetime. Hence, optimization of process parameters must be performed to reach the best performance of the manufactured part with the given polymer. A fractional design of experiments is performed with the ARBURG plastic freeforming using a medical-grade poly (methyl methacrylate) to improve the overall mechanical performance. Tensile specimens are produced, tested, and the impact of different parameter settings is analyzed to identify the factors with the highest impact on the mechanical performance. Based on the results, further parameter optimization is performed. A direct correlation between the density and the tensile properties of the printed parts is observed. Further, an influence of the processing pressure resulting from changes in the processing temperature was detected. Optimization for good mechanical performance is performed, and a relation between the filling of the parts, the nozzle temperature, and the discharge pressure on to the tensile properties is found. This investigation reveals that shrinkage due to changes in temperature and pressure has an essential role in determining the tensile properties of specimens produced by ARBURG plastic freeforming.

Introduction

Additive manufacturing (AM), also known as 3D-printing, has become an important manufacturing method, especially in the medical field. AM enables patient specific instruments, prosthetics, prototypes, pre-operative models, implants, surgical cutting and drill guides, and even organ replacements, which are costlier if manufactured in other ways.[110, 119, 125, 126, 182] Nevertheless, this technology still must overcome some limitations to ensure a safe and reproduceable performance, for invasive medical applications. In particular, for long term applications such as permanent implants, the material and the printed part have to fulfil strict requirements in terms of biocompatibility and mechanical performance.[190] Additively manufactured specimens most likely show anisotropic and weaker mechanical properties compared to specimens produced via injection molding or subtractive manufacturing, mainly due to the lower in inter- and intra-layer bonding as well as the presence of numerous weld lines. This is specifically true for parts manufactured by material extrusion (MEX) additive manufacturing methods.[179, 242, 248] However, several investigations on setting different parameters in MEX and their influence on the mechanical properties of printed specimens have already been performed with the aim of maximizing the mechanical performance of MEX parts.[34, 94, 106, 145, 158, 241, 242] On the contrary, not much work has yet been done with the novel AM technology known as the ARBURG plastic freeforming (APF),[34, 94, 97, 106] and the effects of some crucial APF setting parameters have not been investigated at all. Therefore, this study will mainly focus on understanding APF process parameters to maximize the tensile mechanical properties of produced specimens.

Previous studies show a high potential of the APF method in terms of mechanical properties.[34, 97, 206, 211] Depending on the material and the process settings, mechanical properties comparable to injection molded parts can be reached. This might be related to a lower porosity resulting in APF compared to parts produced by MEX technologies.[206] To figure out the specific influences of process parameters, a design of experiments (DoE) can be applied. Selected parameters are set in two different states, a high and a low value and variated to get every possible combination. By introducing a middle point, non-linear behaviors can also be detected. The number of samples develops to the power of the number of parameters in a full DoE. In order to reduce the effort a fractional DoE can be performed to identify the most significant impact factors, since not every combination is considered. The only drawback of this type of DoE is that interactions of higher orders are not covered; however, these interactions are rather rare.[12]

Some studies already have been performed to characterize the individual influences of the processing parameters on mechanical or geometrical parameters of the APF method.[34, 94, 106, 206] A linear increase of the tensile properties with rising nozzle temperature was found, but no correlation between stiffness or strength and the building

chamber temperature. The overlap parameter, on the other hand, showed a highly non-linear correlation with the maximum in the tensile stress at around 80 % for the used acrylonitrile-butadiene-styrene copolymer.[34] However, parameters such as the rotational screw speed and the drop aspect ratio were not studied until now. Thus, they were included in this study. Further the influence of the processing pressure on tensile properties was analyzed for a better understanding of the process.

For this study, a medical grade poly (methyl methacrylate) (PMMA) was selected, due to its inert, biocompatible, and robust character.[204] It is a transparent thermoplastic material and widely used in the medical field for intraocular and hard contact lenses or microfluidic analytic devices [108, 213]. A different form of PMMA, also referred to as bone cement is used for cranial implants and as anchor for hip implants.[184, 213] This type of PMMA is one of the most used materials for intraoperative construction of cranial reconstruction implants.[62, 138, 161, 216] Such implants were formerly shaped by hand but have now been replaced by the production of molds for casting via thermoforming,[180] wax elimination[37] or additive manufacturing[43, 63, 130, 178, 219, 254, 267]. Nowadays, direct additive manufacturing of cranial implants is also being studied,[125, 126, 203] and this investigation based on a previous performed work[97] demonstrates the potential of additively manufactured PMMA parts.

Experimental

Material

An amorphous thermoplastic compound based on PMMA (CYROLITE® MD H12, Roehm GmbH, Darmstadt, Germany) was used as pellets. This polymer is usually used in the medical diagnostics industry and is processed via extrusion or injection molding. Hence, the material fulfills the requirements according to ISO 10993-1 and United States Pharmaceutical (USP) Class VI [39] but is not yet approved for permanent in-vivo applications (i.e. as implant for more than 30 days). Some relevant material properties supplied by the manufacturer are summarized in Table 12. The material was dried at 80 °C in a dehumidified circulating air drier (Drymax Wittmann Kunststoffgeraete GmbH, Vienna, Austria) for at least 24 hours and kept dry with the build-in hot air drier (Helios Geraetebau fuer Kunststofftechnik GmbH, Rosenheim, Germany) at the hopper of the APF machine.

Table 12   Material properties of the used PMMA material as supplied by the producer [218].

Parameter	Testing method	Typical value
Tensile strength	ASTM D 638	65.5 MPa
Tensile modulus	ASTM D 638	3.2 GPa
Tensile elongation at break	ASTM D 638	4-6 %
Melt flow rate at 230°C/3.8 kg	ASTM D 1238	7.0 g 10 min^{-1}
Specific gravity	ASTM D 792	1.19

Material Processing
ARBURG plastic freeforming

The APF process was developed by ARBURG GmbH + Co KG (Lossburg, Germany) and combines the material processing from the conventional injection molding and AM process and is therefore able to process nearly any thermoplastic material available in pellets form into complex shapes in a layer-by-layer approach. The APF is categorized as material jetting additive manufacturing technology according to ISO/ASTM 52900,[5] due to the deposition of droplets. In principle, the polymer is molten by a plasticization unit similar to an injection molding screw also providing the needed process pressure. After plasticization the material enters the discharge unit, consisting of a piezo electrical shut-off nozzle, which opens the nozzle up to 250 times per second.[94, 97] Hence, the material is extruded in form of droplets instead of a continuous string. However, since the frequency is so high, a chain of droplets forms during calibration of the pressure. The specific appearance of the drop is related to the material, and the used machine settings. The form is characterized by the drop aspect ratio (*DAR*), defined as the ratio between the drop width to the drop height (*DAR* = *W*/*H*). This ratio is one of the most important building parameters that are specified in the preparation/slicing software.[97] A schematic overview of the APF process and an illustration of the *DAR* is given in Figure 23.
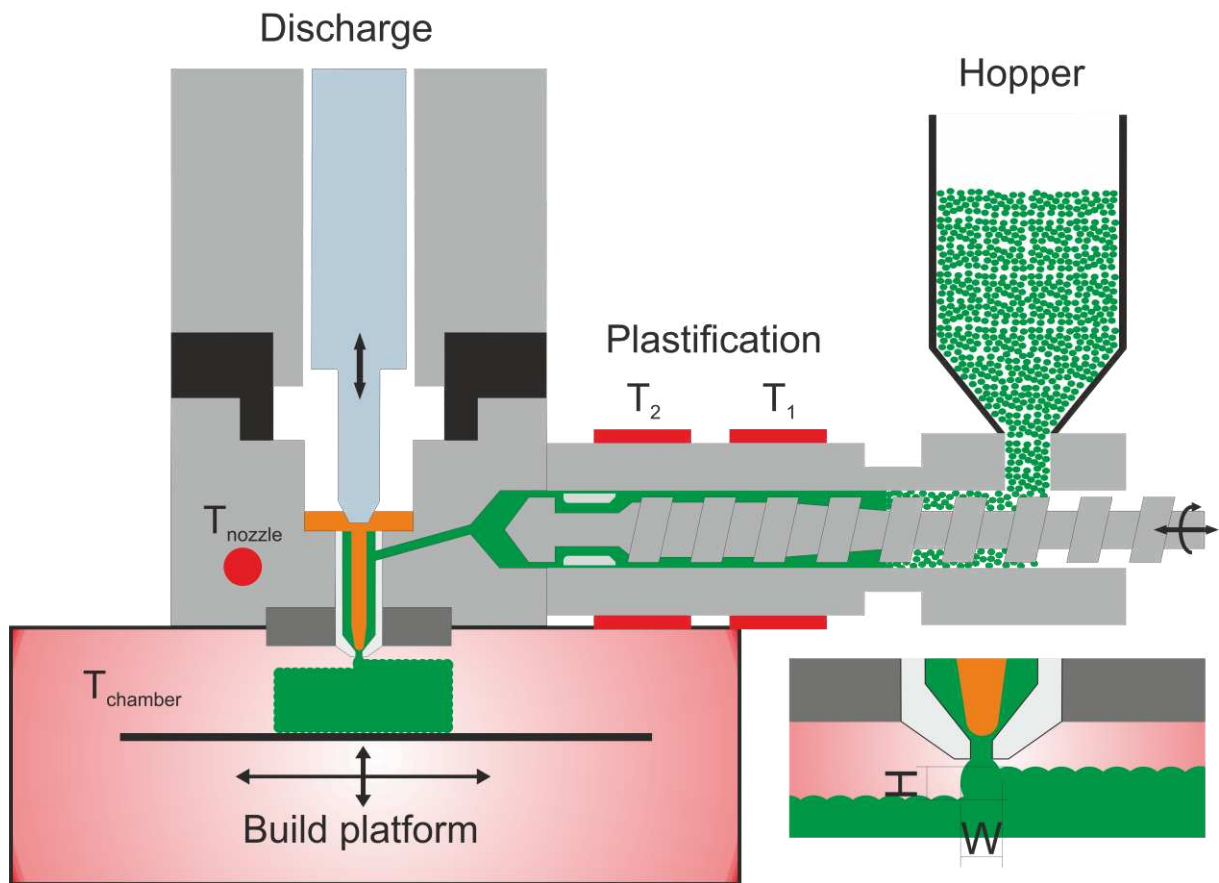
Figure 23   Schematic working principle of the ARBURG plastic freeforming process. Temperatures for plasticization zone 1 and 2 (T_1, T_2), the nozzle (T_{Nozzle}) and the heated chamber ($T_{Chamber}$), as well as the drop height (H) and width (W)are indicated.[97]

Basically, the setting for a successfully manufactured sample can be split into machine parameters and building parameters. Machine parameters include the different temperatures, rotational screw speed, back pressure and are directly set on the machine. Building parameters, on the other hand, are those responsible for rebuilding the CAD-model with the 3D-printing process. The *DAR* is a static value and is needed to calculate the trace width of the individual paths and the distance the machine must travel in between one nozzle opening cycle. Further building parameters are quite similar to other conventional slicing software and include the layer height, overlap, infill ratio, orientation and support settings. For this investigation the influence of the nozzle temperature (T_{Nozzle}), the chamber temperature ($T_{Chamber}$), and the rotational screw speed (v_{screw}) during the dosing as part of the machine parameters are varied. To further include building parameters the drop aspect ratio (*DAR)* and the overlap (*OL*), which defines the overlap of the infill lines with the previously laid contour lines, were chosen.

Design of Experiments

All specimens were additively manufactured in an ARBURG freeformer 200-3X (ARBURG GmbH + Co KG, Lossburg, Germany). The specific print jobs were prepared by the corresponding ARBURG freeformer software v2.30 (ARBURG GmbH + Co KG, Lossburg, Germany). For all specimens, the same nozzle with a diameter of 0.2 mm was used. A material qualification procedure was previously performed to find suitable processing parameters and these obtained values were applied for all parameters not varied in this work (Table S1) [16]. For the optimization procedure and investigation of the effects, some of the already qualified parameters were varied. The selected parameters and their values are given in Table 13. For evaluation of the DoE, the software Minitab® version 19.2020.1 (Minitav, LLC. State College, Pennsylvania, United States) was used.

Table 13   Parameter settings for the design of experiments for the ARBURG plastic freeforming process.

Parameter	+	o	-
Nozzle temperature (T_{Nozzle}) in °C	260	240	220
Chamber temperature ($T_{Chamber}$) in °C	120	100	80
Screw speed (v_{screw}) in m min^{-1}	8	6	4
Drop aspect ratio (DAR)	1.38	1.30	1.22
Overlap (OL) in %	50	25	0

A fractional 2^{5-1} DoE with a middle point was performed, hence 17 different combinations of the mentioned parameters were set. The individual parameters settings generated by the software Minitab® are listed in Table 14, the experiments were executed in a randomized order. Three replicants were performed for each parameter set and 6 replicants for the middle point. All the samples were manufactured one at a time in YXZ orientation according to ISO/ASTM 52921:2019.11.01 [3] on a removable building platform. The specimens were fabricated with one contour line and ±45° infill strategy. The building platform is made of an acrylonitrile-butadiene-styrene copolymer, polycarbonate blend, and is supplied by ARBURG GmbH + Co KG.

Table 14　List of the parameter combinations used in the 2^{5-1} DoE, generated by the software Minitab®. The actual numerical values and description are given in Table 13.

Parameter set	T_{Nozzle}	$T_{Chamber}$	v_{screw}	DAR	OL
1	-	-	+	+	+
2	-	+	+	+	-
3	-	-	-	+	-
4	-	+	-	+	+
5	-	-	-	-	+
6	-	+	-	-	-
7	-	+	+	-	-
8	-	+	+	-	+
9	o	o	o	o	o
10	+	+	+	+	+
11	+	-	-	+	-
12	+	-	+	+	-
13	+	-	-	+	+
14	+	-	+	-	+
15	+	-	-	-	-
16	+	+	+	-	-
17	+	+	-	-	+

Optimization

After identifying the critical factors on the mechanical properties, optimization by variating the nozzle temperature and the drop aspect ratio was performed. It must be mentioned that for each nozzle temperature, the resulting drop dimensions were measured under the microscope (SZH, Olympus Optical Co., Japan) and variated by a value of $\pm\ 0.05$. However, the lower settings resulted in failed print jobs and had to be adjusted to higher DARs. The values are given in Table 15, where the middle value of the DAR corresponds to the measured value. For the optimization analysis, three replicants were produced each. All non-critical parameters ($T_{Chamber}$, v_{screw}, and OL) were set to the middle value mentioned in Table 14.

Table 15   Drop aspect ratios (*DAR*s) used for analyzing the influence of the nozzle temperature (T_{Nozzle}). The middle values are the microscopically measured values, which are then varied by ±5 % (if possible) for the upper and lower values.

T_{Nozzle} in °C	DAR [-]		
	+	o	-
220	1.22	1.25	1.3
240	1.20	1.23	1.28
260	1.18	1.21	1.26

The aim of the DoE was to understand the influence and the importance of different processing parameters on the mechanical properties of printed specimens. Thus, tensile bars according to DIN EN ISO 527-1A with shortened measurement length were chosen. The length of the specimen was shortened to reduce the building time by ensuring a similar cross-section; the resulting geometry can be seen in Figure 24.
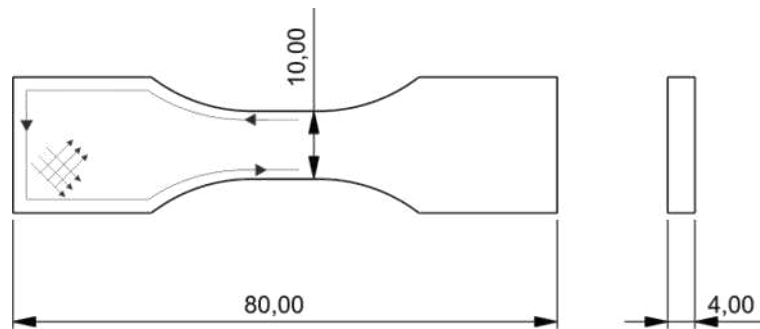

Figure 24   Schematic drawing of the modified specimen used for the design of experiments and the parameter optimization procedure. The dimensions are given in mm and the building strategy is indicated by the arrows.

Material Testing
Density Measurements
    Density measurements were performed on the printed samples to estimate their filling grade. The measurements were performed on a digital scale (KERN & Sohn GmbH, Balingen-Frommern, Germany) by the Archimedes principle and the use of deionized water. Special care was taken that no air bubbles were present, since the printed specimens have a rough surface.

Mechanical Testing
    All tensile tests were performed on the universal testing machine Zwick Z250 (ZwickRoell GmbH + Co KG, Ulm, Germany) at a testing speed of 1 mm min^{-1} up to an elongation of 0.25 %, for evaluation of the Young's modulus and was then increased to 50 mm min^{-1} until the breakage. The used testing speeds are in accordance with DIN EN ISO 527-1. The clamping length was set to 42 mm. Mechanical clamps with riffled grip inserts were used for clamping, and the deformations were evaluated by digital image correlation using a Mercury

RT System (Sobriety s.r.o., Kuřim, Czech Republic). Therefore, a graphite sparkle pattern was applied on the specimens before testing. Young's modulus is determined as the ratio of the incremental change in stress to the incremental change in strain, at strain levels between 0.05 and 0.25 %. Further, the stress and strain values at the moment of the fracture are evaluated and defined as strain or stress at break. All stresses and strains are engineering values considering the initial cross-section of the specimen.

Thermal Analysis

Thermal analyses were performed to identify the application temperature limit of the material. Differential scanning calorimetry (DSC) was performed at 20 K min^{-1} in a temperature range from 30 to 260 °C to measure the glass transition temperature (T_g) by using the middle point of the step-down, under a protective nitrogen atmosphere. Thermogravimetric analysis (TGA) was performed at the same heating rate in a temperature range from 25 to 650 °C and under an oxygen atmosphere to indicate the initial degradation temperature (*IDT*). The *IDT* is defined as the temperature at a weight loss of 1 % or in other words at a relative weight of 99 %. As a second indication of thermal degradation, the temperature at the peak (T_{peak}) of the differential curve of the weight loss is used. Samples weighing between 5 and 10 mg were used for DSC and TGA. Three measurements were carried out on the virgin granules.

pvT – measurements

The specific volume (*v*) as a function of pressure (*p*) and temperature (*T*) provides information on how much a polymeric material shrinks when processed at high pressures and temperatures. This information is very useful when setting the parameters in an injection molding process. The APF shares some of the characteristics of an injection molding machine; therefore, this information brings additional insight into the process. *pvT*-measurements were performed on a *pvT*-measurement device (SWO Polymertechnik GmbH, Krefeld, Germany) from 260 to 50 °C at a cooling rate of 6 K min^{-1}. The analysis was carried out at five different pressure levels, ranging from 200 to 1000 bar. According to Chang et. al [33], the Tait-equation to describe the specific volume of polymers in solid (5) and melt state (6) as a function of pressure and temperature was used.

$$v(p,T) = [b_{1s} + b_{2s} \cdot (T - b_5)] \cdot \left[1 - 0.0894 \cdot ln\left(1 + \frac{p}{b_{3s} \cdot e^{-b_{4s} \cdot (T-b_5)}}\right)\right]$$
$$+ b_7 e^{[b_8 \cdot (T-b_5) - b_9 \cdot p]} \tag{5}$$

$$v(p,T) = [b_{1m} + b_{2m} \cdot (T - b_5)] \cdot \left[1 - 0.0894 \cdot ln\left(1 + \frac{p}{b_{3m} \cdot e^{-b_{4m} \cdot (T-b_5)}}\right)\right] \tag{6}$$

The transition between solid and melt state is defined by the transition temperature (T_{trans}) according to equation (7), where $T < T_{trans}$ means the polymer is in solid state and if $T > T_{trans}$ the polymer is in melt state.

$$T_{trans} = b_5 + b_6 \cdot p \tag{7}$$

For each material the b* values in equation (5)-(7) differ and are used to describe the material behavior. The coefficient b_7 to b_9 became zero for amorphous polymers. A curve fit was performed on the measured data points by adapting all the *b** values in equation (5)-(7). The least squares errors between the measured data and the equation were found by using the differential evolution method [249]. The zero-pressure line was extrapolated using these results.

Fractography

Microscopy images of the fracture surfaces after tensile testing were taken with an Olympus SZH (Olympus Optical Co., Tokio, Japan) light microscope under reflected light at a 16 times magnification.

Results

The thermal analyses resulted in a T_g of 108.6 °C ± 0.5 K, an *IDT* of 284.3 °C ± 0.57 K and a T_{peak} of 305.3 °C ± 3 K with the given material at three replications. One of the measured DSC and TGA curves are exemplary shown in Figure 25.
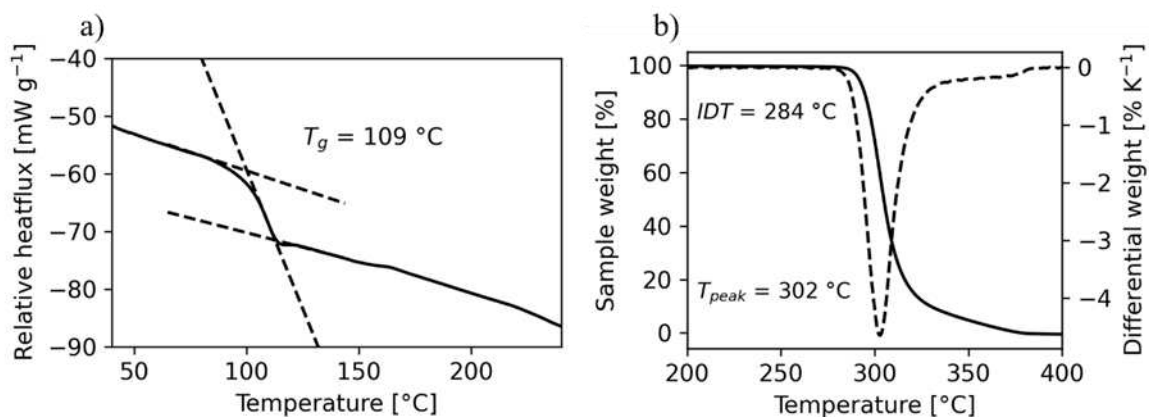

Figure 25   Thermal analysis curves from the DSC (a) and TGA (b) measured for PMMA. The dashed lines represent the approximated straight to evaluate the T_g (a) and the derivative curve from the T_g curve (b).

Furthermore, *pvT*-measurements were performed to characterize the shrinkage behavior of the used material. Curve fitting was performed to describe the material behavior and for extrapolation of the zero-pressure curve. The data set (points) as well as the fitted curves (lines) are displayed in Figure 26.
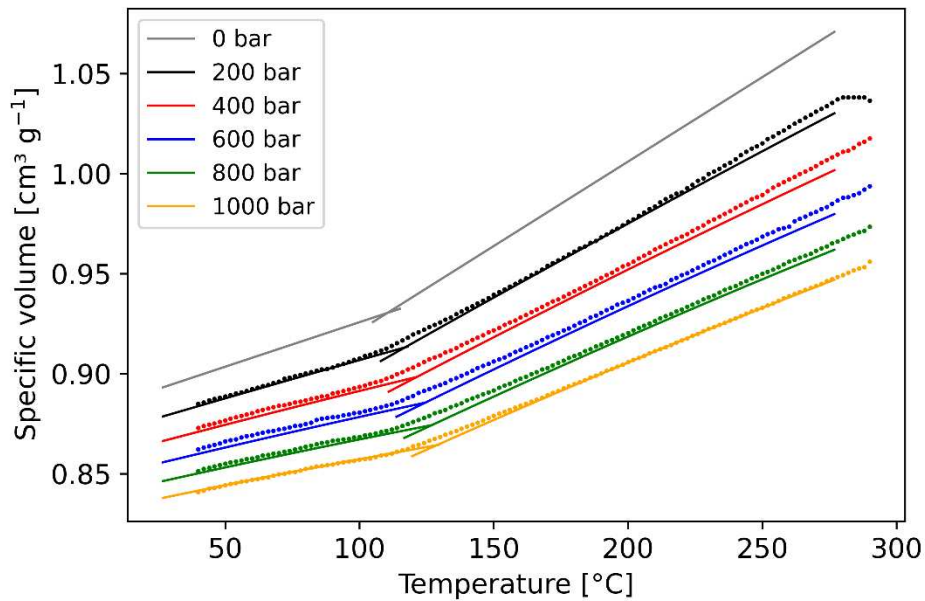
Figure 26   *pvT*-measurements of PMMA at five different pressure levels including the fitted and extrapolated curves.

The resulting coefficients for equation (5)-(7) are given in Table 16, note that the coefficients b_7 to b_9 are zero for amorphous polymers, such as PMMA [33].

Table 16   Coefficients for equation (5)-(7) as a result of the curve fit performed on the measured *pvT* data.

Coefficient	Value	Coefficient	Value	Coefficient	Value
b_{1s}	$0.93 \ 10^{-3}$	b_{1m}	$0.93 \ 10^{-3}$	b_5	383.2
b_{2s}	$0.45 \ 10^{-6}$	b_{2m}	$0.84 \ 10^{-6}$	b_6	$0.14 \ 10^{-6}$
b_{3s}	$75 \ 10^6$	b_{3m}	$65.5 \ 10^6$		
b_{4s}	$3.5 \ 10^{-3}$	b_{4m}	$3.3 \ 10^{-3}$		

The results of the analysis of variance obtained for the DoE can be seen in the support information for each of the tensile properties measured (Table S2 to Table S5). As a result of the DoE, two significant influences out of the five parameters can be identified (Figure 27). The nozzle temperature and the drop aspect ratio show the most significant impact on the stress at break, the strain at break as well as the density and the Young's modulus of the printed specimen. However, the Young's modulus and the density show less significant influences due to the flatter slope and the error bars, resulting from the scattering of the individual specimen. For the other parameters, no significant influences could be observed.
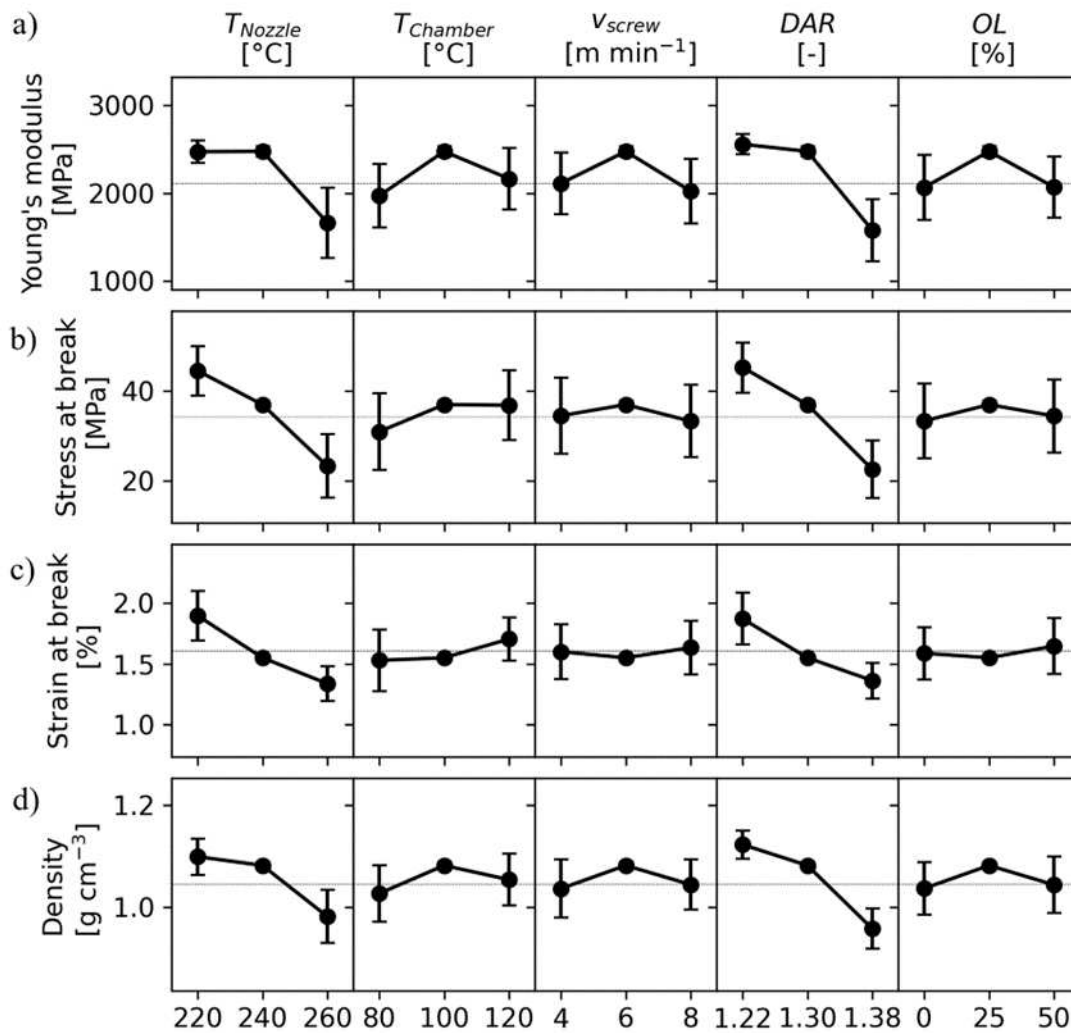
Figure 27 Main effect plot from the results of the design of experiments, split up into the effects on the Young's modulus (a), the stress at break (b), the strain at break (c) and the parts density (d).

The used DoE did not include all variations of parameters resulting in a lack of precision at correlations at higher orders. However, correlations from the second order still can be analyzed in order to understand the influence of two individual parameters in combination. The following plots show these influences on the stress at break for the manufactured specimens. One can see a strong correlation if the two lines (black solid and green dashed) show a different slope, which is true for the interaction of the overlap and the screw speed as can be seen in Figure 28. However, due to the error bars this effect might be more an artefact than a significant interaction.
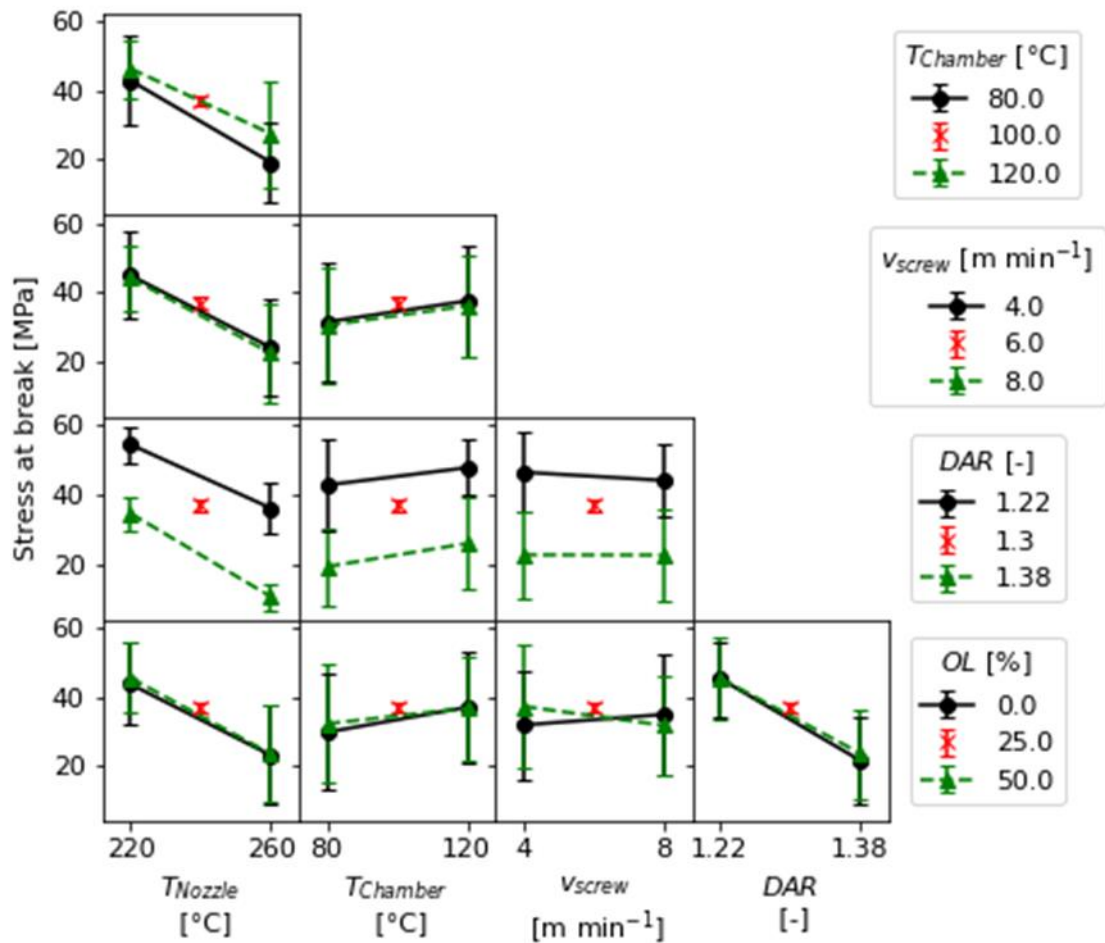
Figure 28   Interaction plots for the visualization of the first order correlation of the individual parameters.

As previously mentioned, the density and the stress at break show similar patterns. Thus, a plot of the stress at break over the measured density was created for a better understanding of this correlation (Figure 29a). The plot shows a significant relation between both values, which is highlighted by the dashed line as a result of a second order polynomial function fitted to the data points. This effect opens the question on the influence of the temperature since the drop formation in the APF not only depends on the temperature but also on the pressure, viscosity, and the discharge values. Therefore, the *DAR* is not independent of the nozzle temperature. An individual *DAR* was defined for each nozzle temperature and variated by 5 % up and down from the evaluated parameter. Tensile tests were performed and split by the nozzle temperature to identify the influence of the temperature and the *DAR*, corresponding to the filling of the specimens (Figure 29b). It can be clearly seen that the temperature alone does not control the density and thus the stress at break.
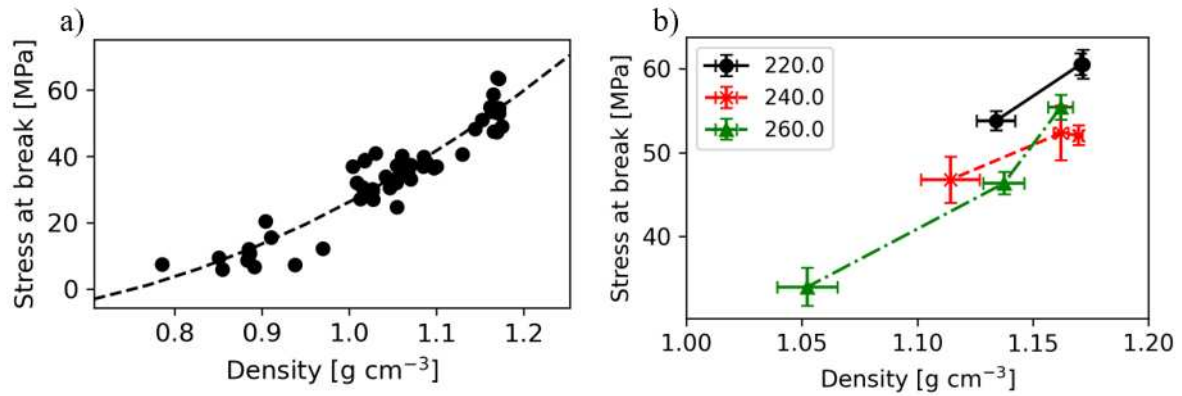
Figure 29 Stress at break values over the individual measured density of the printed PMMA specimens for the design of experiments (a) and the optimization procedure (b) split up into the individual nozzle temperatures.

For a better understanding of the process, the discharge and the pressure acting on the melt during the process is monitored and saved for every individual print job. For a successful process, these values should be relatively constant but can vary due to inhomogeneities in the provided polymer melt. The monitored average values of the pressure are shown in Figure 30a. The error bars in the plot represent the change in processing pressure during the manufacturing process. Different pressure values occurred at different temperatures resulting from the dependence of viscosity on temperature [34]. Since the pressure changes at the different temperature levels, the previous detected influence of the temperature may be a result of the lower processing pressure. Hence, the stress at break values is plotted over the different pressure values (Figure 30b). This figure shows a high dependency of the stress at break on the processing pressure, especially at high nozzle temperatures or lower pressure values.
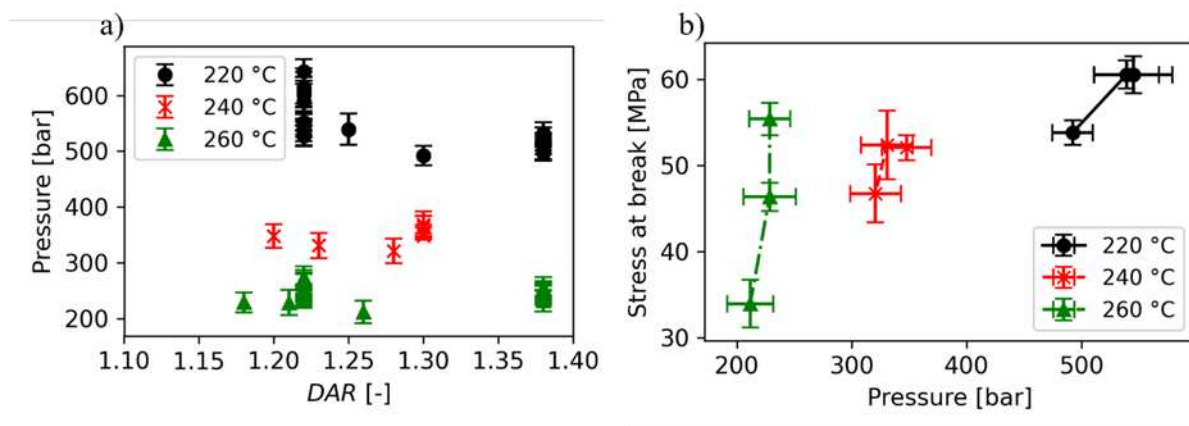

Figure 30 Average processing pressure for the individual printing processes and the standard deviation representing the changes in the pressure during processing at different

nozzle temperatures (a). The stress at break of the optimized specimens processed at different nozzle temperatures over the recorded pressure (b).

After tensile testing, the fracture surfaces were investigated under the light microscope. Figure 31 shows representative fracture surfaces of specimens printed at different nozzle temperatures and drop aspect ratios. The specimen in the upper right corner (DAR = 1.22 and T_{Nozzle} = 220 °C) shows a dense part but also a huge amount of overfilling. This overfilling results in a curvature at the top of the part, which deviates from the sought-after rectangular cross-section. Further, lower DAR led to a higher filling and therefore also to a lower overall porosity (Figure 27d). The samples printed at a DAR = 1.38 are less filled and the weld lines between the layers and the droplet structure are clearly visible. Weld lines can be seen for the parts printed at higher DAR but also at the specimen displayed in the lower right corner.
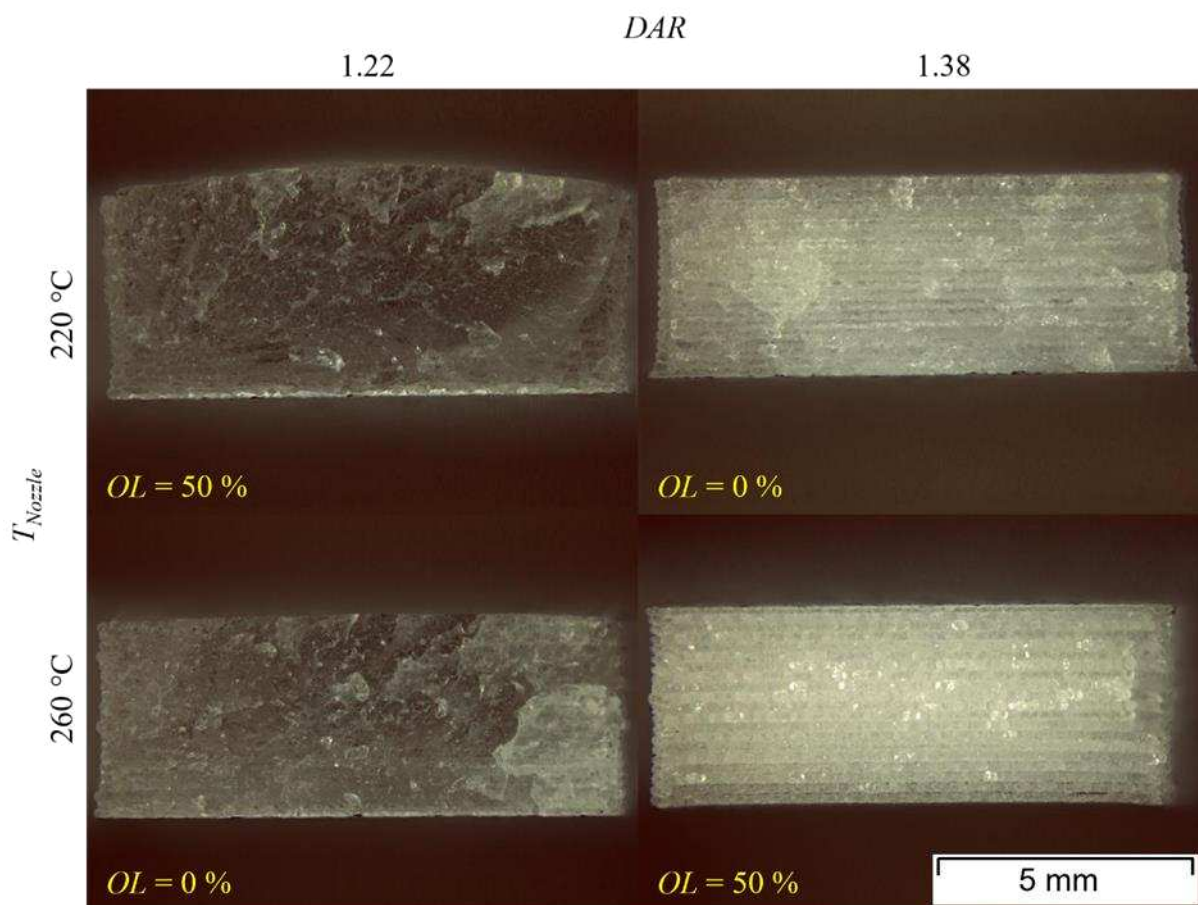
Figure 31 Microscopy images of the fracture surface of PMMA in APF for different processing temperatures (T_{Nozzle}) and drop aspect ratios (DAR) represented for the performed design of experiments. The Chamber temperature ($T_{Chamber}$ = 120 °C) and the screw speed (v_{screw} = 8 m min^{-1}) was the same for the displayed samples. The Overlap value (OL) was different and is given in the figure. The building platform side of each specimen is at the bottom.

The fracture surfaces of the specimens used for the optimization procedure were studied under the light microscope. The images are shown in Figure 32 and are arranged according

to their nozzle temperature and *DAR*. The appearance of the fracture surfaces is comparable to Figure 31 and shows a higher filling at lower *DAR* settings, respectively. Further, more weld lines and more opaque appearance at the same *DAR* settings at higher processing temperatures can be seen. The cross section of the sample produced at 220 °C with a *DAR* of 1.22 shows a high curvature on the top surface, hence a high overfilling of the part resulting in poor geometrical accuracy. The top surface of the specimens became flatter at rising *DAR* values and elevating processing temperatures. The individual layer lines and the droplet structure are also more visible at higher processing temperatures and higher *DAR* values. However, the specimen in the lower right corner of Figure 32 shows the most rectangular cross section.
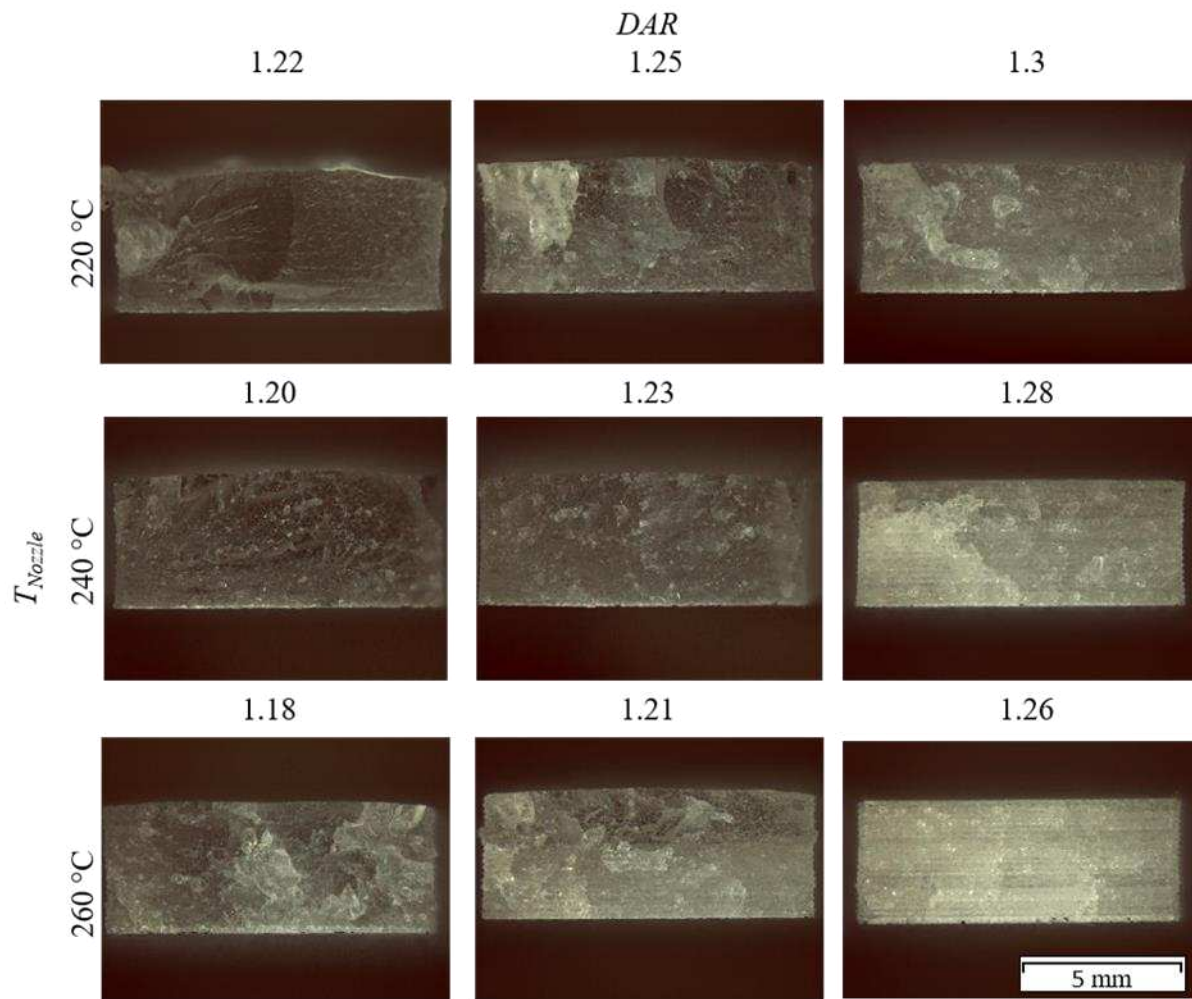
Figure 32   Microscopic images of the fracture surfaces of the optimized PMMA specimens in APF arranged according to the nozzle temperatures (T_{Nozzle}) and the drop aspect ratios (*DAR*). The building platform side of each specimen is at the bottom.

Discussion

The APF technology is a relatively new additive manufacturing method available on the market and offers the main advantage to make use of original polymer granulates traditionally

used for extrusion or injection molding. However, in order to find suitable process parameters for a specific material a qualification procedure must be performed. An example of a qualification process has been shown by Hentschel et al. [97] a further optimization is needed to achieve the desired properties, i.e. high mechanical performance, as shown in this work. Other researchers already applied similar approaches to either go for better optical properties or geometrical accuracy [94, 106]. Table 17 compares the tensile properties of the specimens prepared in this work and the previous work, where the focus was to obtain the best geometrical accuracy. In both studies the same material was used, and the tensile test conditions were similar.

Table 17   Comparison of tensile properties between specimens optimized for mechanical performance (current work) and specimens optimized for geometric accuracy (previous work).

Tensile property	Mechanical performance	Geometrical accuracy [97]
Stress at break in MPa	60.5 ± 2.14	47.6 ± 1.7
Young´s modulus in MPa	2984 ± 83	2982 ± 89
Strain at break in %	2.8 ± 0.07	1.7 ± 0.04

Overall, it was not possible to find processes settings with maximal mechanical properties and high geometrical accuracy. Hence, for each application a compromise must be found by adapting the process parameters. One might define two different standard processing parameter sets for either mechanical strength or improved geometrical accuracy. In this study, individual parameters and their influence on the mechanical behavior were investigated and show similar results for the effect of nozzle temperature and *DAR* values. Although other materials were used in the cited literature the connection between the density and the tensile properties [34, 117, 206] can be seen. However, it seems to be more crucial for brittle materials, such as PMMA, where a residual porosity of 10 % leads to a loss of up to 50 % in tensile strength. The nozzle temperature shows a similar significant influence on tensile properties in the performed design of experiments, which mainly resulted from a lower density at higher nozzle temperatures according to the density results in Figure 27d. Furthermore, samples of lower density showed distinct weld lines in Figure 31, which may also result in lower mechanical performance [242]. Hence, the DAR values were adapted to reach comparable density values, but some deviation at different settings are still present.

Higher tensile strength still can be reached at lower nozzle temperatures at similar densities as can be seen in Figure 29b. In theory, if two individual droplets are deposited next to each other they fuse together through diffusion and coalescence similar to sintering processes [242, 248]. Hence, higher temperatures should lead to better bonding or better welding strength

of the individual drops. However, in this case higher nozzle temperatures resulted in weaker parts, which may be due to thermal degradation during the process but by comparing the *IDT* (284 °C) and T_{peak} (302 °C) of the PMMA and the highest processing temperature (260 °C), no excessive degradation should be present even if overheating due to shear heating is considered, which is unlikely because of the short residence time at the highest shear rates.

Figure 30b shows the stress at break as a function of the processing pressure showing a significant influence. Further, by comparing to Figure 29b, similar patterns of the individual points can be seen. Hence, the influence of the pressure cannot be neglected, and this was also concluded by Moritzer et al. [179]. One reason for the differences in the tensile properties is residual micro-porosity or residual stresses in the part resulting from shrinkage of the material. Considering the specific volume at different temperature and pressure values (Figure 26), the specimens produced at higher temperatures and lower pressure values have a higher specific volume during the droplet deposition (v(260 °C, 220 bar) = 1.02 cm^3 g^{-1}, v(220 °C, 600 bar) = 0.95 cm^3 g^{-1}). This results in a higher shrinkage potential compared to the specimen at lower nozzle temperatures and leads to residual porosity or residual stresses, which might explain the differences in the appearance of the fracture surface in Figure 32. Further, the white dots visible in this figure (T_{Nozzle} = 240 °C, *DAR* = 1.20) may act like weak spots and explain the lower mechanical performance at similar densities. Hence, the loss in stress at break is more an effect of the micro-porosity or residual stresses rather than thermal degradation, and diffusion among droplets and layers.

The influence of the pressure shows higher impact at higher nozzle temperatures as can be seen in Figure 30. Thus, one approach for further improvement of the tensile properties of this PMMA in APF is to increase the extrusion pressure at higher nozzle temperatures. With the APF this value cannot be set directly since it is controlled by the machine for a stable discharge value. However, the pressure can be controlled indirectly, i.e. by increasing the back pressure during the dosing stroke. Hence further improvements are possible, and more investigations are needed to corroborate these initial observations.

Conclusion

The ARBURG plastic freeforming (APF) technology is a rather new additive manufacturing method with a high potential for producing functional parts at relatively high mechanical performance. Parameter optimization by using design of experiments can help to provide better performance and understanding of the process that will lead to the most optimal settings. This investigation showed that the stress at break of a medical-grade poly (methyl methacrylate) (PMMA) was mainly influenced by the porosity either due to the lower filling at higher drop aspect ratio (*DAR*) settings or due to lower processing pressures and its

corresponding shrinkage. Hence, the density of the printed part needs to be optimized in order to provide sufficient mechanical performance.

Similar results have been found in other work, but do not properly explain the loss in stress at break at higher nozzle temperatures. Higher weld strength and diffusion between the individual drops should lead to better inter- and intra-layer strength, but in this case the shrinkage due to changes in temperature and pressure of the individual drops had the higher impact on the overall parts performance.

For further improvement of PMMA parts manufactured by the APF technology, the processing pressure can be increased, especially at higher processing temperatures. One approach might be to increase the back pressure, which on the one hand can influence the melt homogeneity, but further increase the pre-compression of the melt, and thus, the processing pressure. Therefore, further research is necessary to better understand this relationship.

Acknowledgements

3.3.3 Publication C

Influence of the print envelope temperature on the morphology and tensile properties of thermoplastic polyolefins fabricated by material extrusion and material jetting additive manufacturing

L. Hentschel, S. Petersman, F. Kynast, U. Schäfer, C. Holzer and J. Gonzalez-Gutierrez

Abstract

Additive manufacturing (AM) nowadays has become a supportive method of traditional manufacturing. In particular, the medical and healthcare industry can profit from these developments in terms of personalized design and batches ranging from 1 to 5 specimens overall. In terms of polymers, polyolefins are always an interesting topic due to their low prices, inert chemistry, and their crystalline structure resulting in preferable mechanical properties. Their semi-crystalline nature has some advantages but are challenging for AM due to their shrinkage and warping, resulting in geometrical inaccuracies or even layer detaching during the process. To tackle these issues, process parameter optimization is vital, with one important parameter to be studied more in detail, the print envelope temperature. It is well known that higher print envelope temperatures lead to better layer adhesion overall, but this investigation focusses on the mechanical properties and resulting morphology of a semi-crystalline thermoplastic polyolefin. Further, two different AM technologies, namely material jetting (Arburg plastic freeforming - APF) and filament-based material extrusion, were studied and compared in detail. It was shown that higher print envelope temperatures lead to more isotropic behavior based on an evenly distributed morphology but results in geometrical inaccuracies since the material is kept in a molten state during printing. This phenomenon especially could be seen in the stress and strain values at break at high elongations. Furthermore, a different

crystal structure can be achieved by setting a specific temperature and printing time, resulting also in peak values of certain mechanical properties. In comparison better results could be archived by the APF technology in terms of mechanical properties and homogeneous morphology. Nevertheless, real isotropic part behavior could not be managed which was shown by specimen printed vertically. Hence, a sweet spot between geometrical and mechanical properties still has to be found.

Introduction

Additive manufacturing (AM) has become an important manufacturing technology over the last decades due to the high freedom of design and rapid production. Especially in medicine and healthcare, more and more beneficial use cases are found every day [110, 119, 160, 221]. Furthermore, the variety of materials for such applications significantly increased since new materials are being developed and validated consistently for 3D printing, provided in different shapes such as granules, filaments, viscous resins, or powders suiting the different AM methods [83, 256, 278]. Materials used for medical applications must fulfill several criteria depending on the category of the applications according to the Food and Drug Administration (FDA) or Medical Device Directive (MDD). Since every production step needs to be certified, the medical certification of granules may be easier since they have to undergo fewer production steps compared to filaments or powders [97].

More limitations on the material come from the AM method and the machine itself. Material extrusion (MEX) technologies are the most used methods, mainly using filaments as feedstock. Such machines can range from simple desktop printers to large industrial machines, with more features and more accurate control. The basic technology remains the same for filament-based MEX. A feedstock filament is pulled and pushed by a conveying unit, usually consisting of two grooved wheels. Further, the solid filament is fed through the cold end to the hot end, where the material is melted. The cold end is responsible for cooling the area and the filament down to prevent premature liquefaction of the polymer since the filament must still act as a piston to push the molten polymer through the nozzle. The most common diameter used for the nozzle is 0.4 mm; hence, a small strand of the material is then extruded and deposited on a moving platform relative to the nozzle. The tool head is the combination of the conveying unit, hot- and cold end, as well as nozzle. A schematic display of this method is given in Figure 33a. Essential properties of the filament polymer are stiffness to provide the needed extrusion pressure, relatively low viscosity to reduce the extrusion resistance, high heat transfer potential for a uniform temperature distribution, and good welding behavior to provide a reasonable inter- and intra-layer strength [80, 171, 270].

However, other MEX methods and AM technologies, such as the Arburg plastic freeforming (APF) technology, can process granules instead of filaments. The corresponding machine, the

freeformer, uses an injection molding unit for melting the granules and applying the needed processing pressure on the melt. A piezo-electronic shut-off valve, opening and closing, up to 250 times per second, is then used to form polymeric melt droplets. Hence, the extrusion is discontinuous as one of the significant differences between the APF and the previously described MEX technology. Although droplets are theoretically formed, an interconnected chain of droplets is produced and deposited on a moving build platform [34, 97]. The part formation occurs in a heated chamber and hence in a controlled environment, as a further difference to most MEX machines. Consequently, a controlled print envelope temperature can strongly influence the material properties, especially for semi-crystalline polymers [34, 106, 243, 259]. A schematic display is given in Figure 33b. Due to the droplet formation, this method is also referred to as material-jetting technology, according to DIN EN ISO/ASTM 52900 [47].
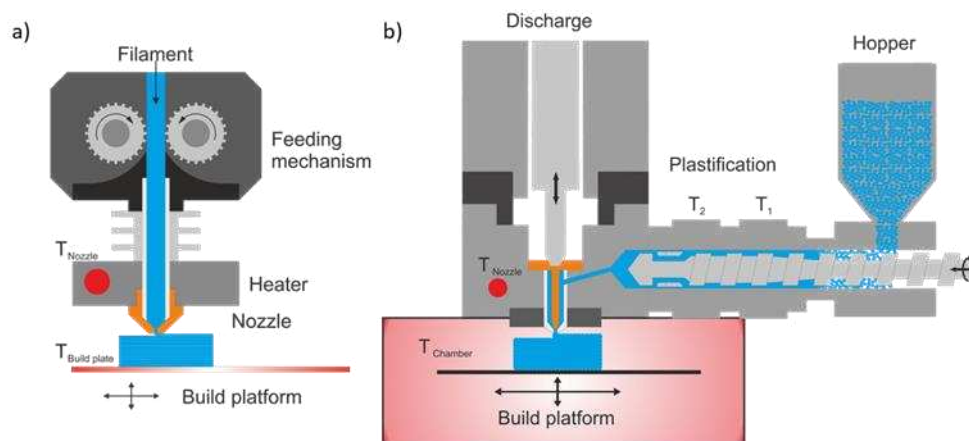
Figure 33   Schematic illustration of the filament-based MEX (a) and the Arburg plastic freeforming (b) technologies.

These technologies show different advantages and disadvantages and clearly have different use cases. The MEX method with a rather easy setup, can provide a rather inexpensive solution for the fabrication of 3D objects, however, might lack accuracy due to machine or filament deviations, as well as filaments slippage. Print jobs can even fail due to filament grinding or buckling, especially when dealing with elastomeric thermoplastics. These problems are not likely to occur in the APF process since granules are molten and due to the shut-off nozzle a controlled extrusion volume is possible. However, the APF is limited in extrusion volume, because of the nozzle size, droplet volume and operation frequencies, whereas the MEX can be applied with nozzle diameters up to 1.2 mm and hence can build big parts rather fast [80]. Nevertheless, Table 18 shows some key parameters of the different technologies as an overview.

Table 18   List of key parameters for the APF [34] and MEX [270] processes.

APF	MEX
Nozzle temperature	Nozzle temperature
Chamber temperature	Bed temperature
Discharge parameter	Nozzle diameter
Drop Aspect Ratio	Layer height
Layer height	Tarce width
Infill density	Infill density
Infill orientation	Infill overlap
Part orientation	Infill orientation
Contour overlap	Part orientation
Printing Speed	Printing speed

Semi-crystalline polymers like polypropylene (PP) are challenging to process using AM technologies due to their crystallization kinetics and accompanying shrinkage and warpage phenomena. However, semi-crystalline polymers show desirable properties for many applications. Hence, some unique grades have been developed to improve their processability [17, 30, 102, 243]. For semi-crystalline polymers, a higher degree of crystallinity and larger crystals generally yield preferable s [187]. Specifically, for generative manufacturing layer-by-layer, weak bonding between individual layers leads to less mechanical performance or even layer detachments [242]. Petersmann et al. [205] showed that increasing the melt temperature of the extrudate and decreasing the printing speed resulted in a more preferable crystalline structure of PP. Ovlaque et al. [191] further studied the temperature evaluation at defined positions during printing at the APF method and analyzed the crystallinity due to the thermal history. It was found that even in a single print, the thermal history in different locations of a printed part can change and lead to different morphology, internal stresses warping, and hence, weak spots of the manufactured parts. It was proven that a bead is remelted several times during the printing cycle. The higher thermal energy input enhances interlayer bonding and mechanical performance. A higher thermal energy input can also be achieved by evaluating ambient temperatures, influencing the cooling behavior and, therefore, crystal growth.

Further physical phenomena influencing the bonding and the mechanical properties are the diffusion and coalescence recently studied by Benié et al. [19]. Diffusion can also be of high interest for semi-crystalline polymers since diffusion is suppressed after forming crystals. Hence, a high cooling rate and, therefore, freezing of the polymer melt lead to a low diffusion and low bonding for semi-crystalline polymers. Further, coalescence is highly linked to diffusion and leads to a reduction of voids. It describes the formation of a single cylinder out of two

individual cylinders over time and can be characterized by the neck growth in the bonding area. This phenomenon is also temperature-dependent and is reasonably faster compared to diffusion [25, 217].

As aforementioned, warping is one of the major issues with 3D-printing semi-crystalline polymers. Warping occurs due to anisotropic shrinkage due to temperature inhomogeneities present in the AM process [13, 195]. This effect is further amplified by the high shrinkage potential caused by a large volume contraction during crystallization. Hence, the shrinkage and warpage behavior can only be improved by changing the polymer morphology, such as the molecular weight, polydispersity, and tacticity, or blending with a rigid filler [244, 245]. Furthermore, by incorporating comonomers such as ethylene, highly elastic thermoplastic materials are obtained, and reduced shrinkage can be observed. These polymers are referred to as thermoplastic polyolefins (TPO) and belong to the thermoplastic elastomers (TPE) group due to their high ductility and low stiffness. Such materials are particularly interesting in numerous applications attributable to their rubber-like properties and thermoplastic processability [17, 18, 69]. However, incorporating ethylene into a polypropylene matrix reduces the polymer's crystallinity, which can improve shrinkage but result in a complex tensile behavior, especially at high elongations [284].

Some studies have already shown the processability of TPEs utilizing filament-based MEX AM, but the use is limited to a specific stiffness/hardness since the needed pressure for the extrusion must be transmitted via the filament. Hence, print processes might suffer from unreliable extrusion or fail due to filament buckling [38, 150, 262, 279]. However, other AM technologies, such as the APF, use polymer pellets unaffected by the material's stiffness. In this study, a specific TPO was processed through filament-based MEX and APF at different build chamber or build platform temperatures to study the influences of the print envelope temperature on the mechanical properties. The influences on the morphology of the fabricated specimen and the consequences of the infill orientation on mechanical properties in additively manufactured samples were investigated in detail. Parts printed at higher envelope temperatures were expected to have more isotropic mechanical properties. Further, more samples were printed along the Z-orientation and were tested for tensile properties.

Materials and Methods

Material

A semi-crystalline polypropylene-ethylene copolymer with the tradename Vistamaxx™ Performance Polymer 3588FL, provided by ExxonMobil Chemical Company (Texas, USA), was used for this investigation. This polypropylene (PP) based on random copolymer has a low ethylene inclusions content, resulting in a softer resin with higher impact strength as compared to the traditional homo PP. Furthermore, the material appears softer, with a Shore

hardness of about 50D. Additional material properties provided by the manufacturer are given in Table 19. The reduced crystallinity and melting temperature arising from the polymer chain arrangement generally results in better printing properties since lower processing temperatures are needed, and less shrinkage and warpage are present [245]. The material was supplied as pellets, which the freeformer can process. Filaments were produced via extrusion, as described in the following section for filament-based MEX.

Table 19   Material properties of VistamaxxTM 3588FL provided by the supplier [61].

Property	Value	Unit
Density	0.889	g/cm³
Melt Mass Flow Rate (230 °C/2.16 kg)	8	g/10 min
Hardness (Shore D)	50	
Tensile Yield Strength	16	MPa
Tensile Stress at Break	26	MPa
Tensile Strain at Break	637	%

Filament Production

Filaments were manufactured with a single screw extruder FT-20 (COLLIN Lab & Pilot Solutions GmbH, Maitenbeth, Germany) equipped with a round-shaped die. This die has an opening diameter of 1.75 mm. The extruded filament was cooled down using a water bath at room temperature. Further, the filament was pulled, measured with an optical measuring device (Sikora AG, Bremen, Germany), and finally winded onto commercially available spools on a self-developed winding unit. The machine settings for the filament extrusion are given in Table 20. The fabricated filaments were further used for the MEX 3D printing method. The rotational speed was varied from 35 to 100 min^{-1} to enhance the production speed.

Table 20   Extrusion processing conditions for the filament production of Vistamaxx™ 3588FL.

Parameter	Value	Unit
Temperature Zone 1	190	°C
Temperature Zone 2	195	°C
Temperature Zone 3	200	°C
Screw Speed	35 – 105	min^{-1}

Additive Manufacturing Process Parameters

Specimens were fabricated by APF and MEX for comparison. The chamber temperature was varied for the APF technology and the building platform temperature for the MEX method

since no temperature-controlled build chamber was available. However, the printer has an enclosed build space, resulting in less air temperature fluctuations. The most important and constant specific settings are given in Table 21. These printing parameters were selected according to published recommendations. The parameter evaluation of the APF method followed a particular procedure and was performed according to Hentschel et al. [97].

Table 21   Processing parameters for the APF and MEX processes

APF			MEX		
Parameter	*Value*	*Unit*	*Parameter*	*Value*	*Unit*
Nozzle Temperature	220	°C	Nozzle Temperature	220	°C
Screw Speed	5	min^{-1}	Printing Speed	20	mm min^{-1}
Drop Aspect Ratio	1.50	-	Filament Diameter	1.75	mm
Chamber Temperature	50, 80, 110	°C	Bed Temperature	50, 80, 110	°C

For the manufacturing of APF samples, an ARBURG freeformer 200-3X by Arburg GmbH & Co KG (Lossburg, Germany) was used. The material was deposited onto an ABS/PC compound single-use build platform held by a vacuum table. The platform gen-erates enough adhesion to complete build jobs, however, some warping and detaching of the build platform were observed at lower temperatures. As default, the nozzle diameter of the APF machine is 0.2 mm for depositing the droplets.

To prepare the MEX samples, a HAEG3D 140L machine provided by HAGE3D (Graz, Austria) was utilized. A unique build platform for polyolefin supplied by PPprint GmbH (Bayreuth, Germany) was used since the polypropylene adhesion to the build platform was insufficient on the standard glass platform. Mainly, at low build platform temperatures more warping and some detachment could be observed during the process. This machine usually is fitted with a 0.4 mm nozzle, which was used for these experi-ments.

Printing Strategy

Tensile bars were printed at different processing settings to investigate the effect of the print envelope temperature on the anisotropy of 3D-printed specimens. To investigate the anisotropy, the infill angle (α) was varied from 0° to 90° and kept constant in every layer. All print envelope temperatures and the printing angles are listed in Table 22a; all setting combinations were manufactured in the first part of the study. Also, no contour line and a layer height of 0.2 mm were used for both processes when preparing the individual G-codes. The software Simplify3D v4.1 (Cincinnati, USA) was used to prepare G-Codes for the MEX, and the ARBURG freeformer software v2.30 (ARBURG GmbH + Co KG) was used to define job files for the APF methods. The used geometry is shown in Figure 34a. To further study the

influence of the contour lines, a combination of infill angle, contour lines, and ambient temperature at three different levels were chosen; the values are given in Table 22b.

Table 22   (a) Print strategies for the APF and MEX samples to study the influence of infill orientation and print envelope temperature without contour line and (b) the second setup to include a specified number of contour lines but only three angles to reduce the number of specimens.

a)

Print Envelope Temperature in °C	50				80				110
Orientation in °	0	10	20	30	45	60	70	80	90

b)

	Print Envelope Temperature in °C	Orientation in °	Number of Contour Lines
Low	50	0	0
Middle	80	45	1
High	110	90	2

By keeping the orientation constant, a specific anisotropic behavior is forced. Hence, the influence of the print envelope temperature on the anisotropy can be deduced based on these setups. Further, tensile bars were prepared in a standing manner (Z-orientation), which was only possible in the APF process due to the availability of support material. Therefore, four tensile bars were arranged in a square slightly touching each other, as shown in Figure 34b and enclosed in solid soluble support material (ARMAT 11). Differential scanning calorimetry (DSC) samples for the thermal analysis were also printed on the building plate and the top of the construction; this is also displayed in Figure 34b. For the MEX samples, printing in Z was impossible since the construction started shaking with increasing layer numbers, resulting in a severe layer shift and failed print jobs. Using soluble support material in the MEX process was also impossible with the used equipment. The APF printed samples were then put in deionized water for around 15 h until the support material was dissolved. The samples were then dried at room temperature to prevent further post-crystallization. At least five specimens have been printed and tested for each setting, except for the Z-orientation, where only four samples were prepared.
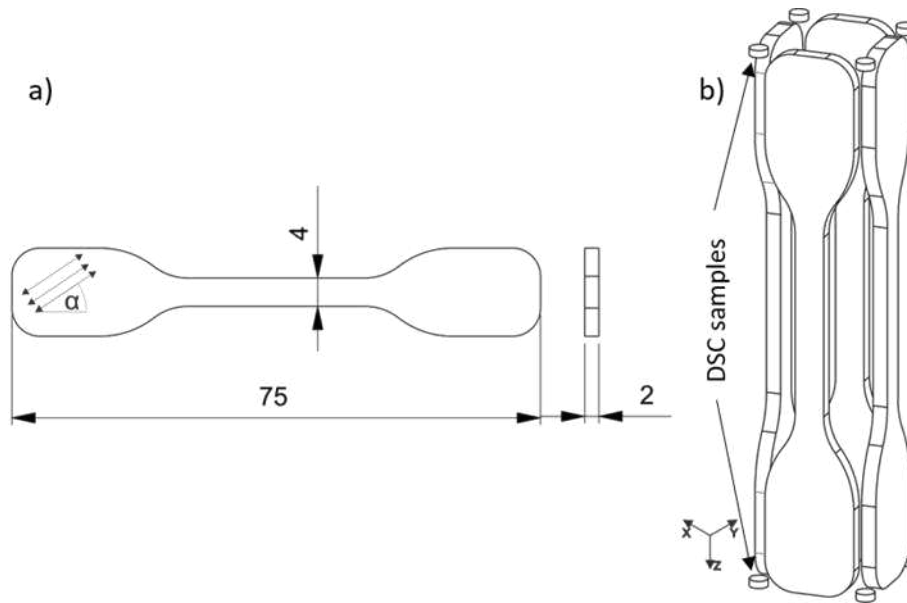
Figure 34   Tensile bar according to ISO 527-5A with the given dimensions in mm and the infill orientation (a) and configuration of tensile bars orientated in Z direction and DSC samples placement (b).

Thermal Experimetal Setup

Differential scanning calorimetry measurements were performed on a Mettler Toledo (Ohio, USA) DSC1. For the standard analysis of the APF and MEX printed samples, the measurement was performed in the temperature range of -50 to 200 °C at a heating rate of 10 K min^{-1}. Further, some experiments were conducted to study the crystallization behavior of the given material. Therefore, samples cut from the virgin granules (ca. 5 mg) were tempered by holding the sample at a given temperature for a specific time using the DSC device. All analyses were performed under a nitrogen atmosphere at a flow rate of 50 ml s^{-1} to prevent any oxidation during the measurements. An example of the temperature progress over time is shown in Figure 35.

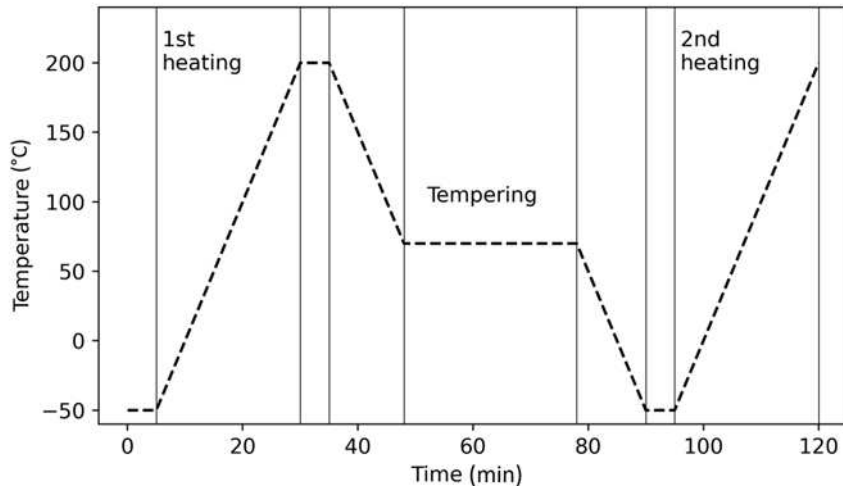Figure 35 Example of temperature progress for the tempering investigations. The temperatures and times were varied for different trials.

Microscopy

In the first step, optical microscopy (SZH, Olympus Optical Co., Japan) images of the central part of the specimens were taken to get an overview of the effects of the print angle and the notches developed in this way. For investigation of the crystalline structure, cross-sectional microtome sections were cut with the Leica RM 2255 (Leica Microsystems GmbH, Germany) microtome. These samples were further put onto a glass slide and wetted with a coverslip. One droplet of paraffinum liquidum with a known refractive index was placed between the samples and the glass slide. Polarized optical microscopy images were taken on the Olympus BX51 (Olympus Life Science Europe GmbH, Germany) at transmitted light mode. That way influences on the morphology of the polymer at different printing parameters could be analyzed.

Mechanical Testing

Tensile tests were done on a universal testing machine, Zwick Z250 (ZwickRoell GmbH + Co KG, Ulm, Germany). Testing speed was set to 1 mm min^{-1} up to an elongation of 0.25 % for the estimation of Young's modulus and was then increased to 50 mm min^{-1} until the breakage to shorten the testing time due to the elastomeric nature of the material. The testing speeds are set according to DIN EN ISO 527-1 [142]. Mechanical clamps with riffed inserts at a defined distance of 42 mm were used to clamp the samples. Deformations were recorded at 1 FPS and evaluated by digital image correlation using a Mercury RT System (Sobriety s.r.o., Kuřim, Czech Republic). This system does communicate directly with the tensile testing machine, to synchronize the deformation and load results. Therefore, a random graphite pattern was sprayed on the specimens before testing. The Young's modulus was evaluated by the ratio of the changes in stress to the changes in strain, measured at the strain levels

between 0.05 and 0.25 %, respectively. For further analysis, the stresses, and strains at the moment of fracture and at the yield point were evaluated. The stresses and strains shown here are engineering values only considering the initial cross-section of the specimen. Correction of these values was not performed in this study.

Results and Discussion

The extruded filaments, produced at higher rotational speed, show a rougher surface, also known as shark-skin effect (Figure 36).
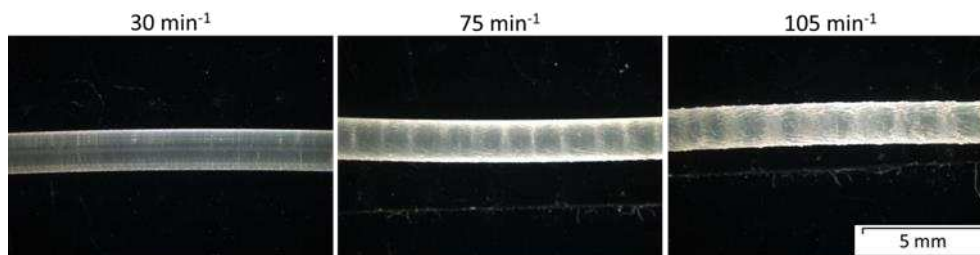
Figure 36 Microscopy images of the Vistamaxx^{TM} 3588FL extruded at different rotational speeds. Images were taken at a magnification of 10.

The filaments produced at 30 min^{-1} show a smooth surface, as seen in the left image. For filaments made at 75 min^{-1}, regular notches or weld lines appeared, which indicate an unstable process resulting in a stick-slip effect or melt breaking due to the high throughput and wall slip. After increasing the rotational speed further, a clear example of the shark skin effect can be seen. Based on these results, only filaments produced at the lowest rotational speed were used for further experiments. Since the sharkskin effect occurred during the filament extrusion process at a higher extrusion speed, it could also happen in the MEX processing at higher speeds [171]. Therefore, the processing speed was limited, and no shark skin was visible on the printed parts (Figure 38).

All parts were printed without any special visible errors on either machine. Only the samples printed at low print envelope temperatures show low bed adhesion and thus some warping. An overview of selected printed parts is displayed in Figure 37, to give an example.
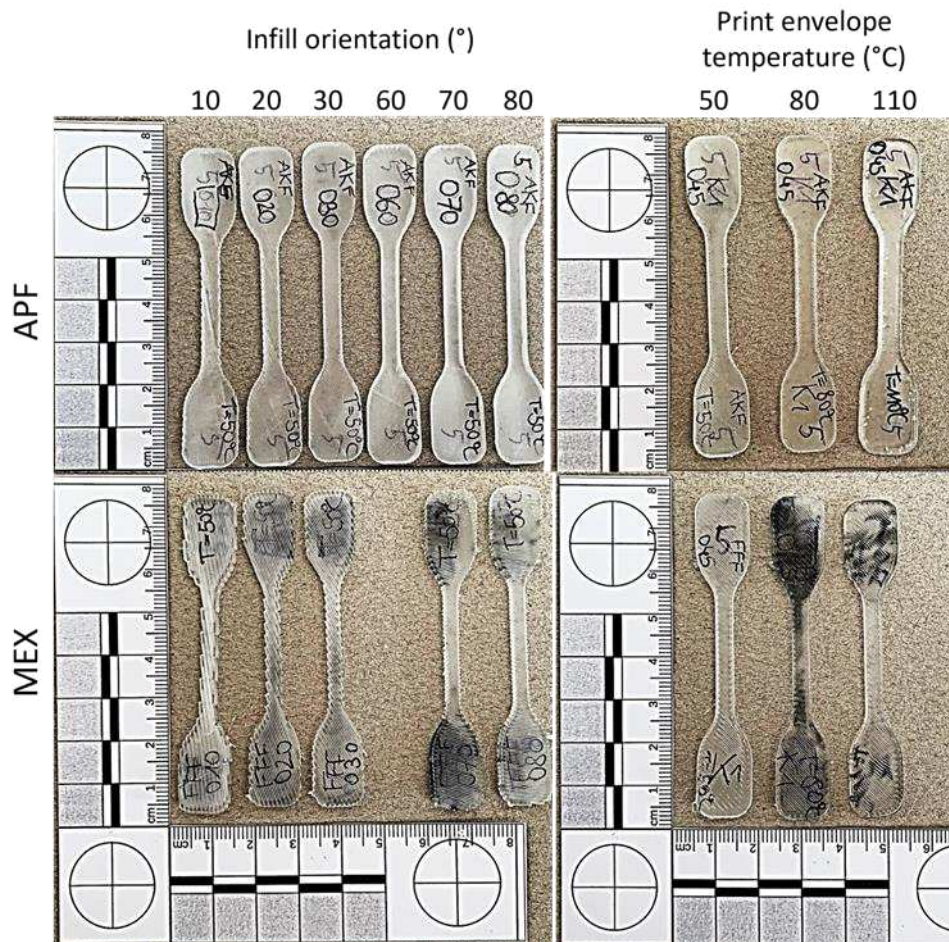
Figure 37 Selection of printed samples at different infill angles (left) and ambient temperatures (right) for the two additive manufacturing methods Arburg plastic freeforming (APF) and material extrusion (MEX).

As one can see, samples printed at different ambient temperatures show different appearances. The specimens, printed on the freeformer at 110 °C chamber temperature, are more transparent but show some voids inside the specimens (see Figure 38b: APF). The black-colored parts on the samples (particularly for MEX) are residuals of the building plate, which were not removeable from the samples. However, such residuals are primarily present on the surface of the clamping areas of the specimens and, hence, do not influence the measurements. Furthermore, the edges of the samples are not smooth for some of the samples since no contour line was used. Especially, the MEX printed samples show predominant notches (Figure 38a: MEX 45° and 90°). For the APF printed samples, notches are neglectable, and even the individual strand lines tend to vanish at elevated ambient temperatures (Figure 38b: APF) and with increasing infill angles (Figure 38a: APF 45° and 90°).
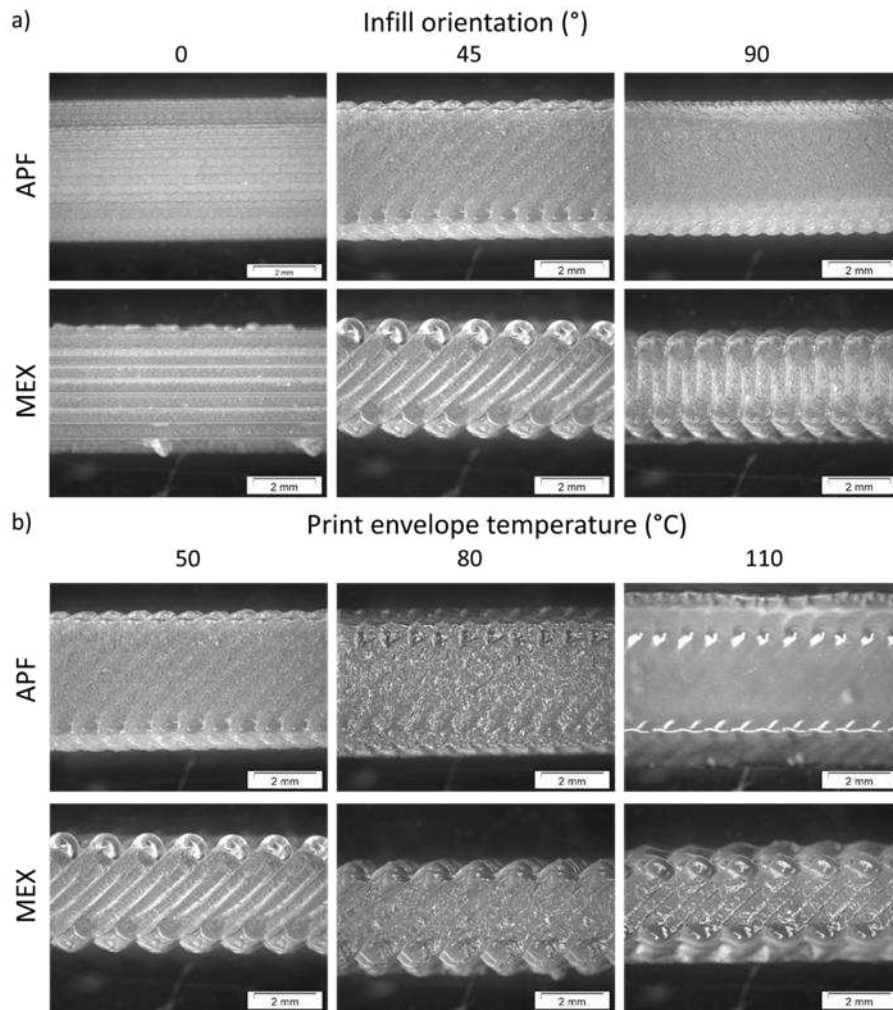
Figure 38   Microscopy images of the top layers of representative samples printed at different
             infill angles, printed at 50 °C print envelope temperature (a) and samples printed
             with 45° infill angle and different print envelope temperatures (b), using the Arburg
             plastic freeforming (APF) and material extrusion (MEX) process.

Comparing the two manufacturing methods, the stands of the APF samples are narrower than for MEX. This is due to the smaller nozzle size used as a standard for APF. The notches in the MEX samples may further lead to weaker performance of the specimens.

Thermal Analysis

To understand the influences of an isothermal holding temperature and time during cooling of the polymer, DSC experiments as described in section "*Thermal Experimental Setup*" were performed. The results of these tempering experiments are shown in Figure 39.
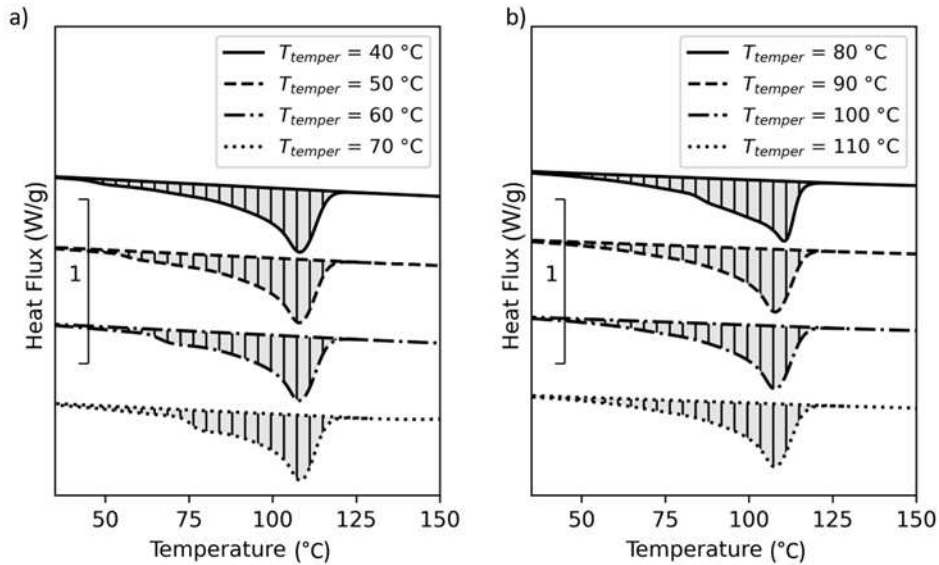
Figure 39   DSC results of tempering trials performed within the DSC device for specimens printed via Arburg plastic freeforming (APF) at different tempering temperatures: 40 to 70 °C (a) and 80 to 110 °C (b).

Comparing the individual curves, differences in the heating curves start to occur at a 60 °C holding temperature and vanish at holding temperatures over 90 °C, which correlates with the onset of the cold crystallization function and the onset of the melting peak for this copolymer. These secondary peaks might indicate the existence of a different crystalline structure due to longer crystallization time. For demonstration, the effective range between the measured onsets at 62 and 97 °C, respectively, is displayed in Figure 40.
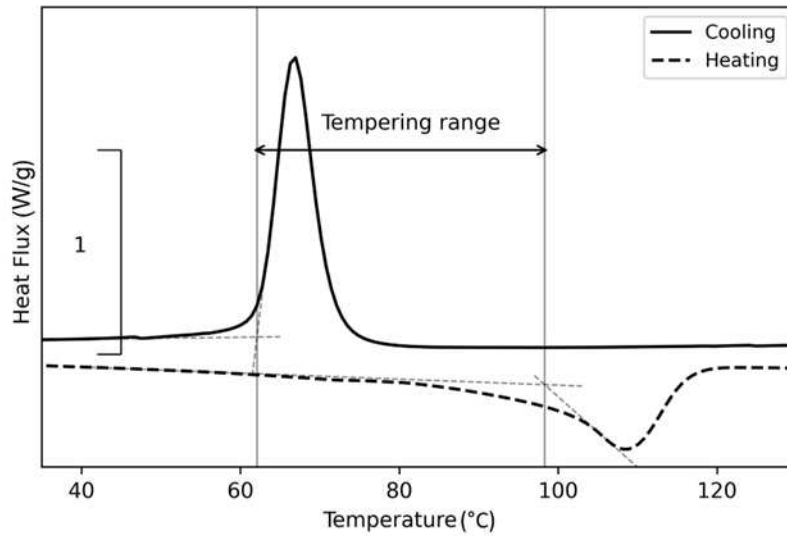
Figure 40 Discovered effective tempering range of the Vistamaxx™ 3588FL, based on the results from the tempering trials from 40 to 110 °C.

The peak temperatures of the results shown in Figure 39 are similar to virgin polypropylene (Figure 40), and the selected temperature range shows similarities to the crystalline mobility temperature range mentioned by Fiebig et al. [64]. The recommended annealing temperature for PP is 85 °C [11], which can also be applied for this copolymer due to its low ethylene content. A further increase in ethylene content leads to a further reduction in melting temperature [35]. Hence, the print envelope temperatures are selected based on these results to be below, in between and above this range.

Further DSC experiments were conducted to study the influence of the tempering time on crystallinity. Unlike the previous experiments the study was performed on pellets at different isothermal holding times and at only three different temperature levels. These results are presented in Figure 41.
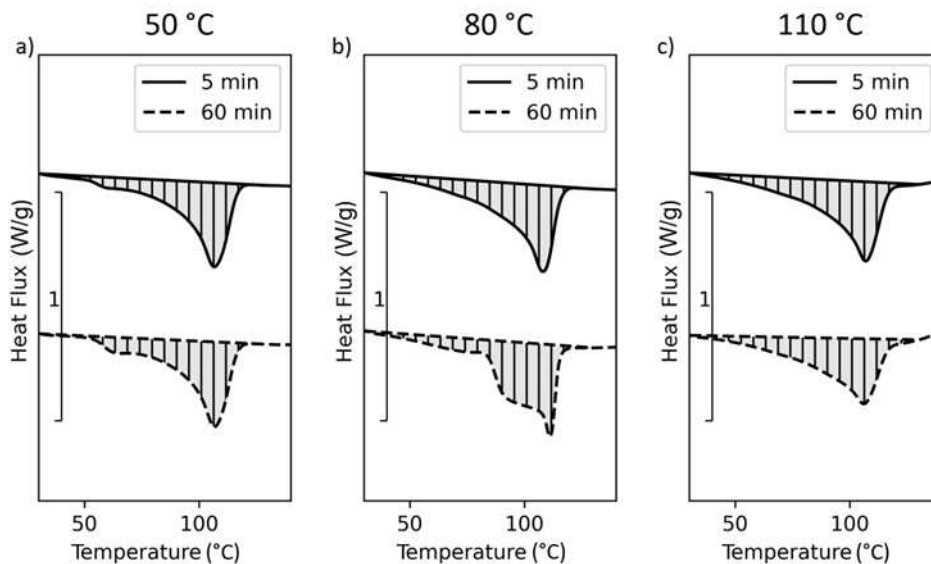
Figure 41 DSC results of tempering trials performed within the DSC device for the material in pellets form at different times and tempering temperatures 50 °C (a), 80 °C (b) and 110 °C (c).

The resulting curves show a significant difference in the melting functions of the samples holding at 80 °C at different times. This indicates the time dependency of the crystallization kinetic and refers to a secondary (β) crystalline structure which can be triggered at a defined undercooling and isothermal holding [266]. Because of the time dependence and the quite slow processing speed in AM, different crystalline structures can occur along the Z-direction of a 3D printed part.

DSC analyses were also performed on printed parts. The resulting curves of the first heating cycle measured on samples taken from samples printed via APF and MEX are presented in Figure 42.
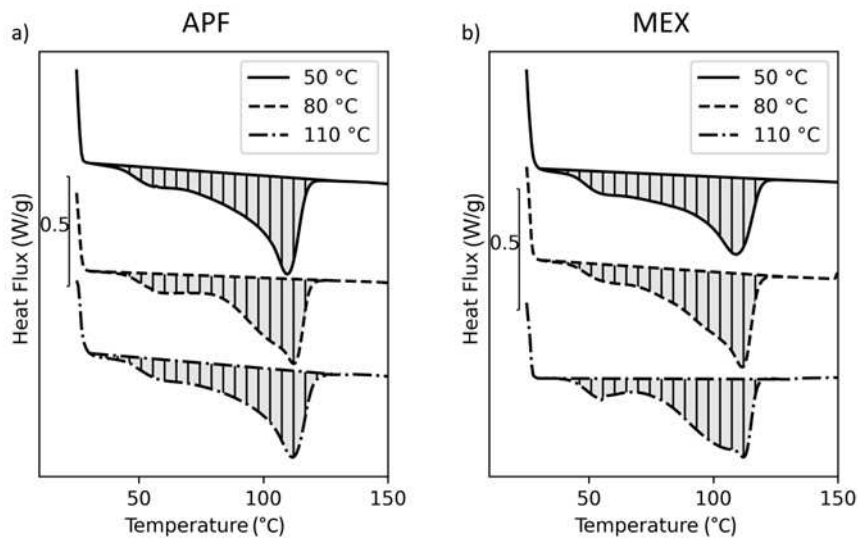
Figure 42 DSC results of specimens printed via Arburg plastic freeforming (APF) (a) and material extrusion (MEX) (b) at different envelope temperatures according to the standard measuring procedure. The melting areas for the calculation of the melting enthalpy are displayed in grey.

Only the first heating curve of samples processed at 80 °C ambient temperature in APF and at 110 °C in MEX show a slightly different behavior at similar settings for the print envelope temperatures. These results also lead to the assumption of a different crystalline structure caused by elevated print envelope temperatures. However, this effect is diminished by even higher temperatures for APF. The secondary melting peak at around 60 °C may be caused by fast cooling during the processes. A similar melting peak occurs in the sample tempered at 50 °C, which may also indicate insufficient cooling due to a low heat conductivity of the polymer and, hence, residual heat within the printed part.

Tensile bars were printed standing in Z-orientation, with DSC samples placed at the bottom and on the top (Figure 34b). The results of the DSC analysis are given in Figure 43.
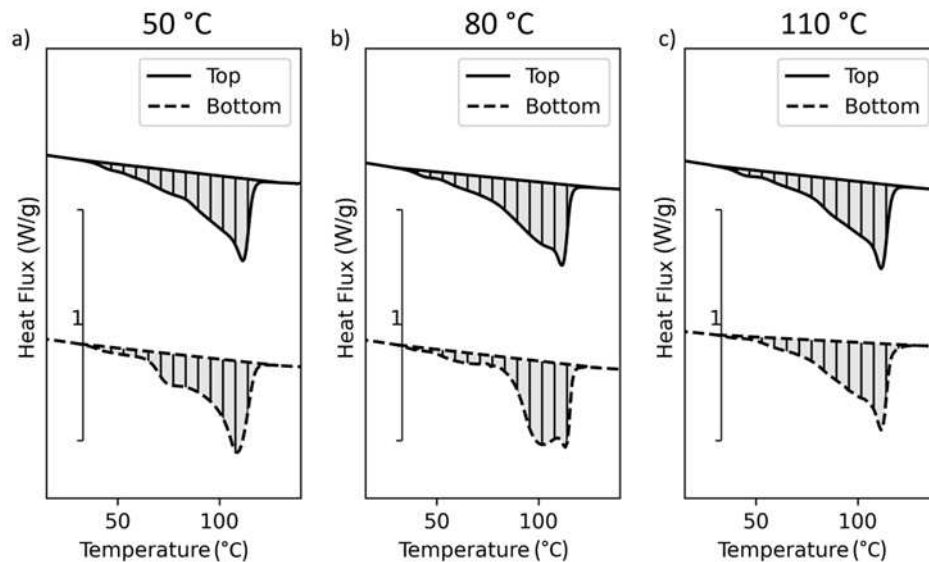
Figure 43   DSC results of tempering trials performed within the DSC device for specimens printed via Arburg plastic freeforming (APF) at different print heights/times and tempering temperatures 50 °C (a), 80 °C (b) and 110 °C (c).

One can spot similar differences as observed within printed samples. Hence, the tempering time significantly influences the crystalline structure, resulting in anisotropy. Thus, if parts with a high expansion in the Z-direction are printed at evaluated temperatures, the time the polymer is exposed to this environment changes from top to bottom. Nevertheless, a more homogeneous crystallinity can be observed if printed at a higher ambient temperature, but the material is still molten. Therefore, the form stability is low and gets lower at rising temperatures due to decreased zero viscosity and melt strength. Further, the polymer starts to flow due to gravity. This flow results in high differences in shape and low accuracy, as seen in Figure 44. Therefore, a compromise between geometrical accuracy and mechanical strength must be found.
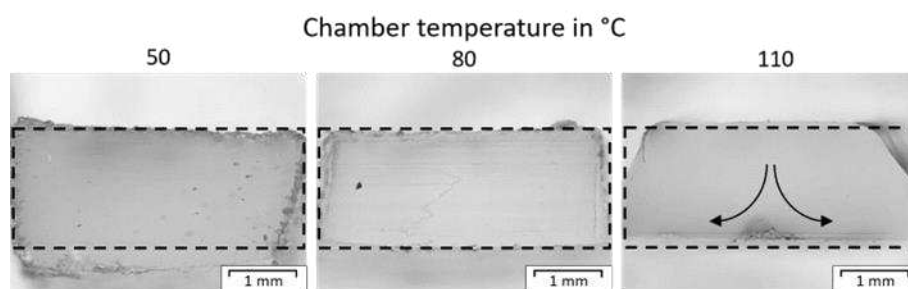
Figure 44   Cross-section of tensile bars printed at different chamber temperatures with the APF and indicated flow direction on the right figure.

However, even if the appearance of the cross-sections did change, the overall mass of the samples and, hence, size did not change at different temperatures. Also, the trace width did

not change with temperature, but as mentioned above, material flow can be present at higher temperatures and lead to deviations in the cross-sections.

Polarization Microscopy

Polarized optical microscopy was performed at the cross-sections of the 0°, 45° and 90° samples, fabricated at different print envelope temperatures. Figure 45 shows the crystalline structures of the MEX printed samples and Figure 46 for APF specimens.
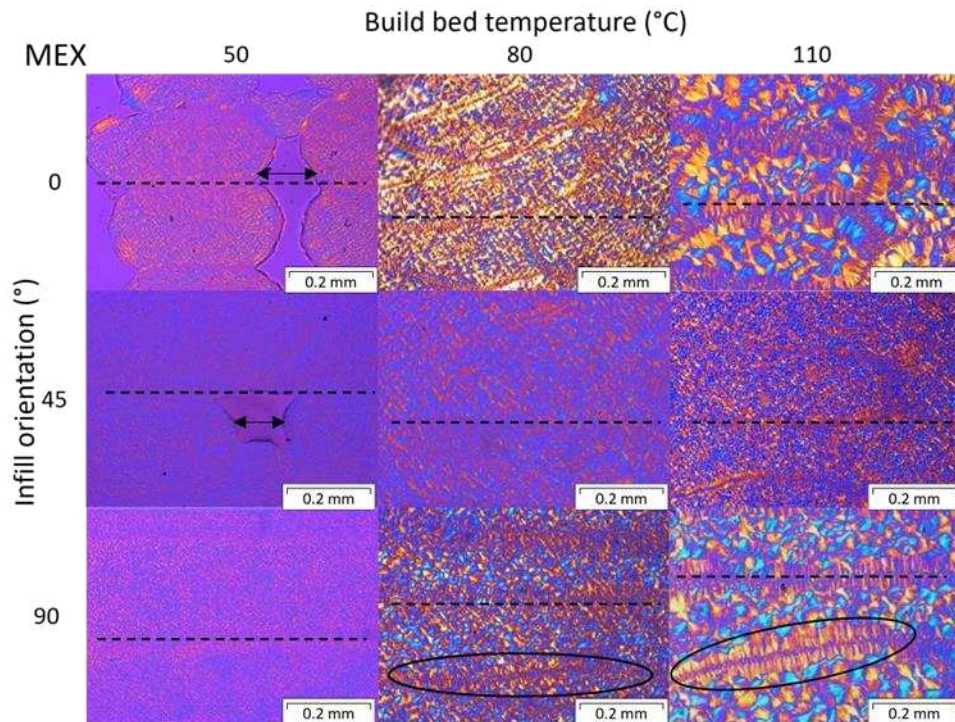
Figure 45   Polarized optical microscopy of samples printed via material extrusion (MEX) at 0°, 45° and 90° infill angle and 50, 80 and 110 °C bed temperature. Visible layer lines are marked by dashed lines, shish-kebab structures are circled in, and voids are shown by the arrows.

One can see the differences in the crystalline structures for different build bed temperatures and print orientations. At higher temperatures, larger spherulites are formed, and so-called shish-kebab structures (black ovals) get more and more present around the connection areas of the individual strands, as similarly observed by Petersmann et al. [205]. Fischer et al. [65] also show increased spherulite size at higher iso-thermal holding temperatures and longer holding times. This larger size of the crystalline structures is probably due to the higher temperature and prolonged crystallization period (i.e., more time is available to grow before solidification). However, the individual layers and strands are still visible in all samples (dashed lines), even more at higher temperatures due to the formed shish-kebab structures. Further, some voids are present in samples printed at low bed temperatures. These voids might be due to under-extrusion during the build process or fast cooling and shrinking, hindering the fusion

of the individual strands. Voids can lead to a loss in strength and a high scattering in the mechanical testing results.
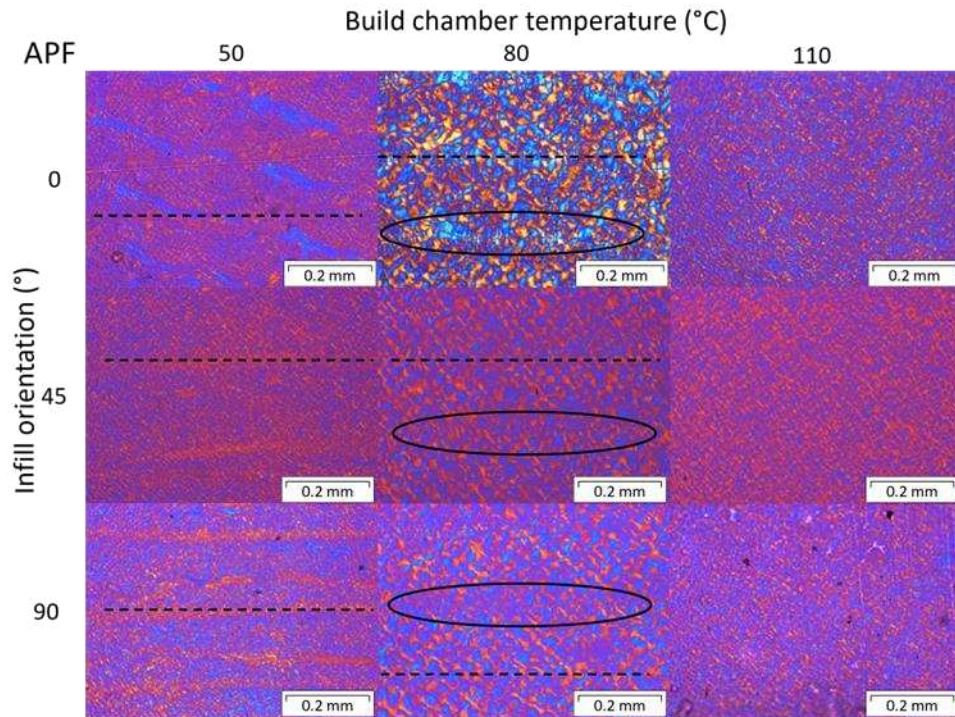
Figure 46   Polarized optical microscopy of specimens prepared by Arburg plastic freeforming (APF) at different print orientations and bed temperatures. Visible layer lines are marked by dashed lines and shish-kebab structures are circled in.

For the APF printed samples, layer lines (dashed lines) can be observed at a chamber temperature of 50 °C and in the 80 °C samples, even though they are not as visible as in the MEX samples. Here as well shish-kebab crystalline structures (black ovals) can be detected at samples printed with 80 °C build chamber temperature. However, the polarized optical microscopy images of samples printed at 110 °C show a homogenous crystallinity, without distinguishable weld lines. This is an indication of a homogeneous material behavior, when printed at higher envelope temperatures. By looking at the figure of the sample printed at 80 °C and 0° infill orientation, a similar crystalline structure on the bonding area can be observed as in the MEX samples printed at 110 °C only at smaller sizes. The smaller size might be due to the thinner strands or droplets deposited with the APF compared to the MEX technology. The internal temperatures of the MEX printed samples may be little lower, compared to the APF printed parts, since only the platform was heated in MEX. This can also be observed from the DSC results (Figure 42), where the heating curve of samples printed at 80 °C with APF are comparable with those of samples printed at 110 °C with MEX.

Tensile Properties

Selected engineering stress-strain curves are shown in Figure 15 with their standard error of the break values. Note that these results are evaluated based on the initial cross-section.

Only the APF samples printed at 110 °C chamber temperature shows a hyperplastic increase at high elongation; all other samples presented break in the plateau. Hence, better bonding was achieved in these settings. The yield strength and the evaluation of the stress-strain curves are similar for all other parameters.
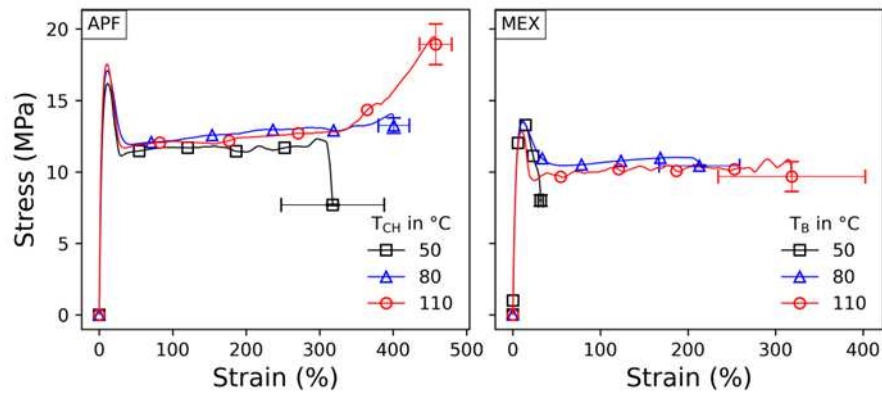
Figure 47   Stress-Strain curve of samples printed with no contour lines and 45° infill angle at different print envelope temperatures for APF (a) and MEX (b)

In comparison, samples printed with the APF show a higher stress level than those printed with MEX. A higher necking behavior can also be observed, but the plateaus show almost the same stress levels. As mentioned, voids may be present more in the MEX samples than in the APF samples, especially at lower print envelope temperatures, which might explain the lower stress and strain values.

The results of the tensile tests from samples printed at different infill angles are displayed in Figure 48. The resulting yield stresses and strain at break values are plotted over the infill angles set for the specimens, for more information the results are listed in Table S6.
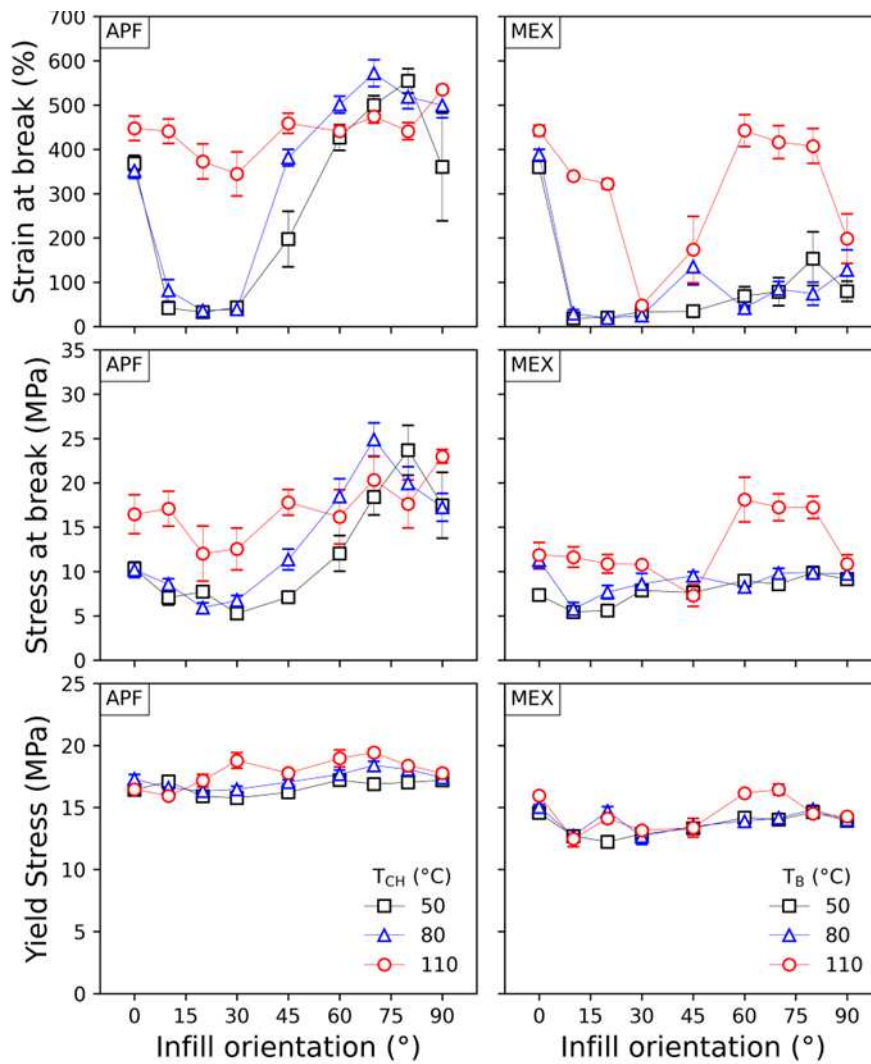
Figure 48   Tensile properties of samples printed via Arburg plastic freeforming (APF) at different chamber temperatures (T_{CH}) and material extrusion (MEX) at different print bed temperatures (T_B) and with infill angles.

The yield strengths of the samples are constant within a specific range, while the strain at break values alternate along the different orientations, particularly at lower print envelope temperatures. The yield strength only shows minor variances, which may be due to the ductile nature of the material. A drop in tensile strength over the infill angle was expected, similar to the results of Dudescu et al. [50]. However, by comparing the different print envelope temperatures, one can see the effect of the infill orientation lowering at 110 °C, making the parts more isotropic in such a manner. Also, no significant changes in strain at break were shown in the mentioned investigation [50] in contrast to the results obtained in this study. The increasing strain at break values for MEX samples printed at 110 °C bed temperature and infill angles of 70°, 80°, and 90° compared to samples printed at lower infill angles may be due to a better intra-layer bonding of the individual strands. At higher infill angles, the time between the next strand laid to the previous shortens significantly, resulting in better welding [19, 25, 40, 205]. Similar behavior can be seen for the APF printed parts but at all temperature

levels. In contrast to the literature, no significant better mechanical performance was detected [89, 155].

Furthermore, the APF samples show higher values at a 90° infill angle than at 0°, which might have been the case due to better bonding between adjacent strands caused by the shorter travel distance, hence higher residual temperatures due to less time for cooling. A similar result was observed by Charlon et al. [34] and Ramezani Dana et al. [211] for ABS. The highest impact of the print envelope temperature was observed at the strain at break values. At this stage, the specimen is highly elongated; hence, minor imperfections can lead to ultimate failure. Thus, a higher scattering can be seen in the results from the strain and stress at break values. It can also indicate the best bonding for the low infill angle specimens for the APF method and samples printed at 110 °C bed temperature with the MEX method.

Nevertheless, additively manufactured samples are mostly printed with a specific number of contour lines since it helps to achieve a better visual appearance (i.e., no jagged edges). According to Table 22b, more samples were prepared and tested to determine the influence of this feature on mechanical properties. The results are shown in Figure 49 and are further listed in Table S7 and Table S8 for more details.
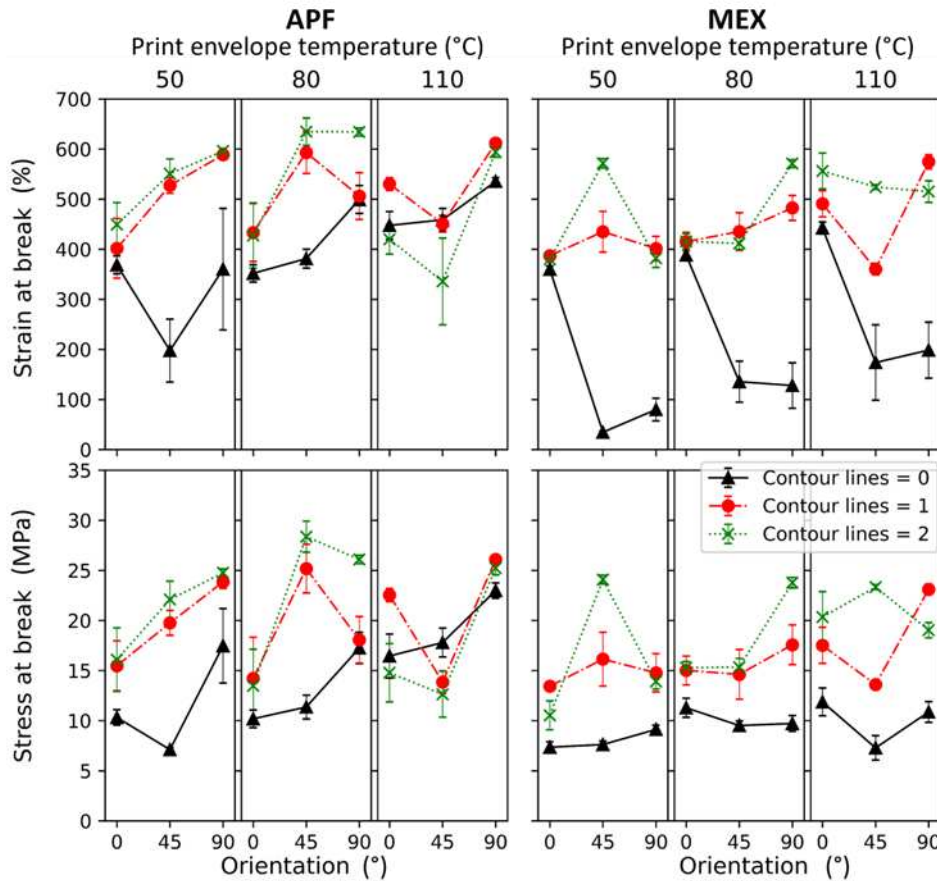
Figure 49   Tensile properties of samples printed via Arburg plastic freeforming (APF) and material extrusion (MEX) at different envelope temperatures, infill angles and contour lines.

Here again, APF samples printed at 90° infill angle show higher stress and strain values than APF samples printed at lower angles overall. The samples printed with zero contour lines show the lowest values for both methods. In the case of the APF process, this was also observed by Charlon et al. [34]. Further, the effect of contour lines vanishes for the APF samples printed at 110 °C chamber temperature, and a drop for the samples printed with a 45° infill angle appears. This result might arise from a more considerable void concentration at the border between infill and contour, resulting from the infill path orientation. These voids can more easily develop at the higher chamber temperature, leading to lower stress and strain results at break. The formation of such voids or micro voids was also discussed by Hentschel et al. [99]. Another explanation for the slight increase in stress at break might be reduced internal stress. Samy et al. [13] found a reduction of up to 2 MPa in internal stress when printed PP at evaluated ambient temperatures. Besides those effects, no significant patterns could be observed. However, it must be highlighted that the highest mechanical performance for both methods was reached at an infill angle of 45° and with two contour lines, which was also concluded by Hirsch et al. [106]. These fabrication strategies correspond with the recommended setting for 3D printing, at least for MEX methods. Furthermore, the differences

in the results between non and single-contour line samples led to the assumption that notches cause a significant drop in performance in angled samples. Due to the ductile nature of the polymer, this has a higher influence on stress and strain at break than on the yield strength.

To further prove decreased anisotropy and higher interlayer adhesion, tensile samples were printed standing in Z-orientation at different chamber temperatures. As mentioned, it was not possible to print them with the MEX technology since the material is too soft and started to wobble with progressing height. Further, it was not possible to use support material due to hardware limitations. The results of these tensile tests are displayed in box plots in Figure 50.

Regardless of the chamber temperature, the stress and stress at break for the specimens printed vertically (z-orientation) were significantly lower than those printed horizontally (xy-orientation), as other researchers observed [106, 162, 283].
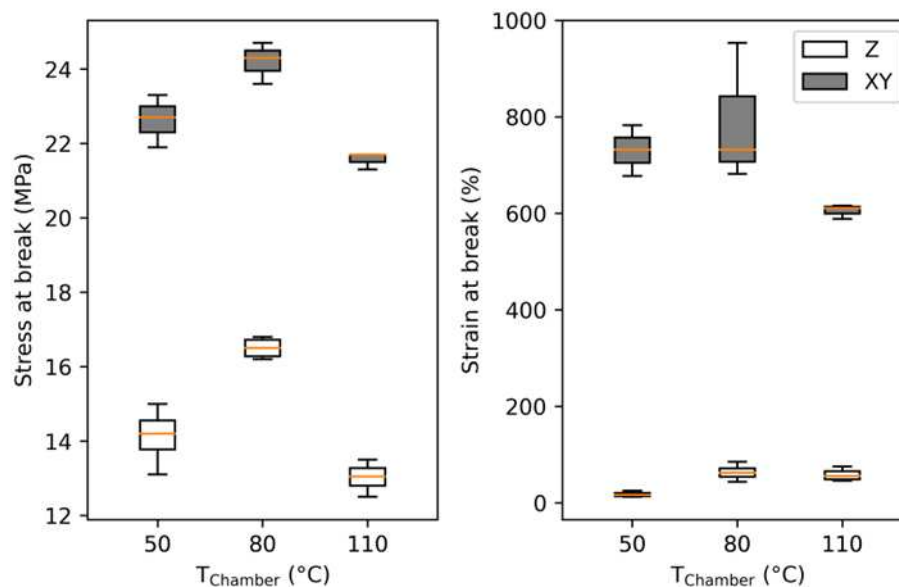
Figure 50   Tensile results of Arburg plastic freeforming (APF) samples printed in Z-orientation at different chamber temperatures and compared to XY-orientated samples.

The results of samples, printed at 80 °C chamber temperature, are way below the stresses and strains observed in the previous samples. Notoriously, the strain values dropped dramatically, resulting in a less ductile behavior. However, the values for stress at break measured for samples printed at 50 °C show a very high scattering. Samples printed at the highest chamber temperatures performed the worst, which may result from poor printing accuracy due to high material flow. These samples also obtained a rough surface, which could have acted as notches and drastically reduced the stress and strain at break values. Hence, thin samples or features printed vertically with this polymer should be printed at room or even lower chamber temperatures for better layer stacking and, thus, better layer adhesion.

Further optimization can be performed by optimizing the printing speed of the APF method, increasing the heating time, and reducing the acceleration forces acting on the printed samples. Interlayer diffusion can be enhanced at longer diffusion times or crystallization times. More extended diffusion can be realized at higher chamber temperatures or slower processing speeds. The results show that higher chamber temperatures lead to weaker samples; thus, slower processing might produce better results. However, in-depth optimization of the diffusion, coalescence, and crystallization may further improve iso-tropic material behavior.

Conclusions

In a nutshell, additively manufactured parts, with the used polyolefin, show anisotropy in mechanical behavior and morphology, among other properties, due to the generative addition of material and thermal history. Among other machines and process parameters, the environment of printing significantly matters. Especially for semi-crystalline materials, the print envelope temperature can strongly influence the morphology and resulting material properties. The idea behind this study was to generate an isotropic additively manufactured part by evaluating print envelope temperatures in two corresponding processes, namely material extrusion (MEX) and Arburg plastic freeforming (APF). The main conclusion of this study can be summarized as follows:

- A different crystalline structure in samples printed at 80 °C by APF and 110 °C by MEX was observed, and a time dependency was shown for the formation of a secondary crystalline structure.

- Weld lines between individual layers or even strands or droplets are no longer present, resulting in a homogeneous crystallinity over the cross-section when a chamber temperature of 110 °C was used in the APF process. This observation leads to the assumption that a more isotropic behavior can be expected at this chamber temperature.

- The yield strength of samples printed with different infill angles and at different envelope temperatures shows no significant difference. However, stress and strain values at break show an influence of the infill angles, which diminishes at higher print envelope temperatures. Hence, the intralayer bonding can be improved by increasing the print envelope temperatures.

- At higher envelope temperatures, crystallization times are prolonged, leading to better welding, resulting in a higher isotropic mechanical behavior for samples printed at higher print envelope temperatures. However, isotropy was not observed in samples printed along the Z-direction. The samples printed at 80 °C chamber temperature show the best performance but still are significantly lower than samples prepared in the XY-direction.

- APF specimens show better overall mechanical performance than MEX samples, most likely due to the lower porosity obtained by the APF method [206]. Since the chamber of the MEX machine was not actively heated, similar morphology could be observed but at higher print build platform temperatures. The influence of the infill orientation remains similar for APF and MEX.
- The effect of contour lines in the mechanical properties was similar for MEX and APF processes. It was found that tensile properties peaked at 45° infill with two contour lines but at different ambient temperatures for the two evaluated processes.
- At higher envelope temperatures, the TPO material is partially molten during printing, and hence, the material tends to flow, resulting in low geometrical stability. Therefore, the envelope temperature must be reduced if the printing time is extended, or high geometrical accuracy is needed. As a recommendation, the print envelope temperature should be kept in the range of the cold crystallization and the melting onset (i.e., 62 and 97 °C).

Future work

DMA analysis can be performed to understand better the crystallinity, phase formations, and influences on the segmentation behavior[154]. This characterization might also be interesting when applying similar approaches to materials with higher ethylene content, which are commercially available. However, regarding 3D printing, the selected TPO might already be on the edge of reliable printability, but others might be interesting for research because their melting temperatures and crystallinity decrease with increased ethylene content [69]. Printability of these copolymers is planned in future works. Also, a study on the diffusion and coalescence properties can further improve mechanical properties, especially in Z- Orientation as proposed by Beniè et. al. [19].

3.3.4 Closing Remarks on Publications B and C

Publication B provides an optimization procedure for mechanical properties for amorphous polymers like the investigated PMMA grade. Using a fractional DoE for screening of different parameters and further optimization of the higher impacting factors by defining a full DoE. It was shown that optimization of the part filling leads to optimized tensile properties for brittle polymers. Further, the correlation of the specific volume and processing conditions of the APF was discussed and provides a novel approach for better understanding of the processing conditions. In Publication C the chamber temperature was proven to be critical for semi-crystalline polymers. The morphology can be optimized to reduce the anisotropy of the tensile properties. However, still lower mechanical properties are present in Z-Orientation, which was also shown for other polymers in the literature [93, 106, 162, 283]. A full DoE was also used in this publication, showing the potential for parameter optimization for semi-crystalline polymers. Therefore, the second hypothesis "*A Design of Experiments approach on processing parameters of the Arburg plastic freeforming can be used to improve the mechanical performance of 3D-printed parts.*" was proven by Publications B and C. Further, hypothesis three "*Process parameters optimization can improve anisotropy in APF-manufactured parts from semicrystalline polymers.*" can be accepted based on Publication C.

4 Medical Applications of Arburg Plastic Freeforming

4.1. State of the Art

The APF is a unique and promising material jetting AM technology. The machine, supplied by the company ARBURG GmbH & Co KG (Lossburg, Germany) is suitable for a clean room environment with slight adaptations [14]. Therefore, it is interesting for the fabrication of personal medical items like patient-specific implants (PSIs). APF is already in use in the manufacturing of medical implants at the company Samaplast AG (St. Margrethen, Switzerland) [223, 226, 227]. Therefore, already established polymers are processed, which are usually used in traditional manufacturing like injection molding or extrusion. As an example, the medical grade PC-U Bionate® supplied by DSM Biomedical (Geleen, Netherlands) and the bioresorbable poly(L-lactide) Resomer® supplied by Evonik Industries AG (Hessen, Germany). However, academic studies dealing with the fabrication of PSIs using the APF are limited. Welsh et al. [276] studied the drug releasing rates from vaginal rings manufactured by APF. They concluded that APF can be used for the processing of drug loaded polymers in various complex geometries. Mele et al. [169] studied the impact behavior of 3D printed PC-U cranial PSIs. They showed that these implants can withstand impact energy up to 12 J and concluded that the integrity of the implant in daily life loads is provided. Additionally, they showed the high potential of the APF technology in the fabrication of complex PSIs, which was also presented by Neff and Petereit [186]. However, optimization of the APF processing parameters to improve the mechanical properties of the printed polymer and optimization of design considerations are still needed.

Further, Additive Manufacturing can be used to produce multi-material parts, like a hard-soft combinations to improve an overall part performance [185]. Therefore, it is important to provide a good inter material adhesion for proper load transfer and functionality of the part. Since parts are generated by layer stacking complex geometrical bonding technologies, knowledge from traditional woodwork can be applied to these multi-material parts. Ermolai et al. [56, 57] showed the enhanced mechanical performance of interlocking geometries for two incompatible polymer grades. Heyndrickx et al. [103] presented a better mechanical performance for non-interlocking geometries for polymers with similar polymer chemistry. Furthermore, multi-material printing was already studied for drug releasing supplies like vaginal

rings [52] or 3D-printed pills [165]. They showed the high potential of delayed drug release due to personalized shell thicknesses of the drug delivery devices. Later, they also used the APF technology to combine the potential of multi-material parts and medical applications as presented in the literature [185, 186].

4.2. Implants fabricated by ARBURG Plastic Freeforming

4.2.1 Introduction to Publications D and E

Publication D provides a mechanical study of cranial implants manufactured from different polymers using the APF technology. As a benchmark, a comparable implant from bone cement was produced by indirect AM as already shown in the literature [123, 130, 254]. Publication D shows the effect of different part orientations on mechanical properties and processing time of structural parts for medical applications.

Publication E demonstrates the concept of a multi-material rib replacement produced in a single step AM procedure. The implant was designed based on a CT-scan model and was manufactured from two different Bionate® grades. A suitable connection interface was tested prior using multi-material tensile specimens. According to the literature, the mechanical performance of a multi-material is greatly related to the interface [56, 57]. The implant samples were then fabricated by the APF technology, using two polymers. A needed support structure was manufactured from the harder grade and removed manually after the AM procedure. The implant was then implanted into a human body donor as part of the feasibility study.

The presented publication D is slightly different from the original, to fit the style and language of this work. The original was submitted as: _Hentschel, L., Petersmann, S., Waly, C., Schuschnigg, S., Salinas, M., Arbeiter, F., Schäfer, U. & Holzer, C. (2023). Impact properties of cranial implants fabricated by Arburg plastic freeforming, Journal of Applied Science_

Publication E was originally submitted and accepted as: _Hentschel, L., Petersmann, S, Gradischar, A., Lebschy, C., Lindenmann, J., Smolle-Juettner, F., Gonzalez-Gutierrez, J., Dias, A., Kynast, F., Hammer, N., Schäfer, U. & Holzer, C. (2023). Mulit-Material Implant Structures with Medical-Grade Polyurethane via Additive Manufacturing AIP Conference Proceedings (PPS-38)_

Beside these publications other related work was published in relation to this topic but is not included into the thesis and listed below:

- Conference contribution: _Hentschel, L., Chawla, C., Gonzalez-Gutierrez, J., Petersmann, S., Kynast, F., Gardischar, A. & Schäfer, U. (2021). Clinical_

implementation of patient specific polymeric implants, Surface in Biomaterials Foundation – BioInterface 2021 (online)

- Conference contribution: Holzer, C., Hentschel, L., Petersmann, S., Gardischar, A., Chawla, C., Kynast, F (2022). *Systematic Development of Additive Manufactured thermoplastic Rib replacement implants*, International Conference of the Polymer Processing Society, Fukuoka, Japan (online)

- Conference contribution: Heyndrickx, A., Hentschel, L., Cardon, L., Holzer, C. (2022) *Production of multi-material parts for medical applications, considering the bonding and adhesion strength of deposited materials by use of the freeforming additive manufacturing technology,* 2nd International Polymer Process Innovation Conference, Lavrion, Greece

Impact Properties of Cranial Implants Fabricated by Arburg Plastic Freeforming

L. Hentschel, S. Petersmann, C. Waly, S. Schuschnigg, M. Salinas, F. Arbeiter, U. Schäfer & C. Holzer

Abstract

Additive manufacturing offers tremendous potential for patient-specific implants (PSI) for the medical sector. These PSIs profit from the high accuracy, accessibility, lower cost, and shorter production times. Mostly expensive inorganic materials and polyetheretherketone are used for such applications. In this study, promising low-cost polymers polymethylmethacrylate (PMMA), polycarbonate (PC), and polycarbonate-urethane (PC-U) are studied for their impact behavior in comparison to a traditional bone cement implant. Implant samples are printed in different orientations using Arburg plastic freeforming, a material jetting process, and tested by an instrumented drop weight test. It was shown that printed samples could not reach the mechanical performance of the bone cement samples and did not show a significant influence on the orientations. Further, tensile, flexural, and Charpy impact samples have been printed in two different orientations. It has been shown that samples printed in XZ orientation have higher impact values and flexural strength, but lower stiffness and tensile strength. The influence of part orientation on the impact behavior of printed parts was analyzed and presented as alternative polymers for PSIs in the craniomaxillofacial region. PMMA might be a considerable choice due to the results from the impact testing, whereas PC-U is already established as implant material.

Introduction

Additive manufacturing (AM) has become an important production technology in almost every industry area. Especially complex geometries, prototypes, and products at low quantities are points of interest for AM methods. Due to low quantities and personalized products, AM

gained more interest in the field of medicine and healthcare, including surgical models, tools, prototypes, or even implants [110, 119, 212, 221, 230]. Craniofacial reconstruction is of particular interest for patient-specific implants (PSI) due to the individual and complex geometry in this region of the human body. Accurate reconstruction in this region is further important due to aesthetic reasons, to protect the patient from any social side effects. Reconstruction of the craniofacial region mostly takes place due to a tumor seduction or trauma [109, 116, 163, 202]. Some PSIs have already been produced additively and implanted in human beings and are made of metals [177, 196, 251], ceramics [26, 222, 234], and rare cases of polymers [81, 194]. Polymers do offer some advances due to their lower hardness, x-ray translucency, chemical resistance, and thermal properties but may lack mechanical performance. Therefore, high-temperature thermoplastics like polyetheretherketone (PEEK), are used for such applications, which are expensive and difficult to process in AM [169, 202]. Materials used for implantable devices must fulfill certain standards, biomechanical and mechanical properties, and criteria according to the Food and Drug Administration (FDA) or Medical Device Directive (MDD), depending on the application and location, which makes the application of new materials more difficult [45, 59, 97].

Former studies show the potential of other polymeric materials such as polypropylene (PP) [31, 125, 229], polycarbonate (PC) [198], polymethylmethacrylate (PMMA) [1, 24, 115, 280], and thermoplastic polyurethanes (TPU) [127, 281] (e.g. polycarbonate-urethan (PC-U) [55, 74, 169]) among others to be used in medical applications. Compared to PEEK these polymers are more affordable and better processable but show worse mechanical performance and biomechanical properties [280][261]. PMMA, PP and PC-U are already used for implants in specific areas due to their unique properties but are limited in charge of bone replacements due to the significantly lower stiffness and ultimate strength. However, it is reported that implants made from inorganic materials are too hard and stiff for their purpose and hence harm the healthy sections of the bone or may lead to bone fatigue instead of the implant [175, 261]. Furthermore, metallic bone replacements in the craniofacial region show other uncomfortable properties like increased sensitivity to temperatures and they are also not x-ray translucent, making further cancer investigation impossible [175, 202].

PMMA was also already used for cranial reconstruction as a two-component reactive material, formerly known as bone cement. It is delivered as a liquid and powder material in a sterile package and is mixed and formed traditionally by hand during the operation. The manual forming results in a low geometrical accuracy in terms of fitting and reconstruction of the curvature and hence leads to a deformation of the appearance of the patient. To improve the geometrical accuracy of the resulting implants, wax elimination, milling, AM, and indirect AM were used. By indirect AM, personalized molds were produced to form the implants with bone cement directly in the operation theater. Some studies show the application of this technology

and its advantages [115, 203, 221, 252, 280]. Further, the durability of the PMMA bone cement was already shown [265]. However, the production of such a mold is time and material consuming. Additionally, PC already has been shown as possible material for cranial reconstruction [198]. This material does not have a long medical history but shows a high processability in AM technology and became a material of choice for material extrusion-based AM [39, 214]. However, many types have been improved for additive manufacturing and are commercially available, but none have medical approval. PC-Us, on the other hand, which exhibit especially high biocompatibility and are already in use for human implants, are not yet available in filament form [20, 55, 74, 169, 207]. Such materials are available in different fractions of hard and soft segments, in detail in the range of 80A to 75D Shore hardness. This polymer is used i.e. for spinal disc replacement or other types of soft tissue due to its low hardness [55, 74, 223]. Conversely, these polymers show low rigidity when it comes to bone replacement but may still be sufficient. Further, these materials are tricky to process and must be kept in a dry state to avoid any hydrolysis during processing [169, 201]. The hydrophilic nature also leads to a small swelling and reduction in mechanical performance when kept in liquid as shown by Petersmann et al. [201].

When it comes to AM of PSIs, a reliable and accurate method such as ARBURG plastic freeforming (APF), invented by ARBURG GmbH & Co KG (Lossburg, Germany), among others, is a good choice. The machine itself is mostly manufactured with stainless steel and can further prevent contamination due to the closed building environment [14, 224, 226, 227]. Furthermore, the machine is suitable for clean room applications with a few adaptations. The working principle of this machine differs from every other technology used for AM and is patented by the company. In a nutshell, the machine is composed of two small injection molding units to melt the polymeric granules (build and support material) by rotation of the screw and provides the needed processing pressure by the screw stroke. After the plasticization unit, a piezo-electronic shut-off nozzle operating at a frequency of up to 250 Hz is used to partially deposit the polymeric melt in the form of a droplet at a size of roughly 0.2 to 0.3 mm [34, 97, 179]. However, the droplet aspect ratio (DAR), defined by the ratio of the drop width to height, is influenced by the nozzle diameter, which is 0.2 mm by default. APF has already been proven for its good performance when it comes to mechanical properties and reliability [34, 99, 106, 206, 276]. Further, the feedstock does not have to be formed into a filament in a previous step, which is especially important in the medical field. Hence, already-approved polymers can be used in this process [97]. One downside of the technology is the relatively high afford of material qualification and optimization [53, 97, 99, 106]. Benié et al. [19] further proposed another approach of parametrical optimization for AM, for the APF process. The print orientation also shows a high impact on the mechanical performance of a printed part [34, 82, 97, 211]. Simple specimens or cantilever beams can be printed optimized

for the force path, but more complex shapes such as cranial reconstructions are restricted by geometric constraints such as overhangs, ground surfaces, and limited building space. Hence, an anisotropic behavior is present in complex parts and can impact part performance [93, 100, 162].

In this study, three different kinds of polymers, namely PC-U, PMMA, and PC, are used to form an example cranial implant in three different printing orientations. These samples are tested for impact strength on a drop weight measurement device. The results are compared to each other and further to an indirect AM-formed bone cement sample, as a benchmark. The results show alternative materials and processes for cranial implants and further applications.

Material and Methods

Materials

Four different polymers are tested and compared to each other. Three of them are available as granules and the last one is delivered as a two-component reactive powder and liquid combination also known as bone cement. This *bone* cement is a special type of PMMA and was supplied by Heraeus GmbH (Hanau, Germany) under the tradename Palacos® R+G. The material was supplied by the Medical University of Graz after the material expired but still was usable for these experiments.

Further, a granule-type PMMA, Cyrolite® MD H12 supplied by Röhm GmbH (Darmstadt, Germany) was used for processing in the APF process. The material was dried in a vacuum dryer at 80 °C for at least 6 h, as recommended. This polymer was designed for the extrusion process and has a relatively high viscosity, which leads to high processing pressures. The polymer shows a high stiffness and is transparent due to the amorphous morphology.

The PC used was supplied by Mitsubishi Chemical Europe GmbH (MCE, Duesseldorf, Germany) under the tradename Xantar®. It is usually used for injection molding and already has some applications in the healthcare area. It shows a lower viscosity compared to the PMMA type since it is built for injection molding and hence is more suitable for the APF process. It shows lower stiffness than PMMA and is also transparent due to its amorphous nature.

The third polymer used for printing is PC-U with the tradename Bionate® 75D supplied by DSM Biomedical N.V. (Geleen, The Netherlands). Prior to processing the material was dried at 80 °C for at least 4 h in a vacuum dryer and was further kept in a dry state during processing. Since this polymer is already approved for invasive usage, it has the highest potential to be used in clinical studies due to its medical history. It is the hardest grade available yet and hence has the highest stiffness but is still orders of magnitude below the other investigated polymers. Furthermore, the polymer shows a semi-crystalline nature in contrast to the other polymers. In Table 23 some reported properties from the used polymers are listed.

Table 23 Physical properties from Palacos® R+G [51], Cyrolite® MD H12 [218], Xantar™ 22 UR [29] and Bionate® 75D [49] given by their individual suppliers.

	Palacos® R+G	Cyrolite® MD H12		Xantar™ 22 UR		Bionate® 75D	
Melt Volume Rate [cm³ 10min⁻¹]		6[a]	230 °C 3.8 kg	10	300 °C 1.2 kg	14	224 °C 5 kg
Density [g cm⁻³]	1.18	1.18		1.2		1.22	
Young's Modulus [GPa]	3	3.2		2.3			
Tensile Strength [MPa]	47.9	65.5		60		63.23	
Elongation at Break [%]				50		241	
Flexural Modulus [GPa]	2.7	3.4				1.79	
Flexural Strength [MPa]	71.56	117.2				70.3	
Impact Strength [J m⁻²]	4.64	19					
Vicat Softening Temperature [°C]		105		148		56	

[a] This value was calculated from the given melt flow rate and density from the reference.

In addition, a soluble support material was used to form the complex structures especially for the different orientations. The support material used was ARMAT® 11 supplied by Arburg GmbH + Co KG and is soluble in water. Depending on the orientation the amount of support material differed and hence dissolving of the support structure could last up to 6 h.

Specimen preparation

Some materials have been qualified in a previous step as already published for PMMA [97]. PC-U and PC have been qualified in a similar approach. In a nutshell, processing temperatures for a stable process pressure are set for each material. Plates (20 x 20 x 5) mm³ are printed at different settings of the *DAR* on a single build platform. Later their appearances are controlled visually, and densities are measured by the Archimedes principle. The *DAR* setting, at which the bulk density or the highest value of density is reached, defines the optimal *DAR* range. For better mechanical performance a lower value is chosen, to force a slight overfilling, which is especially important for brittle polymers [99]. Table 24 gives an overview of the used processing parameters in the APF process.

Table 24   Processing parameters for the Arburg plastic freeforming for the used PMMA, PC and PC-U.

	PMMA	PC	PC-U
Temperature zone 1 [°C]	215	230	210
Temperature zone 2 [°C]	230	250	225
Nozzle temperature [°C]	235	295	220
Chamber temperature [°C]	100	120	80
Dosing stroke [mm]	8	6	7
Backpressure [bar]	170	80	50
Screw speed in [m s^{-1}]	4	4	4
Discharge value [%]	67	50	65
Drop aspect ratio (DAR)	1.30	1.095	1.30

Additionally, tensile bars according to ISO 527-1A [142] and Charpy testing bars according to ISO 179-1 [140] were printed in two different orientations, namely XY and XZ. Five samples have been printed in parallel on one build plate, in total five tensile bars and 15 Charpy testing bars have been printed for each polymer and each orientation. Figure 51 shows the building plates with the different orientations and geometries. For the tensile bars printed in XZ-orientation, support material was needed and later removed by dissolving in water.
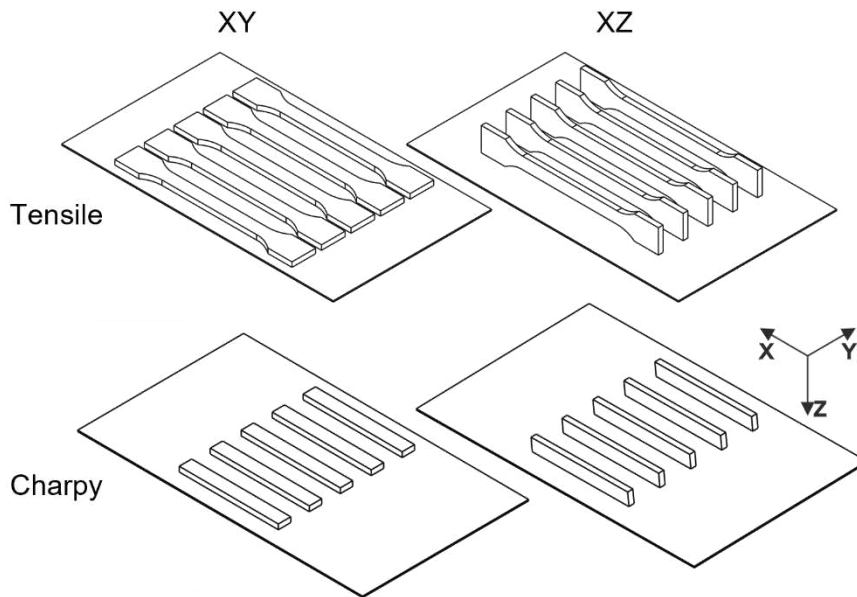
Figure 51 Arrangement of tensile and Charpy specimen on the building plate in two different orientations: XY and XZ.

Printing of the implant samples was performed on an Arburg freeformer 200-3X supplied by Arburg GmbH + Co KG on disposable PC/ABS blend rough building plates. Circulating air driers, attached to both hoppers, keep the polymers in a dry state during the processes. This is especially important for the long printing jobs as the samples are rather large and can last up to 7 h. Cranial implant samples are printed in three different printing orientations (XY, XZ and XY45) as demonstrated in Figure 52.
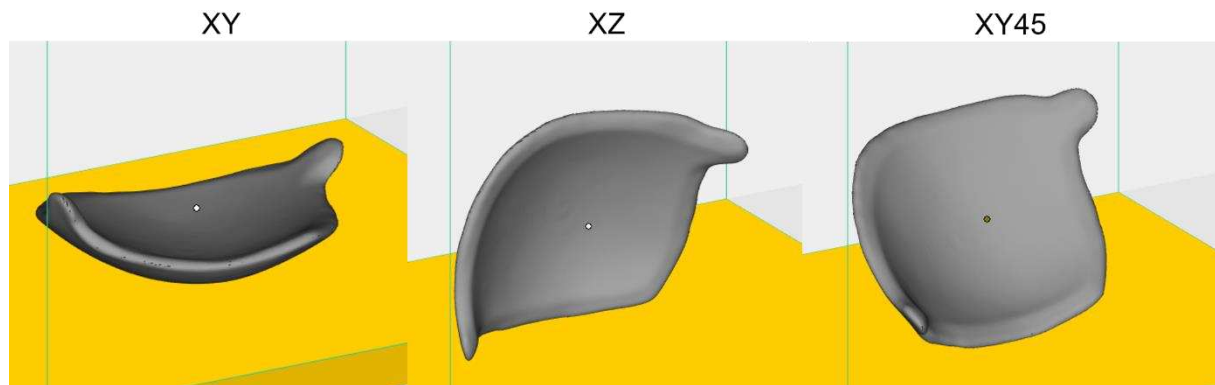
Figure 52 Representations of the implant models at different print orientations.

Based on the implant model shown in Figure 52, a mold was designed and printed on a Prusa i3 MK3 (Prusa, Czech Republic). A PET-G filament supplied by Mitsubishi Chemical Europe GmbH (MCE, Duesseldorf, Germany) was used and processed with a 0.4 mm nozzle and standard settings, provided by the manufacturer. After printing, the separation plane of the mold was sanded by hand, to ensure sufficient closing of the mold halves. For easier separation of the final part from the mold, a foil was laid into the mold. For mixing, the powder

component was put into a polymeric cup, the liquid component was added and mixed by hand until a homogeneous mass was archived. The mass was then placed in the mold at a given mass and distributed using a small spoon, before the mold was closed. The mold halves were then clamped (Figure 53a), and the polymer rested for at least ten minutes as recommended by the supplier. Afterwards, the finished part (Figure 53b) was removed from the mold and the edges were smoothed by hand. In total four samples from two molds have been fabricated.
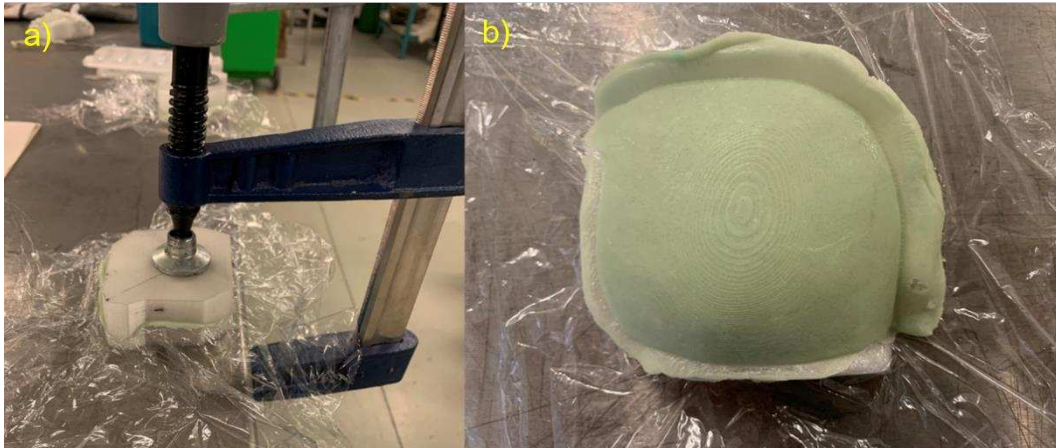
Figure 53   Pictures of the manufacturing of the bone cement samples using the 3D-printed mold.

Mechanical and physical testing

The tensile, bending, charpy and impact tests were carried out at 23 °C and 50% r.h. and for each polymer and printing conditions at least five specimens were tested.

A universal testing machine Zwick Z250 (ZwickRoell GmbH + Co KG, Ulm, Germany) was used for tensile testing. A testing speed of 1 mm min^{-1} was applied until an elongation of 0.25% was reached for measuring of the tensile modulus and later increased to 50 mm min^{-1} until failure. This testing procedure is in accordance with ISO 527-1, to accelerate the testing procedure, for high elongations. The machine was equipped with a 10 kN load cell. For clamping, mechanical grips were used and deformations were evaluated by the travel distance of the grips.

Further, 3-point bending analyses were performed using a universal testing machine Zwick Z10 (Zwick Roell, Germany). The machine was equipped with a 10 kN load cell and the three-point measurement setup. The tests were carried out at a testing speed of 2 mm min^{-1}, according to EN ISO 178. Deformations were measured using the makroXtens extensometer for deflections up to 10 mm if no other failure occurred beforehand. The support distance was 64 mm. Supports and loading edges were 5 mm in radius. The flexural modulus (E_f) and the maximum flexural stress (σ_{fM}) of the test specimens were evaluated according to EN ISO 178 [139]. E_f is evaluated by the slope of the flexural stress-flexural strain curve between 0.05 and 0.25% flexural strain. For tensile and flexural tests, it must be noticed that all stresses and

strains are considered as engineering values only taking into account the initial cross-section of the specimen.

For Charpy impact testing, the pendulum impact tester HIT25/50P (Zwick Roell, Germany) set up with a 2 J pendulum was used. Specimens were tested according to DIN EN ISO 179-2 [141] standard in notched and unnotched state. The notch was cut according to ISO 179-1A at 2 mm depth and 0.25 mm tip radius on the edgewise plane. The impact speed was set at 2.9 m s^{-1} according to standard. The Charpy unnotched (a_{cU}) and notched (a_{cN}) impact strength were evaluated according to standard (EN ISO 179-2).

A CEAST 9350 drop tower impact system (Instron Deutschland GmbH, Germany) was used to carry out impact tests on the implant samples. The machine fulfills the requirements of ISO 6603-2 [143]. For data acquisition, the CEAST DAS 64K (Instron Deutschland GmbH, Germany) was used. A drop height of 1 m was applied for the testing procedure and resulted in a testing speed of approximately 4.43 m s^{-1}. A hemispheric 22 kN piezo striker with a diameter of 20 mm and the model number M2098 was used. To minimize the reduction of velocity during testing, a mass of 10 kg was added on top of the holder mass of 4.3 kg. Further, a lubricant was applied to the striker to reduce the friction between the implant and the drop weight. During the measurement, values for time and force were recorded. Energy, displacement, and velocity were calculated using these measured values. Force-displacement curves were evaluated for each polymer and individual printing conditions. The damage force (F_D), which is defined as the first peak in the force-displacement curve, the maximum force (F_M), as well as the displacement at damage force (l_D) and the displacement until a maximum force (l_M) were evaluated.

In addition, density was measured for the tested samples using the Archimedes principle. Therefore, a digital scale supplied by KERN & SOHN GmbH (Balingen, Germany) and the corresponding measurement setup. For all density measurements, deionized water was used. The reference density of the water was corrected for the temperature, measured by a mercury thermometer. Samples were shaken in the water to prevent bubbles on the samples surface and inaccurate results of the analysis. For the material qualification procedure, printed cubes at different DAR values were measured. Furthermore, fractures of the implant samples have been analyzed after impact testing as well.

Results and Discussion

To validate the processing conditions of the different polymers, density measurements were performed. The goal is to reach the highest possible density (most likely the bulk density of the polymer) to ensure proper mechanical performance. However, due to changes in the morphology such as the crystalline structure, the frozen free volume or voids, the densities of printed parts can alter and the parts show weaker mechanical properties [99, 206, 211]. Figure

54 represents the results of the density measurements for the qualification of the process parameters. For PC-U and PMMA, the *DAR* values are about the same ranges and show similar flattening to lower settings. Even though the density values are different, the *DAR* setting of 1.30 was considered suitable for both polymers. For the PC samples, this flattening cannot be seen; instead, the density drops again at lower *DAR* settings. Hence, a *DAR* value of 1.095 was used for further samples made from PC. It should be noticed that the settings for the polymers PMMA [99] and PC-U [98] have already been optimized in previous works, but the values for PC have not yet been further developed. The values can further be optimized through variation of parameters such as the nozzle temperature, dosing, and the discharge parameters, but this is beyond the scope of this work.
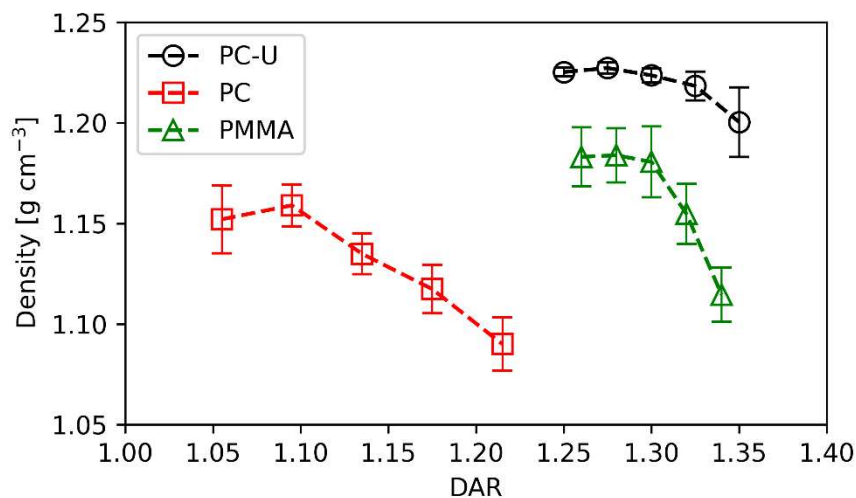
Figure 54   Density measurement of samples printed at the freeformer with changing *DAR* settings. Mean and standard deviation for n=5.

Figure 55 gives the results of the tensile tests performed on the printed specimens. As expected, PC-U shows a significantly lower Young's modulus compared to PMMA and PC (Figure 55a). However, a higher dependency on the printing orientation can be seen for PC-U, which is also true for the tensile strength (Figure 55b). The PMMA specimens show the highest stiffness, but lower strength compared to the PC samples. Also, there are no significant differences for samples printed in XY or XZ orientation. Comparing the strain at break values of the polymers, PC-U gives the highest results of around 90 % due to the more ductile nature of this material (Figure 55c). PC and PMMA are more brittle materials, hence the elongation at break will not exceed 10 %. Nevertheless, printed specimens usually show lower mechanical performance in comparison to traditionally manufactured samples [97, 206].

Figure 55   Tensile test results of the samples printed at the freeformer with three different materials (PC-U, PC, PMMA) and two different orientations (XY, XZ). The results are evaluated for Young's modulus (a), tensile strength (b) and elongation at break (c). Mean and standard deviation for n=5.

Figure 56 shows the results of the 3P-bending tests executed on the printed samples. PMMA and PC show comparable results in flexural modulus (Figure 56a) and flexural strength (Figure 56b), while the PC-U samples have an overall lower mechanical performance. Due to the thermoplastic and elastomeric nature of the PC-U these results were expected. However, the values reached with samples printed in XY or XZ orientation are similar; hence, there is no influence of the orientation in contrast to the tensile results. With the other two amorphous polymers the differences are noticeable and show lower values for flexural modulus but higher values in flexural strength when printed in XZ direction. The higher flexural stress values obtained at the XZ samples are due to a higher residual heat on the print surface due to lower layer building time. However, the differences in the flexural modulus cannot be explained that way. Considering the placement of the samples, internal stresses due to inhomogeneous cooling may enhance the measured flexural modulus slightly. Hence, this small enhancement, also slightly visible for the PC-U samples, results in no real changes in that property. It was also observed in previous studies, that the stiffness of printed tension samples are not or only slightly affected by different processing conditions [34, 211].

Figure 56   3P-bending results of samples printed at the freeformer with three different materials (PC-U, PC, PMMA) and two different orientations (XY, XZ). evaluated for flexural modulus (a) and flexural strength (b). Mean and standard deviation for n=5.

Furthermore, Charpy impact tests were performed in both un- and notched state. The results are given in Figure 57. Again, the PC-U shows a lower performance compared to the other polymers; however, the differences between un- and notched samples, in maximum force and impact strength is lower compared to the PMMA and PC samples. These results were expected due to the more brittle nature of PMMA and PC. PMMA is more brittle than PC, which can be seen in the impact strength results. Overall, the differences in XY and XZ direction are higher than in the 3P-bending results. One explanation can be given by the different surfaces due to the layer lines, which may act as little notches. Hence the differences are reduced in the notched samples, as demonstrated in Figure 57b and Figure 57d. The differences in impact strength for PC-U printed at different orientations are of further interest. In Figure 57c, the impact strength of the unnotched samples is higher if printed in the XZ-direction, whereas Figure 57d shows higher impact strength for PC-U when printed in XY direction. It must be mentioned that warping was observed for PC-U samples printed in XZ-orientation; hence, internal stresses occurred and may influence the measurement results. Another explanation may be the presence of residuals from the build plate for XZ-samples. This might enhance the impact performance of the printed samples but are cut if the notch is inserted. Therefore, there are no changes from the polymer itself, but more likely from the process.

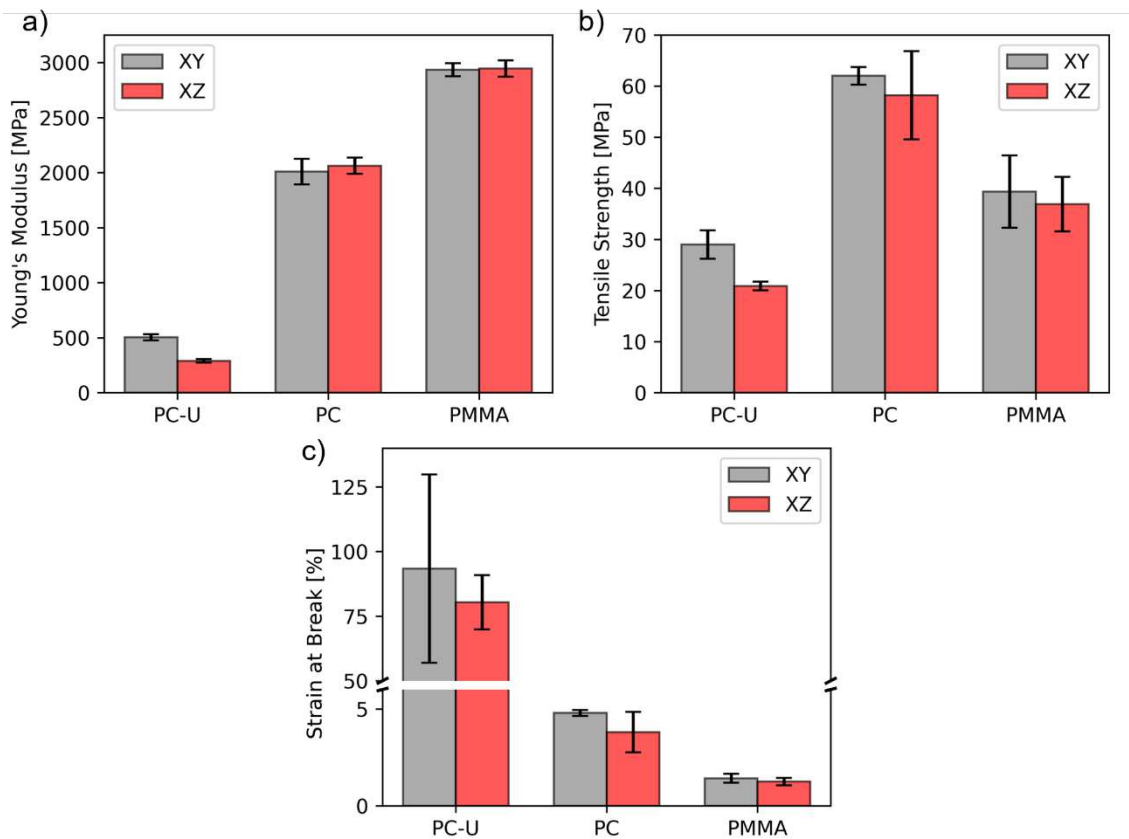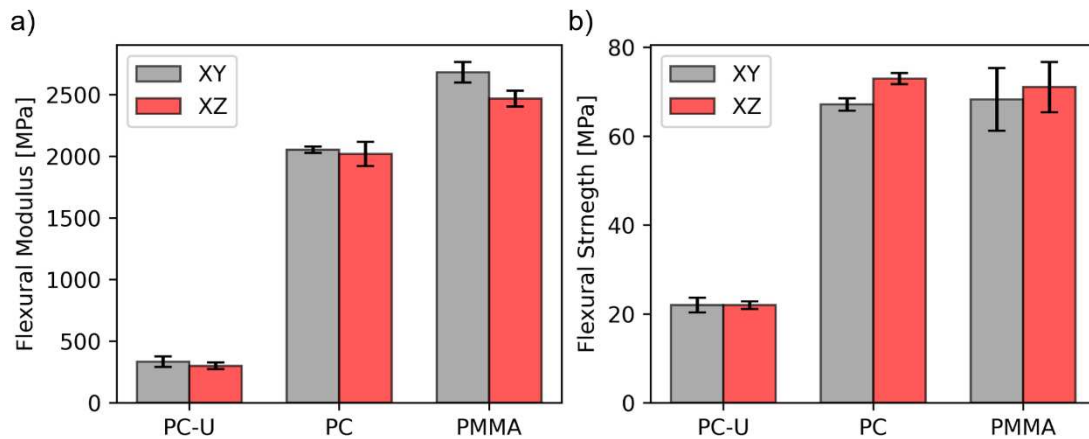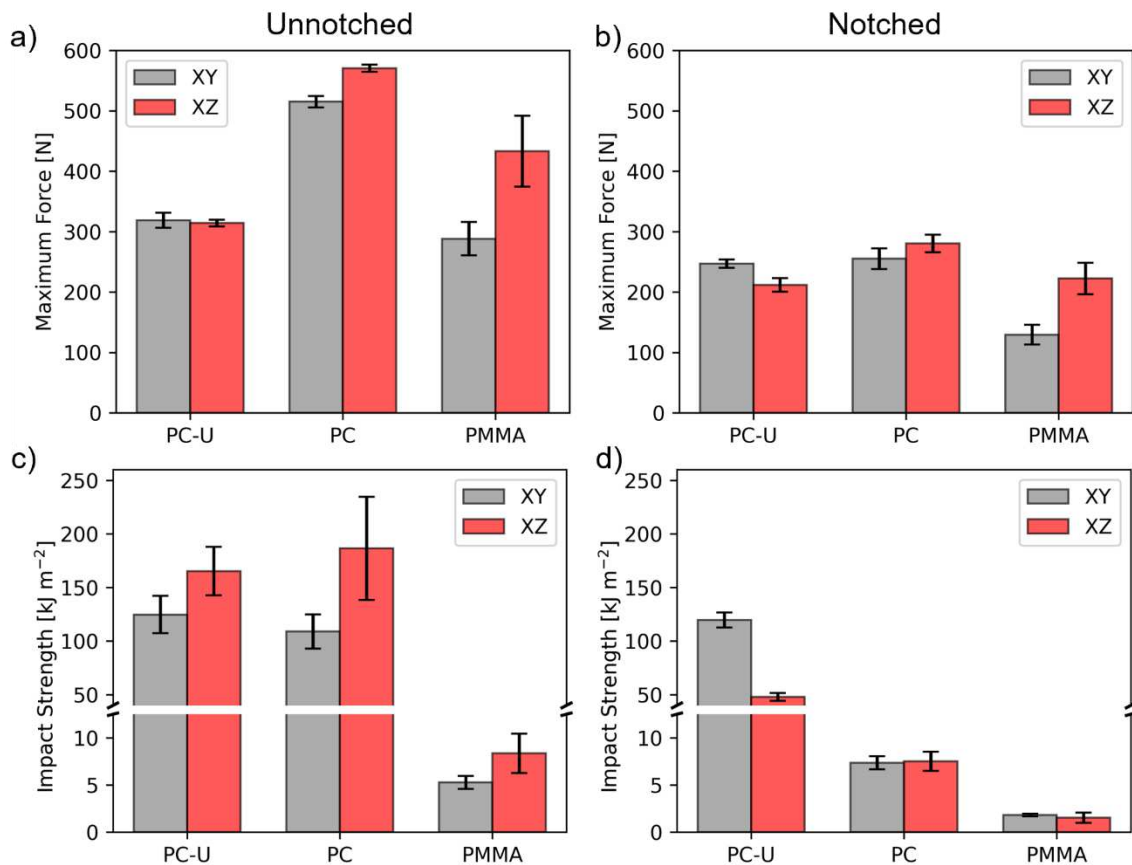Figure 57   Charpy impact test results of samples printed at the freeformer with three different materials (PC-U, PC, PMMA) and two different orientations (XY, XZ) evaluated for the unnotched maximal force (a), notched maximal force (b), unnotched impact strength (c) and notched impact strength (d). Mean and standard deviation for n=5.

As the main part of this study, implant samples were printed by means of the APF process at different orientations. Figure 58 shows the resulting samples, where one can suspect the different layer lines over the different part orientations. For the implants printed in XY-orientation, concentric ellipses can be detected, which are also visible in the bone cement sample since the negative was printed in a similar orientation. For the XZ and XY45 samples, a similar pattern of layer lines is visible, however, differences are still noticeable. The PC-U/XY45 samples must be pointed out due to visible artifacts on the inner surface. These might be a result of the in-situ warping of the sample. Hence, a shift in the part geometry occurs. Based on that, a low adhesion of the support material to the PC-U can be concluded, making ARMAT® 11 not the optimal solution for this polymer. However, the support material was suitable for the other geometries and polymers, and is still preferable for medical applications due to the water solubility. The surface of the implants was not further examined, but it was noticeable that the PC-U samples showed the worst surface appearance compared to the other materials. Further optimization of the processing parameters might be necessary for longer print jobs.
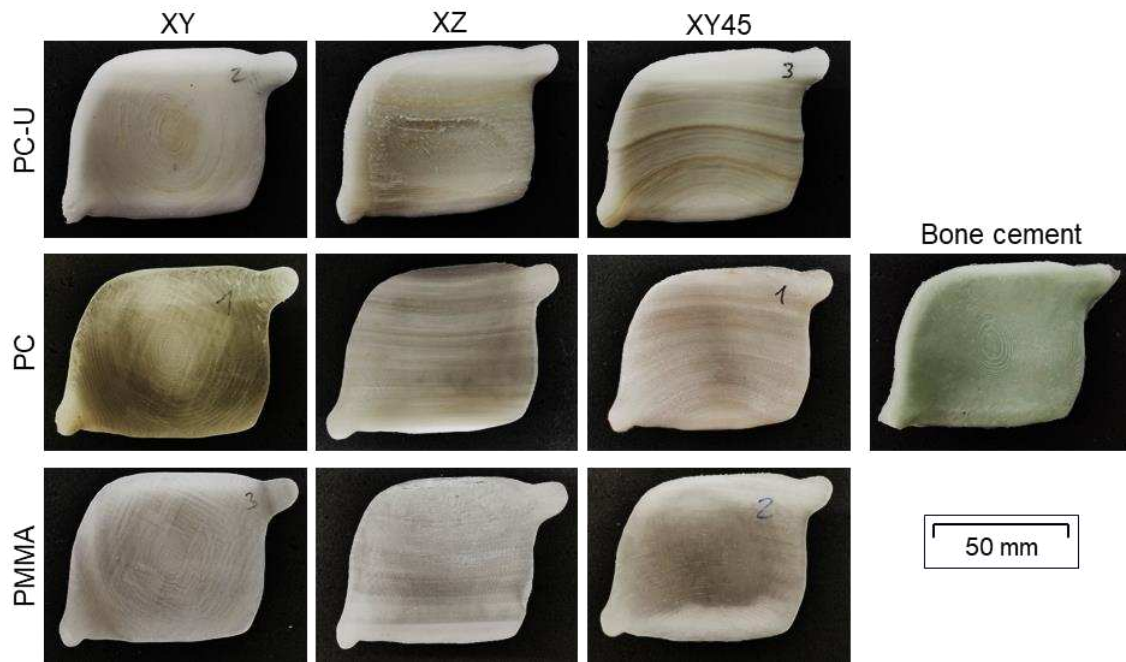
Figure 58 Photographs of representative implants printed at different orientations and with different polymers. A representative bone cement sample is also displayed.

The bone cement sample has a different contour, due to insufficient sealing of the separation line of the mold. However, this does neither affect the mechanical testing nor was considered in any other comparison, since all samples can undergo some post-processing. Further noticeable are the discoloring of the PC-U, mainly referred to local degradation of the polymer or a different crystalline structure due to the processing conditions. The PC samples also show a slight coloring effect noticeable in the XZ and XZ45 parts and a kind of regular pattern. This pattern may either interfere with the differences in the overhanging angle or the processing cycle. The machine must dose the molten polymer at a given dosing length, usually around 4-8 mm, and discharge the polymer until the melt cushion is reached. To deposit this amount of melt, 5 to 20 minutes can pass by, depending on the geometry and the usage of support material. Hence, a very large residual time of the polymer is present with this method and can lead to changes in the polymer morphology or even to degradation as can be detected in the PC-U samples.

Figure 59 displays the samples after impact testing with the resulting break patterns. Since the bone cement samples were prepared as the benchmark, the break patterns of these samples are aimed for. These samples are broken into three pieces of approximately the same size. The brake lines originate exactly at the impact point. It had to be noticed that no small fragments have been found after testing, which may interfere with the human body. Similar break patterns can be seen for the samples PC-U/XZ, PC-U/XY45 and PC/XY45. These three samples show break lines that are not in line with the printing layers. Only one breaking line in the samples PC-U/XZ shows a correlation with the layer orientation. PC-U/XY, PC/XZ,

PMMA/XY, and PMMA/XY45 broke into four pieces and PC/XY and PMMA/XZ even into five fragments. For the other samples, only a few break lines follow the layer lines of the printing orientation. In detail, the horizontal break line of all samples printed in XZ orientation. It can be concluded that the inter-layer bonding of the samples is sufficient even for more complex parts printed by APF with the given profiles. Further, it needs to be pointed out that the samples PC-U/XY and PC/XY tend to form small fragments. This is not recommended for implants since small fragments are difficult to remove and can lead to complications in the real application.
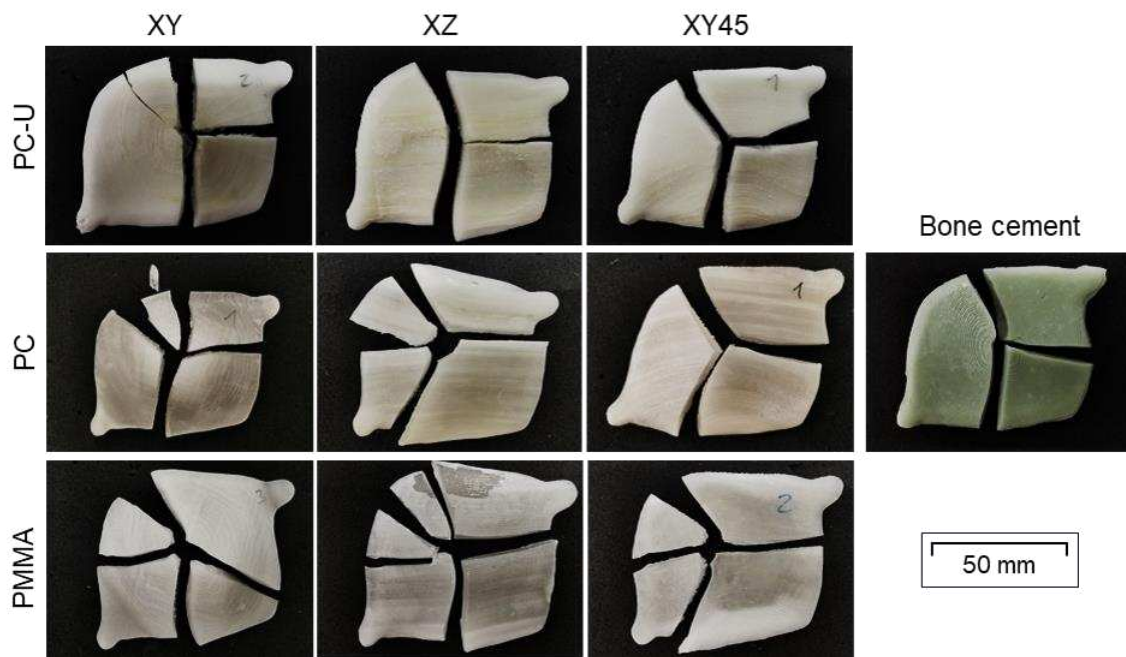
Figure 59   Photographs of representative implants printed with different orientations (XY, XZ and XY45) and polymers (PC-U, PC, PMMA) as well as a representative reference implant manufactured with bone cement after impact testing.

In Figure 60 the measurement results of the drop weight tests are displayed. The measured force is plotted over the displacement and split into the different print orientations with the bone cement samples as reference in all subplots. It clearly can be seen that the bone cement samples outplay the printed samples. However, PC/XY samples show a high maximum force, but at higher displacements. Further, these peaks appear after the damage force, which is considered as the first peak in the force-displacement curve. For most of the tests, the first damage has already been reached at low displacements of around 1 mm. Even though PC-U does show a ductile nature, the force-displacement curves show similar behavior for all the polymers. Nonetheless, PC-U samples withstand the lowest forces of all prepared samples, the PC/XY sample reached the highest maximum force of all samples. PC and PC-U samples show a higher displacement than the PMMA and bone cement samples, representing the higher stiffness of the PMMA-type polymers. However, the higher stiffness of the samples also leads to higher damage forces, for example, the PMMA/XZ samples can compete with the

bone cement samples also in damage force. Similar experiments have been conducted with PEEK implants, also considering different printing orientations. They found comparable results of printed samples and commercially available samples at specific processing settings [202]. In this case, the benchmark of the bone cement can almost be reached at the lower end.
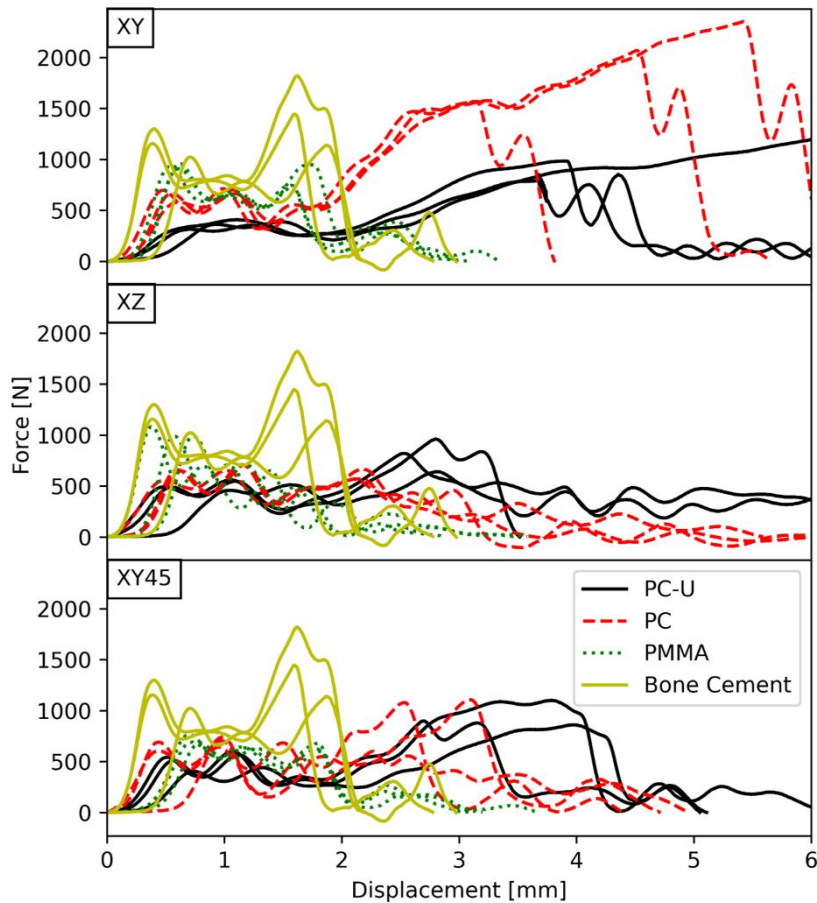
Figure 60   Impact force over displacement of the individual implant samples printed with different orientations (XY, XY45, XZ) and materials (PC-U, PC, PMMA) as well as the reference implants made of bone cement evaluated on the drop weight experiment.

Figure 61 shows the results of the impact tests in form of a box plot of the damaging force and the maximal force measured on the drop weight test. The yellow region represents the area measured for the bone cement samples, which cannot be allocated to a certain orientation. The results of the damage force again show that none of the printed samples are as resistant as the bone cement samples, only the PMMA/XZ samples are near the low end of the area. On the other hand, results of the maximum force show that the samples PC/XY and PC-U/XY are within the same range or even beyond. Comparing the different print orientations of the polymers PC and PC-U, either a constant damage force or a linear decrease from XY to XZ of the maximum force was detected. The samples printed from PMMA break the pattern and show comparable low values for the samples printed in PMMA/XY45 orientation. Compared to a similar study performed by Petersmann et al. [202] on PEEK implants printed

by means of filament based material extrusion, a lower impact of the orientation on APF printed samples was detected. The appearances of the fracture surfaces also altered a lot for these PEEK samples, which was not the case for the APF printed samples.
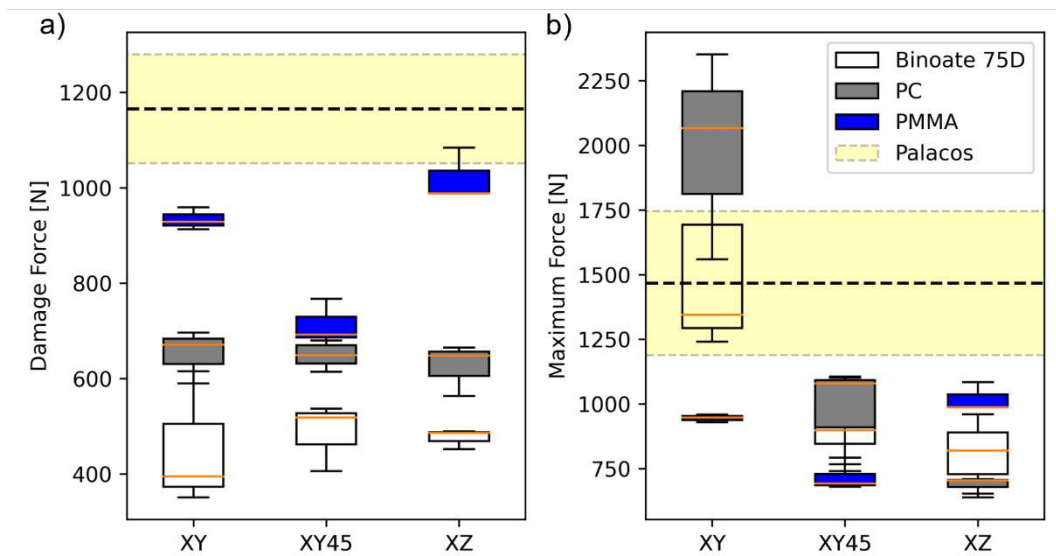
Figure 61   Results of the drop weight tests preformed on the individual implant samples printed with different orientations (XY, XY45, XZ) and materials (PC-U, PC, PMMA) as well as the reference implants made of bone cement. Five samples were tested per type.

To better understand the influence of orientation, the results are plotted against density. In addition, for a better comparison of the individual printed polymers, the results were set in relation to the highest archived values. Figure 62 shows the results of the relative damage force and the relative maximum force over the relative density, respectively. For PC and PC-U, there is a clear trend towards higher damage forces at higher densities. However, for PMMA this is not true for a single data point. In contrast, PC-U samples show a decline in maximum force to higher densities. Moreover, PC samples show exponential growth of maximum force to higher relative densities. The PMMA samples show a similar distribution of maximum force over density and again the same outlier. These PMMA samples were printed on XY45 orientation and obtained the lowest damage and maximum force but the highest density values. It was seen that due to overhang issues the contour lines did not bond to the infill in some areas, which may lead to a reduction in cross-section and hence weakening of the part. The correlation between the densities and the mechanical strength of polymeric specimens printed by APF has already been shown in previous publications [99, 206]. Therefore, it can be concluded that orientations have an impact on the printed samples, in particular for PMMA. A similar testing procedure was performed by Mele M. et al. [169], which concluded a high potential of PC-U Bionate® 75D to be used for PSI in the craniomaxillofacial region, ensuring the integrity of the implant up to an impact energy of 20 J. At this energy level, the first

indications of failure were detected. However, in this study, all samples were damaged but were tested with an impact energy of approximately 140 J. Based on that, other polymers show an even better impact performance but lack biocompatibility compared to PC-U. On the other hand, experimental studies comparing PMMA and Ti6Al4V cranial implants concluded a better overall performance of the titanium alloy implant. In fact, the higher stiffness and toughness of this material lead to a high energy absorption and less stress concentration in critical areas. Therefore, higher forces are needed to fracture the skull for implants with higher stiffness [261]. Since the most critical area for damage is likely to be the interface between the implant and the skull, the need for increased implant stiffness is questionable. Nevertheless, it was shown that higher deflections occur on the less stiff PMMA samples which is also considered as undesirable, due to possible damaging of the surrounding soft tissues in the real application [202, 261].
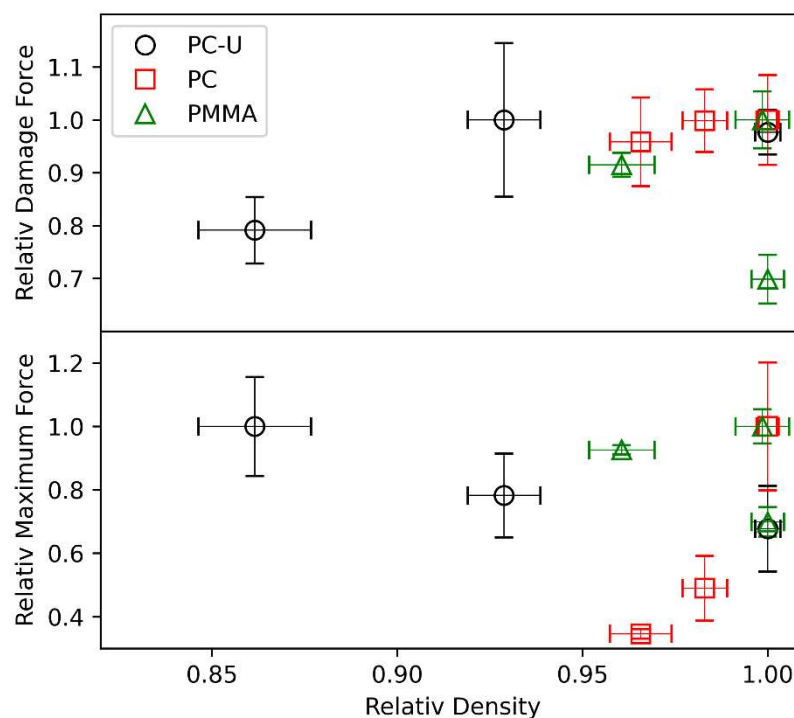
Figure 62   Results of the relative damage force over the relative density of the impact tests on printed implants for the different polymers. The relative values are calculated from the maximum values of the individual polymers. Mean and standard deviation for n=5.

Since most orientations show similar results, except for PMMA/XY45 samples, the processing data were analyzed for further evaluation. In particular, the manufacturing times until the implants are available are of interest. Figure 63 shows the building time, number of layers and the mean pressure of the different polymers and orientations. Interesting are the differences in building time with different polymers (Figure 63a), which is related to the different DAR values, explaining the slightly higher building times for PC samples. Nevertheless, PC

and PC-U show the same time changes at the print jobs. PMMA, on the other hand, obtains similar build times for the XY45 and XZ orientation. During longer processes with this material, bridging can occur which can lead to longer dosing times and hence prolong the building process. This might be an explanation for the longer building times in XZ direction compared to the other materials. The layer counts are the same for all polymers and gradually increase from XY, over XY45 to XZ as expected (Figure 63b). The pressure plot can be used as an indicator for quality control and must not display a high standard deviation or differences at the different orientations. High standard deviations can indicate an unstable process, while differences in comparing the other orientations may indicate other problems such as warping, wrong offset settings, or an unsuitable chamber temperature. The pressure looks constant overall for PC and PMMA, with slight changes for the different orientations (Figure 63c). For PC-U, higher fluctuations in the pressure, especially in the XZ samples, were recorded. It must be noticed that this material is rather tricky to process since thermal degradation can occur easily. The long residual times of this process can lead to degradation in the polymer melt which can be noticed in the process pressure. In this case, the XY direction caused the least deviation in pressure for PC-U. Also, the XY direction had the lowest building time, which makes this orientation preferable from this point of view. However, the support removal must be considered too in terms of production times.
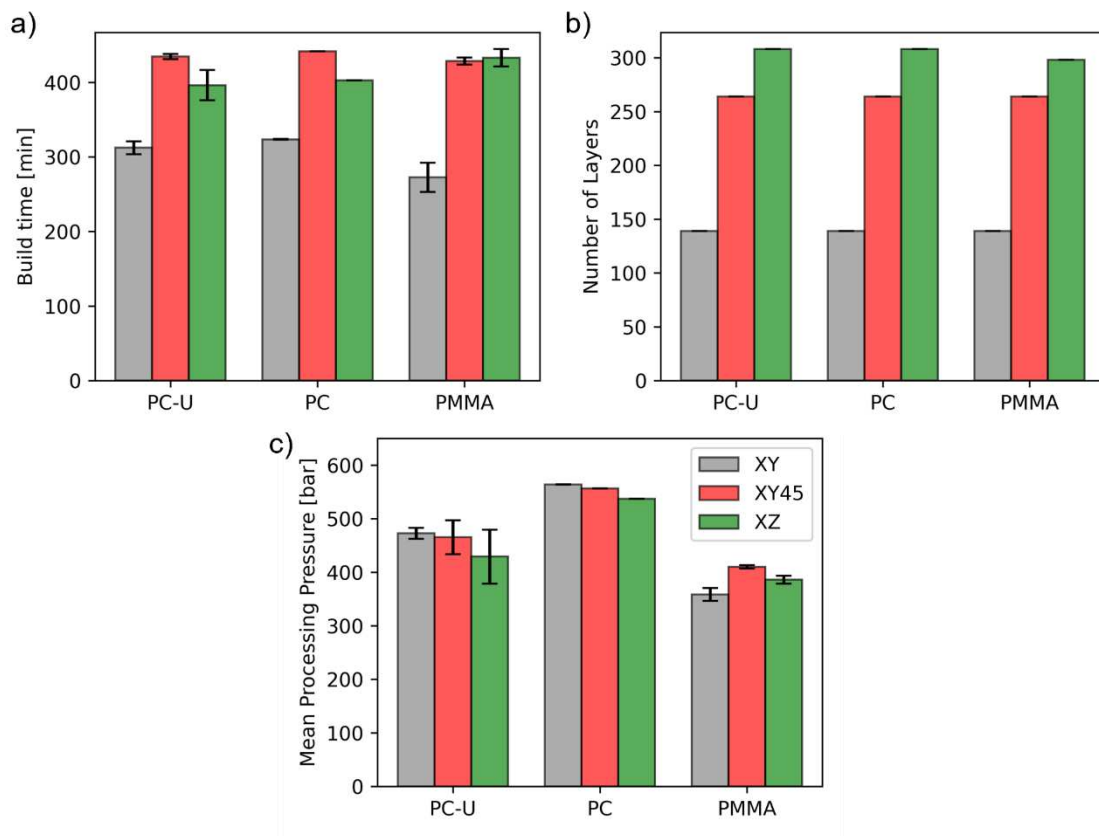
Figure 63   Process data of the APF process for different orientations (XY, XY45, XZ) and materials (PC-U, PC, PMMA) of the tested implant samples: The building time (a), the number of layers (b) and the mean pressure during the process.

The support material is removed by dissolving in water. The time for support removal is highly related to the support volume and the water temperatures. The highest volume of support polymer was used for the XY45 orientation, the second most for the XY and the least amount for the XZ orientation. Further, a huge amount of the support volume could already be removed manually for most of the XZ-orientated samples. This led to a short dissolution time and in the end a fast production time. Overall, considering the removal of the support material, all samples needed a similar production time of around 10 h in total, for starting the process to the finished product.

For the bone cement samples, the production time of the mold was around 12 h. The whole process of mixing, pressing, and removal of the finished samples took around 30 min. Further, the time for the design of the mold must be considered as well. Which can take up to 10 h, in addition to the modeling of the implant.

Direct manufacturing of the implants can offer some more advantages, such as the usage of different materials with adjustable properties for different regions in the human body. Furthermore, the implants can be directly incorporated with drugs for better healing or reduced inflammation [276]. AM also offers the possibility to form multi-material parts with unique

properties at specific locations of the part. An example is cranial implants using a PET-G core and a TPU shell with preferable stiffness and impact properties [127].

Conclusion

Tensile, three-point bending and Charpy impact testing were performed on samples printed in two different orientations and with three different materials, namely polymethylmethacrylate (PMMA), polycarbonate (PC), and polycarbonate-urethane (PC-U). Some influences of the orientation on the measured properties could be detected. Samples printed in XZ orientation show higher impact values and flexural strength, but lower stiffness and tensile properties. However, some differences are not significant and can therefore be neglected. As a main reason, the layer building time can be named, resulting in a higher residual heat of the previous layer, and hence improved inter-layer bonding.

Direct additive manufacturing of cranial implants from different feedstocks was researched to find a replacement for the rigid and expensive PEEK-type polymers or inorganic implant materials such as titanium. A standardized implant was manufactured in three different orientations and with three different polymers using the Arburg plastic freeforming (APF) technology. As a benchmark, implant samples of bone cement were produced by indirect additive manufacturing. All samples were tested by a drop weight test and compared to each other. The values of the benchmark samples could not be exceeded by any of the APF samples. However, the PMMA/XZ implants showed the highest damage forces and the PC/XY implants the highest maximum force, but at high deformations. Hence, improvements still must be made in order to fit the requirements. One approach to enhance mechanical performance is to thicken the implants, if the geometry can be altered, for compensation of the lower material properties. Additionally, more in-depth parameter optimization could lead to better results.

Overall, PMMA/XZ showed the most comparable results to the bone cement samples, which may be due to the similar polymeric nature. Bone cement is a PMMA-type polymer and therefore shares the brittle material behavior. PC, on the other hand, showed the highest forces during the test, but the damage force overall was lower compared to the PMMA samples. As expected, the PC-U shows the lowest values, except for the maximum forces for the XY samples. This material is the only medically approved polymer for long period invasive implants but is not as rigid as the bone cement sample. However, considering that the exact properties of bone are not known [181], and fixations are considered as the most critical points [261], the PC-U exhibits a high potential for such applications [169, 207].

In a nutshell, personalized medical implants greatly benefit from additive manufacturing in terms of precision, availability, and costs. However, more research must be performed on this topic to find a suitable selection of polymers, methods, and applications on the human body.

Acknowledgements

4.2.3 Publication E

Multi-Material Implant Structures with Medical-Grade Polyurethane via Additive Manufacturing

L. Hentschel, S. Petersmann, A. Gradischar, C. Lebschy, J. Lindenmann, F. Smolle-Juettner, J. Gonzalez-Gutierrez, A. Dias, F. Kynast, N. Hammer, U. Schäfer & C. Holzer

Abstract

Additive Manufacturing (AM) allows the creation of personalized medical models, tools, and implants. Patient-specific structures can be fabricated faithfully, quickly and reliably. The production of orthopedic implants by means of AM could greatly benefit from multi-material structures. The skeletal system is composed of hard bones and softer cartilage, performing different tasks in the body. Multi-material implant structures require biocompatible materials that can withstand in-body conditions for extended periods of time. Among possible material candidates, polyurethanes have been selected for further investigation. This project studied two medical-grade polyurethanes (with established clinical history for long-term implants) produced by DSM Biomedical with a Shore hardness of 75D and 80A. They were used to fabricate three-dimensional structures with the thermoplastic material jetting technique (MJT) known as Arburg Plastic Freeforming (APF). Tensile and bending specimens were produced for the individual polyurethanes by applying optimized processing parameters. Also, multi-material specimens were manufactured to analyze fracture failure at the interface between the two polyurethanes in tension. Based on information collected in this investigation, recommendations on preparing implantable structures such as rib replacement systems are given.

Introduction

Due to the high freedom of design and rapid production, additive manufacturing (AM) has become an important manufacturing technology over the last decades. Especially in medicine and healthcare, added benefits are found constantly [110, 119, 221]. Furthermore, the variety of materials for 3D printing applications significantly increased since they were developed. Different shaped feedstocks such as granules, filaments, or powders suiting the various manufacturing methods are common [83, 256]. Materials used for medical applications must fulfill several criteria, depending on the category of the applications according to the Food and Drug Administration (FDA) or Medical Device Directive (MDD). Since every production step needs to be certified, the validation of granules may be easier since they have to undergo fewer production steps compared to filaments or powders [97].

Further limitations for medical devices, like implants, come from the AM method or the machine itself. The Arburg plastic freeforming (APF) is a unique technology developed by ARBURG GmbH + Co KG (Lossburg, Germany), which can process original polymer granules. The corresponding machine, the freeformer, uses a plasticization unit similar to an injection molding machine for melting and applying the required processing pressure on the melt. Attached to that unit, a piezo-electronic shut-off valve, opening and closing up to 250 times per second, forms droplets out of the polymeric melt [93, 97, 99]. A schematic display is illustrated in Figure 64. Due to the droplet formation, this method is also referred to as material jetting technology, according to DIN EN ISO/ASTM 52900 [47]. The unique droplet formation of this technology leads to unique processing parameters, particularly the discharge value and the Drop Aspect Ratio (*DAR*), also known as the Form Factor. The DAR is defined as the ratio of the drop width to height (*W/H*) [53, 97, 99]. An advantage of the freeformer is its use of a heated chamber, hence a controlled ambient environment, which prevents contamination. The machine has two individual discharge nozzles and can process two different polymers. One of the nozzles is usually loaded with soluble support material, but other building materials can be used as well. Bigger versions of the freeformer series with three individual nozzles now are also available.
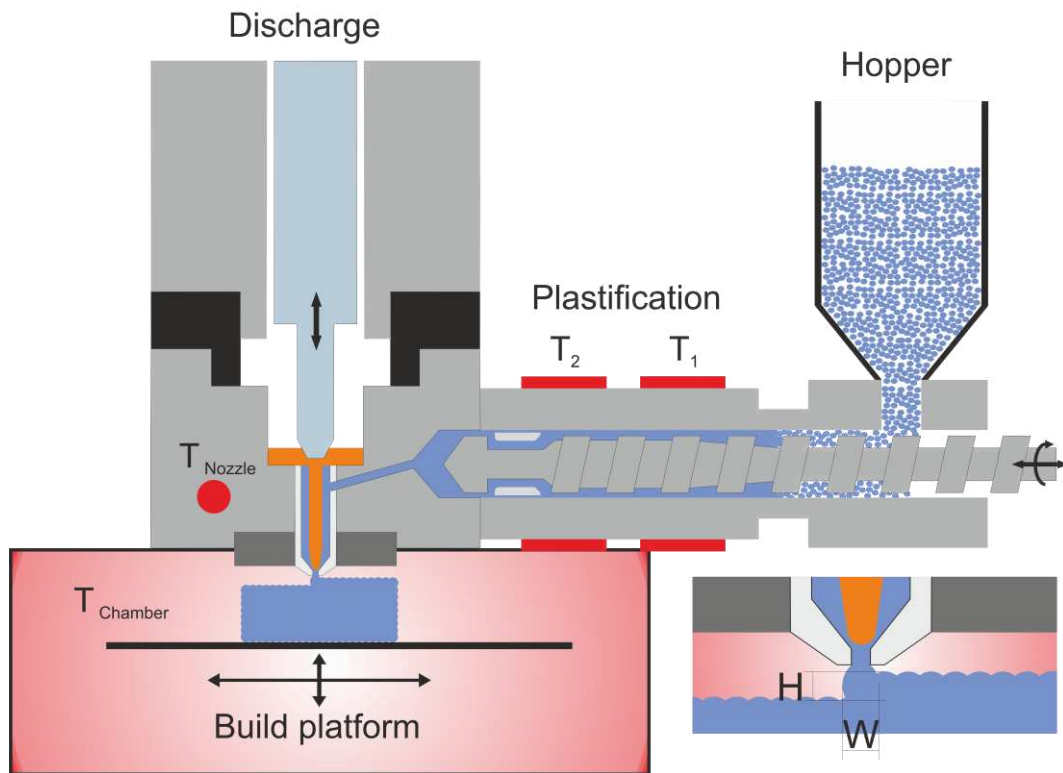
Figure 64 Schematic of the Arburg plastic freeforming principle adapted from Hentschel et. al. [99].

One type of polycarbonate urethane (PCU), manufactured by DSM Biomedical (Geleen, The Netherlands), with the tradename Bionate®, is gaining particular interest for medical AM, especially with the APF [20, 201, 207]. This polymer is available in different Shore hardnesses, ranging from 80A to 75D while maintaining the same polymer chemistry. Hence, the combination of different Bionate® materials is suitable for a multi-material approach, achieving a hard-soft mechanic. Therefore, a study on possible connection designs was performed and applied to a feasibility study on a multi-material rib replacement. With this study, a concept of enhanced multi-material implants shall be demonstrated to improve human healthcare in the future.

Materials and Methods

The materials used were the PCU type Bionate® 80A and Bionate® 75D, provided by DSM Biomedical. These are block-copolymers with different ratios of hard and soft components. The materials are specifically designed for medical devices and are already well-established. However, these materials are prone to hydrolysis at the 3D printing temperatures and must be dried before processing at least at 82 °C for 4 h in a vacuum drier [20, 207] to minimize the risk of hydrolysis attributable to residual moisture. Some material properties are given in Table 25a, and the chosen processing parameters are listed in Table 25b.

Table 25 Material properties provided by the supplier (a) and chosen processing parameters based on previous material qualifications and processing guides (b).

a)

Value	Bionate® 80A		Bionate® 75D	
Shore Hardness	80A		73D	
Density	1.19	g/cm³	1.22	g/cm³
Ultimate Tensile Strength	46.6	MPa	63.2	MPa
Flexural Modulus	28.7	MPa	1792.6	MPa
Melt Flow Rate (224 °C)	22 (1200)	g/10 min (g)	14 (5000)	g/10 min (g)

b)

Parameter	Bionate® 80A		Bionate® 75D	
Temperature Zone 1 (T_1)	180	°C	185	°C
Temperature Zone 2 (T_2)	185	°C	220	°C
Temperature Nozzle (T_{nozzle})	195	°C	217	°C
Temperature Chamber ($T_{Chamber}$)	80	°C	110	°C
Rotational Screw Speed	4	m/s	2	m/s
Back pressure	50	MPa	100	MPa
Discharge Value	60	%	65	%
DAR	1.15-1.20		1.30-1.35	

Specimens were manufactured with an Arburg freeformer 200-3X, provided by ARBURG GmbH + Co KG, with two individual nozzles. The polymers were pre-dried for 8 h at 85 °C within a vacuum drier. The hoppers of the freeformer are attached to circulating air driers, also set to 85 °C, to keep the granules dry during processing. The print job files were prepared in the Arburg freeformer software v2.30 (ARBURG GmbH +Co KG) for a nozzle diameter of 0.2 mm and a layer height of 0.2 mm.

To validate the processing parameters, in detail the DAR values, plates with dimensions of (20 x 20 x 5) mm³ were printed at different DAR settings (Figure 65a). The samples were used for density measurements using the Archimedes principle with a digital balance (KERN & Sohn GmbH, Balingen-Frommern, Germany) and deionized water. Based on these results, two different DAR values for each material were set for further experiments.

Five dog bone specimens according to ISO 527-1 standards were printed in XY direction at once for the single material test. Both DAR settings were applied and compared to injection molded samples. The samples are represented in Figure 65b.
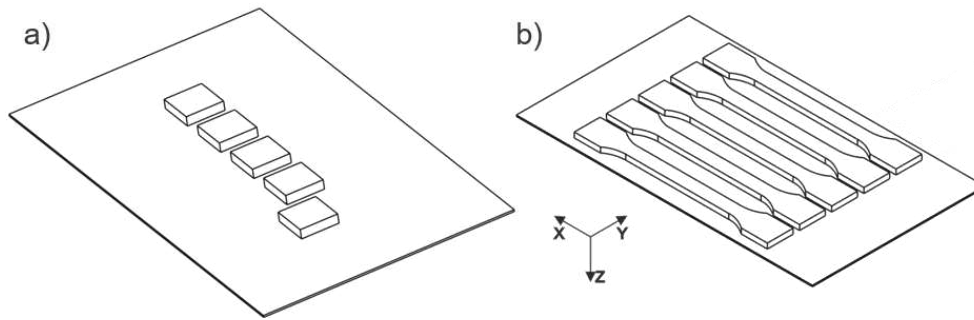
Figure 65   Drawing of the arrangement of the qualifications cubes (a) and standard ISO527-1 tensile bars (b).

To validate the adhesion or the strength of the connection between the two polymers, unique 2K-tensile bars with different designs of the transition areas were applied. These areas ranged from simple plane connections (V1 to V3) via alternating (V4 to V6) to interlocking (V7 and V8) designs. All samples are schematically displayed in Figure 66a. Based on the results a rib replacement implant was redesigned from a CT-scan model. A special connection for the sternum was made to sew the implant to the human tissue. Therefore, an array of holes was introduced into the design. On the other end, the negative form of a commercially available rib clamp was embedded in the CAD model to ensure a good fixation. The implant is supposed to be printed in a hard-soft combination. Since only two individual nozzles are available, a break-away support was designed in order to be printable and was made with the harder material. Figure 66b shows the rib replacement with the soft part in green, the hard part in blue and the support indicated by the transparent part.
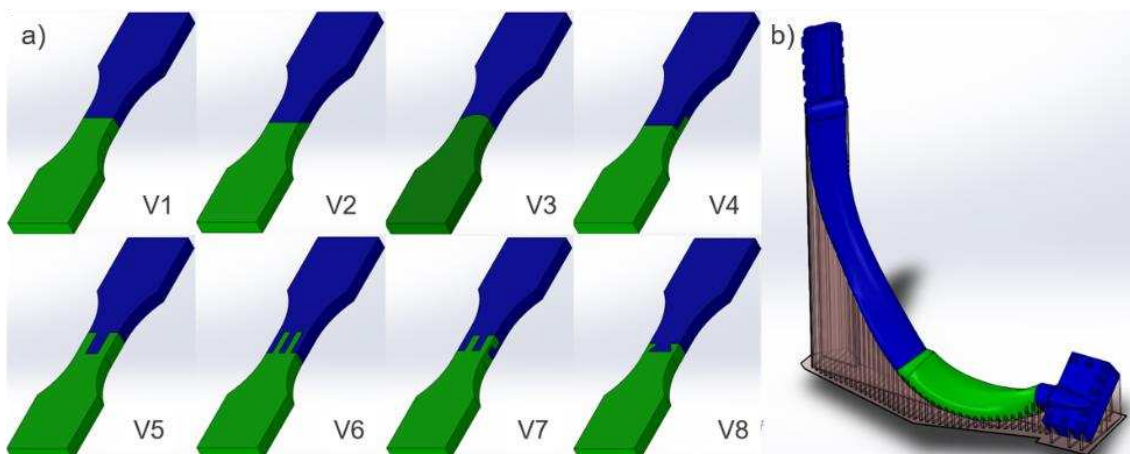
Figure 66   Multi-material tensile bars with different connection designs (a) and rib replacement design (b) in hard (blue) – soft (green) components. The rib replacement needed a break-away support displayed transparent in (b).

The implant was then used in a feasibility study, performed at the Institute for Macroscopic and Clinical Anatomy, Medical University Graz. The study was performed on a human cadaver

for research purposes and was conducted according to the Styrian Death and Funeral Act. The rib cage of the human body donor was set free and the specific rib was removed and consequently replaced by the 3D-printed model. Therefore, the model was sewed to the sternum by using surgical sutures, tunneled through the predefined holes. On the other side a special rib clamp was used to connect the model to the remaining original rib. Manual reanimation was then performed on the open rib cage and the movement of the implant was observed.

All tensile tests were performed on the universal testing machine Zwick Z250 (ZwickRoell GmbH + Co KG, Ulm, Germany) at a testing speed of 1 mm/min up to an elongation of 0.25 % for evaluation of the Young's modulus. The testing speed was then increased to 50 mm/min until breakage occurred. The testing speeds were per DIN EN ISO 527-1. The clamping length was 110 mm for the standard tensile bars and 42 mm for the 2-component tensile bars. Mechanical clamps with riffled grip inserts were used for clamping.

Results and Discussion

Figure 67a shows the density measurements performed on plates printed with different DAR settings. The density values reached the documented bulk densities (horizontal lines) at specific DAR values, usually taken as the DAR settings if better mechanical strength is required. A second DAR value can be taken slightly below the max. density DAR value to force a slight underfilling but enhanced accuracy [94, 99]. However, it is mentioned that the DAR can be optimized for certain dimensions or layer heights to reach an optimal filling degree [53, 94].

Mechanical properties were then analyzed with the selected DAR values and processing parameters in Table 1. The resulting stress-strain curves are displayed in Figure 67b. It is visible that the effect of the DAR is more critical for the Bionate® 75D compared to the Bionate® 80A samples. Hence, the DAR setting affects more the less ductile PCU. Further, for the softer material, the additively manufactured parts show a similar behavior to the injection molded parts, while for the harder material, the curves are very different. In detail, the injection molded samples develop a significant yield peak, which is not present in the printed samples. This behavior might also indicate a different morphology or micro voids within the parts, forcing a less ductile material behavior [53, 99].
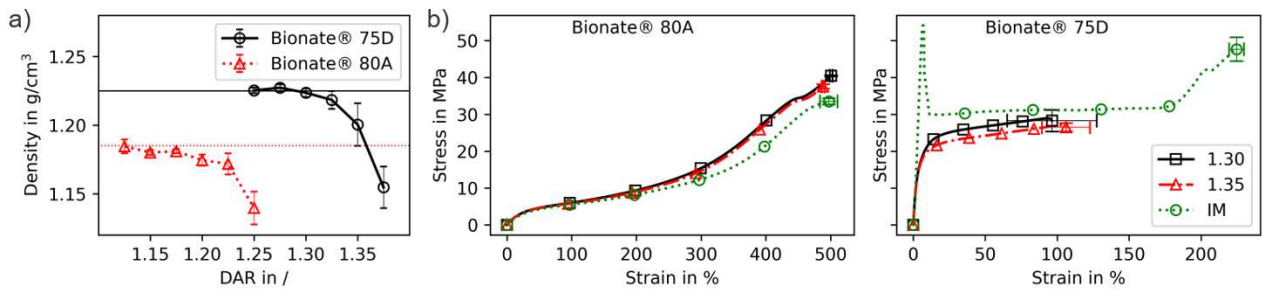
Figure 67   Results of the density measurements, with the bulk densities indicated by the horizontal lines (a), and tensile measurements (b) of samples printed with Bionate® 80A and 75D.

The multi-material specimens have also been tested on the tensile testing machine. Figure 68a shows multi-material specimen (V1) mounted on the tensile testing machine. Here, one can see the different deformation of the two materials. A high transverse contraction in the transition area between the soft and hard material is present since the soft material wants to deform, and the hard one acts against it. Thus, a high shear stress is expected in this region. Nevertheless, the picture does indicate a good bonding of the two PCUs. Figure 68b shows a box plot of the tensile results of the specimens with different connection designs. V2 performs best at stress and strain, with V1 and V8 also giving good results. Regarding strain, V8 even matches V2. V1 to V3 have connections without interlocks, for which high adhesion was not expected. V2 outperformed the other two versions due to its sloped geometry, ensuring less cross-contraction at the interface and less shear stress. The design of V3 has a concave curvature which may cause even higher shear stresses. Furthermore, the stress-strain responses of V1 to V3 are in between the two neat materials, as displayed in Figure 68c. Interlocking designs usually lead to good connectivity in multi-material printing [56, 57]. However, in this case, connections without interlocks led to better results due to their chemical compatibility. One reason for the worse performance of the interlocking designs may originate in the lower content of hard material over the interface cross-sections. Therefore, based on these findings, a non-interlocked connection seems suitable for multi-material parts, like the multi-material rib replacement system prepared in this investigation.
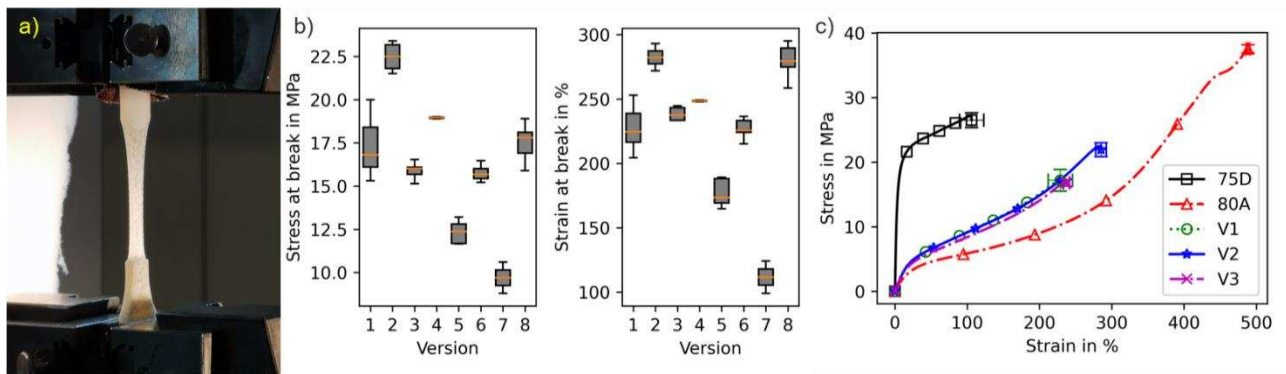
Figure 68   Picture of a multi-material specimen mounted on the tensile testing device (a), the matching results as a box plot (b) and the stress-strain curves of the single materials in comparison with two selected multi-material specimens (c).

Based on the tensile testing results, a rib replacement was designed and manufactured with the APF, as shown in Figure 69a. Some inaccuracies can be seen at the top of the model, which were caused by the wobbling of the specimen during printing. This wobbling was reduced by reinforcing the support structure, as shown in Figure 69b. After successful printing, the model was implanted in a human body donor as described previously. A picture of an implanted rib is provided in Figure 69c. Reanimation was performed on the body after implantation to observe the rib movement, which mainly took place in the soft part, as expected. Furthermore, no breakage of the model was observed, resulting in a successful feasibility study.
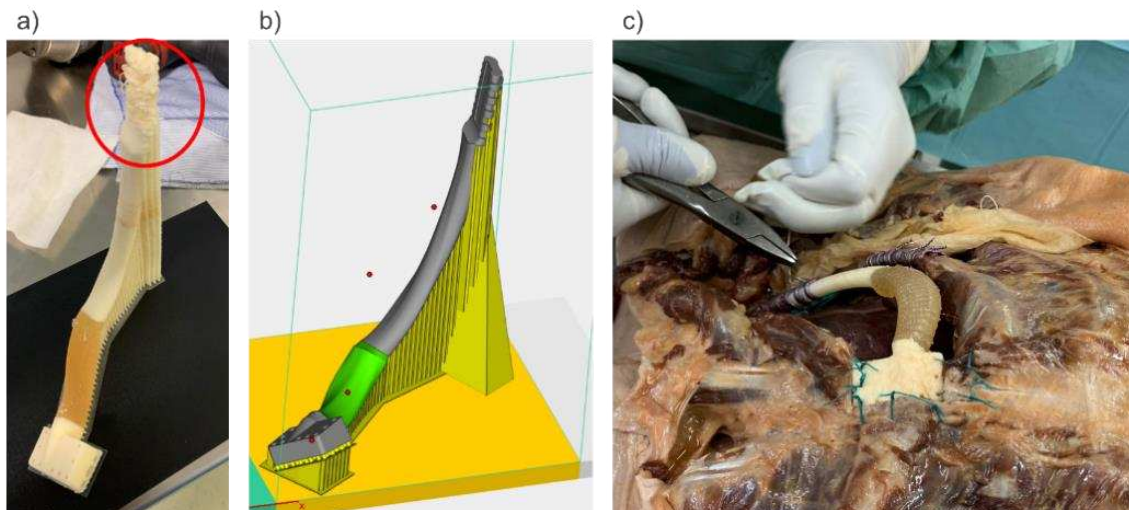
Figure 69   Picture of the printed rib replacement with poor resolution (a), screen shot of the support reinforcement (b) and picture of the implanted rib model (c).

Conclusion

In conclusion, the two used polycarbonate urethanes (PCUs), Bionate® 80A and Bionate® 75D, are suitable for proper hard-soft multi-material additive manufacturing. Compatibility between the materials was shown by tensile testing of specimens with different connection

designs, where non-interlocked connections worked the best, despite other results from the literature [56, 57]. Additional optimization of the process parameters can be done to improve further the mechanical properties of the hard material (75D). A replacement for the hard part made of stiffer or composite reinforced thermoplastic polyurethanes would also be conceivable. Since the PCUs were designed for medical usage, their application for a possible multi-functional rib replacement was studied. A feasibility study performed on a human body donor showed promising results regarding the reanimation behavior and no failure during the procedure. Further experiments need to be carried out with a greater focus on the mechanical performance and stiffness of the design. Additionally, the model itself could be printed on, e.g., the freeformer 750-3X, which has a bigger build volume and a third nozzle, so that the model could be printed with soluble support material. Using a soluble support material would result in a better surface finishing and print orientation, increasing the mechanical properties further and reducing the building time. Therefore, this approach of a multi-material rib replacement may be suitable for clinical trials in the future and will possibly enhance human healthcare.

Acknowledgments

4.2.4 Closing remarks to Publications D and E

Publications D and E proved the feasibility of manufacturing PSI using the APF technology. In detail, Publication D showed the processing of different polymers for the same application to find the best-fitting material for different applications. In addition to Mele et al. [169], the feasibility of APF implants from Bionate® was replicated. However, other polymers even exceed the mechanical performance of the PC-U. In comparison to the bone cement, none of the printed samples showed the same stiffness but nevertheless they are still applicable as implants in the craniomaxillofacial area. To further improve the performance of implants fabricated from softer polymers, the design can be adapted but more studies have to be conducted [169].

Publication E on the other hand showed the feasibility of a multi-material rib replacement implant. It was shown that two grades of Bionate® can be combined to initiate soft and hard tissue in a single part. Technical products, like hinges, using this approach are already presented in the literature [185]. However, more optimization on processing parameters and

design must be performed for commercialization. Nonetheless, the potential of the APF technology for medical applications, like PSIs was shown in the presented studies as well as in the latest literature [165, 169, 186, 223, 226, 227, 276].

5 Conclusion and Research Outlook

5.1. Conclusion

The here studied APF technology is a rather new and promising AM method, enabling the processing of polymer granules of already established materials for medical applications. This is crucial for invasive medical products, like implants. Further, the APF machines are designed for medical fabrication with slight adaptations and can already be found in some companies for such products [14, 169, 223, 224, 226, 227, 276]. AM can be used for in-house production, reducing the transport distances and times leading to a more environmental and economical fabrication of personalized orthodontic devices using the APF method [166].

To ensure a reliable manufacturing process, proper processing parameters must be defined. This is performed by a material qualification procedure, which ensures specific and reproducible part properties. According to DIN SPEC 1707 [2], a material qualification is valid for a single material, parameter set, and printing procedure and must be requalified after any changes. A proper approach for a qualification procedure for the APF process was presented in Publication A and led to the acceptance of hypothesis one. The qualification is especially important to produce medical devices to ensure the mechanical integrity and functionality of the part. Publication A pointed out that part orientation greatly influence mechanical performances, which was also found in the literature [93, 106, 162, 211, 283]. Furthermore, a maximum of geometrical accuracy and mechanical properties cannot be combined with a single parameter set, which was also concluded by Eisele et al. [53]. Therefore, parameter optimization must be performed for a given application and desired properties.

The second hypothesis was defined and tested in Publication B. It was shown that a proper DoE can be used to find higher impacting factors for mechanical properties and can be applied to optimize these. Further, the understanding of the process was enhanced by studying and discussing the specific volume of the polymer during the process. It was observed that the *DAR* parameter shows the highest impact on tensile properties. Moreover, it was demonstrated that tensile properties are related to the part density, which was also evident in the literature [34, 206]. Thus, it was concluded that the density can be used as a quality parameter for 3D-printed parts. In contrast, in the literature [34, 106] a reciprocal influence of the processing temperatures on tensile properties was shown in Publication B. It was assumed that the higher

processing pressure at lower processing temperatures led to a smaller difference in specific volume between the molten and the solid polymer. The smaller difference in specific volume results in a lower shrinkage potential during the processing. Hence, fewer voids and less internal stresses could occur in the fabricated parts and led to better tensile properties. However, the study was only performed on a single amorphous polymer and should be replicated with other similar polymers.

Semi-crystalline materials are rather tricky to process due to the higher shrinkage potential of these types of polymers. This can be reduced by the incorporation of filler materials, or modification of the polymer [244, 245]. On the other hand, semi-crystalline polymers show better weld strength which can enhance the inter-layer adhesion of 3D printed parts, especially at evaluated environmental temperatures. Therefore, it was proposed that higher print envelope temperatures lead to less anisotropic part performances. In general, hypothesis three was able to be accepted due to the results of Publication C, even though specimens printed in Z-orientation resulted in significantly lower tensile properties. Tensile bars were printed at different infill angles and chamber temperatures with the APF technology. The results showed that there is less influence on the printing angle at higher chamber temperatures. The influence of the printing orientation has already been studied in the literature [93, 106, 162, 206, 211]. Publication C showed the potential of higher chamber temperatures on the morphology of semi-crystalline polymers and on the enhanced isotropic properties. However, it was found that the crystalline structure changed along the Z-printing axis in dependence of the printing time and chamber temperature. It was assumed that more of the β-crystals of the PP were formed on the lower layers. This structure is preferred according to some publications [191, 242, 246].

Chapter 4 of this thesis was composed of two case studies of 3D-printed implants. Therefore, personalized cranial implants were produced with different polymer materials and tested for their impact properties. It was shown that implants were able to be manufactured within an acceptable period and have relatable mechanical properties. Samples were prepared in different orientations and compared regarding their processing times and impact properties. Further, the concept of a multi-material rib replacement was presented in Publication E. The novel approach of printing a soft and hard material combination was exhibited to be beneficial for such purposes. The implant can imitate the behavior of the soft tissue as well as the hard tissue of a human body. It was demonstrated in the literature that rib implants made from metals often lead to complications due to the higher stiffness of the material [91, 122, 135, 175, 274]. Publication E also studied the combination of two PC-U polymers with different shore hardnesses and stiffnesses. The results showed that for similar polymer, a non-interlocking contact surface performs better than an interlocking one, in contrast to the results found in the literature [56, 57].

Overall, the PhD. thesis demonstrated the potential of the APF technology for use in the medical sector. It gave qualification and optimization procedures to find suitable and reliable parameter sets for a given medical-approved polymer. It was pointed out that mechanical properties could be improved by using a DoE approach and further that the morphology of semi-crystalline polymers can be manipulated by adapting the printing envelope temperatures. The feasibility of 3D-printing polymer cranial implants from different polymers was shown and the novel concept of a multi-material polymer rib replacement was presented. Whereas the fabrication of cranial prostheses is already in a state of possibility, other applications like rib preplacement still must undergo further investigations. In general, the APF procedure is an innovative AM technology with a high potential for invasive medical applications.

5.2. Concluding Remarks on the Hypotheses

An overview of the concluding remarks on the hypotheses discussed in this PhD thesis are given below.

1. *"A proper qualifications procedure can be used to define suitable processing parameters for the APF technology."*
   The findings in publication A and additional contribution to this paper led to the acceptance of this hypothesis for PMMA. It can be concluded that the tensile strength and the part density can be used as parameters for suitable processing parameters.

2. *"A Design of Experiments approach on processing parameters of the APF can be used to improve the mechanical performance of 3D-printed parts."*
   Based on the results of publication B this hypothesis can be accepted for amorphous thermoplastic polymers like PMMA. Moreover, publication C further showed a similar approach for semi-crystalline polymers and support the acceptance of the hypothesis.

3. *"Process parameters optimization can reduce anisotropic properties in APF-manufactured parts made from semicrystalline polymers."*
   Even though complete isotropic mechanical properties could not be generated by the APF process for the given material, a reduced influence on the printing orientation could be archived. Hence, this Hypothesis can be accepted based on the results of publication C.

4. *Technical or commodity polymers are feasible materials for medical invasive parts, produced by APF.*
   Publication D showed a case study for 3D printable cranial implants. Based on the mechanical testing of the parts, it was concluded that these samples are

applicable for invasive medical usage and led to the acceptance of this hypothesis.

5. *A hard-soft material combination, manufactured by the APF, can improve the performance of medical implants.*

This hypothesis is confirmed by the demonstrations given in publication E. The innovative idea given in that paper is still in its infancy but show the potential of multi-material 3D-printing.

5.3. Research Outlook

The presented work showed the influences on the mechanical properties of 3D-printed parts, fabricated with different processing parameters and part orientations have. In Publication A, a small difference in tensile properties of specimens printed in different batch sizes was observed. The prolonged layer-building time for larger batch numbers may lead to weaker part properties. Since this publication focuses on the parameter qualification, this finding was not studied further but may be interesting for future investigations. A few studies dealing with layer-building time in MEX technologies are already published and show potential for failure prediction [40]. The results of such studies can be used for a better understanding of the AM processes and further parameter optimization.

Moreover, reproducibility is still a huge topic for AM in general [6, 36, 77, 105, 176]. Especially for the fabrication of medical devices, constant and repeatable properties are crucial. DIN SPEC 17075 [2] proposes the use of accompanied specimens for quality management issues. However, no repeatability studies for APF, including a defined parameter set applied to different APF machines on different locations, have been published yet. Such studies will consume a lot of resources but may show the influence of the operator on the part properties. Furthermore, a well-trained staff is essential as well, to ensure properly fabricated parts. To reduce human errors and enhancing the repeatability of part properties, computer software can support the qualification procedure and monitoring of the process.

Artificial intelligence (AI) is nowadays on everyone's mind. In terms of 3D printing, AI may help with the perfect part orientation [71] or in the generation of cranial prostheses [147, 148, 170]. Later it may again help to reduce human error sources in the fabrication of medical implants. Moreover, AI may be used to further improve material qualification, process monitoring, and additional process optimization to ensure constant part properties.

Some degradation was observed during the processing of hygroscopic polymers. It was shown that residual times of the APF process can range up to 20 min. This rather long period

can lead to oxidation, degradation, or chain scission of the polymer feedstock. For unstable polymers, the reduction of the residual time is important to prevent such occurrences. Therefore, the plasticization process should be studied in detail and the influence factors on the residual time must be indicated. Moreover, finite element simulation can be used to understand the process and predict weak spots in the resulting part due to polymer degradation [95].

Multi-material implant systems were proposed in Publication E. This is a rather new idea which is used to mimic soft and hard tissue in a single part and enhance the overall part performance. However, the hard material used still shows significantly lower stiffness compared to the human bone. Therefore, more investigation into this concept is necessary and a good point of interest.

One of the main topics of this PhD. thesis was the feasibility of 3D-printing medical implants using the APF technology. The advantages of 3D printing in the medical sector are already known and well-studied [114, 119, 119, 194, 230, 277]. However, AM-manufactured polymeric implants are rare and mostly individual cases. Therefore, clinical trials must be conducted as a subsequent step to establish the use of the APF process in the fabrication of medical implants. For these studies also the in-house production of such implants must be considered. The main issues of in-house production are the implementation of the quality management system, qualification, and validation due to standards and qualified staff. Further, proposed AI or software support can help to reduce human errors, which is crucial for reproducibility and repeatability. Additionally, manufactured cranial implants have been studied intensively in the last decade. Thus, the author believes that the establishment of 3D-printed PSIs is soon possible whereas in-house production may still take some more time.

In the end, this PhD. study showed impact factors on the mechanical properties of the APF process and a qualification procedure to ensure proper parameter sets. The potential of the application for cranial implants and a novel concept of multi-material implant systems was demonstrated. The thesis was only possible by interdisciplinary work from polymer science, mechanical engineering, and medical research which led to these unique and astonishing findings. Research in the field of AM and human healthcare will be enhanced in the future based on the results presented in this work.

6 References

[1] Abdulai, A.E.; Iddrissu, M.I.; Dakurah, T.K.: Cranioplasty Using Polymethyl Methacrylate Implant Constructed from an Alginate Impression and Wax Elimination Technique, Ghana Med. J. 40 (1), 2006, pp. 18–21

[2] DIN SPEC 1707: Additive Fertigung - Anforderungen an qualitätsgesicherte Prozesse für additive Fertigungszentren, 2019

[3] OENORM EN ISO ASTM 52921: Additive Fertigung - Grundlagen - Standardpraxis Positionierung, Koordinaten und Aurichtung des bauteiles, 01.11.2019

[4] OENORM EN ISO ASTM 52900: Additive Fertigung - Grundlagen - Terminologie, 15.06.2018

[5] ISO ASTM 52900: Additive manufacturing — General principles — Fundamentals and vocabulary, 01.11.2021

[6] Ahlinder, A.; Charlon, S.; Fuoco, T.; Soulestin, J.; Finne-Wistrand, A.: Minimise thermo-mechanical batch variations when processing medical grade lactide based copolymers in additive manufacturing, Polymer Degradation and Stability 181, 2020, pp. 109372

[7] Ajinjeru, C.; Kishore, V.; Liu, P.; Lindahl, J.; Hassen, A.A.; Kunc, V.; Post, B.; Love, L.; Duty, C.: Determination of melt processing conditions for high performance amorphous thermoplastics for large format additive manufacturing, Additive Manufacturing 21, 2018, pp. 125–132

[8] Alharbi, N.; Osman, R.; Wismeijer, D.: Effects of build direction on the mechanical properties of 3D-printed complete coverage interim dental restorations, The Journal of prosthetic dentistry 115 (6), 2016, pp. 760–767

[9] Ali, U.; Karim, K.J.B.A.; Buang, N.A.: A Review of the Properties and Applications of Poly (Methyl Methacrylate) (PMMA), Polymer Reviews 55 (4), 2015, pp. 678–705

[10] Alonso-Rodriguez, E.; Cebrian, J.L.; Nieto, M.J.; Del Castillo, J.L.; Hernandez-Godoy, J.; Burgueno, M.: Polyetheretherketone custom-made implants for craniofacial defects: Report of 14 cases and review of the literature, Journal of cranio-maxillo-facial surgery : official publication of the European Association for Cranio-Maxillo-Facial Surgery 43 (7), 2015, pp. 1232–1238

[11] Annealing Guidelines for Plastic Stock Shapes | Boedeker, 2023, https://www.boedeker.com/Technical-Resources/Technical-Library/Plastic-Annealing-Guidelines (Retrieved on: 16.05.2023)

[12] Antony, J.: Design of Experiments for Engineers and Scientists, Elsevier, 2014

[13]   Antony Samy, A.; Golbang, A.; Harkin-Jones, E.; Archer, E.; Dahale, M.; McIlhagger, A.: Influence of Ambient Temperature on Part Distortion: A Simulation Study on Amorphous and Semi-Crystalline Polymer, Polymers 14 (5), 2022

[14]   ARBURG GMBH + CO. KG: Medizin - Einzigartig einsetzbar: Das Kunststoff-Freiformen, https://www.arburg.com/media/daten/publications/brochures/ARBURG_Medizintechnik _682108_DE/# (Retrieved on: 04.12.2023)

[15]   Arefin, A.M.E.; Khatri, N.R.; Kulkarni, N.; Egan, P.F.: Polymer 3D Printing Review: Materials, Process, and Design Strategies for Medical Applications, Polymers 13 (9), 2021

[16]   Bandyopadhyay, A.; Bose, S.: Additive manufacturing, CRC Press, Boca Raton, FL, 2016

[17]   Banerjee, S.S.; Burbine, S.; Kodihalli Shivaprakash, N.; Mead, J.: 3D-Printable PP/SEBS Thermoplastic Elastomeric Blends: Preparation and Properties, Polymers 11 (2), 2019

[18]   Banerjee, S.S.; Kumar, K.D.; Sikder, A.K.; Bhowmick, A.K.: Nanomechanics and Origin of Rubber Elasticity of Novel Nanostructured Thermoplastic Elastomeric Blends Using Atomic Force Microscopy, Macromolecular Chemistry and Physics 216 (15), 2015, pp. 1666–1674

[19]   Benié, K.; Barrière, T.; Placet, V.; Cherouat, A.: Introducing a new optimization parameter based on diffusion, coalescence and crystallization to maximize the tensile properties of additive manufacturing parts, Additive Manufacturing 69, 2023, pp. 103538

[20]   Berkmortel, C.; Langohr, G.D.G.; King, G.; Johnson, J.: Hemiarthroplasty implants should have very low stiffness to optimize cartilage contact stress, Journal of orthopaedic research : official publication of the Orthopaedic Research Society 38 (8), 2020, pp. 1719–1726

[21]   Berman, B.: 3-D printing: The new industrial revolution, Business Horizons 55 (2), 2012, pp. 155–162

[22]   OENORM EN ISO 10993-1: Biologische Beurteilung von Medizinprodukten, 15.03.2011

[23]   Bos, F.; Wolfs, R.; Ahmed, Z.; Salet, T.: Additive manufacturing of concrete in construction: potentials and challenges of 3D concrete printing, Virtual and Physical Prototyping 11 (3), 2016, pp. 209–225

[24]   Bot, G.M.; Ismail, N.J.; Usman, B.; Shilong, D.J.; Obande, J.O.; Aliu, S.; Sale, D.; Shehu, B.B.: Using the head as a mould for cranioplasty with methylmethacrylate, Journal of Neurosciences in Rural Practice 4 (4), 2013, pp. 471–474

[25] Brenken, B.; Barocio, E.; Favaloro, A.; Kunc, V.; Pipes, R.B.: Fused filament fabrication of fiber-reinforced polymers: A review, Additive Manufacturing 21, 2018, pp. 1–16

[26] Brie, J.; Chartier, T.; Chaput, C.; Delage, C.; Pradeau, B.; Caire, F.; Boncoeur, M.-P.; Moreau, J.-J.: A new custom made bioceramic implant for the repair of large and complex craniofacial bone defects, Journal of cranio-maxillo-facial surgery : official publication of the European Association for Cranio-Maxillo-Facial Surgery 41 (5), 2013, pp. 403–407

[27] Bryant, F.D.; Sui, G.; Leu, M.C.: A study on effects of process parameters in rapid freeze prototyping, Rapid Prototyping Journal

[28] BV Med: Kunststoffe in der Medizintechnik: Geschichte(n) und Trends, https://www.bvmed.de/de/technologien/geschichte/kunststoffe-in-medizinprodukten (Retrieved on: 02.12.2023)

[29] Campus: Xantar™ 22 UR, 2023, https://www.campusplastics.com/campus/en/datasheet/XANTAR%E2%84%A2+22+UR /Mitsubishi+Chemical+Group/107/59cf12e8/SI?pos=10 (Retrieved on: 09.11.2023)

[30] Carneiro, O.S.; Silva, A.F.; Gomes, R.: Fused deposition modeling with polypropylene, Materials & Design 83, 2015, pp. 768–776

[31] Cervigni, M.; Natale, F.; La Penna, C.; Saltari, M.; Padoa, A.; Agostini, M.: Collagen-coated polypropylene mesh in vaginal prolapse surgery: an observational study, European journal of obstetrics, gynecology, and reproductive biology 156 (2), 2011, pp. 223–227

[32] Chacón, J.M.; Caminero, M.A.; García-Plaza, E.; Núñez, P.J.: Additive manufacturing of PLA structures using fused deposition modelling: Effect of process parameters on mechanical properties and their optimal selection, Materials & Design 124, 2017, pp. 143–157

[33] Chang, R.Y.; Chen, C.H.; Su, K.S.: Modifying the tait equation with cooling-rate effects to predict the pressure-volume-temperature behaviors of amorphous polymers: Modeling and experiments, Polymer Engineering & Science 36 (13), 1996, pp. 1789–1795

[34] Charlon, S.; Soulestin, J.: Thermal and geometry impacts on the structure and mechanical properties of part produced by polymer additive manufacturing, Journal of Applied Polymer Science, 2020

[35] Chen, J.; Cao, Y.; Kang, J.; Li, H.: Effect of Temperature and Comonomer Content on Thermal Behavior and Crystallization Property of the Propylene–Ethylene Random Copolymers, Journal of Macromolecular Science, Part B 50 (2), 2010, pp. 248–265

[36]   Chen, L.; Lin, W.-S.; Polido, W.D.; Eckert, G.J.; Morton, D.: Accuracy, reproducibility, and dimensional stability of additively manufactured surgical templates, The Journal of prosthetic dentistry 122 (3), 2019, pp. 309–314

[37]   Chiarini, L.; Figurelli, S.; Pollastri, G.; Torcia, E.; Ferrari, F.; Albanese, M.; Nocini, P.F.: Cranioplasty using acrylic material: a new technical procedure, J. Cranio-MaxilloFac. Surg. 32 (1), 2004, pp. 5–9

[38]   Christ, J.F.; Aliheidari, N.; Ameli, A.; Pötschke, P.: 3D printed highly elastic strain sensors of multiwalled carbon nanotube/thermoplastic polyurethane nanocomposites, Materials & Design 131, 2017, pp. 394–401

[39]   Cole, D.P.; Gardea, F.; Henry, T.C.; Seppala, J.E.; Garboczi, E.J.; Migler, K.D.; Shumeyko, C.M.; Westrich, J.R.; Orski, S.V.; Gair, J.L.: AMB2018-03: Benchmark Physical Property Measurements for Material Extrusion Additive Manufacturing of Polycarbonate, Integrating Materials and Manufacturing Innovation 9 (4), 2020, pp. 358–375

[40]   Coogan, T.J.; Kazmer, D.O.: Prediction of interlayer strength in material extrusion additive manufacturing, Additive Manufacturing 35, 2020, pp. 101368

[41]   Cooper, K.: Rapid Prototyping Technology, CRC Press, 2001

[42]   Culmone, C.; Smit, G.; Breedveld, P.: Additive manufacturing of medical instruments: A state-of-the-art review, Additive Manufacturing 27, 2019, pp. 461–473

[43]   De La Peña, A.; De La Peña-Brambila, J.; Pérez-De la Torre, J.; Ochoa, M.; Gallardo, G.J.: Low-cost customized cranioplasty using a 3D digital printing model: a case report, J. 3D Print. Med. 4, 2018

[44]   Deb, S.: Orthopaedic bone cements, Woodhead Publishing in materials, Woodhead Pub. Ltd, Cambridge, s.l., 2008

[45]   FDA Guidance: Design Control Guidance For Medical Device Manufacturers, 11.03.1997

[46]   Diegel, O.: Additive Manufacturing, AN Overview, In: Comprehensive Materials Processing, Elsevier, 2014, pp. 3–18

[47]   DIN EN ISO/ASTM 52900:2022-03, Additive Fertigung_- Grundlagen_- Terminologie (ISO/ASTM 52900:2021); Deutsche Fassung EN_ISO/ASTM 52900:2021

[48]   Domininghaus, H.; Elsner, P.: Kunststoffe, Eigenschaften und Anwendungen, 7. Ed., Springer, Berlin, New York, 2008

[49]   DSM Biomedical: Bionate®Thermoplastic polycarbonate polyurethane, 2020, https://www.dsm.com/content/dam/dsm/biomedical/en_us/documents/document-bionate-pcu-productsheet.pdf (Retrieved on: 31.05.2023)

[50] Dudescu, C.; Racz, L.: Effects of Raster Orientation, Infill Rate and Infill Pattern on the Mechanical Properties of 3D Printed Materials, ACTA Universitatis Cibiniensis 69 (1), 2017, pp. 23–30

[51] Dunne, N.: Mechanical properties of bone cements, In: Deb S. (Ed.): Orthopaedic bone cements, Woodhead Publishing in materials, Woodhead Pub. Ltd, Cambridge, s.l., 2008, pp. 233–264

[52] Eder, S.; Kuchler, L.; Katschnig, M.; Brandl, B.; Wolfgang, M.; Koutsamanis, I.; Hentschel, L.; Arbeiter, F.; Roblegg, E.; Spoerk, M.: Personalization of Complex Vaginal Inserts of Ethylene Vinyl Acetate via 3D-Printing, Advanced Materials Technologies 8 (17), 2023

[53] Eisele, L.; Heuer, A.; Weidenmann, K.A.; Liebig, W.V.: Can Different Parameter Sets Lead to Equivalent Optima between Geometric Accuracy and Mechanical Properties in Arburg Plastic Freeforming?, Polymers 15 (6), 2023, pp. 1516

[54] El Halabi, F.; Rodriguez, J.F.; Rebolledo, L.; Hurtós, E.; Doblaré, M.: Mechanical characterization and numerical simulation of polyether-ether-ketone (PEEK) cranial implants, Journal of the mechanical behavior of biomedical materials 4 (8), 2011, pp. 1819–1832

[55] Elsner, J.J.; McKeon, B.P.: Orthopedic Application of Polycarbonate Urethanes: A Review, Techniques in Orthopaedics 32 (3), 2017, pp. 132–140

[56] Ermolai, V.; Sover, A.; Boca, M.A.; Hriţuc, A.; Slătineanu, L.; Nagîţ, G.; Stavarache, R.C.: Mechanical Behaviour of Macroscopic Interfaces for 3D Printed Multi-material Samples, MATEC Web of Conferences 368, 2022, pp. 1004

[57] Ermolai, V.; Sover, A.; Nagîţ, G.: Influence of contact geometry over the filament bond of polylactic acid blends, IOP Conference Series: Materials Science and Engineering 1235 (1), 2022, pp. 12004

[58] Essig, H.; Lindhorst, D.; Gander, T.; Schumann, P.; Konu, D.; Altermatt, S.; Rucker, M.: Patient-specific biodegradable implant in pediatric craniofacial surgery, Journal of cranio-maxillo-facial surgery : official publication of the European Association for Cranio-Maxillo-Facial Surgery 45 (2), 2017, pp. 216–222

[59] EU Regulation: EU Medical Device Directive 2017/745, 05.04.2017

[60] European plastic product manufacturer: Freeformer is a big hit in Denmark, EPPM, 2015

[61] ExxonMobile Chemical Company: Product Datasheet Vistamaxx 3980FL

[62] Fernandes da Silva, A.L.; Borba, A.M.; Simão, N.R.; Pedro, F.L.M.; Borges, A.H.; Miloro, M.: Customized Polymethyl Methacrylate Implants for the Reconstruction of Craniofacial Osseous Defects, Hindawi 358569, 2014, pp. 8

[63] Fiaschi, P.; Pavanello, M.; Imperato, A.; Dallolio, V.; Accogli, A.; Capra, V.; Consales, A.; Cama, A.; Piatelli, G.: Surgical results of cranioplasty with a polymethylmethacrylate customized cranial implant in pediatric patients: a single-center experience, J. Neurosurg. 17 (6), 2016, pp. 705–710

[64] Fiebig, J.; Gahleitner, M.; Paulik, C.; Wolfschwenger, J.: Ageing of polypropylene: processes and consequences, Polymer Testing 18 (4), 1999, pp. 257–266

[65] Fischer, C.; Drummer, D.: Crystallization and Mechanical Properties of Polypropylene under Processing-Relevant Cooling Conditions with respect to Isothermal Holding Time, International Journal of Polymer Science 2016, 2016, pp. 1–11

[66] Fleisch, A.F.; Sheffield, P.E.; Chinn, C.; Edelstein, B.L.; Landrigan, P.J.: Bisphenol A and related compounds in dental materials, Pediatrics 126 (4), 2010, pp. 760–768

[67] Ford, S.; Despeisse, M.: Additive manufacturing and sustainability: an exploratory study of the advantages and challenges, Journal of Cleaner Production 137, 2016, pp. 1573–1587

[68] Frauenhofer IGB: Biomaterialien, Entwicklung, Synthese und Charakterisierung von Materialien für den Kontakt mit biologischen Systemen, https://www.igb.fraunhofer.de/content/dam/igb/documents/brochures/materialien/hydro gel/1803_BR_biomaterialien_de.pdf (Retrieved on: 02.12.2023)

[69] Gahleitner, M.; Jääskeläinen, P.; Ratajski, E.; Paulik, C.; Reussner, J.; Wolfschwenger, J.; Neißl, W.: Propylene-ethylene random copolymers: Comonomer effects on crystallinity and application properties, Journal of Applied Polymer Science 95 (5), 2005, pp. 1073–1081

[70] Gander, T.; Essig, H.; Metzler, P.; Lindhorst, D.; Dubois, L.; Rucker, M.; Schumann, P.: Patient specific implants (PSI) in reconstruction of orbital floor and wall fractures, Journal of cranio-maxillo-facial surgery : official publication of the European Association for Cranio-Maxillo-Facial Surgery 43 (1), 2015, pp. 126–130

[71] García Galicia, J.A.; Benes, B.: Improving printing orientation for Fused Deposition Modeling printers by analyzing connected components, Additive Manufacturing 22, 2018, pp. 720–728

[72] Garcia-Gonzalez, D.; Rusinek, A.; Jankowiak, T.; Arias, A.: Mechanical impact behavior of polyether–ether–ketone (PEEK), Composite Structures 124, 2015, pp. 88–99

[73] Gaub, H.: Customization of mass-produced parts by combining injection molding and additive manufacturing with Industry 4.0 technologies, Reinforced Plastics 6 (60), 2016, pp. 401–404

[74]   Geary, C.; Birkinshaw, C.; Jones, E.: Characterisation of Bionate polycarbonate polyurethanes for orthopaedic applications, Journal of Materials Science. Materials in Medicine 19 (11), 2008, pp. 3355–3363

[75]   Gebhardt, A.: 3D-Drucken, Grundlagen und Anwendungen des Additive Manufacturing (AM), Hanser eLibrary, Hanser, München, 2014

[76]   GEHR Plastics: GEHR Plastics PE-UHMW Polyethylene, Ultra High Molecular Weight, https://www.matweb.com/search/datasheet_print.aspx?matguid=22492cabc9c3487493 a3dd214fc4a3dd (Retrieved on: 02.12.2023)

[77]   George, E.; Liacouras, P.; Rybicki, F.J.; Mitsouras, D.: Measuring and Establishing the Accuracy and Reproducibility of 3D Printed Medical Models, Radiographics : a review publication of the Radiological Society of North America, Inc 37 (5), 2017, pp. 1424–1450

[78]   Gibson, I.; Rosen, D.W.; Stucker, B.: Additive manufacturing technologies, 3D printing, rapid prototyping and direct digital manufacturing, Springer, New York [etc.], 2015

[79]   Go, J.; Hart, A.J.: Fast Desktop-Scale Extrusion Additive Manufacturing, Additive Manufacturing 18, 2017, pp. 276–284

[80]   Go, J.; Schiffres, S.N.; Stevens, A.G.; Hart, A.J.: Rate limits of additive manufacturing by fused filament fabrication and guidelines for high-throughput system design, Additive Manufacturing 16, 2017, pp. 1–11

[81]   Goh, B.T.; Teh, L.Y.; Tan, D.B.P.; Zhang, Z.; Teoh, S.H.: Novel 3D polycaprolactone scaffold for ridge preservation--a pilot randomised controlled clinical trial, Clinical oral implants research 26 (3), 2015, pp. 271–277

[82]   Gómez-Gras, G.; Abad, M.D.; Pérez, M.A.: Mechanical Performance of 3D-Printed Biocompatible Polycarbonate for Biomechanical Applications, Polymers 13 (21), 2021

[83]   González-Henríquez, C.M.; Sarabia-Vallejos, M.A.; Rodriguez-Hernandez, J.: Polymers for additive manufacturing and 4D-printing: Materials, methodologies, and biomedical applications, Progress in Polymer Science 94, 2019, pp. 57–116

[84]   Govindaraj, S.; Muthurama, M.S.: Systematic Review on Sterilization Methods of Implants and Medical Devices, International Journal of ChemTech Research (8), 2015, pp. 897–911

[85]   Graham, A.D.; Olof, S.N.; Burke, M.J.; Armstrong, J.P.K.; Mikhailova, E.A.; Nicholson, J.G.; Box, S.J.; Szele, F.G.; Perriman, A.W.; Bayley, H.: High-Resolution Patterned Cellular Constructs by Droplet-Based 3D Printing, Scientific Reports 7 (1), 2017, pp. 7004

[86]   Graphite Additive Manufacturing: How are 3D Printing proces calculated?, https://www.graphite-am.co.uk/graphite-additive-manufacturing/how-are-3d-printing-prices-calculated/ (Retrieved on: 08.01.2024)

[87] Greeff, G.P.; Schilling, M.: Closed loop control of slippage during filament transport in molten material extrusion, Additive Manufacturing 14, 2017, pp. 31–38

[88] Gross, B.C.; Erkal, J.L.; Lockwood, S.Y.; Chen, C.; Sence, D.M.: Evaluation of 3D Printing and Its Potential Impact on Biotechnology and the Chemical Sciences

[89] Hanon, M.M.; Marczis, R.; Zsidai, L.: Anisotropy Evaluation of Different Raster Directions, Spatial Orientations, and Fill Percentage of 3D Printed PETG Tensile Test Specimens, Key Engineering Materials 821, 2019, pp. 167–173

[90] Hashmi, S.: Comprehensive Materials Processing, Elsevier, Oxford, 2014

[91] Hazel, K.; Weyant, M.J.: Chest Wall Resection and Reconstruction: Management of Complications, Thoracic surgery clinics 25 (4), 2015, pp. 517–521

[92] Hecker, F.: SFF_Paper_Comparison of Component Properties and Economic Efficiency

[93] Hecker, F.; Driediger, C.; Hirsch, A.; Moritzer, E.: Comparison of Component Properties and Economic Efficiency of the Arburg Plastic Freeforming and Fused Deposition Modeling, Solid Freeform Fabrication 2021: Proceedings of the 32th Annual International, 2021

[94] Hecker, F.; Elsner, C.L.; Hirsch, A.; Moritzer, E.: Investigations for the Optimization of Visual and Geometrical Properties of Arburg Plastic Freeforming Components, Solid Freeform Fabrication 2021: Proceedings of the 32th Annual International

[95] Hecker, F.; Hirsch, A.; Moritzer, E.: Investigation and Modeling of the Residence Time Dependent Material Degradation in the Arburg Plastic Freeforming, 2021

[96] Hentschel, L.; Gonzalez-Gutierrez, J.; Holzer, C.: Eingliederung von Additiven Fertigungstechnologien in einen klinischen Prozess zur Herstellung von medizinischen Implantaten, Jahresmagazin Kunststofftechnik : Ingenieurwissenschaften … : im Fokus 2020, 2020, pp. 56–61

[97] Hentschel, L.; Kynast, F.; Petersmann, S.; Holzer, C.; Gonzalez-Gutierrez, J.: Processing Conditions of a Medical Grade Poly(Methyl Methacrylate) with the Arburg Plastic Freeforming Additive Manufacturing Process, Polymers 12 (11), 2020

[98] Hentschel, L.; Petersmann, S.; Gonzalez-Gutierrez, J.; Arbeiter, F.; Dias, A.; Kynast, F.; Holzer, C.: Mulit-material implant structures with medical-grade polyurethanes via Arburg Plastic Freeforming, International Conference of the Polymer Processing Society, St. Gallen, 2023

[99] Hentschel, L.; Petersmann, S.; Gonzalez-Gutierrez, J.; Kynast, F.; Schäfer, U.; Arbeiter, F.; Holzer, C.: Parameter Optimization of the ARBURG Plastic Freeforming Process by Means of a Design of Experiments Approach, Advanced Engineering Materials, 2022, pp. 2200279

[100] Hentschel, L.; Petersmann, S.; Kynast, F.; Schäfer, U.; Holzer, C.; Gonzalez-Gutierrez, J.: Influence of the Print Envelope Temperature on the Morphology and Tensile Properties of Thermoplastic Polyolefins Fabricated by Material Extrusion and Material Jetting Additive Manufacturing, Polymers 15 (18), 2023

[101] Heraeus Medical: PALACOS® Knochenzemente, https://www.heraeus-medical.com/de/healthcare-professionals/brands/palacos/ (Retrieved on: 20.12.2023)

[102] Hertle, S.; Drexler, M.; Drummer, D.: Additive Manufacturing of Poly(propylene) by Means of Melt Extrusion, Macromolecular Materials and Engineering 301 (12), 2016, pp. 1482–1493

[103] Heyndrickx, A.; Hentschel, L.; Cardon, L.; Holzer, C.: Production of multi-material parts for medical applications, considering the bonding and adhesion strength of deposited materials by use of the freeforming additive manufacturing technology, In: PPI 2022 : 2nd International Polymer Process Innovation Conference, Abstracts, 2022, pp. 97

[104] Hieu, L.C.; Bohez, E.; Vander Sloten, J.; Oris, P.; Phien, H.N.; Vatcharaporn, E.; Binh, P.H.: Design and manufacturing of cranioplasty implants by 3-axis CNC milling, Technol Health Care 10 (5), 2002, pp. 413–423

[105] Hirsch, A.; Dalmer, C.; Moritzer, E.: Investigation of Plastic Freeformed, Open-Pored Structures with Regard to Producibility, Reproducibility and Liquid Permeability, In: Meboldt M.; Klahn C. (Ed.), Industrializing Additive Manufacturing, Proceedings of AMPA2020, Springer International Publishing; Imprint Springer, Cham, 2021 ;, pp. 112–129

[106] Hirsch, A.; Hecker, F.; Moritzer, E.: Process Parameter Optimization to Improve the Mechanical Properties of Arburg Plastic Freeformed Components, Solid Freeform Fabrication 2019: Proceedings of the 30th Annual International, 2019, pp. 705–714

[107] Holzmond, O.; Li, X.: In situ real time defect detection of 3D printed parts, Additive Manufacturing 17, 2017, pp. 135–142

[108] Hong, T.-F.; Ju, W.-J.; Wu, M.-C.; Tai, C.-H.; Tsai, C.-H.; Fu, L.-M.: Rapid prototyping of PMMA microfluidic chips utilizing a CO2 laser, Microfluidics and Nanofluidics 9 (6), 2010, pp. 1125–1133

[109] Honigmann, P.; Sharma, N.; Okolo, B.; Popp, U.; Msallem, B.; Thieringer, F.M.: Patient-Specific Surgical Implants Made of 3D Printed PEEK: Material, Technology, and Scope of Surgical Application, BioMed research international 2018, 2018, pp. 4520636

[110] Hornick, J.: 3D printing in Healthcare, Journal of 3D Printing in Medicine 1 (1), 2017, pp. 13–17

[111] Huang, S.H.; Liu, P.; Mokasdar, A.; Hou, L.: Additive manufacturing and its societal impact: a literature review, The International Journal of Advanced Manufacturing Technology 67 (5), 2013, pp. 1191–1203

[112] Ignatius, A.A.; Claes, L.E.: In vitro biocompatibility of bioresorbable polymers: poly(L, DL-lactide) and poly(L-lactide-co-glycolide), Biomaterials 17 (8), 1996, pp. 831–839

[113] INDUSTRIALIZING ADDITIVE MANUFACTURING, Proceedings of ampa2020, SPRINGER NATURE, [S.l.], 2020

[114] Izdebska-Podsiadły, J.: Polymers for 3D printing, Methods, properties, and characteristics, Plastics Design Library, Elsevier Science & Technology Books, San Diego, 2022

[115] Jain, R.; Mahendru, S.; Aggarwal, A.; Brajesh, V.; Aulakh, H.S.; Singh, S.; Jain, A.; Khazanchi, R.K.: Feasibility of Customised Polymethyl Methacrylate Implants Fabricated Using 3D Printed Flexible Moulds for Correction of Facial Skeletal Deformities, The Journal of craniofacial surgery 32 (6), 2021, pp. 1981–1985

[116] Jalbert, F.; Boetto, S.; Nadon, F.; Lauwers, F.; Schmidt, E.; Lopez, R.: One-step primary reconstruction for complex craniofacial resection with PEEK custom-made implants, Journal of cranio-maxillo-facial surgery : official publication of the European Association for Cranio-Maxillo-Facial Surgery 42 (2), 2014, pp. 141–148

[117] James Brackett, Dakota Cauthen, Justin Condon, Tyler Smith, Nidia Gallego, Vlastamil Kunc, and Chad Duty: Characterizing the Influence of PrintParameters on Porosity and Resulting Density, Solid Freeform Fabrication 2019: Proceedings of the 30th Annual International, 2019

[118] Jaroschek, C.: Spritzgießen für Praktiker, 2. Ed., Hanser, München, 2008

[119] Javaid, M.; Haleem, A.: Additive manufacturing applications in medical cases: A literature based review, Alexandria Journal of Medicine 54 (4), 2018, pp. 411–422

[120] Jonkergouw, J.; van de Vijfeijken, S.E.C.M.; Nout, E.; Theys, T.; van de Casteele, E.; Folkersma, H.; Depauw, P.R.A.M.; Becking, A.G.: Outcome in patient-specific PEEK cranioplasty: A two-center cohort study of 40 implants, Journal of cranio-maxillo-facial surgery : official publication of the European Association for Cranio-Maxillo-Facial Surgery 44 (9), 2016, pp. 1266–1272

[121] Kaiser, W.: Kunststoffchemie für Ingenieure, Von der Synthese bis zur Anwendung, 4. Ed., Hanser, München, 2016

[122] Kang, J.; Wang, L.; Yang, C.; Wang, L.; Yi, C.; He, J.; Li, D.: Custom design and biomechanical analysis of 3D-printed PEEK rib prostheses, Biomechanics and modeling in mechanobiology 17 (4), 2018, pp. 1083–1092

[123] Katalenic, M.: A Better Mold of Cranioplasties, stratasys, 2017

[124] Katschnig, M.: Biofunktionelle Kunststoffimplantate durch additive Fertigung für die kraniomaxillofaziale Chirurgie, Dissertation at Montanuniversitaet Leoben, Leoben, 2019

[125] Katschnig, M.; Arbeiter, F.; Haar, B.; van Campe, G.; Holzer, C.: Cranial Polypropylene Implants by Fused Filament Fabrication, Advanced Engineering Materials 19 (4), 2017, pp. 1600676

[126] Katschnig, M.; Holzer, C.: Cranial polyetheretherketone implants by extrusion–based additive manufacturing: state of the art and prospects, Material Science & Engineering International Journal 2 (3), 2018, pp. 66–68

[127] Katschnig, M.; Wallner, J.; Janics, T.; Burgstaller, C.; Zemann, W.; Holzer, C.: Biofunctional Glycol-Modified Polyethylene Terephthalate and Thermoplastic Polyurethane Implants by Extrusion-Based Additive Manufacturing for Medical 3D Maxillofacial Defect Reconstruction, Polymers 12 (8), 2020

[128] Kaut, F.; Cepus, V.; Grellmann, W.; Lach, R.: Struktur-Eigenschafts-Beziehungen additiv gefertigter thermo-plastischer Polymere am Beispiel der ARBURGFreeformer-Technologie, In: Kynast M.;Eichmann M.; Witt G. (Ed.): Rapid.Tech + FabCon 3.D - International Trade Show & Conference for Additive Manufacturing, Proceedings of the 15th Rapid.Tech Conference, Erfurt, Germany, 5-7 June 2018, Hanser, München, 2018, pp. 217–235

[129] Keating, S.J.; Leland, J.C.; Cai, L.; Oxman, N.: Toward site-specific and self-sufficient robotic fabrication on architectural scales, Science Robotics

[130] Kim, B.-J.; Hong, K.-S.; Park, K.-J.; Park, D.-H.; Chung, Y.-G.; Kang, S.-H.: Customized Cranioplasty Implants Using Three-Dimensional Printers and Polymethyl-Methacrylate Casting, J. Korean Neurosurg. Soc. 52 (6), 2012, pp. 541–546

[131] Kim, B.S.; Lee, J.-S.; Gao, G.; Cho, D.-W.: Direct 3D cell-printing of human skin with functional transwell system, Biofabrication 9 (2), 2017, pp. 25034

[132] Kleppmann, W.: Versuchsplanung, Produkte und Prozesse optimieren, Hanser eLibrary, 9. Ed., Hanser, Carl, München, 2016

[133] Klipper documentation, https://www.klipper3d.org/ (Retrieved on: 30.11.2023)

[134] KLS Martin: Individual Patient Solutions: IPS Implants®, https://www.klsmartin.com/de/produkte/individual-patient-solutions-mkg/ips-implants/ (Retrieved on: 02.12.2023)

[135] Kocher, G.J.; Al-Hurani, M.; Minervini, F.: Surgical fixation of rib fractures: how I do it, Journal of Visualized Surgery 6 (0), 2019

[136] Korpela, J.; Kokkari, A.; Korhonen, H.; Malin, M.; Närhi, T.; Seppälä, J.: Biodegradable and bioactive porous scaffold structures prepared using fused deposition modeling,

Journal of biomedical materials research. Part B, Applied biomaterials 101 (4), 2013, pp. 610–619

[137] Kotz, F.; Arnold, K.; Bauer, W.; Schild, D.; Keller, N.; Sachsenheimer, K.; Nargang, T.M.; Richter, C.; Helmer, D.; Rapp, B.E.: Three-dimensional printing of transparent fused silica glass, Nature 544 (7650), 2017, pp. 337–339

[138] Kriegel, R.J.: Kalottenplastik für große Schädeldefekte mit PMMA (Polymethylmethacrylat) oder Tutoplast-prozessierten autogenen Knochentransplantaten, Inaugural-Dissertation at Rheinischen Friedrich-Wilhelms-Universität Bonn, 2006

[139] DIN EN ISO 178: Kunststoffe_- Bestimmung der Biegeeigenschaften (ISO 178:2019), 01.08.2019

[140] DIN EN ISO 179-1: Kunststoffe_- Bestimmung der Charpy-Schlageigenschaften - Teil 1: Nicht instrumentierte Schlagzähigkeitsprüfung (ISO 179-1:2010), 01.11.2010

[141] DIN EN ISO 179-2: Kunststoffe_- Bestimmung der Charpy-Schlageigenschaften_- Teil_2: Instrumentierte Schlagzähigkeitsprüfung (ISO_179-2:2020), 01.09.2020

[142] DIN EN ISO 527-1: Kunststoffe_- Bestimmung der Zugeigenschaften_- Teil_1: Allgemeine Grundsätze (ISO_527-1:2019), 01.12.2019

[143] DIN EN ISO 6603-2: Kunststoffe_- Bestimmung des Durchstoßverhaltens von festen Kunststoffen_- Teil_2: Instrumentierter Schlagversuch (ISO_6603-2:2000), 01.04.2002

[144] Kurtz, S.M.; Devine, J.N.: PEEK biomaterials in trauma, orthopedic, and spinal implants, Biomaterials 28 (32), 2007, pp. 4845–4869

[145] Lanzotti, A.; Martorelli, M.; Staiano, G.: Understanding Process Parameter Effects of RepRap Open-Source Three-Dimensional Printers Through a Design of Experiments Approach, Journal of Manufacturing Science and Engineering (137), 2015

[146] Lee, C.-Y.; Liu, C.-Y.: The influence of forced-air cooling on a 3D printed PLA part manufactured by fused filament fabrication, Additive Manufacturing 25, 2019, pp. 196–203

[147] Li, J.; Ellis, D.G.; Kodym, O.; Rauschenbach, L.; Rieß, C.; Sure, U.; Wrede, K.H.; Alvarez, C.M.; Wodzinski, M.; Daniol, M.; Hemmerling, D.; Mahdi, H.; Clement, A.; Kim, E.; Fishman, Z.; Whyne, C.M.; Mainprize, J.G.; Hardisty, M.R.; Pathak, S.; Sindhura, C.; Gorthi, R.K.S.S.; Kiran, D.V.; Gorthi, S.; Yang, B.; Fang, K.; Li, X.; Kroviakov, A.; Yu, L.; Jin, Y.; Pepe, A.; Gsaxner, C.; Herout, A.; Alves, V.; Španěl, M.; Aizenberg, M.R.; Kleesiek, J.; Egger, J.: Towards clinical applicability and computational efficiency in automatic cranial implant design: An overview of the AutoImplant 2021 cranial implant design challenge, Medical image analysis 88, 2023, pp. 102865

[148] Li, J.; Gsaxner, C.; Pepe, A.; Morais, A.; Alves, V.; Campe, G. von; Wallner, J.; Egger, J.: Synthetic skull bone defects for automatic patient-specific craniofacial implant design, Scientific data 8 (1), 2021, pp. 36

[149] Ligon, S.C.; Liska, R.; Stampfl, J.; Gurr, M.; Mulhaupt, R.: Polymers for 3D Printing and Customized Additive Manufacturing, Chemical reviews 117 (15), 2017, pp. 10212–10290

[150] Lin, X.; Coates, P.; Hebda, M.; Wang, R.; Lu, Y.; Zhang, L.: Experimental analysis of the tensile property of FFF-printed elastomers, Polymer Testing 90, 2020, pp. 106687

[151] Liu, F.; Wang, X.: Synthetic Polymers for Organ 3D Printing, Polymers 12 (8), 2020

[152] Liu, X.; Yuk, H.; Lin, S.; Parada, G.A.; Tang, T.-C.; Tham, E.; La Fuente-Nunez, C. de; Lu, T.K.; Zhao, X.: 3D Printing of Living Responsive Materials and Devices, Advanced Materials 30 (4), 2018, pp. 1704821

[153] Liu, Y.; Yi, N.; Davies, R.; McCutchion, P.; Ghita, O.: Powder Bed Fusion Versus Material Extrusion: A Comparative Case Study on Polyether-Ether-Ketone Cranial Implants, 3D Printing and Additive Manufacturing 10 (5), 2023, pp. 941–954

[154] Liu, Z.: Review and prospect of thermal analysis technology applied to study thermal properties of energetic materials, FirePhysChem 1 (3), 2021, pp. 129–138

[155] Lorenzo-Bañuelos, M.; Díaz, A.; Cuesta, I.I.: Influence of raster orientation on the determination of fracture properties of polypropylene thin components produced by additive manufacturing, Theoretical and Applied Fracture Mechanics 107, 2020, pp. 102536

[156] Lu, J.: Orthopedic Bone Cements, In: Poitout D.G. (Ed.): Biomechanics and Biomaterials in Orthopedics, Springer London, London, 2004, pp. 86–100

[157] Lu, Y.; Chen, S.C.: Micro and nano-fabrication of biodegradable polymers for drug delivery, Advanced drug delivery reviews 56 (11), 2004, pp. 1621–1633

[158] Luiz Fernando C. S. Durão; Richard Barkoczy; Eduardo Zancul; Linda Lee Ho; Renan Bonnard: Optimizing additive manufacturing parameters for the fused deposition modeling technology using a design of experiments, Progress in Additive Manufacturing 4 (3), 2019, pp. 291–313

[159] Mahmood, S.; Qureshi, A.J.; Talamona, D.: Taguchi based process optimization for dimension and tolerance control for fused deposition modelling, Additive Manufacturing 21, 2018, pp. 183–190

[160] Malik, H.H.; Darwood, A.R.J.; Shaunak, S.; Kulatilake, P.; El-Hilly, A.A.; Mulki, O.; Baskaradas, A.: Three-dimensional printing in surgery: a review of current surgical applications, The Journal of surgical research 199 (2), 2015, pp. 512–522

[161] Marchac, D.; Greensmith, A.: Long-term experience with methylmethacrylate cranioplasty in craniofacial surgery, J Plast Reconstr Aesthet Surg. 61 (7), 2008, 744-52; discussion 753

[162] Maroti, P.; Varga, P.; Abraham, H.; Falk, G.; Zsebe, T.; Meiszterics, Z.; Mano, S.; Csernatony, Z.; Rendeki, S.; Nyitrai, M.: Printing orientation defines anisotropic mechanical properties in additive manufacturing of upper limb prosthetics, Materials Research Express 6 (3), 2019, pp. 35403

[163] Maroulakos, M.; Kamperos, G.; Tayebi, L.; Halazonetis, D.; Ren, Y.: Applications of 3D printing on craniofacial bone repair: A systematic review, Journal of Dentistry 80, 2019, pp. 1–14

[164] Matyjaszewski, K.; Möller, M.; Müllen, K.; Ober, C.K.: Polymers for advanced functional materials, Polymer Science, a comprehensive reference / Ed.-in-chief Krzysztof Matyjaszewski; Martin Möller ; Vol. 8, Elsevier, Amsterdam, 2012

[165] McDonagh, T.; Belton, P.; Qi, S.: Manipulating drug release from 3D printed dual-drug loaded polypills using challenging polymer compositions, International Journal of Pharmaceutics 637, 2023, pp. 122895

[166] Medical University of Graz: CAMed - Clinical additive manufacturing for medical applications, Graz, Austria, 2020, https://www.medunigraz.at/en/camed/ (Retrieved on: 22.07.2020)

[167] ÖNORM EN ISO 14971: Medizinprodukte - Anwendung des Risikomanagements auf Medizinprodukte, 01.03.2013

[168] ÖNORM EN ISO 13485: Medizinprodukte - Qualitätsmanagementsysteme - Anforderungen für regulatorische Zwecke, 01.08.2017

[169] Mele, M.; Cercenelli, L.; Pisabeschi, G.; Fiorini, M.; Zucchelli, A.; Campana, G.; Tarsitano, A.; Marcelli, E.: 3D printing of a cranial implant with energy-absorbing polymer via ARBURG plastic freeforming technology, Journal of Mechanics in Medicine and Biology, 2023

[170] Memon, A.R.; Li, J.; Egger, J.; Chen, X.: A review on patient-specific facial and cranial implant design using Artificial Intelligence (AI) techniques, Expert review of medical devices 18 (10), 2021, pp. 985–994

[171] Michael E. Mackay: The importance of rheological behavior in the additive manufacturing technique material extrusion, Journal of Rheology 62 (6), 2018, pp. 1549

[172] Minitab Inc.: Factorial and fractional factorial designs, https://support.minitab.com/en-us/minitab/20/help-and-how-to/statistical-modeling/doe/supporting-topics/factorial-and-screening-designs/factorial-and-fractional-factorial-designs/ (Retrieved on: 02.12.2023)

[173] Minitab Inc.: What is the design resolution in a factorial design?, https://support.minitab.com/en-us/minitab/20/help-and-how-to/statistical-modeling/doe/supporting-topics/factorial-and-screening-designs/what-is-design-resolution/ (Retrieved on: 02.12.2023)

[174] Mishra, A.; Seethamraju, K.; Delaney, J.; Willoughby, P.; Faust, R.: Long-term in vitro hydrolytic stability of thermoplastic polyurethanes, Journal of biomedical materials research. Part A 103 (12), 2015, pp. 3798–3806

[175] Moghadasi, K.; Mohd Isa, M.S.; Ariffin, M.A.; Mohd jamil, M.Z.; Raja, S.; Wu, B.; Yamani, M.; Bin Muhamad, M.R.; Yusof, F.; Jamaludin, M.F.; Ab Karim, Mohd Sayuti bin; Abdul Razak, B.b.; Yusoff, N.b.: A review on biomedical implant materials and the effect of friction stir based techniques on their mechanical and tribological properties, Journal of Materials Research and Technology 17, 2022, pp. 1054–1121

[176] Mohamed, O.A.; Masood, S.H.; Bhowmik, J.L.: Investigation of dimensional variation in parts manufactured by fused deposition modeling using Gauge Repeatability and Reproducibility, IOP Conference Series: Materials Science and Engineering 310, 2018, pp. 12090

[177] Moiduddin, K.; Darwish, S.; Al-Ahmari, A.; ElWatidy, S.; Mohammad, A.; Ameen, W.: Structural and mechanical characterization of custom design cranial implant created using additive manufacturing, Electronic Journal of Biotechnology 29, 2017, pp. 22–31

[178] Morales-Gómez, J.A.; Garcia-Estrada, E.; Leos-Bortoni, J.E.; Delgado-Brito, M.; Flores-Huerta, L.E.; La Cruz-Arriaga, A.A. de; Torres-Díaz, L.J.; León, Á.R.M.-P. de: Cranioplasty with a low-cost customized polymethylmethacrylate implant using a desktop 3D printer, J. Neurosurg., 2018, pp. 1–7

[179] Moritzer, E.; Hirsch, A.; Heim, H.-P.; Cherif, C.; Truemper, W.: Plastic droplet welding: bond strength between plastic freeforming structures and continuous fiber-reinforced thermoplastic composites, Welding in the World 63 (3), 2019, pp. 867–873

[180] Moser, M.; Schmid, R.; Schindel, R.; Hildebrandt, G.: Patient-specific polymethylmethacrylate prostheses for secondary reconstruction of large calvarial defects:, A retrospective feasibility study of a new intraoperative moulding device for cranioplasty, J. Cranio-MaxilloFac. Surg. 45 (2), 2017, pp. 295–303

[181] Motherway, J.A.; Verschueren, P.; van der Perre, G.; Vander Sloten, J.; Gilchrist, M.D.: The mechanical properties of cranial bone: the effect of loading rate and cranial sampling position, Journal of biomechanics 42 (13), 2009, pp. 2129–2135

[182] Msallem, B.; Sharma, N.; Cao, S.; Halbeisen, F.S.; Zeilhofer, H.-F.; Thieringer, F.M.: Evaluation of the Dimensional Accuracy of 3D-Printed Anatomical Mandibular Models Using FFF, SLA, SLS, MJ, and BJ Printing Technology, Journal of clinical medicine 9 (3), 2020, pp. 817

[183] Muhammad Iqbal Sabir; Xiaoxue Xu; Li Li: A review on biodegradable polymeric materials for bone tissue engineering applications, Journal of Materials Science 44 (21), 2009, pp. 5713–5724

[184] Navarro, M.; Michiardi, A.; Castaño, O.; Planell, J.A.: Biomaterials in orthopaedics, Journal of the Royal Society, Interface 5 (27), 2008, pp. 1137–1158

[185] Neff, M.; Pawelczyk, L.: Resilient Hard-soft Combinations with Plastic Freeforming, ATZproduction worldwide 6 (2), 2019, pp. 36–39

[186] Neff, M.; Petereit, S.: The Promise of 3D-Printed Implants, 1136 Pages / Transactions on Additive Manufacturing Meets Medicine, Vol. 5 No. S1 (2023): Trans. AMMM Supplement, 2023

[187] O'kane, W.J.; Young, R.J.; Ryan, A.J.: The effect of annealing on the structure and properties of isotactic polypropylene films, Journal of Macromolecular Science, Part B 34 (4), 1995, pp. 427–458

[188] Omnexus: Comprehensive Guide on Polymethyl methacrylate (PMMA or Acrylic), https://omnexus.specialchem.com/selection-guide/polymethyl-methacrylate-pmma-acrylic-plastic (Retrieved on: 02.12.2023)

[189] Osswald, T.A.; Hernández-Ortiz, J.P.: Polymer processing, Modeling and simulation, Hanser Publishers, Munich, Cincinnati, 2008

[190] Otero, J.J.; Vijverman, A.; Mommaerts, M.Y.: Use of fused deposit modeling for additive manufacturing in hospital facilities: European certification directives, Journal of cranio-maxillo-facial surgery : official publication of the European Association for Cranio-Maxillo-Facial Surgery 45 (9), 2017, pp. 1542–1546

[191] Ovlaque, P.; Bayart, M.; Soulestin, J.; Trolez, Y.; Olivier, D.; Bujeau, B.; Charlon, S.: On the temperature evolution and related crystallinity of polypropylene parts processed via material extrusion, Additive Manufacturing 58, 2022, pp. 103065

[192] Pagac, M.; Hajnys, J.; Ma, Q.-P.; Jancar, L.; Jansa, J.; Stefek, P.; Mesicek, J.: A Review of Vat Photopolymerization Technology: Materials, Applications, Challenges, and Future Trends of 3D Printing, Polymers 13 (4), 2021

[193] Palanisamy, C.; Raman, R.; Dhanraj, P.k.: Additive manufacturing: a review on mechanical properties of polyjet and FDM printed parts, Polymer Bulletin 79 (9), 2022, pp. 7065–7116

[194] Panayotov, I.V.; Orti, V.; Cuisinier, F.; Yachouh, J.: Polyetheretherketone (PEEK) for medical applications, Journal of Materials Science. Materials in Medicine 27 (7), 2016, pp. 118

[195] Panda, B.N.; Shankhwar, K.; Garg, A.; Jian, Z.: Performance evaluation of warping characteristic of fused deposition modelling process, The International Journal of Advanced Manufacturing Technology 88 (5-8), 2017, pp. 1799–1811

[196] Park, E.-K.; Lim, J.-Y.; Yun, I.-S.; Kim, J.-S.; Woo, S.-H.; Kim, D.-S.; Shim, K.-W.: Cranioplasty Enhanced by Three-Dimensional Printing: Custom-Made Three-Dimensional-Printed Titanium Implants for Skull Defects, The Journal of craniofacial surgery 27 (4), 2016, pp. 943–949

[197] Park, G.-J.: Analytic Methods for Design Practice, Springer London, London, 2007

[198] Park, G.-Y.: Osteoblastenspezifische Biokompatibilität und mechanische Eigenschaften von etablierten und nichtetablierten Polymeren im Hinblick auf den Einsatz als Schädelimplantat, Dissertation at Ruhr-Universitaet Bochum, Bochum, 2012

[199] Petersen, E.E.; Kidd, R.W.; Pearce, J.M.: Impact of DIY Home Manufacturing with 3D Printing on the Toy and Game Market, Technologies 5 (3), 2017, pp. 45

[200] Petersmann, S.; Hentschel, L.; Gonzalez-Gutierrez, J.; Tödtling, M.; Schäfer, U.; Arbeiter, F.; Üçal, M.: The Effects of Washing and Formaldehyde Sterilization on the Mechanical Performance of Poly(methyl Methacrylate) (PMMA) Parts Produced by Material Extrusion-Based Additive Manufacturing or Material Jetting, Advanced Engineering Materials, 2022, pp. 2200225

[201] Petersmann, S.; Huemer, M.; Hentschel, L.; Arbeiter, F.: Effects of simulated body fluid on the mechanical properties of polycarbonate polyurethane produced via material jetting, Polymer Testing 120, 2023, pp. 107977

[202] Petersmann, S.; Smith, J.A.; Schäfer, U.; Arbeiter, F.: Material extrusion-based additive manufacturing of polyetheretherketone cranial implants: Mechanical performance and print quality, Journal of Materials Research and Technology 22, 2023, pp. 642–657

[203] Petersmann, S.; Spoerk, M.; Huber, P.; Lang, M.; Pinter, G.; Arbeiter, F.: Impact Optimization of 3D-Printed Poly(methyl methacrylate) for Cranial Implants, Macromolecular Materials and Engineering 304 (11), 2019

[204] Petersmann, S.; Spoerk, M.; van de Steene, W.; Üçal, M.; Wiener, J.; Pinter, G.; Arbeiter, F.: Mechanical properties of polymeric implant materials produced by extrusion-based additive manufacturing, Journal of the mechanical behavior of biomedical materials 104, 2020, pp. 103611

[205] Petersmann, S.; Spoerk-Erdely, P.; Feuchter, M.; Wieme, T.; Arbeiter, F.; Spoerk, M.: Process-induced morphological features in material extrusion-based additive manufacturing of polypropylene, Additive Manufacturing 35, 2020, pp. 101384

[206] Pinter, P.; Baumann, S.; Lohr, C.; Heuer, A.; Englert, L.; Weidemann, K.A.: Mechanical Properties of Additively Manufactured Polymer Samples using a Piezo Controlled Injection Moulding unit and Fused Filament Fabrication compared with a conventional Injection Molding Process, Solid Freeform Fabrication 2018: Proceedings of the 29th Annual International, 2018, pp. 2219–2227

[207] Pisaneschi, G.; Mele, M.; Zucchelli, A.; Fiorini, M.; Campana, G.; Marcelli, E.; Tarsitano, A.; Lucchi, E.; Cercenelli, L.: Numerical and experimental investigation of a 3D-printed PCU patient-specific cranial implant, Progress in Additive Manufacturing, 2023, pp. 1–15

[208] Poukens, J.; Laeven, P.; Beerens, M.; Nijenhuis, G.; Sloten, J.V.; Stoelinga, P.; Kessler, P.: A classification of cranial implants based on the degree of difficulty in computer design and manufacture, The international journal of medical robotics + computer assisted surgery : MRCAS 4 (1), 2008, pp. 46–50

[209] Powell, D.G.: Medical Applications of Polycarbonate, 1998, https://www.mddionline.com/product-development/medical-applications-of-polycarbonate (Retrieved on: 02.12.2023)

[210] Ramakrishna, S.; Mayer, J.; Wintermantel, E.; Leong, K.W.: Biomedical applications of polymer-composite materials: a review, Composites Science and Technology 61 (9), 2001, pp. 1189–1224

[211] Ramezani Dana, H.; Barbe, F.; Delbreilh, L.; Azzouna, M.B.; Guillet, A.; Breteau, T.: Polymer additive manufacturing of ABS structure: Influence of printing direction on mechanical properties, Journal of Manufacturing Processes 44, 2019, pp. 288–298

[212] Rankin, T.M.; Giovinco, N.A.; Cucher, D.J.; Watts, G.; Hurwitz, B.; Armstrong, D.G.: Three-dimensional printing surgical instruments: are we there yet?, The Journal of surgical research 189 (2), 2014, pp. 193–197

[213] Ratner, B.D.: Biomaterials science, An introduction to materials in medicine, 2. Ed., Elsevier Academic Press, Amsterdam, Boston, 2004

[214] Reich, M.J.; Woern, A.L.; Tanikella, N.G.; Pearce, J.M.: Mechanical Properties and Applications of Recycled Polycarbonate Particle Material Extrusion-Based Additive Manufacturing, Materials (Basel, Switzerland) 12 (10), 2019

[215] RepRap, 2023, https://reprap.org/wiki/RepRap (Retrieved on: 30.11.2023)

[216] Ridwan-Pramana, A.; Marcián, P.; Borák, L.; Narra, N.; Forouzanfar, T.; Wolff, J.: Structural and mechanical implications of PMMA implant shape and interface geometry in cranioplasty--A finite element study, Journal of cranio-maxillo-facial surgery : official publication of the European Association for Cranio-Maxillo-Facial Surgery 44 (1), 2016, pp. 34–44

[217] Robert W. Hopper: Coalescence of Two Equal Cylinders: Exact Results for Creeping Viscous Plane Flow Driven by Capillarity, 1993

[218] Roehm America LLC: CYROLITE MD H12 polymer, Parsippany, NJ, USA, 2018, https://www.cyrolite.com/en/cyrolite-md (Retrieved on: 19.08.2020)

[219] Rotaru, H.; Baciut, M.; Stan, H.; Bran, S.; Chezan, H.; Iosif, A.; Tomescu, M.; Kim, S.-G.; Rotaru, A.; Baciut, G.: Silicone rubber mould cast polyethylmethacrylate-

hydroxyapatite plate used for repairing a large skull defect, J. Cranio-MaxilloFac. Surg. 34 (4), 2006, pp. 242–246

[220] Roth, S.; Seul, T.: Kunststoffe in der Medizintechnik, Von der Idee bis zur Industrialisierung, Hanser, Carl, München, 2020

[221] Sahal, M.; Chen, M.T.; Sharma, S.; Nair, S.S.; Nair, V.G.: 3DP materials and methods for orthopedic, dental and maxillofacial implants: a brief comparative report, Journal of 3D Printing in Medicine 3 (3), 2019, pp. 127–134

[222] Saijo, H.; Igawa, K.; Kanno, Y.; Mori, Y.; Kondo, K.; Shimizu, K.; Suzuki, S.; Chikazu, D.; Iino, M.; Anzai, M.; Sasaki, N.; Chung, U.; Takato, T.: Maxillofacial reconstruction using custom-made artificial bones fabricated by inkjet printing technology, Journal of Artificial Organs 12 (3), 2009, pp. 200–205

[223] Samaplast AG: Mit Additiver Fertigung bereit für die Medical Zukunft

[224] Samaplast AG: AM in zertifizierter Umgebung nach DIN SPEC 1701, 2021, https://samaplast.ch/wp-content/uploads/SAMA-White-Paper-A4_D_26.1_neu.pdf (Retrieved on: 04.12.2023)

[225] Sastri, V.R.: Plastics in medical devices, Properties, requirements, and applications, Plastics Design Library, Elsevier, William Andrew Applied Science Publishers, San Diego, 2022

[226] Scheffknecht, B.: Additive Fertigung - Implantate für Mensch und Tier, 2020, https://samaplast.ch/wp-content/uploads/200603-D-sc-Beitrag-in-Medplast-2020-Seite-32-und-33.pdf

[227] Scheffknecht, B.: Potenziale für Implantate heben, 2022, https://samaplast.ch/wp-content/uploads/SAMA-White-Paper-A4_D_26.1_neu.pdf (Retrieved on: 04.12.23)

[228] Sebastian W. Pattinson; A. John Hart: Additive Manufacturing of Cellulosic Materials with Robust Mechanics and Antimicrobial Functionality, Advanced Materials Technologies 2 (4), 2017, pp. 1600084

[229] Sergent, F.; Desilles, N.; Lacoume, Y.; Tuech, J.-J.; Marie, J.-P.; Bunel, C.: Biomechanical analysis of polypropylene prosthetic implants for hernia repair: an experimental study, American journal of surgery 200 (3), 2010, pp. 406–412

[230] Shafiee, A.; Atala, A.: Printing Technologies for Medical Applications, Trends in molecular medicine 22 (3), 2016, pp. 254–265

[231] Sharma, N.; Aghlmandi, S.; Cao, S.; Kunz, C.; Honigmann, P.; Thieringer, F.M.: Quality Characteristics and Clinical Relevance of In-House 3D-Printed Customized Polyetheretherketone (PEEK) Implants for Craniofacial Reconstruction, Journal of clinical medicine 9 (9), 2020

[232] Sharma, N.; Honigmann, P.; Cao, S.; Thieringer, F.: Dimensional characteristics of FDM 3D printed PEEK implant for craniofacial reconstructions, Transactions on Additive Manufacturing Meets Medicine, Vol 2 No 1 (2020): Trans. AMMM, 2020

[233] Sheikh, Z.; Najeeb, S.; Khurshid, Z.; Verma, V.; Rashid, H.; Glogauer, M.: Biodegradable Materials for Bone Repair and Tissue Engineering Applications, Materials (Basel, Switzerland) 8 (9), 2015, pp. 5744–5794

[234] Shen, C.; Zhang, Y.; Li, Q.; Zhu, M.; Hou, Y.; Qu, M.; Xu, Y.; Chai, G.: Application of three-dimensional printing technique in artificial bone fabrication for bone defect after mandibular angle ostectomy, Zhongguo xiu fu chong jian wai ke za zhi = Zhongguo xiufu chongjian waike zazhi = Chinese journal of reparative and reconstructive surgery 28 (3), 2014, pp. 300–303

[235] Shusteff, M.; Browar, A.M.; Kelly, B.E.; Henriksson, J.; Weisgraber, T.H.; Panas, R.M.; Fang, N.X.; Spadaccini, C.M.: One-step volumetric additive manufacturing of complex polymer structures, Science Advances

[236] Silva, L.B.; Oliveira, R.O. de; Barbosa, G.F.; Shiki, S.B.; Fu, K.: Influence of the single-screw extruder nozzle diameter on pellet-based filaments for additive manufacturing, Journal of the Brazilian Society of Mechanical Sciences and Engineering 44 (7), 2022, pp. 1–11

[237] Sinn, D.P.; Bedrossian, E.; Vest, A.K.: Craniofacial implant surgery, Oral and maxillofacial surgery clinics of North America 23 (2), 2011, 321-35, vi-vii

[238] Sivarupan, T.; Balasubramani, N.; Saxena, P.; Nagarajan, D.; El Mansori, M.; Salonitis, K.; Jolly, M.; Dargusch, M.S.: A review on the progress and challenges of binder jet 3D printing of sand moulds for advanced casting, Additive Manufacturing 40, 2021, pp. 101889

[239] Splavski, B.; Lakicevic, G.; Kovacevic, M.; Godec, D.: Customized alloplastic cranioplasty of large bone defects by 3D-printed prefabricated mold template after posttraumatic decompressive craniectomy: A technical note, Surgical neurology international 13, 2022, pp. 169

[240] Splavski, B.; Lakičević, G.; Rotim, K.; Božić, B.; Godec, D.: A 4-case study of alloplastic cranioplasty by additive manufacturing of 3D printed modified mold, In: 2018, pp. 72

[241] Spoerk, M.: Optimisation of the Mechanical Properties and Processing of Polypropylene and Poly(Lactic Acid) Parts Produced by Extrusion-Based Additive Manufacturing, PhD thesis at Montanuniversitaet Leoben, 2018

[242] Spoerk, M.; Arbeiter, F.; Cajner, H.; Sapkota, J.; Holzer, C.: Parametric optimization of intra- and inter-layer strengths in parts produced by extrusion-based additive

manufacturing of poly(lactic acid), Journal of Applied Polymer Science 134 (41), 2017, pp. 45401

[243] Spoerk, M.; Arbeiter, F.; Raguž, I.; Weingrill, G.; Fischinger, T.; Traxler, G.; Schuschnigg, S.; Cardon, L.; Holzer, C.: Polypropylene Filled With Glass Spheres in Extrusion-Based Additive Manufacturing: Effect of Filler Size and Printing Chamber Temperature, Macromolecular Materials and Engineering 303 (7), 2018, pp. 1800179

[244] Spoerk, M.; Holzer, C.; Gonzalez-Gutierrez, J.: Material extrusion-based additive manufacturing of polypropylene: A review on how to improve dimensional inaccuracy and warpage, Journal of Applied Polymer Science 137 (12), 2020, pp. 48545

[245] Spoerk, M.; Sapkota, J.; Weingrill, G.; Fischinger, T.; Arbeiter, F.; Holzer, C.: Shrinkage and Warpage Optimization of Expanded-Perlite-Filled Polypropylene Composites in Extrusion-Based Additive Manufacturing, Macromolecular Materials and Engineering 302 (10), 2017, pp. 1700143

[246] Spoerk, M.; Savandaiah, C.; Arbeiter, F.; Sapkota, J.; Holzer, C.: Optimization of mechanical properties of glass-spheres-filled polypropylene composites for extrusion-based additive manufacturing, Polymer Composites 40 (2), 2019, pp. 638–651

[247] Spoerk, M.; Savandaiah, C.; Arbeiter, F.; Traxler, G.; Cardon, L.; Holzer, C.; Sapkota, J.: Anisotropic properties of oriented short carbon fibre filled polypropylene parts fabricated by extrusion-based additive manufacturing, Composites Part A: Applied Science and Manufacturing 113, 2018, pp. 95–104

[248] Srinivas, V.; van Hooy-Corstjens, C.S.; Rastogi, S.; Harings, J.A.: Promotion of molecular diffusion and/or crystallization in fused deposition modeled poly(lactide) welds, Polymer 202, 2020, pp. 122637

[249] Storn, R.; Price, K.: Differential Evolution – A Simple and Efficient Heuristic for global Optimization over Continuous Spaces, Journal of Global Optimization 11 (4), 1997, pp. 341–359

[250] Stratasys: A better mold for cranioplasties: 3D printing enables faster, cheaper, more predictable outcomes., https://www.stratasys.com/en/resources/case-studies/university-of-zagrebs-centre-for-additive-technologies/ (Retrieved on: 13.03.2024)

[251] Sumida, T.; Otawa, N.; Kamata, Y.U.; Kamakura, S.; Mtsushita, T.; Kitagaki, H.; Mori, S.; Sasaki, K.; Fujibayashi, S.; Takemoto, M.; Yamaguchi, A.; Sohmura, T.; Nakamura, T.; Mori, Y.: Custom-made titanium devices as membranes for bone augmentation in implant treatment: Clinical application and the comparison with conventional titanium mesh, Journal of cranio-maxillo-facial surgery : official publication of the European Association for Cranio-Maxillo-Facial Surgery 43 (10), 2015, pp. 2183–2188

[252] Sutradhar, A.; Paulino, G.H.; Miller, M.J.; Nguyen, T.H.: Topological optimization for designing patient-specific large craniofacial segmental bone replacements, Proceedings of the National Academy of Sciences of the United States of America 107 (30), 2010, pp. 13222–13227

[253] Svetlizky, D.; Das, M.; Zheng, B.; Vyatskikh, A.L.; Bose, S.; Bandyopadhyay, A.; Schoenung, J.M.; Lavernia, E.J.; Eliaz, N.: Directed energy deposition (DED) additive manufacturing: Physical characteristics, defects, challenges and applications, Materials Today 49, 2021, pp. 271–295

[254] Tan, E.T.W.; Ling, J.M.; Dinesh, S.K.: The feasibility of producing patient-specific acrylic cranioplasty implants with a low-cost 3D printer, J. Neurosurg. 124 (5), 2016, pp. 1531–1537

[255] Tan, Z.; Parisi, C.; Di Silvio, L.; Dini, D.; Forte, A.E.: Cryogenic 3D Printing of Super Soft Hydrogels, Scientific Reports 7 (1), 2017, pp. 16293

[256] Teo, A.J.; Mishra, A.; Park, I.; Kim, Y.-J.; Park, W.-T.; Yoon, Y.-J.: Polymeric Biomaterials for Medical Implants and Devices, ACS Biomaterials Science & Engineering 2 (4), 2016, pp. 454–472

[257] Teoh, S.H.: Engineering materials for biomedical applications, Biomaterials engineering and processing series, Vol. 1, World Scientific Pub, Singapore, 2004

[258] Thompson, M.K.; Moroni, G.; Vaneker, T.; Fadel, G.; Campbell, R.I.; Gibson, I.; Bernard, A.; Schulz, J.; Graf, P.; Ahuja, B.; Martina, F.: Design for Additive Manufacturing: Trends, opportunities, considerations, and constraints, CIRP Annals 65 (2), 2016, pp. 737–760

[259] Thumsorn, S.; Prasong, W.; Ishigami, A.; Kurose, T.; Kobayashi, Y.; Ito, H.: Influence of Ambient Temperature and Crystalline Structure on Fracture Toughness and Production of Thermoplastic by Enclosure FDM 3D Printer, Journal of Manufacturing and Materials Processing 7 (1), 2023, pp. 44

[260] Timothy J. Coogan; David O. Kazmer: In-line rheological monitoring of fused deposition modeling, Journal of Rheology 63 (1), 2018, pp. 141

[261] Tsouknidas, A.; Maropoulos, S.; Savvakis, S.; Michailidis, N.: FEM assisted evaluation of PMMA and Ti6Al4V as materials for cranioplasty resulting mechanical behaviour and the neurocranial protection, Bio-medical materials and engineering 21 (3), 2011, pp. 139–147

[262] Turner, B.N.; Strong, R.; Gold, S.A.: A review of melt extrusion additive manufacturing processes: I. Process design and modeling, Rapid Prototyping Journal

[263] Umweltbundesamt: BISPHENOL A Massenchemikalie mit unerwünschten Nebenwirkungen,

https://www.umweltbundesamt.de/sites/default/files/medien/publikation/long/3782.pdf
(Retrieved on: 02.12.2023)

[264] Valkenares, H.; Vogeler, F.; Voet, A.; Kurth, J.P.: Screw extrusion based 3D printing, a novel additive manufacturing technology, 2013

[265] van de Vijfeijken, Sophie E.C.M.; Münker, T.J.; Jager, N. de; Vandertop, W.P.; Becking, A.G.; Kleverlaan, C.J.; Becking, A.G.; Dubois, L.; Karssemakers, L.; Milstein, D.; van de Vijfeijken, S.; Depauw, P.; Hoefnagels, F.; Vandertop, W.P.; Kleverlaan, C.J.; Münker, T.; Maal, T.; Nout, E.; Riool, M.; Zaat, S.: Properties of an In Vivo Fractured Poly(Methyl Methacrylate) Cranioplasty After 15 Years, World Neurosurgery 123, 2019, e60-e68

[266] Varga, J.; Tóth, F.; Hummel, D.O.: Annealing of the β-modification of polypropylene, Makromolekulare Chemie. Macromolecular Symposia 5 (1), 1986, pp. 213–223

[267] Verius, M.; Marreiros, F.; Heuze, Y.; Unterhofer, C.; Recheis, W.: A novel approach for implant design of large cranial defects using PMMA and rapid prototyping techniques, European Congress of Radiology 2011, Vienna, Austria, 2011, https://epos.myesr.org/poster/esr/ecr2011/C-0950 (Retrieved on: 25.08.2020)

[268] Visser, C.W.; Kamperman, T.; Karbaat, L.P.; Lohse, D.; Karperien, M.: In-air microfluidics enables rapid fabrication of emulsions, suspensions, and 3D modular (bio)materials, Science Advances 4 (1), 2018, eaao1175

[269] Voron Design, https://vorondesign.com/ (Retrieved on: 30.11.2023)

[270] Vyavahare, S.; Teraiya, S.; Panghal, D.; Kumar, S.: Fused deposition modelling: a review, Rapid Prototyping Journal, 2019

[271] Walenkamp, G.H.I.M.; Murray, D.W.; Henze, U.; Kock, H.-J.: Bone Cements and Cementing Technique, Springer Berlin Heidelberg, Berlin, Heidelberg, 2001

[272] Wang, J.; Lee, M.K.; Park, S.-M.; Hong, S.; Kim, N.: A study on the mechanical properties and deformation behavior of injection molded PMMA-TSP laminated composite, Korea-Australia Rheology Journal 24 (1), 2012, pp. 23–33

[273] Wang, J.Y.; Xu, D.D.; Sun, W.; Du, S.M.; Guo, J.J.; Xu, G.J.: Effects of nozzle-bed distance on the surface quality and mechanical properties of fused filament fabrication parts, IOP Conference Series: Materials Science and Engineering 479, 2019, pp. 12094

[274] Warden, S.J.; Gutschlag, F.R.; Wajswelner, H.; Crossley, K.M.: Aetiology of rib stress fractures in rowers, Sports medicine (Auckland, N.Z.) 32 (13), 2002, pp. 819–836

[275] Weller, C.; Kleer, R.; Piller, F.T.: Economic implications of 3D printing: Market structure models in light of additive manufacturing revisited, International Journal of Production Economics 164, 2015, pp. 43–56

[276] Welsh, N.R.; Malcolm, R.K.; Devlin, B.; Boyd, P.: Dapivirine-releasing vaginal rings produced by plastic freeforming additive manufacturing, International Journal of Pharmaceutics 572, 2019, pp. 118725

[277] Wintermantel, E.; Ha, S.-W.: Medizintechnik, Interdisziplinarität, Biokompatibilität, Technologien, Implantate, Diagnostik, Werkstoffe, Business ; mit 200 Tabellen = Life science engineering, 4. Ed., Springer, Berlin, 2008

[278] Wohlers Associates: Wohlers report 2016, 3D printing and additive manufacturing state of the industry : annual worldwide progress report, Wohlers Associates, Inc., Fort Collins, USA, 2016

[279] Xiao, J.; Gao, Y.: The manufacture of 3D printing of medical grade TPU, Progress in Additive Manufacturing 2 (3), 2017, pp. 117–123

[280] Xu, A.; Venugopal, V.; Aryal, M.R.; Alfawares, Y.; Matur, A.V.; Cheng, J.; Kosco, E.; McConaha, M.; Ghalsasi, O.; Lockett, D.; Bal, G.; Andaluz, N.; Ngwenya, L.B.; Anand, S.; Forbes, J.: Toward global availability of low-cost, patient-specific cranial implants: creation and validation of automated CranialRebuild freeware application, Acta Neurochirurgica 165 (8), 2023, pp. 2219–2224

[281] Yarwindran, M.; Azwani Sa'aban, N.; Ibrahim, M.; Periyasamy, R.: Thermoplastic Elastomer Infill Pattern Impact on Mechanical Properties 3D Printed Customized Orthotic Insole, ARPN Journal of Engineering and Applied Sciences, 2016

[282] Yuan, S.; Shen, F.; Chua, C.K.; Zhou, K.: Polymeric composites for powder-based additive manufacturing: Materials and applications, Progress in Polymer Science 91, 2019, pp. 141–168

[283] Zaldivar, R.J.; Witkin, D.B.; McLouth, T.; Patel, D.N.; Schmitt, K.; Nokes, J.P.: Influence of processing and orientation print effects on the mechanical and thermal behavior of 3D-Printed ULTEM® 9085 Material, Additive Manufacturing 13, 2017, pp. 71–80

[284] Zhao, J.; Sun, Y.; Men, Y.: Elasticity Reinforcement in Propylene–Ethylene Random Copolymer Stretched at Elevated Temperature in Large Deformation Regime, Macromolecules 49 (2), 2016, pp. 609–615

[285] Ziaee, M.; Crane, N.B.: Binder jetting: A review of process, materials, and methods, Additive Manufacturing 28, 2019, pp. 781–801

[286] Zolfagharian, A.; Mahmud, M.A.P.; Gharaie, S.; Bodaghi, M.; Kouzani, A.Z.; Kaynak, A.: 3D/4D-printed bending-type soft pneumatic actuators: fabrication, modelling, and control, Virtual and Physical Prototyping 15 (4), 2020, pp. 373–402

7.1. Supplementary Information

7.1.1 Supplementary Information to Publication A
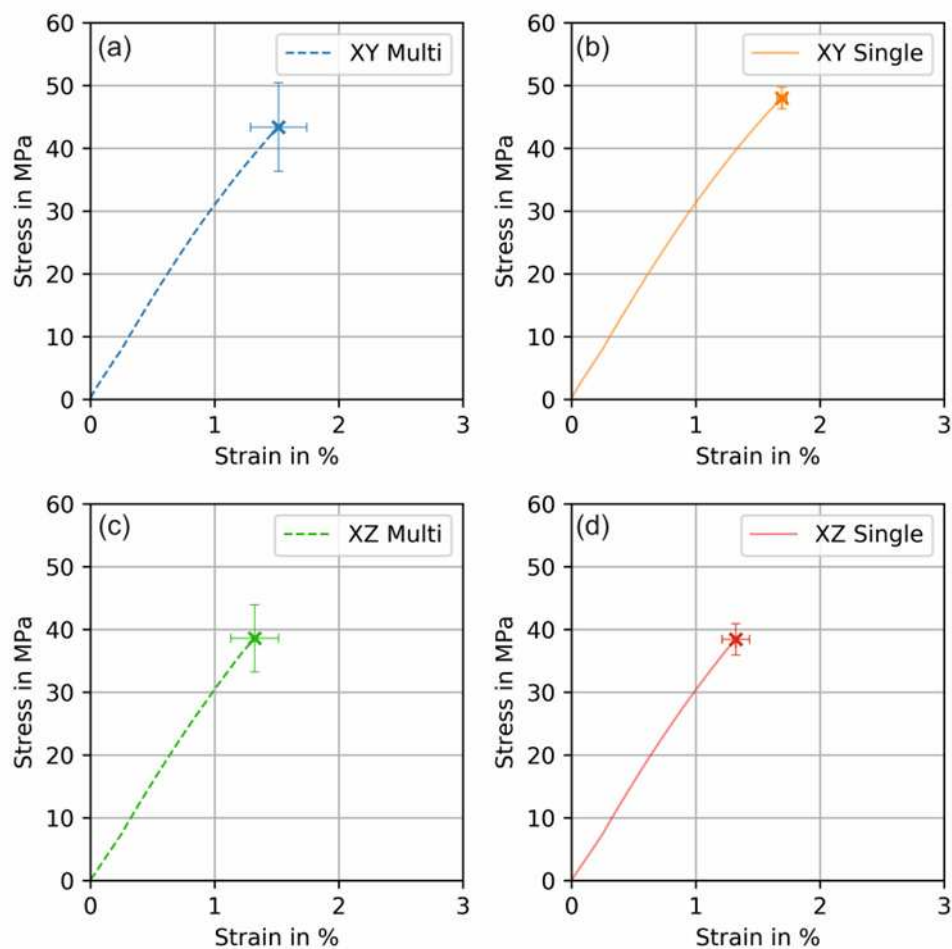
Figure S1   Stress-strain curves for the individual treatments investigated: (a) Print orientation XY multiple specimens per batch, (b) print orientation XY and single specimen per batch, (c) print orientation XZ and multiple specimens per batch, and (d) orientation XZ and single specimens per batch.

7.1.2 Supplementary Information to Publication B

Material processing

To improve the repeatability of the experiments all missing APF parameters are given in Table S1.

Table S1   Printing conditions for PMMA and the support material.

Parameter	Values	Unit
Temperature zone 1 (T_1)	200	°C
Temperature zone 2 (T_2)	230	°C
Dosing stroke	8	mm
Backpressure	40	bar
Discharge rate	67	%
Layer height	0.2	mm
Scale factor X-direction	1.015	/
Scale factor Y-direction	1.015	/
Scale factor Z-direction	1.000	/

Design of Experiments

In order to support the results of the design of experiments performed in this work, the results of the analysis of variances (ANOVA) carried out with the software Minitab® are given in Table S3 for the Young's modulus, Table S3 for the stress at break, Table S4 for the strain at break and Table S5 for the density results.

Table S2   ANOVA table for the Young's modulus response of the tensile tests. The designation A refers to the nozzle temperature, B to the building chamber temperature, C to the rotational screw speed, D to the drop aspect ratio and E to the overlap.

Source	Degrees of freedom	Sum of squares	Mean square	F-value	p-value
Model	16	24714485	1544655	70.83	$<10^{-4}$
Linear	5	19812642	3962528	181.70	$<10^{-4}$
A	1	7803644	7803644	357.84	$<10^{-4}$
B	1	447330	447330	20.51	$<10^{-4}$
C	1	93736	93736	4.30	0.045
D	1	11467787	11467787	525.86	$<10^{-4}$
E	1	146	146	0.01	0.935
2-Way-interactions	10	4018452	401845	18.43	$<10^{-4}$
A*B	1	101305	101305	4.65	0.038
A*C	1	271	271	0.01	0.912
A*D	1	3718756	3718756	170.53	$<10^{-4}$
A*E	1	574	574	0.03	0.872
B*C	1	50223	50223	2.30	0.138
B*D	1	7775	7775	0.36	0.554
B*E	1	57599	57599	2.64	0.113
C*D	1	7264	7264	0.33	0.567
C*E	1	1011	1011	0.05	0.831
D*E	1	73674	73674	3.38	0.074
Curvature	1	883391	883391	40.51	$<10^{-4}$
Error	37	806882	21808		
Total	53	25521367			

Table S3 ANOVA table for the stress at break response of the tensile tests. The designation A refers to the nozzle temperature, B to the building chamber temperature, C to the rotational screw speed, D to the drop aspect ratio and E to the overlap.

Source	Degrees of freedom	Sum of squares	Mean square	F-value	p-value
Model	16	12474.9	779.68	44.56	$<10^{-4}$
Linear	5	11979.3	2395.86	136.93	$<10^{-4}$
A	1	5382.6	5382.64	307.64	$<10^{-4}$
B	1	410.0	410.04	23.44	$<10^{-4}$
C	1	17.8	17.77	1.02	0.320
D	1	6155.0	6155.04	351.78	$<10^{-4}$
E	1	13.8	13.82	0.79	0.380
2-Way-interactions	10	445.8	44.58	2.55	0.019
A*B	1	68.1	68.09	3.89	0.056
A*C	1	2.0	2.03	0.12	0.735
A*D	1	97.5	97.51	5.57	0.024
A*E	1	5.8	5.76	0.33	0.570
B*C	1	0.5	0.51	0.03	0.866
B*D	1	8.9	8.87	0.51	0.481
B*E	1	21.4	21.40	1.22	0.276
C*D	1	16.0	16.03	0.92	0.345
C*E	1	214.8	214.82	12.28	10^{-3}
D*E	1	10.7	10.74	0.61	0.438
Curvature	1	49.9	49.88	2.85	0.100
Error	37	647.4	17.50		
Total	53	13122.3			

Table S4 ANOVA table for the strain at break response of the tensile tests. The designation A refers to the nozzle temperature, B to the building chamber temperature, C to the rotational screw speed, D to the drop aspect ratio and E to the overlap.

Source	Degrees of freedom	Sum of squares	Mean square	F-value	p-value
Model	16	8.78	0.54	17.94	$<10^{-4}$
Linear	5	7.53	1.50	49.22	$<10^{-4}$
A	1	4.03	4.02	131.76	$<10^{-4}$
B	1	0.37	0.37	12.05	0.001
C	1	0.01	0.01	0.44	0.514
D	1	3.05	3.05	99.73	$<10^{-4}$
E	1	0.06	0.06	2.10	0.156
2-Way-interactions	10	1.22	0.12	4.00	0.001
A*B	1	0.09	0.09	3.03	0.090
A*C	1	0.02	0.02	0.79	0.379
A*D	1	0.23	0.23	7.55	0.009
A*E	1	0.01	0.01	0.38	0.543
B*C	1	0.04	0.04	1.46	0.234
B*D	1	0.19	0.19	6.26	0.017
B*E	1	$<10^{-4}$	$<10^{-4}$	0.01	0.928
C*D	1	0.06	0.06	2.04	0.162
C*E	1	0.56	0.56	18.46	$<10^{-4}$
D*E	1	$<10^{-3}$	$<10^{-3}$	0.05	0.833
Curvature	1	0.03	0.03	0.92	0.343
Error	37	1.13	0.03		
Total	53	9.91			

Table S5   ANOVA table for the density response of the tensile tests. The designation A refers to the nozzle temperature, B to the building chamber temperature, C to the rotational screw speed, D to the drop aspect ratio and E to the overlap.

Source	Degrees of freedom	Sum of squares	Mean square	F-value	p-value
Model	16	0.53	0.033	50.05	$<10^{-4}$
Linear	5	0.50	0.100	150.46	$<10^{-4}$
A	1	0.16	0.165	247.88	$<10^{-4}$
B	1	0.01	0.009	13.17	0.001
C	1	$<10^{-4}$	0.001	1.14	0.293
D	1	0.32	0.325	489.20	$<10^{-4}$
E	1	$<10^{-4}$	0.001	0.91	0.346
2-Way-interactions	10	0.02	0.002	3.48	0.003
A*B	1	0.01	0.007	11.03	0.002
A*C	1	$<10^{-4}$	0.002	2.78	0.104
A*D	1	0.01	0.008	11.57	0.002
A*E	1	$<10^{-4}$	$<10^{-4}$	0.67	0.417
B*C	1	$<10^{-4}$	0.002	2.32	0.136
B*D	1	$<10^{-4}$	$<10^{-4}$	0.67	0.419
B*E	1	$<10^{-3}$	0.003	4.03	0.052
C*D	1	$<10^{-4}$	0.001	0.93	0.340
C*E	1	$<10^{-4}$	0.001	0.76	0.388
D*E	1	$<10^{-4}$	$<10^{-5}$	0.03	0.863
Curvature	1	0.01	0.009	13.75	0.001
Error	37	0.02	0.001		
Total	53	0.56			

7.1.3 Supplementary Information to Publication C

Table S6   Tensile test results from the samples printed at different infill orientations and print envelope temperatures. For a comparison stresses at break (a), strain at break (b) and yield stresses (c) are listed here.

a)   Stress at break (MPa)

	APF			MEX		
	50 °C	80 °C	110 °C	50 °C	80 °C	110 °C
0°	10.3 ± 0.8	10.2 ± 0.9	16.5 ± 2.2	7.3 ± 0.5	11.3 ± 1	11.9 ± 1.4
10°	7 ± 0.8	8.6 ± 0.6	17.1 ± 2	5.4 ± 0.2	5.8 ± 0.8	11.6 ± 1.1
20°	7.7 ± 0.4	5.9 ± 0.5	12 ± 3.1	5.6 ± 0.1	7.7 ± 0.7	10.9 ± 1.1
30°	5.3 ± 0.5	6.7 ± 0.5	12.5 ± 2.3	7.9 ± 0.5	8.6 ± 1.2	10.8 ± 0.3
45°	7.1 ± 0.2	11.4 ± 1.2	17.8 ± 1.4	7.6 ± 0.4	9.5 ± 0.5	7.3 ± 1.2
60°	12 ± 2	18.5 ± 2	16.2 ± 3.1	9 ± 0.4	8.3 ± 0.5	18.1 ± 2.5
70°	18.4 ± 2	24.9 ± 1.9	20.3 ± 2.6	8.6 ± 0.5	9.8 ± 0.5	17.2 ± 1.5
80°	23.7 ± 2.8	20 ± 1.9	17.6 ± 2.7	9.8 ± 0.5	9.8 ± 0.7	17.2 ± 1.3
90°	17.5 ± 3.7	17.2 ± 1.6	23 ± 0.8	9.1 ± 0.4	9.7 ± 0.8	10.9 ± 1

b)   Stain at break (%)

	APF			MEX		
	50 °C	80 °C	110 °C	50 °C	80 °C	110 °C
0°	369 ± 18	352 ± 17	447 ± 28	360 ± 6	388 ± 12	442 ± 12
10°	42 ± 5	82 ± 24	441 ± 28	19 ± 0.5	30 ± 8	340 ± 4
20°	33 ± 5	36 ± 2	373 ± 40	20 ± 2	19 ± 2	322 ± 11
30°	43 ± 11	39 ± 2	345 ± 50	34 ± 8	25 ± 11	48 ± 4
45°	198 ± 63	381 ± 19	459 ± 23	35 ± 2	135 ± 41	174 ± 75
60°	427 ± 29	501 ± 19	441 ± 13	69 ± 21	42 ± 2	442 ± 36
70°	500 ± 21	572 ± 30	474 ± 15	79 ± 31	84 ± 17	416 ± 37
80°	555 ± 28	518 ± 27	441 ± 19	153 ± 61	74 ± 26	408 ± 39
90°	360 ± 121	499 ± 28	535 ± 8	80 ± 23	128 ± 45	198 ± 56

c)   Yield stress (MPa)

	APF			MEX		
	50 °C	80 °C	110 °C	50 °C	80 °C	110 °C
0°	16.4 ± 0.3	17.3 ± 0.4	16.5 ± 0.2	14.6 ± 0.2	15 ± 0.2	16 ± 0.2
10°	17.1 ± 0.2	16.6 ± 0.1	15.9 ± 0.2	12.7 ± 0.1	12.7 ± 0.2	12.5 ± 0.6
20°	15.9 ± 0.4	16.3 ± 0.1	17.2 ± 0.5	12.2 ± 0.2	14.7 ± 0.4	14.1 ± 0.3
30°	15.8 ± 0.5	16.5 ± 0.3	18.8 ± 0.6	12.9 ± 0.1	12.7 ± 0.7	13.2 ± 0.2
45°	16.2 ± 0	17 ± 0.2	17.8 ± 0.3	13.3 ± 0.2	13.5 ± 0.1	13.4 ± 0.8
60°	17.2 ± 0.4	17.7 ± 0.4	19 ± 0.7	14.2 ± 0.1	13.9 ± 0.2	16.1 ± 0.2
70°	16.9 ± 0.4	18.4 ± 0.3	19.4 ± 0.3	14 ± 0.1	14.2 ± 0.3	16.4 ± 0.4
80°	17 ± 0.2	18.1 ± 0.1	18.4 ± 0.2	14.6 ± 0.1	14.8 ± 0.3	14.5 ± 0.2
90°	17.2 ± 0.3	17.4 ± 0.1	17.8 ± 0.3	13.9 ± 0.2	14 ± 0.1	14.3 ± 0.2

Table S7   Tensile results for the specimen printed with the APF method at different infill orientations, chamber temperatures and number of contour lines. Values for stresses at break (a) and Strain at break (b) are listed.

a)	Stress at break (MPa)			
Chamber temperature →		50 °C	80 °C	110 °C
Orientation ↓	Number of contour lines ↓			
	0	10.3 ± 1.7	10.2 ± 2	16.5 ± 4.9
0°	1	15.5 ± 5.6	14.2 ± 9.2	22.5 ± 1.5
	2	16.1 ± 7.1	13.5 ± 8.2	14.8 ± 6.5
	0	7.1 ± 0.5	11.4 ± 2.6	17.8 ± 3.2
45°	1	19.8 ± 2.8	25.2 ± 5.4	13.9 ± 2.5
	2	22.1 ± 4.1	28.4 ± 3.5	12.6 ± 5.1
	0	17.5 ± 8.3	17.2 ± 3.5	23 ± 1.7
90°	1	23.8 ± 1.5	18.1 ± 5.2	26.1 ± 0.9
	2	24.8 ± 0.9	26.1 ± 1	25.2 ± 1.5

b)	Strain at break (MPa)			
Chamber temperature →		50 °C	80 °C	110 °C
Orientation ↓	Number of contour lines ↓			
	0	369 ± 40	352 ± 39	447 ± 62
0°	1	402 ± 133	433 ± 129	530 ± 28
	2	449 ± 98	427 ± 145	420 ± 67
	0	198 ± 140	381 ± 42	459 ± 51
45°	1	527 ± 35	593 ± 93	451 ± 38
	2	551 ± 66	635 ± 61	336 ± 193
	0	360 ± 271	499 ± 62	535 ± 17
90°	1	589 ± 8	506 ± 104	612 ± 12
	2	596 ± 12	634 ± 18	594 ± 23

Table S8　Tensile results for the specimen printed with the MEX method at different infill orientations, chamber temperatures and number of contour lines. Values for stresses at break (a) and Strain at break (b) are listed.

a) **Stress at break (MPa)**

Chamber temperature →		50 °C	80 °C	110 °C
Orientation ↓	Number of contour lines ↓			
0°	0	7.3 ± 1.2	11.3 ± 2.1	11.9 ± 3.1
	1	13.4 ± 1	15 ± 3.2	17.5 ± 4
	2	10.5 ± 3.2	15.3 ± 1.3	20.3 ± 5.7
45°	0	7.6 ± 0.8	9.5 ± 1	7.3 ± 2.7
	1	16.1 ± 6	14.6 ± 5.5	13.6 ± 0.5
	2	24.1 ± 1	15.3 ± 2	23.3 ± 0.6
90°	0	9.1 ± 1	9.7 ± 1.8	10.9 ± 2.3
	1	14.8 ± 4.3	17.6 ± 4.4	23.1 ± 1.2
	2	13.9 ± 1.7	23.8 ± 1.2	19 ± 1.7

b) Strain at break (MPa)

Chamber temperature →		50 °C	80 °C	110 °C
Orientation ↓	Number of contour lines ↓			
0°	0	360 ± 14	388 ± 26	442 ± 27
	1	387 ± 3	415 ± 41	491 ± 59
	2	380 ± 13	415 ± 35	556 ± 80
45°	0	35 ± 5	135 ± 92	174 ± 168
	1	435 ± 91	435 ± 84	360 ± 26
	2	572 ± 21	412 ± 27	524 ± 11
90°	0	80 ± 51	128 ± 101	198 ± 125
	1	401 ± 54	482 ± 55	574 ± 32
	2	382 ± 41	571 ± 18	515 ± 48

7.2. Abbreviations

Designation	Description
3D	three-dimensional
ABS	Acrylnitrile Butadien Styrene
a_{cN}	Charpy impact strength notched in KJ m^{-2}
a_{cU}	Charpy impact strength unnotched in KJ m^{-2}
AI	Artificial intelligence
α	infill angle
α_0	Constant coefficient of linear regression in equation (4)
α_A	Coefficient of factor A inequation (4)
α_{AB}	Coefficient of interaction AB in equation (4)
AM	Additive Manufacturing
APF	Arburg plastic freeforming
b_{1m}	Coefficient of melt function of the specific volume (6)
b_{1S}	Coefficient of solid function of the specific volume (5)
b_{2m}	Coefficient of melt function of the specific volume (6)
b_{2S}	Coefficient of solid function of the specific volume (5)
b_{3m}	Coefficient of melt function of the specific volume (6)
b_{3S}	Coefficient of solid function of the specific volume (5)
b_{4m}	Coefficient of melt function of the specific volume (6)
b_{4S}	Coefficient of solid function of the specific volume (5)
b_5	Coeffcent of pvt equations (5-7)
b_6	Coeffcent of Ttrans equation (7)
b_7	Coefficient of solid function of the specific volume for semi-crystalline polymers (5)
b_8	Coefficient of solid function of the specific volume for semi-crystalline polymers (5)

b_9	Coefficient of solid function of the specific volume for semi-crystalline polymers (5)
BJT	Binder jetting
BMDW	Austrian Federal Ministry for Digital and Economic Affairs
BMVIT	Austrian Federal Ministry of Transport, Innovation and Technology
CAD	Computer aided Design
CAMed	COMET-K project, Clinical additive Manufacturing for medical applications
CD	Compact discs
CNC	Computer numerical control
CO_2	Carbondioxide
CT	Computer tomography
DAR	Drop aspect ratio
DED	Direct energy deposition
DLP	Digital light processing
DoE	Design of experiments
DSC	Differential scanning calorimetry, thermal material analysis
EBM	Electron beam melting
E_f	Flexurar modulus in GPa
F_D	Damage force on drop weight testing in N
FDA	Food and Drug Administration in the United States
FDM®	Fused deposition modeling
FFF	Fused filament fabrication
F_M	Maximum force in drop weight testing in N
g	Generator in DoE
G-code	Maschine code for 3D printer
I_D	Displacement at damage force in mm

IDT	Initial degradation temperature in °C
IM	Injection molding
l_M	Displacement at maximum force in mm
k	factor in DoE
LCD	Liquide crystal display
MDD	Medical device directive, regulation of medical device production in the EU
MEX	Material Extrusion
MJT	Material Jetting
MRT	Magnet resonance tomography
OL	Overlap, design parameter in the ARBURG slicer software
p	pressure
PBF	Powder bed fusion
PC	Polycarbonate
PCL	Polycaprolactone
PC-U	Polycarbonate urethane
PE	Polyethylene
PEEK	Polyetheretherketone
PEG	Polyethylene-glycol
PET-G	Glycole modified Polyethylenetherephtalat
Ph.D.	Doctor of Philosophy
PLA	Polylactide-acid
PMMA	Polymethylmethacrylate
PP	Polypropylene
PS	Polystyrene
PSI	Patient specific implant
PVA	Polyvinyl alcohol

pvT	Pressure, specific volume, and temperature relation measurement of polymeric materials
SFG	Styrian Business Promotion
SHL	Sheet lamination
σ_{fM}	Maximum flexural Stress in MPa
SLA	Stereolithography
SLM	Selective laser melting
SLS	Selective laser sintering
STL	Standard triangle language
T	Temperature
T_1	Temperature in Zone 1 in °C
T_2	Temperature in Zone 2 in °C
T_B	Building plate temperature in °C
T_{CH}	Chamber Temperature in °C
$T_{chamber}$	Chamber Temperature in °C
T_g	Glass transition temperature in °C
TGA	Thermalgravimetric analysis
Ti6Al4V	Titanium alloy
T_{nozzle}	Nozzle temperature in °C
TPE	Thernoplastic polyethylene
T_{peak}	Temperature at the peak of the differential curve from the TGA experiment
TPO	Thermoplastic polyolefine
T_{temper}	Holding temperature during the tempering process in °C
T_{trans}	Transition temperature of *pvt* functions in °C
UHMWPE	Ultra high molecularweight Polyethylene
UID	Unique identification number

USP	United States Pharmaceutical, regulation for medical materials in the United States
UV	ultraviolette
v	specific volume
VPP	Vat Photopolymerization
Screw	Rotational screw speed of the freeformer